

Algorithms for Separation  
of Secondary Surveillance Radar Replies



Algorithms for Separation  
of Secondary Surveillance Radar Replies

PROEFSCHRIFT

ter verkrijging van de graad van doctor  
aan de Technische Universiteit Delft,  
op gezag van de Rector Magnificus prof.dr.ir. J.T. Fokkema,  
voorzitter van het College van Promoties,  
in het openbaar te verdedigen

op maandag 9 december 2002, om 13:30 uur

door

Nicolas Laurent Regis PETROCHILOS

Agrégé-Normalien  
Ecole Normale Supérieure de Lyon.  
Diplôme d'Étude Approfondie aan de  
ENSEA, Cergy-Pontoise  
geboren te Paris, France

Dit proefschrift is goedgekeurd door de promotoren:

Prof.dr.ir. P. Dewilde

Prof.dr. P. Comon

Prof.ir. P. van Genderen

Samenstelling promotiecommissie:

Rector magnificus	voorzitter
Prof.dr.ir. P. Dewilde	Technische Universiteit Delft, promotor
Prof.dr. P. Comon	Universite de Nice, promotor
Prof.ir. P. van Genderen	Technische Universiteit Delft, promotor
Prof.dr.ir. A.J. van der Veen	Technische Universiteit Delft
Prof.ir. G. Galati	Universita di Tor Vergata, Rome
Prof.dr. M. Moonen	Katholieke Universiteit, Leuven
Prof.dr. Ph. A. Regalia	Institut National des Telecommunication, Evry

*Published and distributed by:* DUP Science

DUP Science is an imprint of  
Delft University Press  
P.O. Box 98  
2600 MG Delft  
The Netherlands  
Telephone: +31 152785678  
Telefax: +31 152785706  
E-mail: [Info@Library.TUdelft.NL](mailto:Info@Library.TUdelft.NL)

ISBN 90-407-2371-0

Keywords: Array signal processing/ Source separation/ Secondary Surveillance Radar

Copyright©2002 by Nicolas Petrochilos

All rights reserved. No part of the material protected by this copyright notice may be reproduced or utilized in any form or by any means, electronic or mechanical, including photocopying, recording or by any information storage and retrieval system, without written permission from the publisher: Delft University Press.

Cover photo by Silke Fisher-Witrisal.

Cover design by Arnold Zwanenburg (<http://www.polipo.com>)

Printed in The Netherlands

*To Lea and my family.*



# Contents

<b>Contents</b>	<b>i</b>
<b>List of Tables</b>	<b>v</b>
<b>1 Introduction</b>	<b>1</b>
1.1 Air-traffic control and the SSR system . . . . .	1
1.2 Problems with mode S . . . . .	2
1.3 A distributed groundstation based solution . . . . .	3
1.4 Scope of the thesis . . . . .	5
1.5 Contributions . . . . .	5
1.6 Outline of the thesis . . . . .	7
1.7 Notation . . . . .	8
<b>2 Secondary Surveillance Radar</b>	<b>11</b>
2.1 System summary . . . . .	11
2.2 Mode A/C and mode S replies . . . . .	14
2.2.1 Mode A/C reply message . . . . .	14
2.2.2 SSR mode S reply . . . . .	15
2.3 Traffic Advisory and Collision Avoidance System . . . . .	16
2.4 Problems . . . . .	17
2.4.1 Well-known mode A/C problems . . . . .	17
2.4.2 Foreseen mode S problems . . . . .	18
2.5 A distributed groundstation network . . . . .	18
2.6 Conclusion . . . . .	20
<b>3 Data model, and state of the art</b>	<b>21</b>
3.1 Data Model . . . . .	21
3.1.1 The emitted replies . . . . .	21
3.1.2 Received data model . . . . .	24
3.1.3 Multipath . . . . .	27
3.2 Statistical properties of the SSR source . . . . .	27
3.3 Algorithmic survey . . . . .	30
3.3.1 MMSE and ZF approach . . . . .	31
3.3.2 ESPRIT . . . . .	32

---

3.3.3	A Decision-Directed Beamformer . . . . .	34
3.3.4	The ILSP and ILSE method . . . . .	35
3.3.5	ACMA . . . . .	36
3.3.6	ACPA . . . . .	37
3.3.7	SOBI . . . . .	38
3.4	Conclusion . . . . .	38
<b>4</b>	<b>Identifiability in the noiseless case</b>	<b>41</b>
4.1	Model and assumptions . . . . .	41
4.2	The infinite sample case . . . . .	43
4.3	The finite sample case . . . . .	44
4.3.1	Method using the binary data property . . . . .	44
4.3.2	Method using the ZCM property . . . . .	47
4.3.3	Simulations . . . . .	50
4.4	Conclusion . . . . .	52
<b>5</b>	<b>Cramer-Rao Bounds</b>	<b>55</b>
5.1	Introduction . . . . .	55
5.1.1	Definition of Cramer-Rao Bound . . . . .	55
5.1.2	Modeling . . . . .	57
5.2	Cramer-Rao Bounds . . . . .	57
5.2.1	Case $\alpha$ : Deterministic known $\mathbf{B}$ . . . . .	57
5.2.2	Case $\beta$ : Stochastic $\mathbf{B}$ . . . . .	59
5.2.3	Case $\gamma$ : Deterministic unknown $\mathbf{B}$ . . . . .	60
5.3	Simulations . . . . .	61
5.4	Conclusion . . . . .	62
<b>6</b>	<b>Algorithms</b>	<b>65</b>
6.1	The problem statement and useful results . . . . .	65
6.1.1	The problem statement . . . . .	65
6.1.2	Prior processing . . . . .	66
6.2	Zero/Constant modulus algorithms . . . . .	68
6.2.1	ZCM properties . . . . .	68
6.2.2	The existing algorithms . . . . .	70
6.2.3	The matrix pencil problem . . . . .	72
6.2.4	The multi-shift ZCMA . . . . .	77
6.2.5	Discussion . . . . .	80
6.3	ESPRIT-Second-Order Blind Identification algorithm . . . . .	80
6.3.1	The original SOBI: principle . . . . .	81
6.3.2	An evolution: ESPRIT-SOBI . . . . .	82
6.3.3	Discussion . . . . .	84
6.4	Manchester Decoding Algorithm . . . . .	85
6.4.1	Principle of the MDA2 . . . . .	85
6.4.2	Principle of the MDA3 . . . . .	88
6.4.3	The third-order joint diagonalization . . . . .	91



---

6.4.4	Discussion . . . . .	92
6.4.5	Mode A/C replies . . . . .	93
6.5	Post-processing . . . . .	93
6.6	Conclusion . . . . .	94
<b>7</b>	<b>Simulations</b>	<b>95</b>
7.1	Simulation scenario . . . . .	95
7.2	SNR . . . . .	96
7.3	Number of Samples . . . . .	99
7.4	Angle difference . . . . .	101
7.5	Frequency difference . . . . .	105
7.6	Power Ratio . . . . .	107
7.7	Packet overlapping . . . . .	110
7.8	Conclusions . . . . .	113
<b>8</b>	<b>Experimental results</b>	<b>115</b>
8.1	Experimental setup . . . . .	115
8.1.1	Design of the receivers . . . . .	115
8.1.2	The digital part . . . . .	117
8.2	Experimental considerations . . . . .	118
8.2.1	Reply density . . . . .	118
8.2.2	Verification of the signal model . . . . .	118
8.3	Experimental results . . . . .	122
8.3.1	Semi-synthesized results . . . . .	122
8.3.2	Real case data: influence of the down-sampling . . . . .	124
8.4	Conclusion . . . . .	128
<b>9</b>	<b>Conclusion</b>	<b>129</b>
<b>A</b>	<b>Proof of Lemma 4.3.5</b>	<b>131</b>
A.1	Reminder . . . . .	131
A.2	Proof of Lemma 4.3.5 . . . . .	132
<b>B</b>	<b>CRB proofs</b>	<b>141</b>
B.1	Inversion of $\mathcal{I}_\gamma$ by the Schur complement theorem . . . . .	141
B.2	Proof for lemma (5.2.3) . . . . .	141
B.2.1	Reminders . . . . .	141
B.2.2	Preliminary lemmas . . . . .	142
B.2.3	Main body . . . . .	144
	<b>Bibliography</b>	<b>147</b>
	<b>Summary</b>	<b>151</b>
	<b>samenvatting</b>	<b>153</b>

<b>Acknowledgments</b>	<b>155</b>
<b>Curriculum vitae</b>	<b>157</b>

# List of Tables

2.1	Various evolutions of the TACAS. . . . .	16
6.1	Multi-shift ZCM Algorithm. . . . .	79
6.2	ESPRIT-SOBI algorithm. . . . .	84
6.3	MDA2 Algorithm. . . . .	88
6.4	MDA3 Algorithm. . . . .	92
8.1	<i>Failure rate over all the possible starts of the down-sampling.</i> . . . .	128



# Chapter 1

## Introduction

### 1.1 Air-traffic control and the SSR system

Air-Traffic Control centers (ATC) have the mission to assure the safety of the aircraft cruising in their area. To fulfill this mission, the ATC operator has at his disposal a Plan Position Indicator (PPI). The PPI displays several kinds of information such as the position and the altitude of all planes in the area for which the operator is responsible. The data for this display is provided by two radar systems, the primary radar and the Secondary Surveillance Radar (SSR). The first one indicates the presence of a plane, whilst the second radar informs moreover on its identity and its altitude.

The primary radar uses a rotating antenna to send pulses in a narrow beam in the direction of sight. If a plane is in the line of sight of the radar, then its body will reflect the pulses. The primary radar detects these reflections to determine the presence of a plane.

A SSR mode A/C uses a conventional rotating antenna as well, but functions more like a cooperative two-way communication system. Indeed, the groundstation emits in a narrow beam in the line of sight an up-link signal, called the “interrogation”, which contains an un-addressed question. A plane illuminated by the radar detects the interrogation packet and responds by emitting a down-link signal, called the “reply”. An omnidirectional antenna on the plane assures the reception of the request. A transponder onboard the aircraft is used to decode the request, to obtain the requested information, and to encode it in a short reply (12 bits), which contains either the altitude or the identity. This reply is transmitted back to the groundstation at a different frequency, using the same omnidirectional antenna. At the groundstation, the received message is decoded and sent to the Air Traffic Control center.

Originally the system was created during the last world war to identify the planes detected by a primary radar, for which reason the radar was called “Identify, Friend or Foe” (IFF). Later it was opened to civilian usage, and now SSR is mandatory on all aircraft. In the USA the SSR system is frequently called the ATC Radar Beacon

System (ATCRBS).

The SSR mode A/C system has some problems, such as “Garble”, which means that replies from two or more airplanes arrive at the same time on the antenna. But also it can endure what is called “FRUIT”, which means that a plane had its transponder triggered by an adjacent SSR groundstation, and emits an undesired answer, which can create a garble situation and/or fool the groundstation. Multipath brings also some additional problems, such as the appearance of ghost planes. Loss of some replies due to garbling is solved by the fact that the interrogation is repeated around 12 times per antenna scan. Due to the increase of air traffic, the density of replies has increased as well, and the SSR mode A/C became more and more overloaded.

To reduce the reply density, in 1999 an updated SSR was supposed to be commissioned: the Secondary Surveillance Radar mode S, where S stands for selective. This update was intended to reduce the density of replies, and as a consequence the quantity of lost replies. It is mainly a protocol update, and differs from SSR mode A/C in two respects. First, the interrogation is selective, the groundstation may address planes separately. Second, the data-length of the replies is longer: while 12 bits are used for mode A/C, mode S has either 64 or 112 bits, called “short” and “long” replies. Furthermore, this protocol allows to have Extended Long Messages (ELM), which consist of several (2 to 8) long replies linked together to form the answer to a request. This new mode provides a data link between the aircraft and the groundstation. This data link is supposed to be part of the Aeronautical Telecommunication Network (ATN), which links aircraft, groundstations and ATC-centers. The upgrade is being delayed by the principal actors of the field (the airline companies and the airports), while Eurocontrol, as well as other federal agencies, tries to enforce it.

Chapter 2, [1], [2], and [3] give more information on SSR.

## 1.2 Problems with mode S

We foresee for this new system some shortcomings. Because the ground antenna is rotating, the time during which the aircraft is illuminated is quite limited, around 30 ms per scan. For a mode A/C link there are up to 15 request-reply exchanges in this time, and this is sufficient to ensure that the answer has been properly decoded. But the mode S datalink requires more time, indeed only one or two ELM are possible in one illumination (or antenna scan). Furthermore, the time between two illuminations is as long as the antenna revolution time, 4-10 seconds. An undesired effect is that an ELM might be received by fractions over different scans, which is unacceptable because the transaction time will be too long. By reducing the density of replies from different aircraft by selectivity, SSR mode S should reduce as well the Garble, FRUIT and Multipath problems. However, these problems will still contribute to fool the ground system. Finally, due to the increase of air traffic, we expect that the currently proposed SSR mode S system will not be able to cope with future traffic densities, at least not in areas with a dense concentration of planes, like in Western

Europe or south-west Asia.

### 1.3 A distributed groundstation based solution

In this thesis, we propose a solution to the problems described in section 1.2 by innovating the ground-based component of the SSR system, while maintaining the current airborne component. The idea is to replace the present rotating antenna by a distributed groundsystem, consisting of a network of groundstations on different geographical positions, as shown in Figure 1.1. These groundstations can be divided into two classes: transmitters, which send the request, and receivers, which receive the transponders' replies. The distributed groundsystem consists of one transmitter and at least three receivers, which work cooperatively. The transmitter sends the

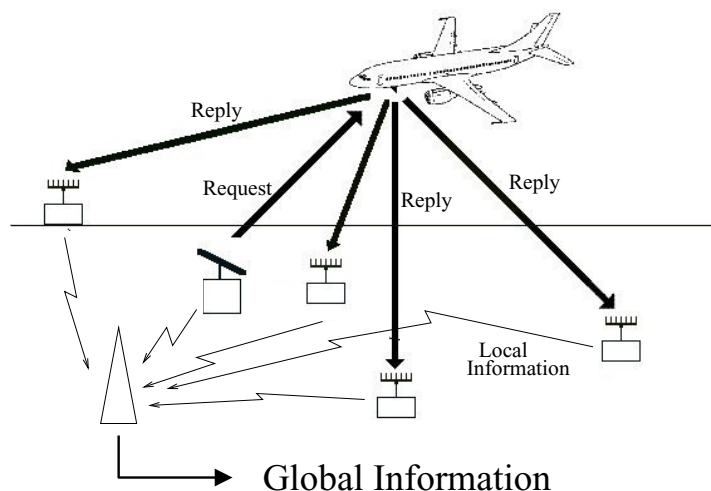


Figure 1.1: *The distributed system: the interrogator, the plane, the receiving stations, and the central management.*

requests and the other groundstations receive the replies on an array antenna. Each array antenna consists of an array of elements attached to a processing unit. The elements are omnidirectional antennas; having several elements gives access to differently phased versions of each impinging signal. Sources from different directions give rise to different phases, and by properly combining this information, the impinging SSR sources can be separated and their directions of arrival estimated. The groundstations send the relevant information, such as the angles of arrival (DOA), the messages, and the times of arrival (TOA) of the SSR signals to a central management system. With this information, and knowledge on the positions of the groundstations, the central management system can estimate the position of the planes by means of triangulation, and confirm the down-link messages. While two

receiving stations suffice in theory, having three or more stations would result in a more accurate location estimation. The principle of this solution is summarized in Figure 1.2.

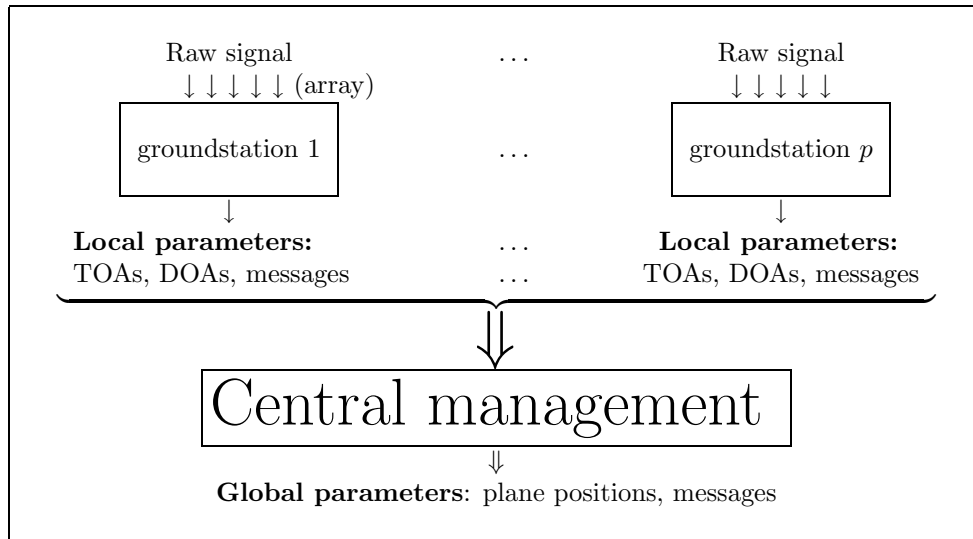


Figure 1.2: Scheme of the proposed solution.

The distributed radar receiver concept has already been applied in the past to other problems, such as tracking radar jitter with the MUlti RAadar Trajectory REConstruction method in [4] and [3], and for Wind Speed Measurement [5]. Furthermore, a study made by J. Tol [6] shows that a distributed ground system can increase the quality of the reception over the usual SSR system. This triangulation principle has been successfully applied recently by a Czech company and became a reliable commercial product, see the corresponding article [7]. The authors only use existing signal decoder linked to one omnidirectional element to obtain the times of arrival of the replies. Our design incorporates an antenna array at each receiving station, which improves the reliability of the separation and allows for direction of arrival estimation. With this additional information, the accuracy of the airplane position would be enhanced compared to the commercial system. Moreover, our design needs only two receivers as a minimum requirement, while this commercial product requires three receivers at least.

The proposed design does not impose any additional requirements on the interrogating antenna, which can be a conventional rotating antenna or a fixed array of several elements. Ultimately, a transmitting array would have the advantage to point instantly to the plane of interest, without having to wait for the rotation of the conventional antenna. Nevertheless, in a transition period, the emitter can keep the actual rotating antenna in order to assess the concept.



## 1.4 Scope of the thesis

As any radar design is a multi-disciplinary exercise, our design involves issues from several diverse expertise fields: creating a receiving array (antenna theory and analog electronics), processing the data (array signal processing), communication between the stations (asynchronous network communication), determining the airplanes position (data fusion and clustering), and presenting the information to the air-traffic controllers (human-machine interface). Among the issues to be solved, we were interested in one particular problem that was worth a separate study: to extract from the raw signal received by the array at each groundstation the meaningful parameters by means of an array Signal Processing (SP) algorithm. Usually, the SP community appreciates the following qualities in an algorithm: robustness, *i.e.* the algorithm does not miss any plane, accuracy, *i.e.* the extracted parameters have a small error variance, and speed, *i.e.* the algorithm is computationally “fast” enough to be implemented in practice. The focus of my thesis is to develop and assess receivers algorithms that solve the problem under consideration and that possess the desired qualities mentioned above. Such an algorithm has two components, firstly it has to separate the incoming overlapping source signals and detect the reply messages, secondly it has to estimate the Direction Of Arrival (DOA) and the Time Of Arrival (TOA) of each source.

To perform source separation, an algorithm has to exploit mathematical properties, resulting from the model of the problem under investigation. Generally, these properties are divided into two categories: spatial and source properties. Spatial properties rely on the propagation channel and the array configuration only, and a good survey can be found in [8, 9]. Source properties are structural properties of the transmitted signals such as their modulation properties and statistical independence. The most used are: cyclostationarity [10], high-order statistics [11], constant modulus [12], finite alphabet [13, 14, 15, 16], or self-coherence [17].

SSR replies have a very structured but unusual source model, it is a binary signal taken from the alphabet  $\{0, 1\}$ , multiplied by a complex phase, which depends on the residual carrier frequency such that this phase is a complex exponential of time. In the literature, we have found algorithms that rely on the residual carrier property [18, 19]. Specifically for a mixture of SSR replies, there is an article [20] that uses a general property, the cumulants, to separate the sources. The only article that proposed SSR separation based on the structural properties of the sources was [21], which presented the Analytical Zero Constant Modulus Algorithm (AZCMA).

## 1.5 Contributions

The main contribution of this thesis is four-fold:

- *Identifiability*, *i.e.* the ability to extract the model parameters from a given set of observations. For a small number of observations, this is not always possible. Using the source symbol properties, I derive an identifiability proposition for an infinite number of observations, and two propositions valid for a finite batch of

samples, the latter propositions state bounds for the identification probability of a mixture of SSR sources.

- *Cramer-Rao Bound:* The CRB gives a lower bound on the estimation accuracy of any unbiased estimator. It is frequently used as a benchmark for algorithms. Assuming a high SNR, I derive Cramer-Rao bounds for two data models: one where the SSR signals is considered stochastic, and one where it is considered deterministic.
- *Receiver algorithms:* I propose a new algorithm that uses the specific encoding of the data in the SSR reply system. I propose as well two evolutions of existing algorithms: the multi-shift-ZCMA and the ESPRIT-SOBI. These algorithms overcome some of the shortcomings of the initial algorithms. The multi-shift ZCMA will even be shown to be quite robust in a variety of circumstances.
- *Experimental platform:* I designed a complete 4 elements phased array, from the antenna dipoles to the receiving chains, which was subsequently built by our technician. With this setup, we were able to obtain real measurement data to confront the algorithms. I report on the setup and the initial results.

During the preparation of the thesis, I also worked on several other topics such as:

- *Synchronization and channel equalization:* Orthogonal Frequency Division multiplexed (OFDM) is a promising scheme for future communication systems: digital video broadcast (DVB), digital audio broadcast (DAB), IEEE 802.11a, W-LAN, Hyperlan II and xDSL, and is well placed for widespread adoption in future broadband wireless networks. This high-data rate multi-carrier scheme is unfortunately sensitive to symbol timing offset, to frequency offset, and to time-varying channels. In [22, 23, 24], we proposed several algorithms to cope with these problems.
- *Blind time delay estimation via subspace intersection and ESPRIT:* In Code division Multiple Acces (CDMA) receiver systems, knowledge of the times of arrival of the dominant paths is required. In [25] we have presented a method to blindly estimate them by taking advantage of several signal space invariances, and lastly an application of ESPRIT.
- *Wind-speed measurement system:* Using a multi-static configuration of passive array antennas with a highly directional emitter, we propose a new scheme to measure air speed in the atmosphere [5]. Two direct important applications are remote-sensing for environmental study, and wind profile measurement at airport sites to improve security for aircrafts during landing.
- *Blind identification of linear-quadratic channel:* In [26], using High-Order Statistics (HOS) of the input we obtain a set of equations which are quadratic in the unknown coefficients of the channel. Several algorithms are then developed to solve these equations.

- *Non-linear channel identification:* Unlike the Schetzen method, the non-blind identification method proposed in [27] can identify non-linear systems whose inputs have discrete distributions, accepts kernels of any length, tolerates signal-independent zero-mean additive noise irrespective of its color and distribution, and leads to a closed form solution.
- *Identifiability of a mixture of constant modulus signals with a finite number of samples:* Identifiability has the same definition as in the first item of the section, but the source model is different, we consider sources whose absolute value is equal to one: Constant Modulus sources. In the literature, unique identifiability of mixtures of CM signals results were developed only for an infinite number of available observations. In [28] we derived a rigorous proof for a finite sample identifiability theorem.

## 1.6 Outline of the thesis

The thesis is organized as follows:

- Chapter **2** contains a short introduction for non-specialists to the present SSR system, and reminds our proposed design for a distributed SSR system.
- Chapter **3** describes the mathematical model of the SSR replies, and after simplification the model that we use throughout this thesis. The chapter presents the statistical properties of the replies and finishes with a short survey of signal processing algorithms for source separation.
- Before deriving any estimation algorithm, we have to be insured that there is a unique identifiability of the parameters. Chapter **4** presents the propositions and theorems derived towards this goal.
- In Chapter **5**, various Cramer-Rao Bounds are derived for SSR replies. A stochastic bound is derived and compared to a deterministic one.
- In Chapter **6**, the algorithms invented during this thesis work are presented. The extension of the AZCMA, the multi-shift ZCMA is first described, then the ESPRIT-SOBI is presented. At the end of the chapter, a new algorithm, the Manchester Decoding Algorithm, is developed, and both versions of the MDA are presented.
- The algorithms presented in the preceding chapter need to be evaluated. As it would not be possible to measure and record all the possible scenarios, we had to simulate them to establish the strong and weak points of the algorithms. In chapter **7**, the results of the extensive simulations are presented, and some behavior of the algorithms is explained.
- Chapter **8** presents the experimental setup designed and constructed at TU Delft. It also exhibits the preliminary results of the measurement campaign.

In this chapter, we also describe the missing elements to have an operational radar.

- The thesis is concluded by chapter 9, which summarizes the significance of this work and proposes some recommendations for future directions of research.

## 1.7 Notation

We denote scalars by italic lowercase letters, as in  $a$ , vectors by lower case boldface letters, as in  $\mathbf{a}$ , and matrices by upper case boldface letters, as in  $\mathbf{A}$ . Unless specified otherwise,  $\mathbf{I}$  is the identity matrix, and  $\mathbf{0}$  and  $\mathbf{1}$  are the vectors with all entries are equal to 0 and 1, respectively. We denote by  $(\cdot)^*$  the complex conjugation, by  $(\cdot)^T$  the matrix transpose, and by  $(\cdot)^H$  the matrix conjugate transpose.

$E\{\cdot\}$  denotes the mathematical expectation operator, and  $\text{Vec}$  is the operator that stacks the columns of a matrix  $\mathbf{A}$  into a vector  $\mathbf{a}$ .  $\text{Unvec}$  is the reverse operator. Unless specified differently, it is used to transform a  $d^2$  vector into a square  $d \times d$  matrix.  $\text{Diag}$  is the diagonal operator, which from a vector creates a diagonal matrix, whose diagonal entries are the elements of the vector:

$$\text{diag}(\mathbf{a}) = \text{diag}([a_1, \dots, a_d]^T) = \begin{bmatrix} a_1 & & 0 \\ & \ddots & \\ 0 & & a_d \end{bmatrix}$$

The notation  $(\cdot)^\dagger$  refers to the Moore-Penrose inverse (pseudo-inverse). For tall matrices, if  $\mathbf{A}^H \mathbf{A}$  is invertible, then:

$$\mathbf{A}^\dagger = (\mathbf{A}^H \mathbf{A})^{-1} \mathbf{A}^H, \quad \text{and} \quad \mathbf{A}^\dagger \mathbf{A} = \mathbf{I}$$

For wide matrices, if  $\mathbf{A} \mathbf{A}^H$  is invertible, then:

$$\mathbf{A}^\dagger = \mathbf{A}^H (\mathbf{A} \mathbf{A}^H)^{-1}, \quad \text{and} \quad \mathbf{A} \mathbf{A}^\dagger = \mathbf{I}$$

The symbol  $\odot$  denotes the Schur-Hadamard (element-wise) matrix product. For two matrices  $\mathbf{A}$  and  $\mathbf{B}$ , the Kronecker product,  $\otimes$ , is defined by:

$$\mathbf{A} \otimes \mathbf{B} = \begin{bmatrix} a_{11} \mathbf{B} & a_{12} \mathbf{B} & & \\ & \dots & & \\ & & & a_{mn} \mathbf{B} \end{bmatrix}$$

Similarly, the symbol  $\circ$  denotes the Khatri-Rao product, which is a column-wise Kronecker product:

$$\mathbf{A} \circ \mathbf{B} = [\mathbf{a}_1 \otimes \mathbf{b}_1, \mathbf{a}_2 \otimes \mathbf{b}_2, \dots]$$

At this point we recall some Kronecker product properties. For matrices and vectors of compatible size, we have

$$\text{vec}(\mathbf{ab}^H) = \mathbf{b}^* \otimes \mathbf{a} \quad (1.1)$$

$$(\mathbf{AC}) \otimes (\mathbf{BD}) = (\mathbf{A} \otimes \mathbf{B})(\mathbf{C} \otimes \mathbf{D}) \quad (1.2)$$

$$(\mathbf{a}^H \mathbf{c})(\mathbf{b}^H \mathbf{d}) = (\mathbf{a} \otimes \mathbf{b})^H (\mathbf{c} \otimes \mathbf{d}) \quad (1.3)$$

$$\text{vec}(\mathbf{ABC}) = (\mathbf{C}^T \otimes \mathbf{A})\text{vec}(\mathbf{B}) \quad (1.4)$$

$$\text{vec}(\mathbf{A}\text{diag}(\mathbf{b})\mathbf{C}) = (\mathbf{C}^T \circ \mathbf{A})\mathbf{b} \quad (1.5)$$

We can introduce a lemma that will be useful later:

**Lemma 1.7.1** *Assume  $\mathbf{M}$  invertible, then  $\mathbf{M} \otimes \mathbf{M}$  is invertible, and*

$$(\mathbf{M} \otimes \mathbf{M})^{-1} = \mathbf{M}^{-1} \otimes \mathbf{M}^{-1}.$$

**Proof:** Using Equation (1.2):

$$\begin{aligned} (\mathbf{M}^{-1} \otimes \mathbf{M}^{-1})(\mathbf{M} \otimes \mathbf{M}) &= (\mathbf{M}^{-1}\mathbf{M}) \otimes (\mathbf{M}^{-1}\mathbf{M}) \\ &= \mathbf{I} \otimes \mathbf{I} = \mathbf{I} \end{aligned}$$

Hence  $\mathbf{M}^{-1} \otimes \mathbf{M}^{-1}$  is the inverse of  $\mathbf{M} \otimes \mathbf{M}$ . Note that similarly, we can show that  $\mathbf{M} \otimes \mathbf{M}^*$  is invertible as well.  $\square$



## Chapter 2

# Secondary Surveillance Radar

This chapter describes the general design of the current SSR systems, the differences between mode A/C and mode S replies, the Traffic Advisory and Collision Avoidance System (TACAS), the deficiencies of the current SSR systems, and our proposed design to solve some of these problems.

Additional information on SSR systems, such as the evolution from mode A/C to mode S, the protocols for the request, and the precise meaning of each bit of the messages can be found in [1], on which this chapter is mainly based.

### 2.1 System summary

On the ground a conventional SSR groundstation consists of two rotating antennas mounted on top of each other. The top antenna is an omnidirectional transmit/receive antenna whose radiation pattern is equal for all azimuths, its received output is called the control beam. Below, there is a long rotating transmit/receive antenna, split into two equal parts on each side of the rotating axis. The output of both parts goes into a device called a hybrid ring, which produces a sum and a difference beam, see Figure 2.1. For transmission, only the sum beam is used, while for reception purpose, both beams are used.

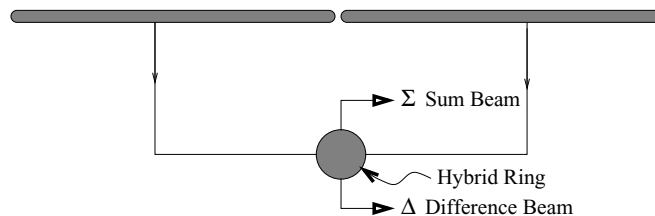


Figure 2.1: *Formation of the sum and difference beams.*

The sum beam is the addition of both sides of the long antenna. This beam has

a narrow main lobe in the boresight direction of the antenna, and some secondary undesired sidelobes. This beam is equal to the resulting beam of the full antenna, and is called the main beam as well. The difference beam is the subtraction of the signals coming from both halves of the long antenna. Its most important property is that in the boresight direction this beam has an amplitude equal to zero and a phase reversal.

Using the sum beam of the rotating long antenna, the ground interrogator sends in the look direction a request modulated by a carrier frequency of 1030 MHz. If there is a plane in this direction, the onboard transponder detects the request and responds to it by a reply containing the desired information modulated by a carrier frequency of 1090 MHz. The use of two different frequencies avoids clutters of the uplink and downlink communications.

In radar systems, one problem is the propagation loss: if the distance between the plane and the radar is  $R$ , a primary radar has a  $R^4$  propagation loss, which corresponds to a factor  $R^2$  for the propagation towards the plane and a factor  $R^2$  for the propagation of the reflection. With the SSR system the reply is emitted by the transponder at the airplane, thus the loss is only proportional to  $R^2$ . This allows for a lower power budget and a better detection.

Since the system is based on active transponders, this request/answer design also avoids typical primary radar problems like false detections from passive elements (raindrops, birds, or mountain reflections). Note that this system needs the cooperation of the airplanes.

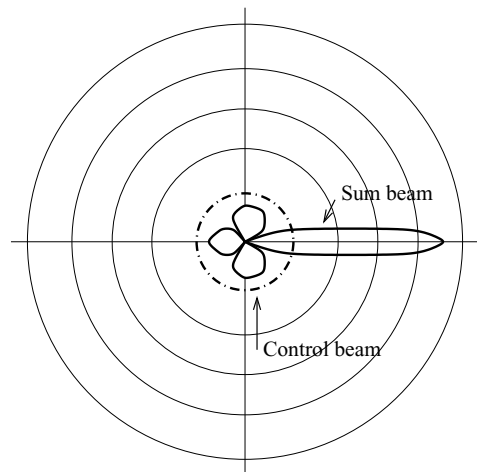


Figure 2.2: *The use of the control beam allows to discard unwanted datalink.*

The control beam is used to avoid errors coming from the sidelobe of the main antenna, see Figure 2.2. During emission, the power of the control beam is weaker than the power of the main lobe of the sum beam, but higher than the power of the secondary lobes of the sum beam. Transponders compare the received powers



of the request and trigger only if they are in the main beam (Interrogator Sidelobe Suppression). Similarly for reception, if the received power in the control beam is larger than the received power in the sum beam, the radar considers that the reply is not in the main lobe of the sum beam, and rejects the detection (Receiver Sidelobe Suppression).

At reception, while the main (sum) beam is very directional, its half beamwidth is still several degrees. This is not sufficient for an accurate measurement of the azimuth and a precise localization of the planes, so additional processing has to be done. Initially, to measure the azimuth the SSR radar used the “sliding window technique”, which takes the average of the boresight angle of the radar between the first and the last received reply in a scan. Nowadays SSR uses a “monopulse technique”, which compares the relative amplitude and phase of the sum and the difference beam. Depending on the result, the groundstation can deduce an accurate azimuth within the main beam.

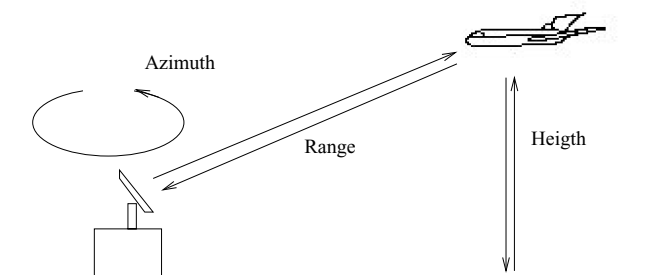


Figure 2.3: *How SSR locates a plane.*

Apart from its datalink capability, SSR can also locate planes, see Figure 2.3. The range between the radar and the plane is measured by the round-trip time, which is the time of propagation plus a time delay for the transponder to answer. This time delay has been specified by the International Civil Aviation Organisation (ICAO) to be  $3\mu s \pm 0.5\mu s$ . The height of the plane is measured by its altimeter, and is sent to the groundstation encoded in a reply (indeed, it is one of the possible requests).

Note that unlike the groundstations, the airborne antennas are small, so these antennas are omnidirectional: the SSR replies go in all directions. Additionally, the transponders emit self-triggered mode S replies to declare their presence. This is called squitter, and its rate is about one per second.

The initial communication protocol used by the SSR is called mode A/C. This protocol allows very little communication, only identity and altitude can be requested. This mode was un-addressed: all planes in the main beam are selected. Because of this non selectivity, all planes in the main lobe of the sum beam answer a reply. In dense regions, the groundstations receive too many replies, and currently the whole system has reached (and passed) its limits.

A new protocol, called mode S where S stands for selective, solves this problem by addressing the requests to specific planes. Only the addressed plane answers, which decreases the density of replies, and the received answer is not garbled by replies of other planes. As a further improvement, mode S enables longer communication messages, which allows also to exchange additional information such as ATC instructions, flight management support, weather forecast, etc... This leads to some automation in air traffic control, and decreases the workload of the controllers and pilots.

However, compatibility between the two modes has to be achieved between zones and planes still using mode A/C and those having mode S. The International Civil Aeronautic Organization (ICAO) proposed to keep the same design with slight modifications. The groundstation processing units must be able to receive and emit both modes. The antennas and the carrier frequencies remain the same. The design of mode S is made such that it acts as a new protocol layer. A clever choice of the pulse positions and powers in the preamble of a mode S request desensitizes mode A/C transponders. So old transponders only answer the mode A/C requests, and ignore the mode S requests. New mode S transponders can reply either mode.

## 2.2 Mode A/C and mode S replies

As the mode A/C and mode S protocols differ, the structure of the replies is also different. We give here a short description of each of them. For more information on the protocol of the request, the reader is relegated to [1].

### 2.2.1 Mode A/C reply message

In mode A/C, the baseband reply message is a frame consisting of 15 pulses with a total duration of  $20.75 \mu\text{s}$ . The pulses are either equal to 1 or 0. The first and the last pulses are called F1 and F2, and are always equal to 1 and limit the boundaries of the reply. The middle pulse, called X, is always equal to 0. The information is encoded on the remaining 12 pulses. Each pulse has a length of  $0.45 \mu\text{s}$  and the spacing between two consecutive pulses is  $1 \mu\text{s}$ , see Figure 2.4.

Depending on whether identity or height is requested, the reply uses all 12 pulses or only 11. For identity requests, 12 pulses provide 4096 different identity numbers to identify the planes. In case of a height request, the 11 used pulses give us 2048 steps of 100 feet.

The shape of a pulse must be within a trapezoid, such that the pulse duration is equal to  $0.8 \pm 0.1 \mu\text{s}$  for the request (and  $0.45 \pm 0.1 \mu\text{s}$  for the answer), the pulse rise time is between 0.05 and  $0.1 \mu\text{s}$ , and the pulse decay time between 0.05 and  $0.2 \mu\text{s}$ . The limitations on rise time and decay time are intended to reduce sideband radiations. The current receivers perform a logarithmic digitization, so a Gaussian pulse meets the requirements (see the DME pulse in Figure 3.1 in [29, p. 28]).

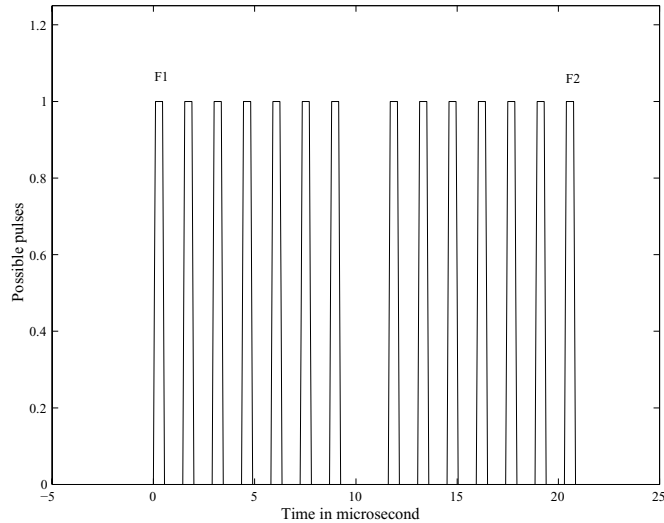


Figure 2.4: Possible pulses for a mode A/C reply.

### 2.2.2 SSR mode S reply

In a mode S reply frame, pulse position modulation is used. The frame starts with a preamble consisting of four pulses. The first four pulses have a duration of  $0.5\mu s$ , and they are placed at 0, 0.5, 3.5, 4.5 $\mu s$  after the beginning of the reply. 8 $\mu s$  after the beginning of the reply begins a 56 or 112-bit binary message. Each bit has a duration of  $1\mu s$ , this time is separated in two periods of  $0.5\mu s$  consisting of a pulse and a non-pulse (the absence of a pulse). A bit equal to 1 is represented by a pulse followed by a non-pulse, and a bit 0 is formed by a non-pulse followed by a pulse. This way of coding is called Manchester encoding and it enables enhanced reception in difficult situations with low Signal to Noise Ratio (SNR). Indeed, the detection of a bit can be done by comparing the respective power of the beginning and the end of the bit time slot.

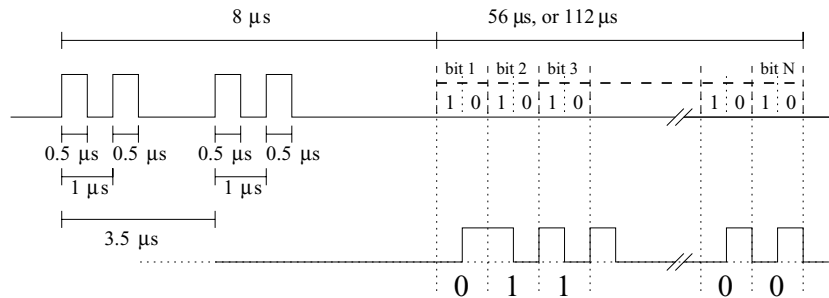


Figure 2.5: Mode S response format.

The precise format of the reply message depends on the type of request that was made: its format matches the format of the request. Although there are 25 possible request and answer messages, only 8 possible exchanges are assigned. The type of request is determined by the first two bits (see [1]).

As for the interrogation, several replies can be linked together to convey a longer message. This is called an Extended Long Message (ELM).

The 56 or 112 bits of information are also coded in order to prevent errors in bit detection. The “parity code” is a modified cyclic redundancy code, which is detailed in [1].

## 2.3 Traffic Advisory and Collision Avoidance System

The TACAS is an airborne system intended for the prevention of a mid-air collision. Instead of creating a whole new system, US engineers conceived to set up an SSR link between two aircraft, with one playing the role of the groundstation. Three versions of this aircraft link exist, from the simplest to the most complete version, see table 2.1. While the power of the inboard equipment to transmit requests is limited to a small range, it still provokes replies from multiple aircraft to be sent in the air.

Version	Description
TACAS I	the system just warns the pilot that a plane is near. The pilot has to locate the hazard visually and decide on the evasive action.
TACAS II	the system also advises the pilot with clues like <i>descend</i> or <i>climb</i> .
TACAS III	the system uses an onboard SSR radar with a directional antenna. The airborne directional antenna allows the plane to have also horizontal angular information on other planes. Because this antenna is much smaller than the ground antenna, the beam width is typically as large as $45^\circ - 90^\circ$ .

Table 2.1: Various evolutions of the TACAS.

The system requires three steps: detection of other planes via an SSR mode A request, track update, and possibly traffic avoidance. The modification is not very simple, because now the transponder should be able to receive and to transmit on both carrier frequencies, 1030 and 1090 MHz.

## 2.4 Problems

This section is organized in chronological order: the well-known problems of SSR mode A/C, and the foreseen problems of SSR mode S.

### 2.4.1 Well-known mode A/C problems

The following list presents the main problems of mode A/C.

- **Garbling:** at least two replies overlap in time at the reception. It may mean that two (or more) transponders have near azimuths and time of arrival within the time duration of the reply. The planes might be at a similar range and direction from the groundstation, however, the height of the aircrafts can be different, and the two planes do not necessarily risk to collide.
- **FRUIT:** False Replies Unsynchronized In Time. This occurs when planes answer to other interrogators, which can be either a groundstation, or the TACAS system of another plane. Since the receiving antenna of the plane is not directional, the transponder answers to all received requests from all interrogators. In turn, the groundstation will receive messages that were not requested by itself. Those answers have random time of arrival and thus indicate random ranges. Based on this property, they are easy to suppress. If FRUIT occurs while a desired answer reaches the groundstation antenna, it leads to a garbling problem.
- **Multipath:** several propagation paths with significant amplitude are present between the plane and the groundstation antenna. Depending on the antenna beam width and the time duration of the response, three categories of non-direct paths may appear:
  1. Non-direct paths with no azimuth angle difference to the line of sight; these are produced by ground reflections on the line of sight. They either have a long time delay (produced far from the antenna, and easy to discard) or they have a short time delay. The last case, more difficult, is caused by ground reflections nearby the antenna, since the antenna has some height above the ground. For the sake of simplicity, let us assume the presence of two paths, a direct one and one produced by the ground reflection. Depending on the time delay and the gain of the ground-reflection, the combination of both paths give rise to interferences like slits of Young. The main consequence is the modification of the antenna elevation pattern and the possible creation of nulls in this pattern. The usual countermeasure is to avoid ground paths. This can be done by installing a rough scattering surface near the antenna, or by using a metallic screen around the antenna, or by using a Large Vertical Aperture antenna (LVA), which nulls the antenna pattern below the horizon.

2. Non-direct paths with small azimuth angle. These can arise when the ground around the groundstation has a slope. Depending on the time delay, it may be quite troublesome to solve.
3. Non-direct paths with large azimuth angle. These do not cause problems: they are quite useful to detect and identify the reflecting objects, see [30].

Typically, the request is sent between 8 and 12 times in a scan, so the usual way to solve a failure in receiving a reply is to listen to the next reply. This can be done only depending on the plane density around the groundstation. In some regions, the mode A/C protocol was overloaded, and an evolution of the system became mandatory.

### 2.4.2 Foreseen mode S problems

The mode S protocol relies on the addressing of the requests to the aircrafts, and on the parity code to correct the received replies. Only one exchange will be necessary where up to 15 could have happened before, thus mode S will decrease the density of replies received, and thus reduce the FRUIT problem. But, the multi-path problem remains unchanged. To conclude, mode S will increase the reliability of the link. However, new problems will appear.

With the rotating transmitter antenna, the dwell time during which the aircraft is illuminated is quite limited, 30 ms, and the time between two scans is quite long, several seconds. For mode A/C links, this time is sufficient to exchange up to 15 data frames between the groundstation and the airplane, so that the required information by the groundstation is obtained. But due to the format of the mode S protocol, the duration of a reply is much longer, and only one or two exchanges are possible within a scan. In the case of difficult situations or for ELM, the system is forced to rely on different scans. This is unacceptable because the total transaction time is then too long, and there is a high access delay.

Furthermore, it is expected that due to the increase in air traffic, the proposed mode S system will not be able to cope with future traffic loads, at least in areas with a dense concentration of planes.

Since there will be less exchanges, it is also expected that the azimuth estimation will be less accurate.

## 2.5 A distributed groundstation network

The natural solution to cope with the expected problems with SSR system is to decouple the emitting and the receiving role at the groundstation. The novel idea is to also decouple the emitting and receiving locations, and to have several receivers. Recall Figure 1.1 and Figure 1.2. Once a request has been sent, at least one groundstation in the receiving network will receive the reply. If several groundstations receive the reply, it is possible to obtain an improved estimate of the aircraft position. Since the receiving groundstations are not placed at the same location

as the emitting station, they receive replies from a large range of directions. Thus the choice of an array of antenna elements is natural, since such arrays allow the estimation of directions and separation of source signals by electronic beamforming.

Our proposed distributed system will also introduce some specific problems. Although the number of desired replies will reduce, the use of an array of omnidirectional antennas will increase the total number of received replies, for two reasons:

- Because of multipath propagation, each SSR reply is received over a direct path, and/or a number of secondary paths. These reflections are avoided in the current SSR system because of the narrow beam and with the help of the control beam. With an array of omni-directional elements, this will no longer be possible; the elements will receive the replies from the line of sight as well as from the secondary paths, see Figure 2.6.

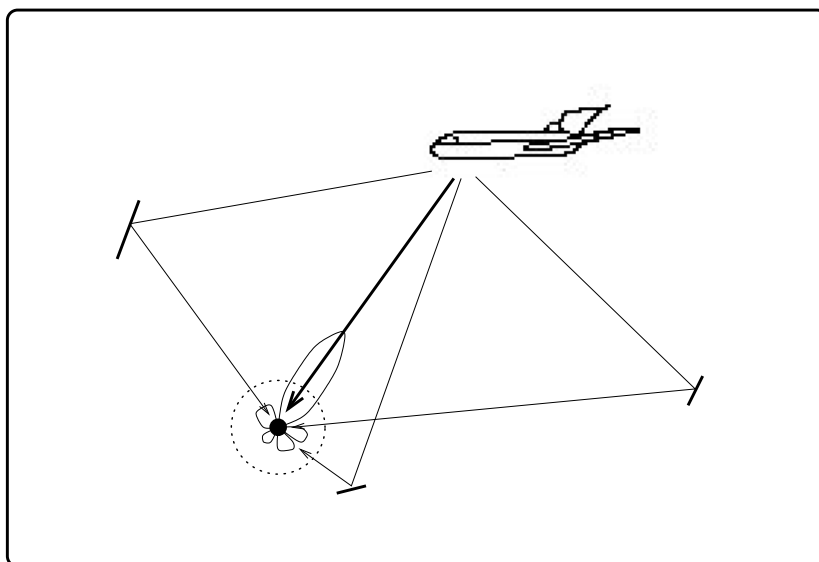


Figure 2.6: An array antenna is more sensitive to multipath than the current system which uses a control beam.

- Due to the omnidirectionality of the elements of the array, the groundstation will receive many more undesired replies: the TACAS replies, the replies triggered by adjacent groundstations, and the squitters (self-triggered replies by the transponder). This leads again to the well-known problem of FRUIT.

It appears that the distributed ground-system will increase the number of replies, desired or FRUIT, which can cause garbling problems. This motivates the use of array signal processing to separate the source signals and estimate their directions.

## 2.6 Conclusion

In this chapter, we explained the principles of the SSR system. We have shown the differences between the replies from both modes. The system limitation was shown, and the need of a new system demonstrated. The chapter also pointed out the possible origins of the replies impinging on a distributed groundstation: the desired replies, the self-triggered replies, and the replies triggered by nearby groundstations or by TACAS.

The last section has shown that the number of instantaneously received replies is expected to increase with the distributed system, and it might appear that the situation is degrading. In fact, it motivates the use of adaptive beamforming, since an array with  $M$  elements can be combined to result in  $M$  spatially very selective antennas.

We can state here the objective of the thesis: with the use of array signal processing, we desire to separate reply signals from different users, partially overlapping in time and frequency. And for each signal, we want to estimate the transmitted symbol and the parameters: DOA and frequency shift.

Further, to obtain estimation performance bounds, we wish to establish identifiability (*i.e.* the fact that the parameters can be uniquely estimated) and to verify the efficacy of the algorithms on simulated and actual data.



## Chapter 3

# Data model, and state of the art

In the end of the previous chapter, we have defined the problem under investigation in this thesis. In the present chapter, we will construct a model of the signal received at the antenna array and identify its properties. This forms the basis of the separation algorithms constructed in subsequent chapters.

The first section presents a model of the received signal due to several SSR replies impinging on a ground array antenna, and is concluded by a summary of the key properties of the model. In the second section, the statistical properties of the sources are analyzed, which leads to the concept of a “pseudo-Gaussian” source, and we connect this to Higher-Order Statistics (HOS) methods. The last section is an overview of several relevant existing algorithms which perform source separation.

### 3.1 Data Model

#### 3.1.1 The emitted replies

We start our data modeling by looking at the emitted data stream before up-conversion, first for mode A/C replies, then for mode S replies.

##### Mode A/C reply frame

Let  $b_n$  be a bit taken from the alphabet  $\{0,1\}$ . A sequence of 12 such bits is the variable data in the reply frame that forms the answer to the request of the transmitting groundstation. We also define  $p_{A/C}(t)$  to be the pulse shape function of the mode A/C pulse which, according to the ICAO, has to satisfy the following conditions, see [29]:

Time ( $\mu s$ )	$t \leq 0$	$0.1 \leq t \leq 0.45$	$t \geq 0.55$
$p_{A/C}(t)$	0	1	0

where we note that the nominal duration of a pulse is  $0.5\mu s$ . The pulse shape is not totally determined by the standard: only the rise and decay times are bounded. Thus, the pulse shape can be different for each transponder. In current practice this is not a problem, since actual groundstations use logarithmic amplifiers and do not perform matched filtering.

The emitted data stream,  $\tilde{\mathbf{b}}$ , contains the 12 data bits  $b_i$  extended by 3 fixed bits,

$$\tilde{\mathbf{b}} = [\tilde{b}_0, \dots, \tilde{b}_{15}] \stackrel{\text{def}}{=} [1, b_1, \dots, b_6, 0, b_7, \dots, b_{12}, 1].$$

The emitted signal is a pulse amplitude modulation (PAM) of the data stream, using the pulse shape function  $p_{A/C}(t)$ . The transponder emits the mode A/C data-stream:

$$b_{A/C}(t) = \sum_{n=0}^{15} \tilde{\mathbf{b}}(n) \cdot p_{A/C}(t - nT_{A/C}) \quad (3.1)$$

where  $\tilde{\mathbf{b}}(n)$  is the  $n$ -th entry of  $\tilde{\mathbf{b}}$ , and  $T_{A/C} = 1.45\mu s$  is the mode A/C period.

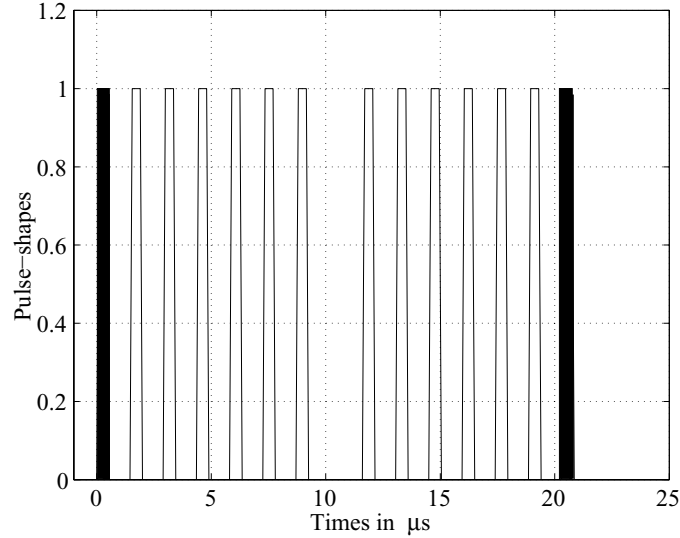


Figure 3.1: *Format of a mode A/C reply frame.*

### Mode S reply frame

Let  $p_S(t)$  be the pulse shape of mode S. According to the ICAO requirements, it must satisfy the following constraints:

Time ( $\mu s$ )	$t \leq 0$	$0.1 \leq t \leq 0.5$	$t > 0.6$
$p_S(t)$	0	1	0

Here again, the standard does not totally enforce the pulse-shape. As before, we denote by  $b_n \in \{0, 1\}$  one of the transmitted bits. For Mode S, the reply frame contains either 56 or 112 bits. The bits are encoded in a ‘‘Manchester Encoding’’ scheme, which means that a bit  $b_n = 0$  is coded as  $\mathbf{b}_n = [0, 1]$ , and a bit  $b_n = 1$  as  $\mathbf{b}_n = [1, 0]$ . The emitted bit stream,  $\tilde{\mathbf{b}}$  consists of a preamble followed by the encoded data bits,

$$\tilde{\mathbf{b}} = [1, 0, 1, 0, 0, 0, 0, 1, 0, 1, 0, 0, 0, 0, 0, 0, 0, \mathbf{b}_1, \mathbf{b}_2, \dots, \mathbf{b}_{56/112}]$$

The preamble is aimed to facilitate the synchronization (detection of the start of a frame).

The Mode S reply signal emitted by the transponder is a pulse amplitude modulation of  $\tilde{\mathbf{b}}$ , and has the form

$$b_S(t) = \sum_{n=0}^{127/239} \tilde{\mathbf{b}}(n) p_S(t - \frac{1}{2}nT_S) \quad (3.2)$$

where  $\tilde{\mathbf{b}}(n)$  is the  $n$ -th entry of  $\tilde{\mathbf{b}}$ , and  $T_S = 1 \mu s$  is the Mode S period.

### Temporal properties

The format of both Mode A/C and Mode S is such that it satisfies interesting temporal correlation properties which are deterministic and independent of the actual transmitted data. For example, note from Figure 3.1 that for any time  $t$ , the product of the data stream and the data stream delayed by half a mode A/C bit-period is equal to zero:

$$b_{A/C}(t) b_{A/C}(t + \frac{1}{2}T_{A/C}) = 0 \quad (3.3)$$

We additionally assume that  $p_S(t) = 0$  for  $t \geq 0.5$ . Then for Mode S, a similar relation holds due to the Manchester encoding, in case the receiver is synchronized. In this case, the product of the data stream with a  $\frac{1}{2}T_S$ -delayed version of itself will always be equal to zero. Otherwise, when unsynchronized, we can still multiply by an additional delayed version, so that we are sure that one of the sub-multiplications is zero.

We summarize the relations in the following proposition.

**Property 3.1.1** *Independent of the transmitted data, a mode A/C transmitted reply signal  $b_C(t)$  satisfies*

$$b_{A/C}(t) b_{A/C}(t + \frac{1}{2}T_{A/C}) = 0, \quad \forall t \in \mathbb{R} \quad (3.4)$$

where  $T_{A/C} = 1.45 \mu s$ .

*Independent of the transmitted data, a mode S reply signal  $b_S(t)$  obeys:*

$$b_S(t) b_S(t + \frac{1}{2}T_S) = 0, \quad t \in \{0, \frac{1}{2}T_S\} + nT_S, n = 0, 1, \dots \quad (3.5)$$

where  $T_S = 1 \mu s$ . More generally,  $b_S(t)$  satisfies

$$b_S(t - \frac{1}{2}T_S) b_S(t) b_S(t + \frac{1}{2}T_S) = 0, \quad \forall t \in \mathbb{R} \quad (3.6)$$

In the remainder of this section, it is not necessary to make a distinction between Mode A/C and Mode S, hence for the sake of simplicity, let  $b(t)$  be either  $b_{A/C}(t)$  or  $b_S(t)$ .

Before being emitted by the antenna, the signal is up-converted to the frequency band  $f_e$ :

$$z(t) = b(t) \cdot \cos(2\pi f_e t)$$

where we neglect the initial phase. The ICAO requires the transponder to emit at nominally the carrier frequency  $f_c = 1090$  MHz, but allows the transponders to have a carrier frequency shift up to  $\pm 3$  MHz, thus,  $f_e \neq f_c$ . In future, this limit should be reduced to  $\pm 1$  MHz.

Due to this frequency carrier mis-match, a residual frequency  $f$  remains after down-conversion by  $f_c$  to baseband. This residual carrier causes significant phase rotations of the symbols (see figure 3.2). Additionally, it hides the Doppler effect due to the radial speed of the aircraft.

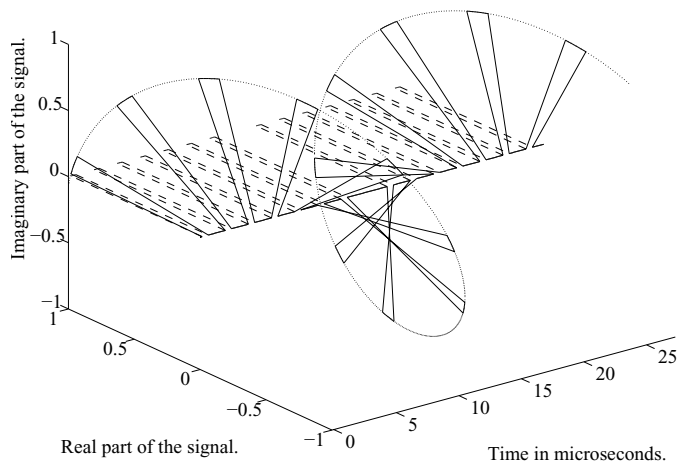


Figure 3.2: *Influence of the carrier frequency shift (50 kHz) on a mode A/C reply. The dashed line is  $b(t)$ , the original reply signal. The residual carrier causes a rotation of  $b(t)$  in the complex plane as a function of time.*

### 3.1.2 Received data model

We will now present complex baseband model for the received signal, as valid after downconversion and sampling. As the derivation of such models is rather standard in the Signal Processing literature (see e.g. [8, 9, 18, 19, 21, 20]), we do not show

the constructing steps. The construction of the model is valid under the following assumptions, which we make from now on:

- As the bandwidth of the signal is  $BW \approx 10$  MHz, and the frequency carrier is  $f_c = 1090$  MHz, we admit a narrow-band assumption, *i.e.*  $BW \ll f_c$ . Consequently, short delays (e.g. propagation delays across the array) are modeled as baseband phase shifts.
- As the array has a size in the order of a few decimeters, and that the airplanes are over a kilometer far away, we admit the far-field assumption: the incoming signal has a planar wavefront.
- As the noise mainly originates from the thermal noise of the receiver, but also from atmospheric sources, we assume that the noise vector is spatially white, and that its entries are Gaussian, independent identically distributed (i.i.d.) with equal variances  $\sigma^2$ .
- We also assume that we know  $\sigma^2$ ; this is reasonable because of the bursty nature of a reply, so that there are many time periods without any signal during which we can estimate the noise variance.
- For simplicity, we assume that the array is a calibrated Uniform Linear Array (ULA), *i.e.* all sensor have an equal behavior, and they are placed in a line at equal distance one from the consecutive other.

At reception, we consider that during a time interval of interest there are  $d$  single-path replies impinging on a  $M$ -element antenna array. We consider the data as a stream of bits and we do not consider synchronization problems. We consider that outside the packet frame, the emitted bit stream is zero, which can be modeled as well by a modulation of bits with value 0. It allows us to not consider time delays between the sources, and to consider all impinging sources present on the full interval as a zero-padded version of the original packets.

For the sake of simplicity, we propose a model **only for mode S** replies, with a sampling period  $T$ . This choice is motivated by the fact that mode S transponders will be mandatory in the future, and by the complexity to handle a combined model that contains both mode A/C and mode S. Due to different (incommensurate) pulse lengths, this would be untractable in the following chapters. Unless specified otherwise, the sampling period is  $T = 0.5 \mu\text{s}$ .

After propagation, reception by the array, and baseband demodulation, the analog signal  $\mathbf{x}(t)$  is sampled and digitized by an Analog-to-Digital Converter (ADC). We denote the digital signal:  $\mathbf{x}[n] \stackrel{\text{def}}{=} \mathbf{x}(nT)$ . After collecting  $N$  samples, we can construct the  $M \times N$  received signal matrix  $\mathbf{X} = [\mathbf{x}[1], \dots, \mathbf{x}[N]]$ . Then we pose the following model for  $\mathbf{X}$ :

$$\mathbf{X} = \mathbf{A} \cdot \mathbf{G} \cdot [\mathbf{F} \odot \mathbf{B}] + \mathbf{N} \quad (3.7)$$

where

- $d$  is the number of sources.

- $\mathbf{A} = [\mathbf{a}(\theta_1), \dots, \mathbf{a}(\theta_d)]$  is the  $M \times d$  steering matrix, with  $\forall i \in \{1, \dots, d\}$  the steering vector defined as

$$\mathbf{a}(\theta_i) = [1, \exp(j\pi \cos(\theta_i)), \dots, \exp(j\pi(M-1)\cos(\theta_i))]^T, \quad (3.8)$$

where  $\theta_i$  is the direction of incidence of the  $i$ -th source with respect to the ULA boresight.

- $\mathbf{G}$  is a  $d \times d$  diagonal gain matrix, with diagonal entries  $g_i = \rho_i \exp(j\psi_i)$   $\forall i \in \{1, \dots, d\}$ , where  $g_i$  is the gain of the  $i$ -th source,  $\rho_i > 0$  its amplitude and  $\psi_i \in [0, 2\pi)$  its phase.
- $\mathbf{F} = [\mathbf{f}_1^T, \dots, \mathbf{f}_d^T]^T$  is a  $d \times N$  matrix, whose  $i$ -th row is  $\mathbf{f}_i = [1, \phi_i, \dots, \phi_i^{N-1}]$  where  $\phi_i = \exp(2\pi j f_i T)$ .  $\mathbf{F}$  is a Vandermonde matrix, which represents the effects of the residual carrier frequencies. We assume  $f_i \in [0, 1/T)$ .
- $\mathbf{B} = [\mathbf{b}[1], \dots, \mathbf{b}[N]]$  is the  $d \times N$  transmitted symbol matrix, whose  $n$ -th column is  $\mathbf{b}[n] = [b_1[n], \dots, b_d[n]]^T$ , where  $b_i[n]$  is the  $n$ -th symbol of the  $i$ -th source. We assume that all  $b_i[n]$  belong to the alphabet  $\{0, 1\}$ .
- $\odot$  the Schur-Hadamard element-wise matrix multiplication.
- $\mathbf{N} = [\mathbf{n}[1] \dots \mathbf{n}[N]]$  is the  $M \times N$  noise matrix, with  $\mathbf{n}[k] \sim \mathcal{CN}(0, \sigma^2 \mathbf{I})$ .

We can also write Equation (3.7) as:

$$\mathbf{X} = \mathbf{A} \cdot \mathbf{G} \cdot \mathbf{S} + \mathbf{N} \quad (3.9)$$

where for simplicity of notation  $\mathbf{S} \stackrel{\text{def}}{=} \mathbf{F} \odot \mathbf{B}$  is the  $d \times N$  source matrix. This equation will be our basic data model throughout the thesis.

Note that the element of the matrix  $\mathbf{S}$  for the  $i$ -th source at integer time  $n$  is equal to:

$$(\mathbf{S})_{i,n} = s_i[n] = b_i[n] \exp(2\pi j n f_i T) \quad (3.10)$$

with  $b_i[n] \in \{0, 1\}$ . From this equation, we can extract the following properties:

**Property 3.1.2** Consider an SSR source  $s[n]$  of the form (3.10).

Static property:  $s[n]$  is a Zero-Constant Modulus (ZCM) source: the source is either zero or of unit norm, i.e.,

$$s[n] = 0 \quad \text{or} \quad |s[n]| = 1, \quad \forall n \in \{1, \dots, N\}$$

This is equivalent to:

$$s[n]s^*[n]s[n] = s[n] \quad (3.11)$$

Dynamic property: For any integer  $k$ , two non-zero samples with a distance of  $\tau = kT$  have a phase difference of  $\phi^k$ , where  $\phi = \exp(2\pi j f T)$ . Consequently,

$$s[n]s^*[n-k] = 0 \quad \text{or} \quad s[n]s^*[n-k] = \phi^k, \quad \forall n \in \{k+1, \dots, N\}. \quad (3.12)$$

Combining the two properties, we obtain the relation:

$$s[n]s^*[n-k]s[n]s^*[n-k] = \phi^k s[n]s^*[n-k], \quad \forall n \in \{k+1, \dots, N\}. \quad (3.13)$$

### 3.1.3 Multipath

The aircraft replies are emitted by means of an omnidirectional antenna. There is always a Line Of Sight (LOS), but depending on the presence or absence of reflecting objects, other paths may exist. In order to simplify this work, we consider only two kinds of secondary paths.

The first type of secondary paths are reflections originated by the ground near the antenna, and have the same direction of arrival. Usually, these reflections are limited by the use of antennas with a large vertical aperture, or by a metallic screen. However, in the experiments conducted at Delft University of Technology, we have used simple dipole antennas for the array, so ground reflections probably occurred. This does not change the data model too much because the time delay between the LOS and the ground reflection signal is much below the inverse of the bandwidth of the replies. So the delay may be represented by a phase shift of the complex baseband signal, *i.e.* the signal due to the second path is a copy of the direct signal multiplied by a complex gain factor dependent on the time delay and the ground reflection coefficient. Both gains can be combined into a factor that alters the received power  $g$  of the reply. While the data model remains the same, the practical consequence is that the final gain can be smaller than the noise or even equal to zero, resulting in the problem that the reply cannot be detected. Let us consider this gain for all the elements. In general, the antenna response will be the sum of the LOS path and the reflected path:

$$\mathbf{a}_{\text{Total}} = g_{\text{LOS}}\mathbf{a}(\theta_{\text{LOS}}) + g_{\text{Ref}}\mathbf{a}(\theta_{\text{Ref}})$$

where the resulting  $\mathbf{a}_{\text{Total}}$  in general does not belong to the array manifold. However, since we are considering a ground reflection, both angles are equal, and  $\mathbf{a}_{\text{Total}} = (g_{\text{LOS}} + g_{\text{Ref}})\mathbf{a}(\theta_{\text{LOS}})$ . Consequently, all antennas fade at the same time. If not in a fade, the estimation of  $\theta_{\text{LOS}}$  is still possible.

Other secondary paths are created by surfaces far from the antenna and are not in the direction of the LOS. They usually show a time delay of several bits, so the matrix  $\mathbf{S}$  is full rank. The secondary paths also have different angles of arrival than the LOS path. Therefore we can consider the two replies as independent signals.

## 3.2 Statistical properties of the SSR source

Our objective in the next chapters will be, given a data matrix  $\mathbf{X}$  of size  $M \times N$ , with  $N$  sufficiently large, to estimate  $d$  and separate the  $d$  source signals  $b_i[n]$ , and the source parameters  $\{f_i, \theta_i\}$ . The separation can be based on deterministic and statistical properties of the sources. Some algorithms use the dynamic properties of the signals, so it is interesting to see if we can adapt these algorithms to the SSR problem.

To simplify the study, we consider a single mode S reply. We consider the model:

$$s[n] = b[n] \exp(2\pi j f T n) = b[n] \phi^n, \quad n = \{1, \dots, N\}$$

where  $T$  is the sampling period,  $f$  the residual frequency,  $\phi = \exp(2\pi j f T)$ , and  $b[n] \in \{0, 1\}$  the bit emitted at time  $n$ . We consider the residual frequency as

an unknown deterministic quantity, rather than as a random variable. We assume that we are synchronised so that the start of the packet is known, without loss of generality it starts at  $n = 1$ . The random part of the signals are the data bits, with values in  $\{0, 1\}$  with equal probability.

Because of the temporal structure of the SSR reply frame, the signal  $s[n]$  is not stationary and we do not use the usual ergodic assumption. At some times  $n$ , the expected value  $E\{b[n]\}$  is zero, at other time instants it is  $\frac{1}{2}$  or 1, multiplied by the residual frequency factor. We first decompose  $b[n]$  for each  $n$  into an expected value and a zero-mean deviation:

$$b[n] = e[n] + a[n]$$

where  $e[n] \stackrel{\text{def}}{=} E\{b[n]\}$  represents the expected value at time  $n$  of the binary signal: it is a constant and zero-padded after expectation.  $a[n]$  represents the random part with  $E\{a[n]\} = 0$ . Figure 3.3 illustrates  $e[n]$  for each kind of SSR mode S.

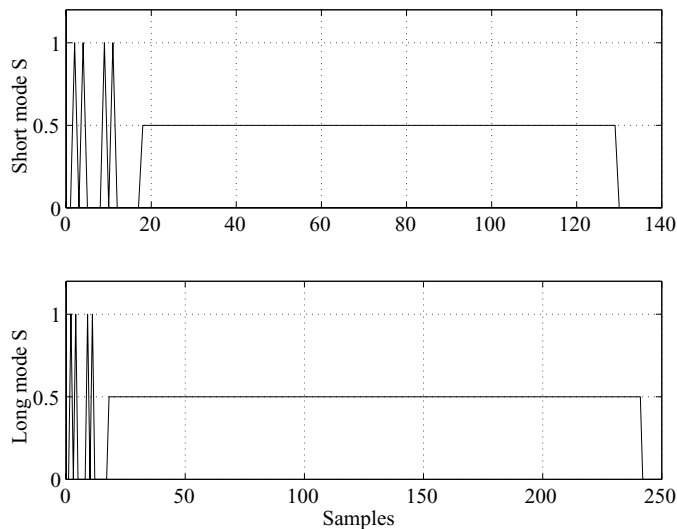


Figure 3.3: The expected value  $e[n]$  of the binary signal  $b[n]$  as a function of times, presented for all modes S.

Note that for certain (known) times  $n$  in a data frame,  $a[n]$  is not random and equal to 0, whereas for other times  $n$ ,  $a[n]$  is random and takes values on the alphabet  $\{\pm\frac{1}{2}\}$ . We define  $T_{\text{det}}$  to be the set of time instants for which  $a[n]$  is not random, and  $T_{\text{rand}}$  to be the time instants for which  $a[n]$  is random. Let  $L$  be the number of independent pulses (the size of  $T_{\text{rand}}$ ). The random elements  $a[n]$  have for  $n \in T_{\text{rand}}$ , the following properties:

$$E\{a[n]\} = 0$$



and

$$\mathbb{E}\{a[n]a[m]\} = \begin{cases} \frac{1}{4} & , \quad m = n \\ -\frac{1}{8} & , \quad m = n \pm 1 \\ 0 & , \quad \text{otherwise} \end{cases} \quad (3.14)$$

The second result of Equation (3.14) is a consequence of the manchester encoding.

Now that we have defined our model and some properties, we consider a non-stationary auto-correlation. First define the un-normalized estimated auto-correlation:

$$\hat{\gamma}[\tau] \stackrel{\text{def}}{=} \sum_{n=1}^{N-\tau} s^*[n]s[n-\tau]$$

then define:

$$\gamma[\tau] \stackrel{\text{def}}{=} \mathbb{E}\{\hat{\gamma}[\tau]\}$$

We obtain after some derivations:

$$\gamma[\tau] = \exp(-2\pi j f T \tau) \left[ \sum_{n=1}^{N-\tau} e^*[n]e[n-\tau] + \frac{L}{8} (2\delta[\tau] - \delta[\tau+1] - \delta[\tau-1]) \right] \quad (3.15)$$

where  $\delta[t]$  is the Kronecker delta, and  $L$  is the number of pulses, 64 or 112 for mode S replies.

Equation (3.15) shows that the auto-correlation is a function depending only on the mode of the source, modulated by exactly the same residual frequency as the source:

$$\gamma[\tau] = \gamma_0[\tau]\phi^{-\tau}$$

where the function  $\gamma_0[\tau]$  depends only on the mode of the reply.

Figure 3.4 presents the auto-correlation  $\gamma_0[\tau]$  for each kind of SSR reply: short mode S, and long mode S. We note that they have a pseudo triangular shape, except for the first 16 samples in the beginning.

### Consequences

To summarize, we consider a single mode S SSR reply, with a residual carrier  $f$ , for which  $\phi = \exp(2\pi j f T)$  where  $T$  is the sampling period. Then the next property holds:

**Property 3.2.1** *For a Mode S SSR reply  $s[n]$ , if  $16 < \tau < T_L - 16$  then  $\gamma[\tau]$  simplifies such that:*

$$\gamma[\tau] = \frac{1}{4}(T_L - \tau)\phi^\tau \quad (3.16)$$

where  $T_L$  is the data length of the data frame (128 or 240 samples). If  $16 < \tau \ll T_L$ , then Equation 3.16 can be further approximated as:

$$\gamma[\tau] = K\phi^\tau \quad (3.17)$$

where the constant  $K$  is equal to  $\frac{T_L}{4}$ .

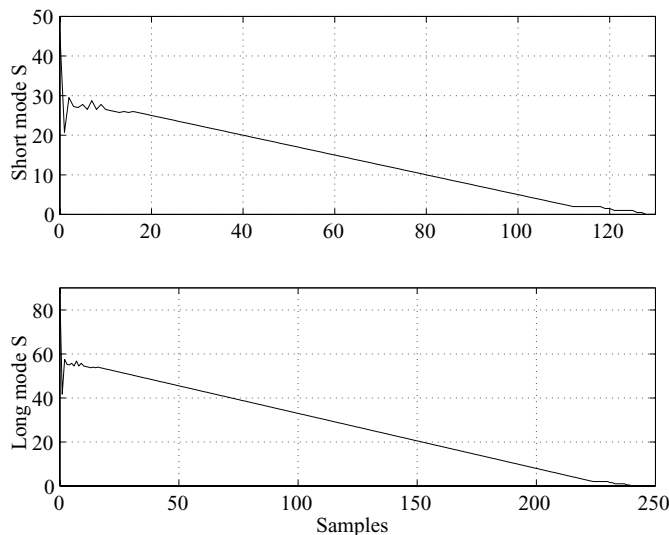


Figure 3.4: Expected auto-correlation  $\gamma_0[\tau]$  of a reply without frequency shift for each mode: short  $S$ , and long  $S$ .

**Mode A/C:** a similar property can be derived for mode A/C. However, the properties cannot easily be combined: one has to take care about the pulse period which is not the same as for mode  $S$ , and the specific encoding for this mode. Since in future chapters we focus mostly on algorithms for mode  $S$ , we omit the corresponding properties for mode A/C.

### 3.3 Algorithmic survey

We present a short survey of the source separation methods which are the most relevant to the principles of the algorithms proposed in the thesis.

First, we recall the difference between a Minimum Mean Square Error (MMSE) beamformer, and a Zero-Forcing (ZF) one. Second, we present an example of a source separation algorithm which is based on spatial properties, *i.e.*, it only uses the knowledge of antenna array, but not of the source structure. The algorithm we choose to present is ESPRIT, because it is an algebraic method that relies on a low rank decomposition of the covariance matrix, and in that sense similar to our approach in future sections. Third, we present several algorithms that use the signal properties. The signal property used in an algorithm can be either quite general or oppositely very specific. Among the specific algorithms, we present the Decision-Directed Beamformer, the ILSP/E algorithm, the ACMA, and the ACPA, which all depend on the constellation or the modulus of the signal. For a more general scheme, we present SOBI, which depend only on statistical independence of the sources. Note that these more general schemes rely on the estimation of certain

statistical moments from the data, and in general require many data samples.

### 3.3.1 MMSE and ZF approach

Consider the linear data model

$$\mathbf{X} = \mathbf{M}\mathbf{S} + \mathbf{N}$$

Note that  $\mathbf{M} = \mathbf{A}\mathbf{G}$  in this thesis, but it can be more general. Note also that we consider  $\mathbf{M}$  tall or square. There are many ways to recover the data matrix  $\mathbf{S}$ , depending on knowledge of  $\mathbf{M}$  or its structure, and knowledge of the structure of  $\mathbf{S}$ . We consider here a linear transformation of the form:

$$\hat{\mathbf{S}} = \mathbf{W}^H \mathbf{X}$$

$\mathbf{W}$  is the beamforming matrix, the  $i$ -th column  $\mathbf{w}_i$  of  $\mathbf{W}$  is a beamformer to receive the  $i$ -th source (row of  $\mathbf{S}$ ). In the presence of noise, we can think of several optimization criteria to obtain the “best” beamformer. Two criteria are commonly used, one to minimize the output noise, the other to reduce the model error.

In the latter case, the cost function to minimize is:

$$\{\mathbf{M}, \mathbf{S}\} = \arg \min_{\mathbf{M}, \mathbf{S}} \|\mathbf{X} - \mathbf{M}\mathbf{S}\|_F^2 \quad (3.18)$$

Without further constraints on  $\mathbf{S}$ , we optimize the cost function keeping  $\mathbf{M}$  constant (or assuming it is known):

$$\hat{\mathbf{S}} = (\mathbf{M}^H \mathbf{M})^{-1} \mathbf{M}^H \mathbf{X} = \mathbf{M}^\dagger \mathbf{X}$$

so the corresponding beamformer is:  $\mathbf{W}^H = \mathbf{M}^\dagger$ , and the solution is:

$$\hat{\mathbf{S}} = \mathbf{M}^\dagger \mathbf{X} = \mathbf{S} + (\mathbf{M}^H \mathbf{M})^{-1} \mathbf{M}^H \mathbf{N}$$

From this result, one can see that each signal is recovered interference-free. The name of the corresponding beamformer is Zero-Forcing, ZF. It yields the best Signal to Interference Ratio, SIR<sup>1</sup>, but unfortunately it might amplify the output noise in case  $\mathbf{M}$  is ill conditioned, thus its output Signal to Noise Ratio, SNR, might be poor. The Signal to Interference and Noise Ratio, SINR, will be equal to SNR.

A second criterion aims at obtaining the lowest output noise after processing. Consider a collection of  $d$  vectors  $\mathbf{w}_i$  such that  $\mathbf{w}_i^H \mathbf{x} = \hat{s}_i$ . Let us stack them in a matrix  $\mathbf{W} = [\mathbf{w}_1, \dots, \mathbf{w}_d]$ , such that  $\hat{\mathbf{S}} = \mathbf{W}^H \mathbf{X}$ , then the criterion to minimize is:

$$\{\hat{\mathbf{W}}, \hat{\mathbf{S}}\} = \arg \min_{\hat{\mathbf{W}}, \hat{\mathbf{S}}} \|\mathbf{S} - \hat{\mathbf{W}}^H \mathbf{X}\|_F^2$$

Keeping  $\mathbf{S}$  constant (or with a known  $\mathbf{S}$ ), we optimize the cost function, and we obtain:

$$\mathbf{W} = (\mathbf{X}\mathbf{X}^H)^{-1} \mathbf{X}\mathbf{S}^H$$

---

<sup>1</sup>In fact the SIR will be infinite in that case.

Note that the first matrix is proportional to the sample covariance matrix:  $\hat{\mathbf{R}}_x \stackrel{\text{def}}{=} \frac{1}{N} \sum_{n=1}^N \mathbf{x}[n] \mathbf{x}^H[n]$ , and the second to  $\hat{\mathbf{R}}_{xs} \stackrel{\text{def}}{=} \frac{1}{N} \sum_{n=1}^N \mathbf{x}[n] \mathbf{s}^H[n]$ . It can be written as  $\mathbf{W} = \hat{\mathbf{R}}_x^{-1} \hat{\mathbf{R}}_{xs}$ . For an infinite number of samples, it tends to  $\mathbf{W} = \mathbf{R}_x^{-1} \mathbf{M}$ . Alternatively, if we know  $\mathbf{M}$  and the sources are uncorrelated, then the optimum beamformer is  $\mathbf{W} = \hat{\mathbf{R}}_x^{-1} \mathbf{M}$ . A beamformer defined in this way will minimize the output noise and the interference, thus it yields the best SINR. This is why it is called the Minimum Mean Square Error beamformer (MMSE).

We define the output Signal to Noise Ratio of a beamformer as the ratio of the output power of the desired source over the power of the output noise. Similarly, the Signal to Interference and Noise Ratio is the ratio of the output power of the desired source over the sum of the output powers of the other sources and the noise. In general, one can say that

$$\begin{aligned} \text{SINR}(\text{MMSE}) &\geq \text{SINR}(\text{ZF}) \\ \text{SIR}(\text{MMSE}) &\leq \text{SIR}(\text{ZF}) \end{aligned}$$

If the mixing matrix  $\mathbf{M}$  is known, tall and full column rank, then the ZF reconstruction of the sources is obtained by the application by the pseudo inverse of  $\mathbf{M}$ , and the SIR is infinite.

### 3.3.2 ESPRIT

Several beamforming and source separation techniques assume that the mixing matrix has the form  $\mathbf{M} = \mathbf{A}\mathbf{G}$ , where  $\mathbf{A}$  is known parametrically as  $\mathbf{A} = [\mathbf{a}(\theta_1), \dots, \mathbf{a}(\theta_d)]$ , and  $\mathbf{G}$  is a diagonal matrix containing the gains of the sources. Classical methods used the sample covariance matrix of  $\mathbf{X}$  directly, as for example the Bartlett method [31], the Minimum Variance Distortionless Response (MVDR, see [32]), or Capon's method [33]. More recent methods first perform a low rank factorization of the covariance matrix (usually obtained by an eigendecomposition, or a Singular Value Decomposition, SVD), and work on the subspace spanned by the left singular vectors; we can cite MUSIC [34, 35], and MODE [36] for general arrays, and ESPRIT [37] for an Uniform Linear Array (ULA). These are all parametric methods to estimate the directions-of-arrival  $\theta_i$ . These in turn determine  $\mathbf{A}$ , and thus for example a zero-forcing beamformer  $\mathbf{W}$ .

We present here the most common implementation of ESPRIT. For an ULA,  $\mathbf{A}$  has the form:

$$\mathbf{A} = \begin{bmatrix} 1 & \dots & 1 \\ \psi_1 & \dots & \psi_d \\ \psi_1^2 & \dots & \psi_d^2 \\ \psi_1^{M-1} & \dots & \psi_d^{M-1} \end{bmatrix}$$

where  $\psi_i = \exp[2\pi j d / \lambda \cos(\theta_i)]$ , and  $\theta_i$  is the direction of arrival of the  $i$ -th source<sup>2</sup>. There are  $d$  sources, and  $\mathbf{A}$  has size  $M \times d$ . We assume  $M > d$ .

<sup>2</sup>In the literature,  $\phi$  is used, here we choose to present ESPRIT with the notation  $\psi$  to not mix the definition.

Define two selection matrices  $\mathbf{J}_1$  and  $\mathbf{J}_2$ , which select the  $(M - 1)$  first and the  $(M - 1)$  last rows, respectively. By applying these matrices to  $\mathbf{A}$ , we get:

$$\begin{aligned}\mathbf{A}_1 &\stackrel{\text{def}}{=} \mathbf{J}_1 \mathbf{A} \\ \mathbf{A}_2 &\stackrel{\text{def}}{=} \mathbf{J}_2 \mathbf{A}\end{aligned}$$

with some simplifications, the special structure of  $\mathbf{A}$  ensures that:

$$\mathbf{A}_2 = \mathbf{J}_1 \mathbf{A} \Phi = \mathbf{A}_1 \Phi$$

where  $\Phi$  is the  $d \times d$  diagonal matrix whose diagonal entries are  $[\psi_1, \dots, \psi_d]$ . This is the fundamental property used by ESPRIT.

Given the data matrix  $\mathbf{X}$ , we perform a low rank decomposition of  $\mathbf{X}$  to obtain an estimate of the subspace spanned by the columns of  $\mathbf{A}$ . It can be done by a Singular Value Decomposition (SVD),  $\mathbf{X} = \mathbf{U} \Sigma \mathbf{V}^H$ , where  $\mathbf{U}$  and  $\mathbf{V}$  are unitary matrices, and  $\Sigma$  is a diagonal matrix containing the singular values in descending order. We construct a matrix  $\mathbf{E}$  consisting of the first  $d$  columns of  $\mathbf{U}$ . If the noise is Gaussian and spatially white, then the column span of  $\mathbf{E}$  tends to the column span of  $\mathbf{A}$  as the number of samples tends to infinity<sup>3</sup>. Thus there exists a  $d \times d$  invertible matrix  $\mathbf{T}$  such that:

$$\mathbf{A} = \mathbf{E} \mathbf{T}$$

We apply the matrices  $\mathbf{J}_1$  and  $\mathbf{J}_2$  to  $\mathbf{E}$  to obtain  $\mathbf{E}_1 = \mathbf{J}_1 \mathbf{E}$  and  $\mathbf{E}_2 = \mathbf{J}_2 \mathbf{E}$ . It follows that

$$\begin{aligned}\mathbf{A}_1 &= \mathbf{E}_1 \mathbf{T} \\ \mathbf{A}_2 &= \mathbf{E}_2 \mathbf{T}\end{aligned}$$

Re-arranging the last Equation gives:

$$\mathbf{A}_1 \Phi = \mathbf{E}_2 \mathbf{T}$$

Using the definition of  $\mathbf{A}_1$ , gives:

$$\mathbf{E}_1 \mathbf{T} \Phi = \mathbf{E}_2 \mathbf{T}$$

This Equation indicates that  $\mathbf{E}_1$  and  $\mathbf{E}_2$  span the same subspace. Since we assumed that  $M > d$ ,  $\mathbf{E}_1$  is tall and we can compute a left inverse of it,  $\mathbf{E}_1^\dagger = (\mathbf{E}_1^H \mathbf{E}_1)^{-1} \mathbf{E}_1^H$ . Applying it, we obtain

$$\begin{aligned}\mathbf{T} \Phi &= \mathbf{E}_1^\dagger \mathbf{E}_2 \mathbf{T} \\ \Rightarrow \mathbf{F} \stackrel{\text{def}}{=} \mathbf{E}_1^\dagger \mathbf{E}_2 &= \mathbf{T} \Phi \mathbf{T}^{-1}\end{aligned}$$

$\mathbf{F}$  can be computed from the data. The model for  $\mathbf{F}$  is an eigenvalue decomposition: the diagonal entries of  $\Phi$  are the eigenvalues of  $\mathbf{F}$  and the vectors of  $\mathbf{T}^{-1}$  are its

<sup>3</sup>There is equality for any  $N$  in the noise-free case.

eigenvectors. Thus, we can compute  $\Phi$ , and from the diagonal elements, the  $\psi_i$ 's ( $i \in \{1, \dots, d\}$ ), we can estimate the directions of arrival. In the absence of noise, the pseudo-inversion of  $\mathbf{A}$  indicates that  $\mathbf{S} = \mathbf{T}^{-1} \mathbf{E}^H \mathbf{X}$ , so we can compute the beamformers  $\mathbf{W}$  as:

$$\mathbf{W} = \mathbf{E} (\mathbf{T}^{-1})^H$$

Over time, many refinements have been added to this algorithm, e.g., multi-dimensional ESPRIT [38, 39], TLS-ESPRIT [40], UNITARY-ESPRIT [41], and VIRTUAL-ESPRIT [42].

### 3.3.3 A Decision-Directed Beamformer

A Decision Directed (DD) Beamforming technique does not use the structure of the array  $\mathbf{A}$ , but of the sources  $\mathbf{S}$ . As all techniques presented in the remaining of this section are not using the structure of the array, we will consider the more general model:

$$\mathbf{X} = \mathbf{M}\mathbf{S} + \mathbf{N}$$

where  $\mathbf{M}$  is unstructured but considered square or tall, and full column rank. The idea in the derivation of a DD beamformer is that  $\mathbf{S}$  is generated by a finite set of unknown discrete variables (the transmitted symbols). The technique in [43] consists of alternately estimating the symbols and the beamformers in order to converge to an optimal solution. In outline, the algorithm is as follows:

1. Obtain by any method a first estimate of the signal, demodulate it to estimate the transmitted symbols, and use a symbol decision (or projection) to regenerate an estimate of the emitted signal:  $\hat{\mathbf{s}}_o[n], \forall n \in \{1, \dots, N\}, k = 0$ .
2. Compute an estimate of the MMSE beamformer  $\mathbf{W}$  as:

$$\mathbf{W}_{MMSE} = \arg \min_{\mathbf{W}} \|\mathbf{W}^H \mathbf{X} - \mathbf{S}\|_F^2 = (\mathbf{S}\mathbf{X}^\dagger)^H = \hat{\mathbf{R}}_{xx}^{-1} \hat{\mathbf{R}}_{xs} \quad (3.19)$$

3. Recompute  $\forall n \in \{1, \dots, N\}$  the signal estimate:

$$\hat{\mathbf{s}}_k[n] = \hat{\mathbf{W}}^H \mathbf{x}[n] \quad (3.20)$$

where the index  $k$  means  $k$ -th iteration.

4. Demodulate  $\hat{\mathbf{s}}_k[n]$  to obtain an estimate of the transmitted symbols:  $\mathbf{q}_{k+1}[n]$ , this is the decision-directed step. Use this stream to regenerate the signal:  $\hat{\mathbf{s}}_{k+1}[n]$ .
5. If  $\mathbf{S}_{k+1} \neq \mathbf{S}_k, k = k + 1$  and go to step 2. Otherwise, we have a stable solution.

The major problem in this method is to find an initial signal to begin the iteration, for which we need some knowledge on  $\mathbf{S}$ , such as a training period. The procedure does not guarantee a global convergence, but only a local convergence is demonstrated in the article, so it may happen that similar sources are found several times (e.g. to have  $\mathbf{W}$  full rank).

### 3.3.4 The ILSP and ILSE method

The article [13] proposed two methods that share the basic ideas of the preceding subsection. The idea is to use the finite alphabet property of the signals to redirect the beams (non-linear step), and to alternately estimate the DOA and the signal (separate the variables).

The model is  $\mathbf{X} = \mathbf{MS} + \mathbf{N}$ , where the noise is additive, spatially white, and Gaussian.  $\mathbf{M}$  is unstructured but considered square or tall, and full column rank.

There are two differences with the preceding algorithm, the first one is that now the entries of  $\mathbf{S}$  are assumed to be the symbols and drawn from a finite alphabet (rather than that  $\mathbf{S}$  is obtained indirectly via some modulation of the symbols). The second is that the authors do not optimize the MMSE criterion but the model error criterion:

$$\min_{\mathbf{M}, \mathbf{S} \in \Omega^{d \times N}} \|\mathbf{X} - \mathbf{MS}\|_F^2 \quad (3.21)$$

where  $(\mathbf{S})_{i,n} \in \Omega$  indicates that the entries of  $\mathbf{S}$  belong to the finite alphabet  $\Omega$ , for example  $\Omega = \{\pm 1\}$ . We define by  $L$  the size of the alphabet set. Using the proof derived in [44], the optimization may be carried out in two steps:

1. For any fixed  $\mathbf{S}$ , the minimization to  $\mathbf{M}$  of equation (3.21) leads to:

$$\hat{\mathbf{M}} = \mathbf{XS}^\dagger = \mathbf{XS}^H (\mathbf{SS}^H)^{-1} \quad (3.22)$$

2. Replacing  $\mathbf{M}$  by  $\hat{\mathbf{M}}$  in 3.21 gives us:

$$\min_{\mathbf{S} \in \Omega} \|\mathbf{X} \mathbf{P}_{\mathbf{S}}^\perp\|_F^2 \quad (3.23)$$

where  $\mathbf{P}_{\mathbf{S}}^\perp = \mathbf{I}_N - \mathbf{S}^H (\mathbf{SS}^H)^{-1} \mathbf{S}$ , is the projection orthogonal to the subspace spanned by the columns of  $\mathbf{S}$ .

The global minimum is found by enumerating  $\mathbf{S}$  over all the possibilities. Since it has an expensive computational cost, the authors propose two simpler algorithms to reduce the computational costs.

- Iterative Least Square with Projection (ILSP): The method consists of projecting the estimate of the signal onto the closest discrete value. The algorithm is outlined below:

1		$k = 0$ , Take a first estimate of $\hat{\mathbf{M}}_0$ .
2	a	$k = k + 1$
	b	$\bar{\mathbf{S}}_k = \left( \hat{\mathbf{M}}_{k-1}^H \hat{\mathbf{M}}_{k-1} \right)^{-1} \hat{\mathbf{M}}_{k-1}^H \mathbf{X} = \hat{\mathbf{M}}_{k-1}^\dagger \mathbf{X}$
	c	$\hat{\mathbf{S}}_k = \text{proj}_{\Omega} [\bar{\mathbf{S}}_k]$
	d	$\hat{\mathbf{M}}_k = \mathbf{X} \hat{\mathbf{S}}_k^H \left( \hat{\mathbf{S}}_k \hat{\mathbf{S}}_k^H \right)^{-1} = \mathbf{X} \hat{\mathbf{S}}_k^\dagger$
3		repeat 2 until $(\hat{\mathbf{M}}, \hat{\mathbf{S}})$ is stable.

The initialization of  $\mathbf{M}$  may be either done by first estimating the DOAs, using ESPRIT or by setting  $\mathbf{M}$  to the identity matrix. An alternative method is to first initialize  $\mathbf{S}$  with a estimate of the signals, which can be obtained by taking the  $d$  rows corresponding to the  $d$  largest singular values of  $\mathbf{X}$ , and then to set the mixing matrix from the step 2.c.

- Iterative Least Square with Enumeration (ILSE): Alternatively, the authors propose to enumerate all the possibilities of the signal over  $\Omega$ . This is quite expensive:  $L^{dN}$  possibilities, but due to the Frobenius norm properties:

$$\|\mathbf{X} - \mathbf{MS}\|_F^2 = \|\mathbf{x}[1] - \mathbf{Ms}[1]\|^2 + \dots + \|\mathbf{x}[N] - \mathbf{Ms}[N]\|^2$$

we may do it for each vector  $\mathbf{s}(k)$  separately, so that we have to enumerate  $N$  times over only  $L^d$  possibilities. The algorithm is outlined below:

1		$k = 0$ , Take a first estimate of $\hat{\mathbf{M}}_0$ .
2	a	$k = k + 1$
	b	By enumeration, $\forall n \in \{1, \dots, N\}$ : $\hat{\mathbf{s}}_k[n] = \arg \left\{ \min_{\mathbf{s}[n] \in \Omega} \ \mathbf{x}[n] - \hat{\mathbf{M}}_k \mathbf{s}[n]\ _F^2 \right\}$ $\hat{\mathbf{S}}_k = [\hat{\mathbf{s}}[1], \dots, \hat{\mathbf{s}}[N]]$
	c	$\hat{\mathbf{M}}_k = \mathbf{X} \hat{\mathbf{S}}_k^H \left( \hat{\mathbf{S}}_k \hat{\mathbf{S}}_k^H \right)^{-1} = \mathbf{X} \hat{\mathbf{S}}_k^\dagger$
3		repeat 2 until $(\hat{\mathbf{M}}, \hat{\mathbf{S}})$ is stable.

As for the Decision-Directed Beamformer, the choice of the initial point is crucial. If the algorithm does not reach a minimum whose cost is close to the noise power  $Nm\sigma^2$ , the authors restart the procedure with a new initial point, otherwise the final estimate is declared correct.

The simulations give good results, even for low angle separation and low SNR. But the computational cost is rather high. ILSE has a cost in the order of  $NMdL^d$  per iteration, where 4 iterations on the average are necessary, while ILSP has a cost in the order  $NMd$  per iteration, but the average number of iterations is now around 10. These algorithms have the best performance for small alphabet set or with initial point near the solution, thus there are perfect for fine-tuning of other algorithms.

### 3.3.5 ACMA

The Analytical Constant Modulus Algorithm (ACMA) [12] also considers the model  $\mathbf{X} = \mathbf{MS} + \mathbf{N}$ . This time, the entries of  $\mathbf{S}$  are supposed to have a constant modulus,  $|S_{ij}| = 1$ . Examples of such signals are FM modulated sources, or discrete sources with a constellation on the unit circle. Another important example is GSM signals.

The algorithm looks for all beamformers  $\{\mathbf{w}\}$  such that the output signal  $\mathbf{w}^H \mathbf{x}[n] = \hat{\mathbf{s}}[n]$  has a constant modulus,

$$|\hat{\mathbf{s}}[n]| = 1, \quad \forall n \in \{1, \dots, N\}$$



For the sake of convenience, we consider  $d$  sources impinging on  $d$  elements. Using the beamformer, an equivalent formulation to the previous Equation is:

$$\mathbf{w}^H \mathbf{x}[n] \mathbf{x}^H[n] \mathbf{w} = 1, \quad \forall n \in \{1, \dots, N\}$$

Using properties of the Kronecker product (see section 1.7, Equation (1.3)), it follows that

$$\mathbf{w}^H \mathbf{x}[n] \mathbf{x}^H[n] \mathbf{w} = 1 \quad \Leftrightarrow \quad (\mathbf{x}[n] \otimes \mathbf{x}[n]^*)^H (\mathbf{w} \otimes \mathbf{w}^*) = 1$$

By stacking for  $n \in \{1, \dots, N\}$  the row vectors  $\mathbf{p}[n] = (\mathbf{x}[n] \otimes \mathbf{x}[n]^*)^H$  into a matrix  $\mathbf{P} \mathbf{P} = [\mathbf{p}^T[1], \dots, \mathbf{p}^T[N]]^T$ , we obtain:

$$\begin{cases} \mathbf{P} \mathbf{y} = \mathbf{1} \\ \mathbf{y} = \mathbf{w} \otimes \mathbf{w}^* \end{cases} \quad (3.25)$$

The next step is to solve the linear system  $\mathbf{P} \mathbf{y} = \mathbf{1}$  independently from the constraint on  $\mathbf{y}$ . We first transform the linear system to an equivalent system  $\hat{\mathbf{P}} \mathbf{y} = \mathbf{0}$ . Let  $\mathbf{Q}$  be an orthonormal (Householder) transformation such that  $\mathbf{Q} \mathbf{1} = [\sqrt{N} \mathbf{0}^T]^T$ , and let  $\hat{\mathbf{P}}$  be the last  $(N - 1)$  rows of  $\mathbf{Q} \mathbf{P}$ , then up to a scaling, solving  $\mathbf{P} \mathbf{y} = \mathbf{1}$  is equivalent to solve:

$$\hat{\mathbf{P}} \mathbf{y} = \mathbf{0}$$

with  $\mathbf{y} \neq \mathbf{0}$ . The solutions of this Equation are in the kernel of  $\hat{\mathbf{P}}$ . If  $N$  is sufficiently large and the sources are sufficiently varying, then it can be shown that the dimension of the kernel is exactly  $d$ . Denote by  $[\mathbf{y}_1, \dots, \mathbf{y}_d]$  its basis, then all solutions  $\mathbf{y}$  are linear combinations of this basis, hence of the form

$$\mathbf{y} = \mathbf{w}_i \otimes \mathbf{w}_i^* = \sum_{j=1}^d \alpha_{ij} \mathbf{y}_j$$

For unknown coefficients  $\alpha_{ij}$ , after some derivations and using the “unvec” operator from Section 1.7, we obtain for  $i \in \{1, \dots, d\}$ :

$$\mathbf{Y}_i = \mathbf{W} \boldsymbol{\Lambda}_i \mathbf{W}^H \quad i = 1, \dots, d$$

where  $\mathbf{Y}_i$  is the  $d \times d$  matrix equal to  $\text{unvec}(\mathbf{y}_i)$ , and  $\boldsymbol{\Lambda}_i$  is a diagonal matrix related to the  $\alpha_{ij}$ . We note that all the  $\mathbf{Y}_i$  have a diagonal form in the same basis,  $\mathbf{W}$ . The only matrix that jointly diagonalizes this collection of matrices  $\{\mathbf{Y}_i\}$  is  $\mathbf{W}$ , up to a column permutation and/or a unit-norm column scaling. The joint diagonalization problem is a generalization of the usual eigenvalue problem. Indeed, assume that  $\mathbf{Y}_1$  is invertible, then note that  $\mathbf{Y}_1^{-1} \mathbf{Y}_2 = \mathbf{W}^{-1} \boldsymbol{\Lambda}_1^{-1} \boldsymbol{\Lambda}_2 \mathbf{W}$ , hence  $\mathbf{W}$  can be computed from the eigenvectors of  $\mathbf{Y}_1^{-1} \mathbf{Y}_2$ . With more than 2 matrices, the joint diagonalization can be computed with the method proposed in [12].

### 3.3.6 ACPA

Proposed in [15, 16], the principle of ACPA differs from the preceding algorithm in the sense that the conditions on the source constellation are more tight. Indeed,

this method is intended to work only for  $n$ -PSK symbol constellations, which are regularly spaced constellations on the unit circle. These distributions are restrictive cases of the more general framework of Constant Modulus distributions.

Since these constellations are the set of the  $L$   $L^{\text{th}}$  roots of unity,  $s$  is in the constellation if  $s^L = 1$ . In the case of  $L = 2$ , this property can be used in the same way as in ACMA [14]. For general  $L$ , let us consider a beamformer  $\mathbf{w}$  such that the output signal is  $\mathbf{w}^H \mathbf{x}[n] = \hat{s}[n]$ , then

$$[\mathbf{w}^H \mathbf{x}[n]]^L = 1, \quad \forall n \in \{1, \dots, N\}$$

Similar to ACMA, it can be shown that this can be written as

$$\mathbf{P} \mathbf{w}^{\circ L} = \mathbf{1}$$

where  $\mathbf{w}^{\circ L}$  is a vector that contains only the non-redundant terms of  $\mathbf{w} \otimes \mathbf{w} \dots \otimes \mathbf{w}$ , and  $\mathbf{P}$  is a tall matrix constructed of  $\mathbf{X}$ . The problem can be solved for all beamformers  $\mathbf{w}$  by solving a linear system and a Joint Diagonalization step, although the latter step is a bit more difficult than in ACMA for  $L > 2$ .

### 3.3.7 SOBI

The Second-Order Blind Identification (SOBI) algorithm [17] is a general technique to blindly separate sources based on differences in second-order spectral content. In contrast to the preceding techniques, it is based on statistical properties of the sources.

Consider the data model  $\mathbf{x}(k) = \mathbf{M}\mathbf{s}(k) + \mathbf{n}(k)$ , where the vector signal  $\mathbf{s}(k)$  consists of  $d$  independent wide-sense stationary sources  $s_i(k)$  with different non-white spectral content. For each  $i \in \{1, \dots, m\}$ , the  $i$ -th component of the noise  $\mathbf{n}_i(k)$  is additive zero-mean Gaussian noise, temporally independently identically distributed.

Let  $\gamma_i(\tau) = \text{E}\{s_i(k)s_i^*(k-\tau)\}$ , and define the non-central auto-covariance of the vector  $\mathbf{x}$  at time-lag  $\tau$  as  $\mathbf{R}_\tau \stackrel{\text{def}}{=} \text{E}\{\mathbf{x}(k)\mathbf{x}^H(k-\tau)\}$ . Then after some derivations, and for  $\tau \neq 0$ ,  $\mathbf{R}_\tau$  becomes:

$$\mathbf{R}_\tau = \mathbf{M}\mathbf{\Gamma}_\tau\mathbf{M}^H$$

where  $\mathbf{\Gamma}_\tau = \text{diag}(\gamma_1(\tau), \dots, \gamma_d(\tau))$ . The authors collect  $L$  matrices  $\mathbf{R}_\tau$  with different  $\tau$ ,  $\tau \in \{\tau_1, \dots, \tau_L\}$ . Note that all the  $\mathbf{R}_\tau$  have a diagonal form in the same basis,  $\mathbf{M}$ . One can prove that if the  $\mathbf{\Gamma}_\tau$  are sufficiently different and  $\mathbf{M}$  is full rank, the only matrix that jointly diagonalizes this collection is  $\mathbf{M}$ , up to a column permutation and/or a unit-norm column scaling. The proposed algorithm in [17] uses the joint diagonalization of Cardoso and Souloumiac [45].

## 3.4 Conclusion

In this chapter we have derived a model for the reception of several SSR sources impinging on an array. For this model, we have extracted several properties that

will be useful to perform source separation. Generic source separation techniques have been reviewed in the preceding section.



## Chapter 4

# Identifiability in the noiseless case

Suppose that we have received a data matrix consisting of a mixture of SSR signals. Our objective in this thesis is to derive algorithms to separate the sources, *i.e.* given the data and a model, estimate all parameters of the model. A general principle in estimation theory is that prior to any signal processing, one has to ensure that the model is identifiable, *i.e.* under noise-free conditions there should be up to a permutation only one unique set of parameters admissible as a solution. In this chapter, we present conditions under which a mixture of SSR replies can be identified.

The identifiability problem is addressed in two different cases: infinite number of samples and finite number of samples. For the finite sample case, only bounds on the probability that identifiability holds can be proposed.

By identifiability, it is meant that the observation  $\mathbf{X} = f(\Theta)$  admits one and only one solution  $\Theta$  in a parameter set  $\Omega$ , e.g. the function  $f(\cdot)$  is bijective. Considering the noiseless case amounts to admit that  $\mathbf{X} \in f(\Omega)$ , which means that  $f(\cdot)$  is surjective by construction. Thus, it remains to prove injectivity of  $f(\cdot)$ , *i.e.* uniqueness of  $\Theta$ .

### 4.1 Model and assumptions

Recall from Chapter 3 the signal model where  $M$  is the number of antennas,  $N$  the number of samples,  $d$  the number of sources, and  $T$  the sampling period. In this chapter, we consider only unframed signals, so that there is no notion of packet here.

Let  $f_i$  be the residual carrier frequency of source  $i$ , and its associated phase  $\phi_i = \exp(2\pi j f_i T)$ ,  $\forall i \in \{1, \dots, d\}$ .  $\mathbf{F}$  is the  $d \times N$  matrix that contains the influences of the residual frequencies: its  $i$ -th row is  $\mathbf{f}_i = [1, \phi_i, \dots, \phi_i^{N-1}]$ . Each source  $s_i$ ,  $\forall i \in \{1, \dots, d\}$ , transmits a bit sequence,  $b_i[n]$ ,  $n \in \{1, \dots, N\}$ , which is taken from the alphabet  $\{0, 1\}$ . We denote the  $d \times N$  data matrix  $\mathbf{B} = [\mathbf{b}_1^T, \dots, \mathbf{b}_d^T]^T$ , whose  $i$ -th row is the binary sequence  $\mathbf{b}_i = [b_i[1], \dots, b_i[N]]$ .  $\odot$  denotes the element-wise

multiplication between two matrices. We define the  $d \times N$  source matrix:

$$\mathbf{S} = \mathbf{F} \odot \mathbf{B}$$

Recall that  $\mathbf{A}$  is the  $M \times d$  steering matrix containing the  $d$  steering vectors  $\mathbf{a}(\theta_i)$ ,  $1 \leq i \leq d$ , where the  $\theta_i$ 's are the directions of arrival of the source.  $\mathbf{a}(\theta)$  is a known function of the parameter  $\theta$ , the DOA, which characterizes the properties of an antenna array.  $\mathbf{G}$  is a  $d \times d$  diagonal gain matrix, which also contains the initial phase of the receivers.  $\mathbf{X} = [\mathbf{x}(1), \dots, \mathbf{x}(N)]$  is a  $M \times N$  matrix that contains the received signal, with  $x_m[k]$  being the signal received on the  $m$ -th sensor at time  $kT$ . The noise-free model is:

$$\mathbf{X} = \mathbf{A}\mathbf{G}[\mathbf{F} \odot \mathbf{B}] = \mathbf{A}\mathbf{G}\mathbf{S} \quad (4.1)$$

At time  $n$ , we receive the  $M$ -vector  $\mathbf{x}[n] = [x_1[n], \dots, x_M[n]]^T$ , corresponding to the binary vector  $\mathbf{b}[n] = [b_1[n], \dots, b_d[n]]^T$ . Last, define the parameter vector  $\Theta$  that contains all the information:  $\Theta = \{\theta_i, g_i, f_i, \mathbf{b}_i, i \in [1, \dots, d]\}$ .

We remind that  $\mathbb{E}\{\cdot\}$  denotes the mathematical expectation operator,  $\mathbf{I}$  the identity matrix, and  $\mathbf{1}$  the vector built of 1's.

**Definition** An array is unambiguous if for any set of  $d$  distinct DOAs,  $\{\theta_1, \dots, \theta_d\}$ , the array response matrix  $[\mathbf{a}(\theta_1), \dots, \mathbf{a}(\theta_d)]$  is full column rank.

Note that in this thesis, we always consider ULA's with a half wavelength separation distance, which is known to be unambiguous in the range  $[0, \dots, 180)$  degrees.

**General assumptions** In this chapter, we make the following assumptions, which are common to all propositions:

- A1.** No noise.
- A2.** The array is an unambiguous ULA. From the definition, the first row of  $\mathbf{A}$  consists of 1.
- A3.** The angles  $\theta_i$  are different,  $\forall i \in \{1, \dots, d\}$ .
- A4.** The residual frequencies belong to the range:  $0 \leq f_i < \frac{1}{T}$ ,  $\forall i \in \{1, \dots, d\}$ .
- A5.** There are more sensors than sources:  $M > d$ . As well, there are more samples than sources:  $N > d$ .
- A6.** We consider unframed streams of bits (no time of arrival identification).
- A7.** The bits,  $b_i[n]$ ,  $\forall i \in \{1, \dots, d\}$  and  $\forall n \in \{1, \dots, N\}$ , are taken from the finite alphabet  $\{0, 1\}$  with an equiprobable distribution. The bit streams are independent, identically distributed, and stationary. Then the following statistical property holds:

$$\mathbb{E}\{\mathbf{b}\mathbf{b}^H\} = \frac{1}{4}\mathbf{1}\mathbf{1}^T + \frac{1}{4}\mathbf{I}$$

- A8.** All gains are non-zero:  $g_i \neq 0$ ,  $\forall i \in \{1, \dots, d\}$ .

In most blind identification problems of the form  $\mathbf{X} = \mathbf{A}\mathbf{G}\mathbf{S}$ , there always remains a permutation and complex scaling uncertainty. The permutation uncertainty is due to the fact that we cannot know the specific ordering of sources in  $\mathbf{S}$ , e.g. for any permutation matrix  $\Pi$ ,  $\mathbf{X} = \mathbf{A}\mathbf{G}\mathbf{S} = \mathbf{A}\Pi\Pi^T\mathbf{G}\mathbf{S}$ . Here, given (i) the data alphabet, (ii) the choice for the phase of the carrier drift at the first sample, and (iii) the definition of the matrix  $\mathbf{A}$ , the complex scaling uncertainty does not hold in our context. Note that this indeterminacy could be resolved by sorting the  $\theta$ 's in increasing order.

Note that as we sample at  $T = 0.5\mu\text{s}$ , the ICAO tolerance on the carrier frequency of  $\pm 3$  MHz precludes an exact identification of the frequency drift, due to aliasing. As we limit  $f$  to the interval  $[0, \frac{1}{T})$  in our model, we obtain the actual carrier residual modulo  $\frac{1}{T}$ .

We consider in this chapter only the noiseless case identification. Parameter estimation in the noisy case is the topic of Chapters 5 and 6.

## 4.2 The infinite sample case

We derive in this section uniqueness conditions for an infinite number of samples.

**Proposition 4.2.1** *Under the assumptions A1 to A8,  $M \geq 2d$ , and an infinite number of samples, then the parameters  $\{\theta_i, g_i, f_i, \mathbf{b}_i\}$ ,  $\forall i \in \{1, \dots, d\}$ , are unique for a given  $\mathbf{X} \in f(\Omega)$ , up to a permutation.*

**Proof** Suppose there are two solutions satisfying the requirements of Proposition 4.2.1:  $\Theta = \{\theta_i, g_i, f_i, \mathbf{b}_i, i \in [1, \dots, d]\}$  and  $\tilde{\Theta} = \{\tilde{\theta}_i, \tilde{g}_i, \tilde{f}_i, \tilde{\mathbf{b}}_i, i \in [1, \dots, d]\}$ . Then:

$$\mathbf{X} = \mathbf{A} \cdot \mathbf{G} \cdot [\mathbf{F} \odot \mathbf{B}] = \tilde{\mathbf{A}} \cdot \tilde{\mathbf{G}} \cdot [\tilde{\mathbf{F}} \odot \tilde{\mathbf{B}}] \quad (4.2)$$

which gives:

$$\mathbf{A} \cdot \mathbf{G} \cdot [\mathbf{F} \odot \mathbf{B}] - \tilde{\mathbf{A}} \cdot \tilde{\mathbf{G}} \cdot [\tilde{\mathbf{F}} \odot \tilde{\mathbf{B}}] = 0$$

Suppose that some of the  $\theta_i$ 's are equal to some of the  $\tilde{\theta}_i$ 's. First re-order the columns of  $\mathbf{A}$  in order to have the common steering vectors,  $\mathbf{A}_c$  in the right block, and the non-common steering vectors,  $\mathbf{A}_{nc}$  in the left block:  $\mathbf{A} = [\mathbf{A}_{nc}, \mathbf{A}_c]$ . The same re-ordering is done on the rows of the matrices  $\mathbf{G}$  and  $\mathbf{F} \odot \mathbf{B}$ . Apply a similar re-ordering to  $\tilde{\mathbf{A}}$  to obtain:  $\tilde{\mathbf{A}} = [\tilde{\mathbf{A}}_c, \tilde{\mathbf{A}}_{nc}]$ . Then:

$$\begin{bmatrix} \mathbf{A}_{nc} & | & \mathbf{A}_c \end{bmatrix} \cdot \begin{bmatrix} \mathbf{G}_{nc} \cdot [\mathbf{F} \odot \mathbf{B}]_{nc} \\ \mathbf{G}_c \cdot [\mathbf{F} \odot \mathbf{B}]_c \end{bmatrix} - \begin{bmatrix} \tilde{\mathbf{A}}_{nc} & | & \tilde{\mathbf{A}}_c \end{bmatrix} \cdot \begin{bmatrix} \tilde{\mathbf{G}}_{nc} \cdot [\tilde{\mathbf{F}} \odot \tilde{\mathbf{B}}]_{nc} \\ \tilde{\mathbf{G}}_c \cdot [\tilde{\mathbf{F}} \odot \tilde{\mathbf{B}}]_c \end{bmatrix} = 0 \quad (4.3)$$

Since  $\mathbf{A}_c = \tilde{\mathbf{A}}_c$ , equation (4.3) can be written as:

$$\begin{bmatrix} \mathbf{A}_{nc} & | & \mathbf{A}_c & | & \tilde{\mathbf{A}}_{nc} \end{bmatrix} \cdot \begin{bmatrix} \mathbf{G}_{nc} \cdot [\mathbf{F} \odot \mathbf{B}]_{nc} \\ \mathbf{G}_c \cdot [\mathbf{F} \odot \mathbf{B}]_c - \tilde{\mathbf{G}}_c \cdot [\tilde{\mathbf{F}} \odot \tilde{\mathbf{B}}]_c \\ \tilde{\mathbf{G}}_{nc} \cdot [\tilde{\mathbf{F}} \odot \tilde{\mathbf{B}}]_{nc} \end{bmatrix} = \mathcal{A}\mathcal{S} = 0 \quad (4.4)$$

The first matrix,  $\mathcal{A}$ , is tall or square and is constructed by a collection of  $\mathbf{a}(\theta_i)$ 's all different. By assumption, we use an unambiguous antenna array, therefore  $\mathcal{A}$  is full column rank, so that the second matrix,  $\mathcal{S}$ , is equal to zero. As the binary signals are non-trivial, for all sources there is an  $n \in \mathbb{N}$ , such that for all the bit is equal to 1 for this time index. Then we obtain  $g_i \phi_i^n = 0$ , which is impossible since  $\mathbf{A}\mathbf{8}$  assumes that  $g_i \neq 0$  and  $|\phi_i| = 1$ . Hence  $\mathbf{G}_{nc} \cdot [\mathbf{F} \odot \mathbf{B}]_{nc}$  and  $\tilde{\mathbf{G}}_{nc} \cdot [\tilde{\mathbf{F}} \odot \tilde{\mathbf{B}}]_{nc}$  have to be zero-dimensional, as well  $\mathbf{A}_{nc}$  and  $\tilde{\mathbf{A}}_{nc}$  are zero-dimensional. We conclude that there were only common DOAs, and we can state that  $\mathcal{A}$ ,  $\mathbf{A}$ , and  $\tilde{\mathbf{A}}$  are equal up to permutation of the columns. After fixing this permutation, we obtain the equality of the rows of  $\mathbf{G}_c \cdot [\mathbf{F} \odot \mathbf{B}]_c$  and  $\tilde{\mathbf{G}}_c \cdot [\tilde{\mathbf{F}} \odot \tilde{\mathbf{B}}]_c$ . For each row  $i = \{1, \dots, d\}$  of the factor  $\mathcal{S}$ , we have:

$$g_i \cdot (\mathbf{f}_i \odot \mathbf{b}_i) = \tilde{g}_i \cdot (\tilde{\mathbf{f}}_i \odot \tilde{\mathbf{b}}_i) \quad (4.5)$$

By taking the absolute value of Equation (4.5), we get:  $|g_i|b_i[n] = |\tilde{g}_i|\tilde{b}_i[n]$ ,  $\forall n \in \{1, \dots, N\}$ . As we consider an infinite number of samples, and that the binary distribution of  $b_i[n]$  is equiprobable, there is almost surely a sample time  $n_0$  for which  $b_i[n_0] = 1$ . Then  $\tilde{b}_i[n_0] = \left| \frac{g_i}{\tilde{g}_i} \right|$  with  $\tilde{b}_i[n_0] \in \{0, 1\}$ , so  $\tilde{b}_i[n_0]$  must be equal to 1 as well, and we obtain:  $|g_i| = |\tilde{g}_i|$ . Then the absolute value of Equation (4.5) results in:  $\tilde{\mathbf{b}}_i = \mathbf{b}_i$ ,  $\forall i \in \{1, \dots, d\}$ .

Yet,  $g_i = |g_i| \cdot e^{j\psi_i}$ , and  $\tilde{g}_i = |\tilde{g}_i| \cdot e^{j\tilde{\psi}_i}$ . Thus Equation (4.5) leads to:

$$\left( e^{j\psi_i} \mathbf{f}_i - e^{j\tilde{\psi}_i} \tilde{\mathbf{f}}_i \right) \odot \mathbf{b}_i = 0$$

It remains to prove that, for all  $i \in \{1, \dots, d\}$ ,  $f_i$  and  $\psi_i$  coincide with  $\tilde{f}_i$  and  $\tilde{\psi}_i$ .

Given an i.i.d. binary equiprobable source  $b_i[n]$ , we can find almost surely two successive time indices,  $n_1$  and  $(n_1 + 1)$ , both belonging to the support of  $b_i$ :  $b_i[n_1] = b_i[n_1 + 1] = 1$ . Then the equations  $\exp[j(2\pi n_1)(f_i - \tilde{f}_i)T + (\psi_i - \tilde{\psi}_i)] = 1$  and  $\exp[j(2\pi(n_1 + 1))(f_i - \tilde{f}_i)T + (\psi_i - \tilde{\psi}_i)] = 1$ , yield that  $(f_i - \tilde{f}_i) = k/T$  for some integer  $k$  and  $\psi_i - \tilde{\psi}_i = 2\tilde{k}\pi$  for some integer  $\tilde{k}$ . So  $g_i = \tilde{g}_i$ ,  $\forall i \in [1, \dots, d]$ , and the  $f_i$ 's are uniquely defined in the range  $[1, T^{-1})$ .  $\square$

### 4.3 The finite sample case

The previous results are of asymptotic nature, and may not hold valid for limited observation lengths. Therefore, we propose another result, which applies to finite observation periods.

#### 4.3.1 Method using the binary data property

Considering a binary matrix  $\mathbf{B}$  of size  $d \times N$  with i.i.d. equiprobable binary entries, we derive the probability to observe, up to a row and a column permutation of  $\mathbf{B}$ , a square sub-matrix of size  $d \times d$ , which is upper-triangular with zeros in the lower



triangle, and ones on the main diagonal. With this probability, we state the finite sample case identifiability, Proposition 4.3.4. This proposition was first presented in [46].

**Lemma 4.3.1** *Let  $\mathbf{B}$  be a  $d \times N$  matrix with i.i.d. equiprobable binary entries. The probability that a column of a  $d \times N$  matrix  $\mathbf{B}$  with independently identically distributed binary entries has the form  $[\ast \cdots \ast, 1, \mathbf{0}_{q-1}]^T$  is:  $p(q, N) = 1 - (1 - 2^{-q})^N$*

*The probability to obtain any column of the aforementioned form, but with the possibility that the 1 has been permuted with one of the 0 is:  $p'(q, N) = 1 - (1 - q \cdot 2^{-q})^N$ .*

**Proof** Only the last  $q$  entries of the column of size  $d$  are imposed, so that the probability to draw such a vector is  $2^{-q}$ . With  $N$  realizations, the probability not to draw such a vector is thus  $(1 - 2^{-q})^N$ .

Similarly, with the permutation, the probability to get a vector of this form up to permutation of the last  $q$  entries is  $q \cdot 2^{-q}$ , and the probability not to get one of those vectors over  $N$  realizations is  $(1 - q \cdot 2^{-q})^N$ .  $\square$

**Lemma 4.3.2** *Let  $\mathbf{B}$  be a  $d \times N$  matrix containing i.i.d. binary random variables with  $N \geq d$ . Denote by  $P_1(d, N)$  the probability that  $\mathbf{B}$  contains an upper triangular matrix with ones on the diagonal up to a row and column permutation. Also denote by  $P_f(d, N)$  the probability that  $\mathbf{B}$  is full rank. Then they are related as:*

$$P_f(d, N) \geq P_1(d, N) = \prod_{q=1}^d [1 - (1 - q \cdot 2^{-q})^{N-d+q}] \quad (4.6)$$

**Proof** A sufficient condition for matrix  $\mathbf{B}$  to be full rank is that there exist  $d$  columns building together an upper triangular matrix with ones along the diagonal, up to a row permutation; thus,  $P_1 \leq P_f$ .

The proof of the expression of  $P_1$  is constructive. First let us extract a column of  $\mathbf{B}$  that contains one 1 and all other elements equal to 0. Lemma 4.3.1 indicates that the probability to draw such a vector is  $p'(d, N)$ . Denote  $i_1$  the index of the 1 in this vector. Now in the remaining  $N - 1$  samples, we look for a column such that there is a 1 at another index than  $i_1$ , 0 elsewhere, and anything at index  $i_1$ ; e.g. a permutation of  $[\ast, 1, \mathbf{0}_{d-2}]^T$ . The probability to obtain such a vector is:  $p'(d - 1, N - 1)$ . Repeating the same argument, we finish by the last column, which consists of a 1 at the last possible index, and anything otherwise. The probability is then  $p'(1, N - d + 1)$ .

The product of the probabilities is the probability that such a set of columns exists, and is:  $P_1 = \prod_{q=1}^d p'(d, N - d + q)$ .  $\square$

Before we can state the Proposition, we need a last lemma:

**Lemma 4.3.3** *Let  $\tilde{\mathbf{B}}$  be a  $(d - 1) \times N$  matrix containing i.i.d. binary random variables with  $N \geq d$ . Let  $\tilde{\mathbf{b}}_i$  be one of the rows of  $\tilde{\mathbf{B}}$ . Construct a  $d \times N$  binary matrix  $\mathbf{B}$  as:*

$$\mathbf{B} = \left[ \tilde{\mathbf{b}}_1^T, \dots, \tilde{\mathbf{b}}_i^T, \tilde{\mathbf{b}}_i^T, \dots, \tilde{\mathbf{b}}_{d-1}^T \right]^T = \left[ \mathbf{b}_1^T, \dots, \mathbf{b}_i^T, \mathbf{b}_{i+1}^T, \dots, \mathbf{b}_d^T \right]^T$$

The probability that  $\mathbf{B}$  contains, up to a row and a column permutation, an upper block triangular matrix with ones on the diagonal and a  $2 \times 2$  block of 1 on the rows  $i$  and  $i + 1$ , is bounded by the probability  $P_1(d, N)$ .

**Proof** Comparing with Lemma 4.6, the difference in the construction occurs during the step  $i$  and  $i + 1$ .

Indeed in the previous lemma, we wish to find two columns as  $\alpha$  and we get two columns as  $\beta$ :

$$\alpha = \begin{bmatrix} * \\ \hline 1 & * \\ 0 & 1 \\ \hline 0 \end{bmatrix} \quad \text{and} \quad \beta = \begin{bmatrix} * \\ \hline 1 & 1 \\ 1 & 1 \\ \hline 0 \end{bmatrix}$$

where the probability for obtaining  $\alpha$  is  $p_\alpha = [1 - (1 - q \cdot 2^{-q})^n][1 - (1 - (q - 1) \cdot 2^{-q+1})^{n-1}]$ . Given that the rows  $i$  and  $i + 1$  are the same, the probability for finding  $\beta$  is  $p_\beta = [1 - (1 - (q - 1) \cdot 2^{-q+1})^n][1 - (1 - (q - 1) \cdot 2^{-q+1})^{n-1}]$ .

Now, we have to compare  $p_\alpha$  and  $p_\beta$ . Note that if  $q \geq 2$ , then  $q \leq 2(q - 1)$ . After numerous steps:

$$[1 - (1 - q \cdot 2^{-q})^n] \leq [1 - (1 - (q - 1) \cdot 2^{-q+1})^n] \quad (4.7)$$

$$p_\alpha \leq p_\beta \quad (4.8)$$

so the probability that we can extract a desired sub-matrix is bounded by  $P_1(d, N)$ .  $\square$

Now, we can state:

**Proposition 4.3.4** *Under the assumptions **A1** to **A8**, for an observation duration  $N \geq d$ , given the matrix  $\mathbf{X}$ , the probability that the parameters  $\{\theta_i, g_i, f_i, i \in [1, \dots, d]\}$  are unique is larger than the probability  $P_1(2d, N)$ , up to a permutation.*

**Proof** Assume there are two solutions to this problem:  $\Theta$  and  $\tilde{\Theta}$ . Then, remind equation (4.2) which gives:

$$\mathbf{A} \cdot \mathbf{G} \cdot [\mathbf{F} \odot \mathbf{B}] - \tilde{\mathbf{A}} \cdot \tilde{\mathbf{G}} \cdot [\tilde{\mathbf{F}} \odot \tilde{\mathbf{B}}] = 0$$

Re-order the rows and the columns of the matrices to bring together the rows containing the same frequencies and the same binary sequences in the two solutions, and bring together the rows containing different frequencies, but identical binary sequences. It gives:

$$\mathcal{A} \cdot \mathcal{S} = 0$$

with:

$$\mathcal{A} \stackrel{\text{def}}{=} \left[ (\mathbf{A}\mathbf{G})_c - (\tilde{\mathbf{A}}\tilde{\mathbf{G}})_c \mid (\mathbf{A}\mathbf{G})_{nc} \mid -(\tilde{\mathbf{A}}\tilde{\mathbf{G}})_{nc} \mid (\mathbf{A}\mathbf{G})_{sc} \mid -(\tilde{\mathbf{A}}\tilde{\mathbf{G}})_{sc} \right]$$

$$\mathcal{S} \stackrel{\text{def}}{=} \begin{bmatrix} (\mathbf{F} \odot \mathbf{B})_c \\ (\mathbf{F} \odot \mathbf{B})_{nc} \\ (\tilde{\mathbf{F}} \odot \tilde{\mathbf{B}})_{nc} \\ (\mathbf{F} \odot \mathbf{B})_{sc} \\ (\tilde{\mathbf{F}} \odot \tilde{\mathbf{B}})_{sc} \end{bmatrix}$$

where the index  $[\cdot]_{sc}$  stands for “semi-common”, e.g. different frequencies, but same binary sequence.  $\mathcal{S}$  is equal to  $\mathcal{F} \odot \mathcal{B}$  by definition, where  $\mathcal{B}$  is a binary matrix as in Lemma 4.3.3. The probability that there exists a sub-matrix of  $\mathcal{B}$ , such that it has the desired form described in Lemma 4.3.3, is bounded by  $P_1(2d, N)$ . This form is block diagonal, with blocks of size 1 and 2, where for the block of size 2, the frequencies are different. So the determinant of these blocks is of the form:  $\det = K(\phi_1^k - \phi_2^k)$ , with  $k$  being a constant, and  $k$  an integer bounded by  $N$ . Such an expression is zero for a finite subset of discrete values taken from an infinite set, so the determinant is almost surely non-zero. Thus, by construction,  $\mathcal{S}$  is full row rank, hence  $\mathcal{A}$  is null. As the first row of any product  $\mathbf{A}\mathbf{G}$  is not zero  $(\mathbf{A}\mathbf{S})$ ,  $(\mathbf{A}\mathbf{G})_{sc}$ ,  $(\tilde{\mathbf{A}}\tilde{\mathbf{G}})_{sc}$ ,  $\mathbf{A}_{nc}$  and  $\tilde{\mathbf{A}}_{nc}$  have to be zero-dimensional, as well  $(\mathbf{F} \odot \mathbf{B})_{sc}$ ,  $(\tilde{\mathbf{F}} \odot \tilde{\mathbf{B}})_{sc}$ ,  $\mathbf{G}_{nc} \cdot [\mathbf{F} \odot \mathbf{B}]_{nc}$  and  $\tilde{\mathbf{G}}_{nc} \cdot [\tilde{\mathbf{F}} \odot \tilde{\mathbf{B}}]_{nc}$  are zero-dimensional. This means that there was only a common part, for which  $(\mathbf{A}\mathbf{G})_c = (\tilde{\mathbf{A}}\tilde{\mathbf{G}})_c$ . Assumption **A2** provides  $\tilde{\mathbf{G}}_c = \mathbf{G}_c$ , and  $\tilde{\mathbf{A}}_c = \mathbf{A}_c$ . This proves identifiability with a probability larger than  $P_1(2d, N)$ .  $\square$

### 4.3.2 Method using the ZCM property

In [47], we proposed a method to identify continuous Constant Modulus (CM) sources. CM signals have unit norm and a uniformly distributed phase over  $[0, 2\pi[$ . The method in [47] uses the linearization technique presented in [12] to create a larger source matrix,  $\Psi$ , which contains all second-order cross-products of the different sources.

We then use an inductive argument to show that  $\Psi$  is full column rank with probability 1 as soon as the number of samples exceeds  $d(d+1)$ . Having this full rank matrix allows to conclude that the sources are identifiable.

Here we use the same methodology applied to Zero-CM (ZCM) sources. First, we recall the ZCM properties and distribution function, and we introduce a matrix  $\Psi$  that will contain all third-order cross-products of the sources. Next, we present a lemma that states the probability for  $\Psi$  to be full column rank, and we state the identifiability proposition based on this lemma.

We remind that the probability distribution function of a ZCM source  $s[n]$  is:

$$P(s[n] = 0) = P(|s[n]| = 1) = \frac{1}{2}$$

with a uniform probability over  $[0, 2\pi[$  for the phase distribution. We remind also Property 3.1.2 for a ZCM source  $s(t)$ :

$$(s^*s^2)[n] = s[n]$$

We consider a collection of stationary i.i.d. ZCM vectors  $\mathbf{s}[n]$ , with  $n \in \{1, \dots, N\}$ , with  $d$  entries:  $s_1[n]$  to  $s_d[n]$ . We denote by  $\Psi$  the  $N \times d^2(d+1)/2$  matrix constructed as:

$$\Psi = [\Psi_a | \Psi_b] \tag{4.9}$$

with:

$$\Psi_a = \left[ \begin{array}{ccc|ccc} s_1[1] & \dots & s_d[1] & (s_1^* s_1 s_2)[1] & \dots & (s_d^* s_d s_{d-1})[1] \\ \vdots & \vdots & \vdots & \vdots & \vdots & \vdots \\ s_1[N] & \dots & s_d[N] & (s_1^* s_1 s_2)[N] & \dots & (s_d^* s_d s_{d-1})[N] \end{array} \right]$$

$$\Psi_b = \left[ \begin{array}{ccc} (s_1^* s_2^2)[1] & \dots & (s_d^* s_{d-1}^2)[1] \\ \vdots & \vdots & \vdots \\ (s_1^* s_2^2)[N] & \dots & (s_d^* s_{d-1}^2)[N] \end{array} \right]$$

whose rows contain all the non redundant elements  $s_i^* s_j s_l[n]$ ,  $\forall \{i, j, l\} \in [1, \dots, d]^3$ ,  $\forall n \in [1, \dots, N]$ . The rows are sorted with the time index, the columns are sorted such that the elements for which  $i = j = l$  are placed first, then the elements with  $j \neq l$ , and lastly the elements such that  $j = l$ , and  $i \neq j$ .

Then, we state:

**Lemma 4.3.5** *Given a matrix  $\mathbf{S}$  of size  $d \times N$  with entries,  $s_i[n]$ , independent identically distributed ZCM samples. Assume that  $N > \frac{1}{2}d^2(d+1)$ , then the probability that the matrix  $\Psi$  has independent columns is larger than:*

$$\begin{cases} P_2(d, N) = P_\alpha(N) \left[ \prod_{i=1}^{d-2} P_T^{(i)}(N-d) \right] p_f, & \text{if } d > 2 \\ P_2(2, N) = p_f P_\alpha(N), & \text{otherwise} \end{cases}$$

where  $P_\alpha(N) = \prod_{i=1}^d \left[ 1 - \left( 1 - \frac{d-i+1}{2^{d-i+1}} \right)^{N-i+1} \right]$ , and

$$P_T^{(i)}(N) = \sum_{N_i=L_{d-i+1}}^{N-L_{d-i+1}} P_C(N_i, N-L_{d-i+1}) \prod_{j=1}^{L_{d-i+1}} p_0(N_i - j + 1)$$

with

$$\begin{aligned} L_{d-i+1} &= \sum_{j=1}^{i-1} l_{d-j+1}, \\ l_d &= d \left\lceil \frac{3d-1}{2} \right\rceil - 1, \\ P_C(N_a, N_b) &= \frac{1}{2^{N_a} (N_a - N_b)! N_b!}, \\ p_f &= \prod_{i=0}^2 \left( 1 - \left( \frac{3}{4} \right)^{N-d-i-L_3} \right), \\ p_0(N) &= 1 - 2^{-N}. \end{aligned}$$

Note that if  $N < d^2(d+1)/2$ , then  $\Psi$  is definitely not full column rank. The proof is given in Appendix A.

Now, let us state:

**Proposition 4.3.6** *Let  $\mathbf{s}[k]$ , for  $k = \{1, \dots, N\}$  be a collection of  $N$  i.i.d ZCM  $d$ -vectors with  $N > \frac{1}{2}d^2(d+1)$ . Assume that there is an invertible linear transformation  $\mathbf{T}$  such that  $\mathbf{y}(k) = \mathbf{T}\mathbf{s}(k)$ ,  $\forall k = 1, \dots, N$ , where all  $\mathbf{y}(k)$  are ZCM  $d$ -vectors as well. Then, with probability larger than  $P_2(d, N)$ ,  $\mathbf{T}$  is unique. In this case,  $\mathbf{T} = \mathbf{\Lambda}\mathbf{P}$ ,  $\mathbf{\Lambda}$  is a diagonal matrix with unit-norm entries and  $\mathbf{P}$  is a permutation.*

**Proof** It is sufficient to prove that each row of  $\mathbf{T}$  contains exactly one non zero element  $t_{ij}$ , which is unit norm:  $|t_{ij}| = 1$ . Since  $\mathbf{T}$  is invertible, it holds also for each column, so that these locations are different for each  $i$ .

From now, we consider separately each row of  $\mathbf{T}$ . Let  $\mathbf{t}_m$  be the  $m$ 'th row of  $\mathbf{T}$ , and let  $\mathbf{t}_m = [t_1, \dots, t_d]$ . Let  $y[k] = \mathbf{y}_m[k]$  be the  $m$ 'th element of  $\mathbf{y}[k]$ . Then  $\forall k \in \{1, \dots, N\}$ , we have

$$y[k] = \sum_{i=1}^d t_i s_i[k] \quad (4.10)$$

The ZCM property can be written as:  $\{y = 0, \text{ or } |y| = 1\}$ , which is equivalent to  $y(yy^* - 1) = 0$ , and  $y = |y|^2 y$ , which leads  $\forall k \in \{1, \dots, N\}$  to:

$$\sum_{l=1}^d t_l s_l[k] = \sum_{i,j,l=1}^d t_i^* t_j t_l s_i^*[k] s_j[k] s_l[k] \quad (4.11)$$

$$= \sum_{i=1}^d |t_i|^2 |s_i[k]|^2 s_i[k] + \sum_{\substack{1 \leq i \\ i \neq j \neq l}}^d 2t_i^* t_j t_l s_i^*[k] s_j[k] s_l[k] \quad (4.12)$$

where the last sum consider all the cross-products such the  $i \neq j$  and  $j \neq l$ . Denote:

$$\mathbf{p}^T = [t_1 (|t_1|^2 - 1), \dots, t_d (|t_d|^2 - 1), 2t_1^* t_1 t_2, \dots, 2t_d^* t_d t_{d-1}, t_1^* t_2^2, \dots, t_d^* t_{d-1}^2]$$

By linearizing (4.12), and using  $s_i^* s_i = s_i$ , we obtain:

$$\mathbf{\Psi} \mathbf{p} = \mathbf{0} \quad (4.13)$$

From Lemma 4.3.5, the probability that  $\mathbf{\Psi}$  is full column rank is larger than  $P_2(d, N)$ . Assuming that  $\mathbf{\Psi}$  is full column rank, the only solution is  $\mathbf{p} = \mathbf{0}$ .

Since  $\mathbf{T}$  is invertible, there is at least one non-zero element (say  $t_i$ ). Then  $\mathbf{p} = \mathbf{0}$  implies that:

$$\begin{cases} t_i (|t_i|^2 - 1) = 0 \\ t_i^* t_j^2 = 0, \quad \forall j \neq i \end{cases} \Rightarrow \begin{cases} |t_i| = 1 \\ t_j = 0, \quad \forall j \neq i \end{cases}$$

Two different rows cannot have their non-zero element in the same column because  $\mathbf{T}$  would not be a bijection. Thus the absolute value of  $\mathbf{T}$  is a permutation, and the identifiability holds with probability  $P_2(d, N)$ .  $\square$

We can now state the identifiability proposition:

**Proposition 4.3.7** *Under the assumptions **A1** to **A8**, for an observation duration  $N \geq d$ , given the matrix  $\mathbf{X}$ , the probability that the parameters  $\{\theta_i, g_i, f_i, i \in [1, \dots, d]\}$  are identifiable is larger than  $P_2'(d, N) = \left[1 - \left(\frac{3}{4}\right)^{N-1}\right]^d P_2(d, N)$ .*

**Proof** Assume there are two solutions to this problem:  $\Theta$  and  $\tilde{\Theta}$ . Then, equation (4.2) tells:

$$\mathbf{A} \cdot \mathbf{G} \cdot \mathbf{S} - \tilde{\mathbf{A}} \cdot \tilde{\mathbf{G}} \cdot \tilde{\mathbf{S}} = \mathbf{0}$$

where  $\mathbf{S} = [\mathbf{F} \odot \mathbf{B}]$  is a ZCM source. As the array is unambiguous and the DOAs are different (**A2** and **A3**),  $\mathbf{A}$  is full column rank. Multiply on the left side by the left inverse of  $\mathbf{A}$  and by the inverse of  $\mathbf{G}$  (**A8**), then:

$$\begin{aligned}\mathbf{S} &= \mathbf{G}^{-1} \mathbf{A}^\dagger \tilde{\mathbf{A}} \tilde{\mathbf{G}} \tilde{\mathbf{S}} \\ &= \mathbf{T} \tilde{\mathbf{S}}\end{aligned}$$

where  $\mathbf{T}$  is an invertible matrix, since the  $\mathbf{A}$  and  $\tilde{\mathbf{A}}$  were spanning the same subspace.

We recognize the situation of the previous Proposition, so with probability  $P_2(d, N)$ ,  $\mathbf{T}$  is a permutation multiplied by a diagonal matrix with unit-norm entries. We deduce the equality up to a permutation and a phase shift:  $\mathbf{S} = \tilde{\mathbf{S}}$ . Using the same argument as in the proof of Proposition 4.2.1, the equality of matrices  $\mathbf{A}$  and  $\tilde{\mathbf{A}}$  can be shown, and hence the equality of matrices  $\mathbf{G}$  and  $\tilde{\mathbf{G}}$ .

It remains to show that  $\mathbf{S} = \tilde{\mathbf{S}}$  implies the equality of the bits and the equality of the frequencies. By taking the absolute value of the equality of the sources we obtain the equality of the binary matrices:  $\mathbf{B} = \tilde{\mathbf{B}}$ . Then, for each source  $i \in \{1, \dots, d\}$ , we have:

$$\mathbf{f}_i \odot \mathbf{b}_i = \tilde{\mathbf{f}}_i \odot \mathbf{b}_i$$

where  $\mathbf{f}_i$  is the  $i$ -th row of  $\mathbf{F}$ . Assume now that we observe two consecutive samples such that  $\mathbf{b}_i[k] = \mathbf{b}_i[k+1] = 1$ , the probability that such an observation occurs is  $\left[1 - \left(\frac{3}{4}\right)^{N-1}\right]$ . Using the same argument as at the end of the proof of Proposition 4.2.1, we obtain the equality of the frequencies.  $\square$

### 4.3.3 Simulations

This section aims at determining to which measure Propositions 4.3.4 and 4.3.6 provide good lower bounds for the actual identifiability probability distribution.

In order to estimate the actual probability distribution, several independent realizations of  $\mathbf{F} \odot \mathbf{B}$  were randomly created by taking randomly a residual carrier and a data-stream. We ran one million independent realizations for the study. For each independent run, we estimated the minimal number of samples  $N$  required to have  $\mathbf{F} \odot \mathbf{B}$  of full row rank. After this collection of results, we performed a histogram to retrieve the probability distribution, which is denoted  $P_F(d, N)$ . As the previous demonstrations use the rank of the source matrices, it is interesting to compare them together.

In Figure 4.1, we compare the bounds for 5 sources with the estimated probability. While the binary bound is better than the ZCM bound, both proposed bounds are not tight, and may be far from the actual probability.

To see the convergence of the bounds, we plot in Figure 4.2 the complementary probability of figure 4.1 for 5 sources. It appears that the ZCM method has a steeper slope than the binary method, so for large numbers of samples, this method can provide a better bound.

Figure 4.3 presents the simulated complementary probability of identifiability. The number of sources varies from 2 to 10. We note that the identifiability reaches

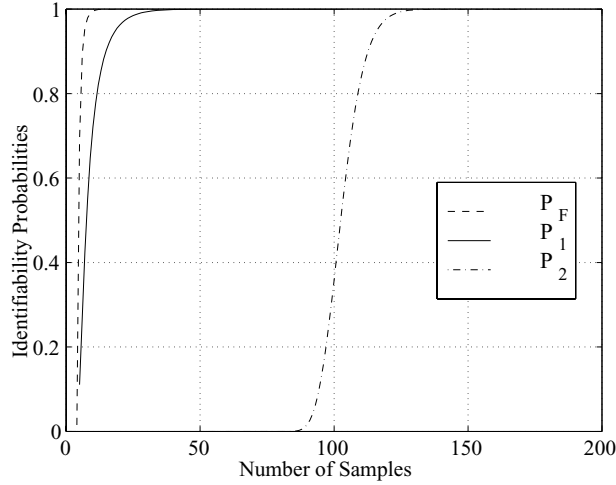


Figure 4.1: Actual probability distribution, and identifiability probabilities bounds as a function of the number of samples with 5 sources, for both cases.

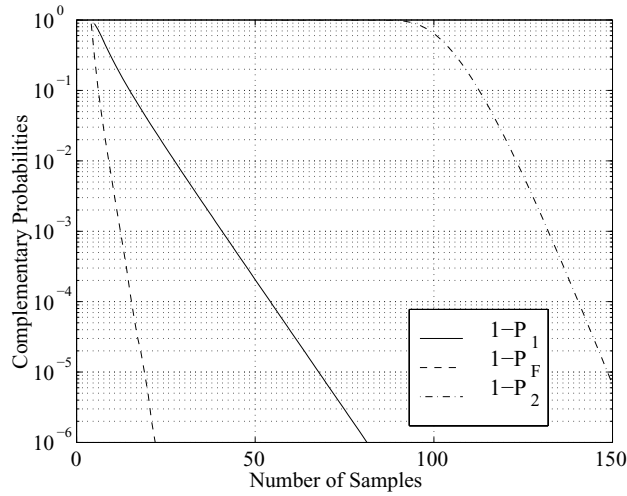


Figure 4.2: Complement of the probabilities of Figure 4.1: Actual probability distribution, and both bounds as a function of the number of samples with 5 sources.

very fast the complementary probability of  $10^{-2}$ , and that the slope of the curves are log-linear with the number of samples and sub-linear with the number of sources. It appears that 100000 Monte-Carlo runs is just sufficient to have probability precision below  $10^{-4}$ .

The results from Proposition 4.3.4 are computed and displayed in Figure 4.4.

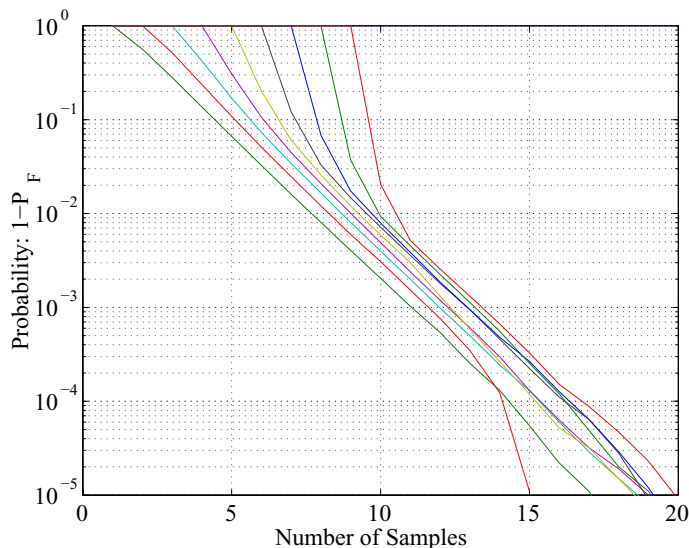


Figure 4.3: *Complement of the identifiability probability computed by simulating 100000 independent runs. The number of sources is from left to right 2 to 10.*

We note first that the number of samples to reach a complementary probability of  $10^{-2}$  is larger than in Figure 4.3. Second, the slopes of the curves become less steep for increasing  $d$  with the number of sources for  $d \geq 3$ .

The results from Proposition 4.3.6 are computed and displayed in Figure 4.5. The number of samples to reach  $1 - P_2 \leq 10^{-2}$  is even larger than with the previous bound. But the slope of the curves is independent of the number of sources, and indicates a behavior in  $10^{-0.12N}$ , which has a better slope than the previous bound.

To conclude, the validity of the bounds is not so good: for a small number of source ( $d$ ), the bound  $P_1$  is correct, but for large number of  $d$  none are good.

## 4.4 Conclusion

In this Chapter, we stated uniqueness propositions for the infinite sample case, and two different bounds for the finite sample case.

The gap between the identification failure probability curves obtained by simulation and the bounds issued by Proposition 4.3.4 and Proposition 4.3.6 demonstrates that the bounds for the finite case are loose, so finite sample identifiability is not a closed problem. One direction for future research could be to improve the final step of the Proof of Lemma 4.3.5.

The assumptions made in this Chapter are mainly relevant to the body part of the mode S sources. We note that for a mixture of 5 overlapping sources, the complementary probability is bounded by  $10^{-4}$  for short mode S (56 samples for



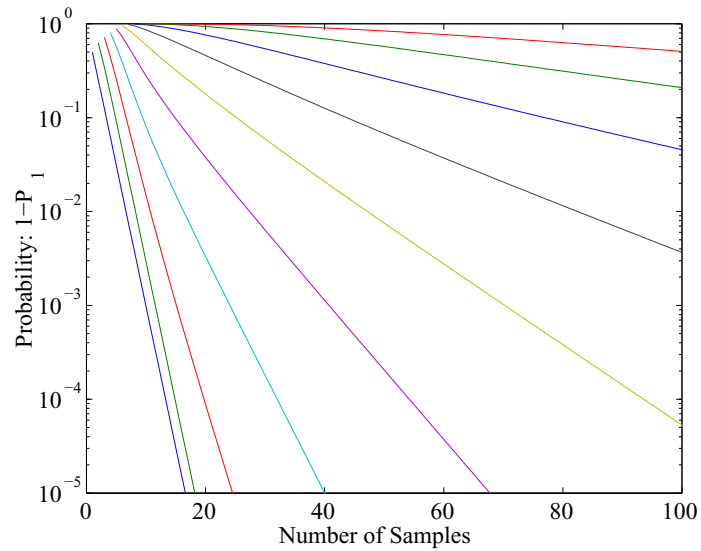


Figure 4.4: *Complementary of the identifiability probability for the binary method. The number of sources are from left to right 2 to 10*

the body), and for long mode S, the bound is below  $10^{-6}$ . We can conclude that the most relevant case, with less than 5 sources, the sources will be “almost surely” identifiable.

While not investigated in this Chapter, one can perhaps show that partly overlapping sources need less samples for a similar probability of uniqueness. This can be a future subject for research.

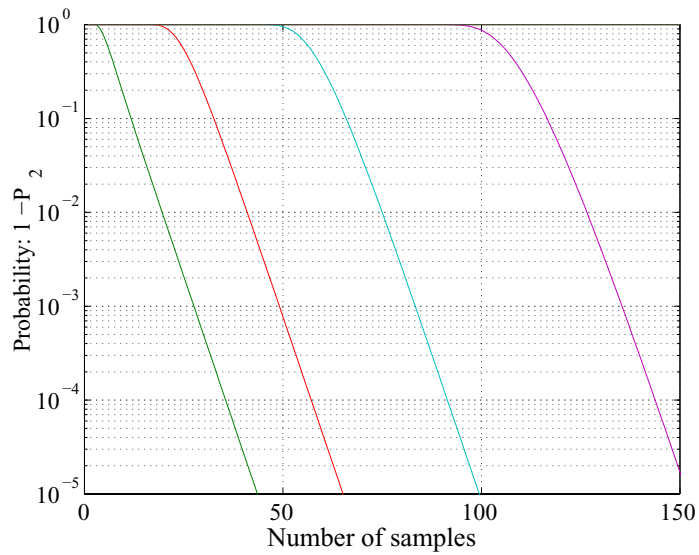


Figure 4.5: Complement of the identifiability probability for the binary method. Here, only the probabilities for 2 to 5 sources are presented.

## Chapter 5

# Cramer-Rao Bounds

After ensuring that an estimation problem has a unique solution in the noise-free case or at least asymptotically, the logical next step is to determine what can be the best result one can obtain in the presence of noise. Indeed, any unbiased estimator of any unknown variable includes some estimation error. The variance of this error is bounded by its Cramer-Rao bound (CRB) [48], which is independent from the estimation algorithm, and depends only on the data model. The difference between the variance and the Cramer-Rao bound is an indication of the quality of this estimator. Note that identifiability ensures that the CRB is finite.

In this chapter, we derive the CRB of the SSR problem for the data model described in Chapter 3. First, we recall the definition of the CRB and our model. We then present the result of our derivations, and the last section presents some simulations.

### 5.1 Introduction

First, we review the general definition of the CRB, then we recall the data model used.

#### 5.1.1 Definition of Cramer-Rao Bound

Consider the data model  $\mathbf{X} = \mathbf{S}(\boldsymbol{\lambda}) + \mathbf{N}$ , where  $\boldsymbol{\lambda}$  is a real-valued parameter vector, and  $\mathbf{N}$  is a complex Gaussian noise matrix with independent identically distributed entries. The matrices are of size  $M \times N$ :  $M$  sensors and  $N$  samples. Define the Fisher Information Matrix, FIM, as in [48], and denote it by  $\mathcal{I}(\boldsymbol{\lambda})$ . The  $(i, j)$ -th entry of  $\mathcal{I}(\boldsymbol{\lambda})$  is defined by:

$$[\mathcal{I}(\boldsymbol{\lambda})]_{ij} \stackrel{\text{def}}{=} -\mathbb{E}_{\mathbf{X}/\boldsymbol{\lambda}} \left\{ \frac{\partial^2 \ln p(\mathbf{X}|\boldsymbol{\lambda})}{\partial \lambda_i \partial \lambda_j} \right\} = \mathbb{E}_{\mathbf{X}/\boldsymbol{\lambda}} \left\{ \frac{\partial \ln p(\mathbf{X}|\boldsymbol{\lambda})}{\partial \lambda_i} \cdot \frac{\partial \ln p(\mathbf{X}|\boldsymbol{\lambda})}{\partial \lambda_j} \right\} \quad (5.1)$$

where the likelihood function  $p(\mathbf{X}|\boldsymbol{\lambda})$  is the probability density of  $\mathbf{X}$  given  $\boldsymbol{\lambda}$ , for our data model:

$$p(\mathbf{X}|\boldsymbol{\lambda}) = [\pi\sigma^2]^{-MN} \cdot \exp \left\{ -\text{trace} \left\{ \frac{1}{\sigma^2} [\mathbf{X} - \mathbf{S}(\boldsymbol{\lambda})]^H [\mathbf{X} - \mathbf{S}(\boldsymbol{\lambda})] \right\} \right\} \quad (5.2)$$

$$= [\pi\sigma^2]^{-MN} \cdot \exp \left\{ -\sum_{k=1}^N \frac{1}{\sigma^2} [\mathbf{x}[k] - \mathbf{s}[k](\boldsymbol{\lambda})]^H [\mathbf{x}[k] - \mathbf{s}[k](\boldsymbol{\lambda})] \right\} \quad (5.3)$$

For a given  $\mathbf{X}$ , any unbiased estimator  $\hat{\boldsymbol{\lambda}}(\mathbf{X})$  of  $\boldsymbol{\lambda}$  is a random variable and its variance is lower bounded by its Cramer-Rao Bound (CRB). For the  $i^{\text{th}}$  element of  $\boldsymbol{\lambda}$ , this bound is the  $i^{\text{th}}$  diagonal element of the inverse of the Fisher Information Matrix (viz. [48]), assuming the inverse exists:

$$\text{Var}(\hat{\boldsymbol{\lambda}}_i) \geq \text{CRB}(\boldsymbol{\lambda}_i) = [\mathcal{I}^{-1}(\boldsymbol{\lambda})]_{ii}$$

We present the next Lemma, as it is useful for later derivations.

**Lemma 5.1.1** *Consider the data model  $\mathbf{X} = \mathbf{S}(\boldsymbol{\lambda}) + \mathbf{N}$ , where  $\boldsymbol{\lambda}$  is a real-valued parameter vector and  $\mathbf{N}$  is white i.i.d complex Gaussian noise with known variance  $\sigma^2$ . The  $(i, j)$  entry of the corresponding FIM is:*

$$\begin{aligned} [\mathcal{I}(\boldsymbol{\lambda})]_{ij} &= \frac{2}{\sigma^2} \sum_{k=1}^N \text{Re} \left\{ \left( \frac{\partial \mathbf{s}[k]}{\partial \boldsymbol{\lambda}_i} \right)^H \cdot \left( \frac{\partial \mathbf{s}[k]}{\partial \boldsymbol{\lambda}_j} \right) \right\} \\ &= \frac{2}{\sigma^2} \text{Re} \left\{ \text{Tr} \left\{ \left( \frac{\partial \mathbf{S}}{\partial \boldsymbol{\lambda}_i} \right)^H \cdot \frac{\partial \mathbf{S}}{\partial \boldsymbol{\lambda}_j} \right\} \right\} \end{aligned} \quad (5.4)$$

where  $\mathbf{s}[k]$  is the  $k$ -th column of  $\mathbf{S}$  corresponding to the time sample  $k$ .

**Proof:** The first derivative of (5.3) with respect to  $\boldsymbol{\lambda}_i$  results in:

$$\frac{\partial \ln p(\mathbf{X}|\boldsymbol{\lambda})}{\partial \boldsymbol{\lambda}_i} = \frac{1}{\sigma^2} \sum_{k=1}^N \left[ \mathbf{n}^H[k] \cdot \frac{\partial \mathbf{s}[k]}{\partial \boldsymbol{\lambda}_i} + \frac{\partial \mathbf{s}^H[k]}{\partial \boldsymbol{\lambda}_i} \cdot \mathbf{n}[k] \right] \quad (5.5)$$

A complex Gaussian distribution is circularly symmetric, so the expectation of odd order terms is zero:

$$\forall \{i, j, k\} \in \mathbb{N}^3 \quad \begin{cases} \mathbb{E} \{ \mathbf{n}^H[i] \mathbf{n}[j] \mathbf{n}[k] \} = 0 \\ \mathbb{E} \{ \mathbf{n}[i] \} = 0 \end{cases}$$

The product of the first derivatives yields the result.  $\square$

Let  $p$  be the size of the parameter vector  $\boldsymbol{\lambda}$ , and define the matrix containing the derivative at the time  $k \in \{1, \dots, N\}$ :

$$\mathbf{D}_k(\boldsymbol{\lambda}) = \left[ \begin{array}{c|c|c} \frac{\partial \mathbf{s}[k]}{\partial \boldsymbol{\lambda}_1} & \dots & \frac{\partial \mathbf{s}[k]}{\partial \boldsymbol{\lambda}_p} \end{array} \right]$$

then from (5.4), the Fisher Information matrix,  $\mathcal{I}(\boldsymbol{\lambda})$  is:

$$\mathcal{I}(\boldsymbol{\lambda}) = \frac{2}{\sigma^2} \text{Re} \left\{ \sum_{k=1}^N \mathbf{D}_k^H(\boldsymbol{\lambda}) \mathbf{D}_k(\boldsymbol{\lambda}) \right\} \quad (5.6)$$

### 5.1.2 Modeling

We recall the SSR data model from the description of Equation (3.9):  $\mathbf{X}$  is the received signal matrix ( $M \times N$ ), which depends on the parameter vector  $\boldsymbol{\lambda} = \{\theta_i, g_i, f_i; 1 \leq i \leq d; \mathbf{B}\}$ :

$$\mathbf{X} = \mathbf{A} \cdot \mathbf{G} \cdot [\mathbf{F} \odot \mathbf{B}] + \mathbf{N}$$

where:

- The array response  $\mathbf{A}$  depends only on the DOAs:  $\theta_i, i \in \{1, \dots, d\}$ .
- The gain matrix depends only on the source powers and initial phases:  $g_i, i \in \{1, \dots, d\}$ . We characterize the diagonal matrix  $\mathbf{G}$  by:  $\mathbf{G}_{ii} = \mathbf{g}_i \stackrel{\text{def}}{=} \rho_i \Psi_{ii}$  with  $\rho_i$  the norm of  $\mathbf{g}_i$ :  $\rho_i = |\mathbf{g}_i|$ , and  $\Psi = \text{diag}[\psi_1, \dots, \psi_d]$  is a diagonal matrix with unit-norm entries such that the diagonal elements contain the initial phases:  $\Psi_{ii}$ .
- The frequency matrix  $\mathbf{F}$  depends only on the residual frequencies:  $f_i, i \in \{1, \dots, d\}$ . Recall that  $\phi_i = \exp(2\pi j f_i T)$ , and  $\Phi = \text{diag}[\phi_1, \dots, \phi_d]$ .
- The binary source signal  $\mathbf{B}$  contains the data-stream :  $b_i[k], i \in \{1, \dots, d\}, k \in \{1, \dots, N\}$ , we assume the binary distribution to have an i.i.d equiprobable outcome out of  $\{0, 1\}$ , so its covariance is:

$$\mathbf{R}_{bb} = \frac{1}{4} (\mathbf{1}\mathbf{1}^T + \mathbf{I})$$

The noise matrix  $\mathbf{N}$  is complex Gaussian, independent identically distributed, and spatially white with identical variance. This noise mainly originates from the thermal noise of the receiver, so we assume we know  $\sigma^2$ .

## 5.2 Cramer-Rao Bounds

In this section, the CRB is derived in various cases. Indeed, the CRB depends on the hypothesis made, and the ‘‘a priori’’ knowledge on the data. The following cases will be under investigation:

- Case  $\alpha$  : Deterministic known  $\mathbf{B}$ .
- Case  $\beta$  : Stochastic  $\mathbf{B}$ .
- Case  $\gamma$  : Deterministic unknown  $\mathbf{B}$ .

We first study the deterministic cases, then the stochastic case.

### 5.2.1 Case $\alpha$ : Deterministic known $\mathbf{B}$

In this subsection, we consider that we know the binary signal matrix  $\mathbf{B}$  with entries  $b_i[k]$ . This strong assumption is relevant in the context of high SNR, because the detection of the bits ( $\{0, 1\}$ ) appears to be almost perfect under these conditions of operation. One consequence is that we consider a reduced parameter vector  $\boldsymbol{\lambda}$ .

Define the following notation:

$$\begin{aligned}\mathbf{D}_A &= \left[ \frac{\partial \mathbf{a}}{\partial \theta}(\theta_1) \cdots \frac{\partial \mathbf{a}}{\partial \theta}(\theta_d) \right] \\ \mathbf{G} &= \text{diag}(\boldsymbol{\rho}) \cdot \boldsymbol{\Psi} \\ \mathbf{C}_T &= j2\pi T [1 \cdots 1]^T \cdot [0 \ 1 \cdots N-1] \\ \mathbf{S} &= \mathbf{F} \odot \mathbf{B}\end{aligned}$$

and we order our parameter vector as:

$$\boldsymbol{\lambda} = [\theta_1, \cdots, \theta_d, f_1, \cdots, f_d, \rho_1, \cdots, \rho_d, \psi_1, \cdots, \psi_d]^T \quad (5.7)$$

**Proposition 5.2.1** *With known binary signal, the FIM for our data model is:*

$$\mathcal{I}_\alpha = \frac{2}{\sigma^2} \begin{bmatrix} \mathbf{I}_{\theta\theta} & \mathbf{I}_{\theta f} & \mathbf{I}_{\theta\rho} & \mathbf{I}_{\theta\psi} \\ \mathbf{I}_{f\theta}^T & \mathbf{I}_{ff} & \mathbf{I}_{f\rho} & \mathbf{I}_{f\psi} \\ \mathbf{I}_{\rho\theta}^T & \mathbf{I}_{\rho f}^T & \mathbf{I}_{\rho\rho} & \mathbf{I}_{\rho\psi} \\ \mathbf{I}_{\psi\theta}^T & \mathbf{I}_{\psi f}^T & \mathbf{I}_{\psi\rho}^T & \mathbf{I}_{\psi\psi} \end{bmatrix} \quad (5.8)$$

where:

$$\begin{aligned}\mathbf{I}_{\theta\theta} &= \text{Re} \left\{ (\mathbf{GSS}^H \mathbf{G}^H) \odot (\mathbf{D}_A^H \mathbf{D}_A)^* \right\} \\ \mathbf{I}_{ff} &= \text{Re} \left\{ (\mathbf{G}(\mathbf{C}_T \odot \mathbf{S})(\mathbf{C}_T \odot \mathbf{S})^H \mathbf{G}^H) \odot (\mathbf{A}^H \mathbf{A})^* \right\} \\ \mathbf{I}_{\theta f} &= \text{Re} \left\{ (\mathbf{GS}(\mathbf{C}_T \odot \mathbf{S})^H \mathbf{G}^H) \odot (\mathbf{D}_A^H \mathbf{A})^* \right\} \\ \mathbf{I}_{\rho\rho} &= \text{Re} \left\{ (\boldsymbol{\Psi} \mathbf{SS}^H \boldsymbol{\Psi}^H) \odot (\mathbf{A}^H \mathbf{A})^* \right\} \\ \mathbf{I}_{\theta\rho} &= \text{Re} \left\{ (\mathbf{GSS}^H \boldsymbol{\Psi}^H) \odot (\mathbf{D}_A^H \mathbf{A})^* \right\} \\ \mathbf{I}_{f\rho} &= \text{Re} \left\{ [(\mathbf{G}(\mathbf{C}_T \odot \mathbf{S}))(\boldsymbol{\Psi} \mathbf{S})^H] \odot (\mathbf{A}^H \mathbf{A})^* \right\} \\ \mathbf{I}_{\psi\psi} &= \text{Re} \left\{ [(\mathbf{GS})(\mathbf{GS})^H] \odot (\mathbf{A}^H \mathbf{A})^* \right\} \\ \mathbf{I}_{\theta\psi} &= \text{Re} \left\{ j [(\mathbf{GS})(\mathbf{GS})^H] \odot (\mathbf{D}_A^H \mathbf{A})^* \right\} \\ \mathbf{I}_{f\psi} &= \text{Re} \left\{ j [(\mathbf{G}(\mathbf{C}_T \odot \mathbf{S}))(\mathbf{GS})^H] \odot (\mathbf{A}^H \mathbf{A})^* \right\} \\ \mathbf{I}_{\rho\psi} &= \text{Re} \left\{ j [(\boldsymbol{\Psi} \mathbf{S})(\mathbf{GS})^H] \odot (\mathbf{A}^H \mathbf{A})^* \right\}\end{aligned}$$

**Proof:** We present the derivation for  $\mathbf{I}_{\theta\rho}$ ; the other submatrices have similar derivations. Recall:

$$\mathbf{s}[k] = \sum_{i=1}^d \mathbf{a}(\theta_i) g_i \phi_i^k b_i[k]$$

then:

$$\begin{aligned}\sum_{k=1}^N \left( \frac{\partial \mathbf{s}[k]}{\partial \theta_i} \right)^H \left( \frac{\partial \mathbf{s}[k]}{\partial \rho_j} \right) &= \sum_{k=1}^N \left[ (g_i \phi_i^k b_i[k])^* \left( \frac{\partial \mathbf{a}}{\partial \theta}(\theta_i) \right)^H \right] [\mathbf{a}(\theta_j) \psi_j \phi_j^k b_j[k]] \\ &= \left( \frac{\partial \mathbf{a}}{\partial \theta}(\theta_i) \right)^H \mathbf{a}(\theta_j) \cdot \sum_{k=1}^N (g_i \phi_i^k b_i[k])^* \psi_j \phi_j^k b_j[k] \\ &= \left( \frac{\partial \mathbf{a}}{\partial \theta}(\theta_i) \right)^H \mathbf{a}(\theta_j) \cdot g_i^* [\mathbf{F} \odot \mathbf{B}]_i^* [\mathbf{F} \odot \mathbf{B}]_j^T \psi_j \\ &= (\mathbf{D}_A^H \mathbf{A})_{ij} \cdot (\mathbf{G}^* [\mathbf{F} \odot \mathbf{B}]^* [\mathbf{F} \odot \mathbf{B}]^T \boldsymbol{\Psi})_{ij}\end{aligned}$$

where  $[\mathbf{F} \odot \mathbf{B}]_i$  denotes the  $i$ -th row of  $[\mathbf{F} \odot \mathbf{B}]$ . It eventually follows from Lemma 5.1.1 that:

$$\mathbf{I}_{\theta\rho} = \frac{2}{\sigma^2} \text{Re} \left\{ (\mathbf{D}_A^H \mathbf{A})^* \odot (\mathbf{GSS}^H \Psi^H) \right\}$$

□

### 5.2.2 Case $\beta$ : Stochastic B

In this subsection, we consider the binary symbols as unwanted parameters with a known probability distribution. Using the binary probability distribution, we derive a stochastic CRB under the assumption that the SNR of each source is high enough. Requiring high SNR is an acceptable condition given the SSR situation. The precise assumption is that the singular values of  $(\mathbf{A}\mathbf{G})$  are one order of magnitude larger than  $M$  times the noise standard deviation. Note that we are again concerned with a reduced vector  $\boldsymbol{\lambda}$  without the binary information as in Equation (5.7).

**Proposition 5.2.2** Define the Töplitz matrix  $\mathbf{C}_B^{(d)} = \frac{1}{4} (\mathbf{1}_{d \times 1} \mathbf{1}_{d \times 1}^T + \mathbf{I}_d)$ , and define:

$$\mathbf{C}_B^D = (\mathbf{1}_{4 \times 1} \mathbf{1}_{4 \times 1}^T) \otimes \mathbf{C}_B^{(d)} = \begin{bmatrix} \mathbf{C}_B^{(d)} & \mathbf{C}_B^{(d)} & \mathbf{C}_B^{(d)} & \mathbf{C}_B^{(d)} \\ \mathbf{C}_B^{(d)} & \mathbf{C}_B^{(d)} & \mathbf{C}_B^{(d)} & \mathbf{C}_B^{(d)} \\ \mathbf{C}_B^{(d)} & \mathbf{C}_B^{(d)} & \mathbf{C}_B^{(d)} & \mathbf{C}_B^{(d)} \\ \mathbf{C}_B^{(d)} & \mathbf{C}_B^{(d)} & \mathbf{C}_B^{(d)} & \mathbf{C}_B^{(d)} \end{bmatrix}$$

assuming that each source has a high SNR, the stochastic Fisher Information Matrix for estimating  $\boldsymbol{\lambda}$  is:

$$\mathcal{I}_\beta(\boldsymbol{\lambda}) = \mathcal{I}_\delta(\boldsymbol{\lambda}) \odot \mathbf{C}_B^D \quad (5.9)$$

where  $\mathcal{I}_\delta(\boldsymbol{\lambda})$  is the FIM for known binary sources all equal to 1:  $b_i[k] = 1, \forall i \in \{1, \dots, d\}$ , and  $\forall k \in \{1, \dots, N\}$ , given by  $\mathcal{I}_\alpha$  for  $\mathbf{S} = \mathbf{F}$ .

The complexity of computing  $\mathcal{I}_\beta$  is of the same order as computing  $\mathcal{I}_\alpha$ . The proof uses the following lemma, and is presented next to it.

**Lemma 5.2.3** Define the simplified model at a time  $k$ :  $\mathbf{x}[k] = \mathbf{M}[k] \mathbf{b}[k] + \mathbf{n}[k]$ , where  $\mathbf{M}[k]$  is the “mixing matrix”, with  $\mathbf{m}^i[k]$  the column of  $\mathbf{M}[k]$  that contains the  $i$ -th parameter  $\lambda_i$  of  $\boldsymbol{\lambda}$ . further define the function  $\delta_s(i-j)$  to be equal to 1 if the parameters  $\lambda_i$  and  $\lambda_j$  correspond to the same source, 0 otherwise<sup>1</sup>.

Assume that the norms of the  $\mathbf{m}^i[k]$  are well above the noise level, then the stochastic  $(i, j)$  entry of FIM is:

$$\mathcal{I}_{i,j}^\beta = \frac{2}{\sigma^2} \left( \frac{1}{4} + \frac{\delta_s(i-j)}{4} \right) \text{Re} \left\{ \sum_{k=1}^N \frac{\partial \mathbf{m}^i[k]}{\partial \lambda_i}^H \frac{\partial \mathbf{m}^j[k]}{\partial \lambda_j} \right\} \quad (5.10)$$

<sup>1</sup>e.g. equal to 1 for  $\lambda_i = f_3$  and  $\lambda_j = \theta_3$ ; 0 for  $\lambda_i = f_3$  and  $\lambda_j = g_1$ .

Since the proof of the Lemma is long, it is postponed to Appendix B.2.

The proof of the proposition 5.2.2 consists only of recognizing in the result of the lemma that the real part is equal to the definition given by Lemma 5.1.1 for a source mixture of sinusoidal (e.g. the bits are all equal to 1). Thus, the term inside the real part is the  $(i, j)$  entry of the FIM  $\mathcal{I}_\delta$ . As we recognize in the first term the entry of  $(i, j)$  entry of  $\mathbf{C}_B^D$ , we conclude that the two matrices are point-wise multiplied.

### 5.2.3 Case $\gamma$ : Deterministic unknown $\mathbf{B}$

In this subsection, we consider the binary signal as an unknown desired parameter. To overcome the fact that the binary signal is based only on a discrete set, and thus non-differentiable, we consider here that the binary signal is a real continuous variable in order to allow the computation of the derivative as a continuous parameter. This hypothesis makes sense considering that the signal is not exactly taken from a discrete set due to the imperfections of the transmitter (or equivalently, we could intellectually consider two very thin Gaussian distributions centered on  $\{0, 1\}$ , which is equivalent to adding a small Gaussian noise).

**Proposition 5.2.4** *Order the parameter vector as:*

$$\boldsymbol{\lambda} = [\mathbf{b}^T[1], \dots, \mathbf{b}^T[N], \theta_1, \dots, \theta_d, f_1, \dots, f_d, |g_1|, \dots, |g_d|, \psi_1, \dots, \psi_d]^T$$

where  $\mathbf{b}[k]$  is the output of the binary sources at time instant  $k$ . Define the following matrices, with  $k \in \{1, \dots, N\}$ :

$$\begin{aligned} \mathbf{H}_k &\stackrel{\text{def}}{=} \text{Re} \{ \Phi^{-k} \mathbf{G}^* \mathbf{A}^H \mathbf{A} \mathbf{G} \Phi^k \} \\ \mathbf{B}[k] &\stackrel{\text{def}}{=} \text{diag} \{ \mathbf{b}[k] \} \\ \mathbf{I}_{\mathbf{b}[k]\theta} &\stackrel{\text{def}}{=} \text{Re} \{ \Phi^{-k} \mathbf{G}^* \mathbf{A}^H \mathbf{D}_A \mathbf{G} \Phi^k \mathbf{B}[k] \} \\ \mathbf{I}_{\mathbf{b}[k]f} &\stackrel{\text{def}}{=} \text{Re} \{ j 2\pi k T \Phi^{-k} \mathbf{G}^* \mathbf{A}^H \mathbf{A} \mathbf{G} \Phi^k \mathbf{B}[k] \} \\ \mathbf{I}_{\mathbf{b}[k]\rho} &\stackrel{\text{def}}{=} \text{Re} \{ \Phi^{-k} \mathbf{G}^* \mathbf{A}^H \mathbf{A} \Psi \Phi^k \mathbf{B}[k] \} \\ \mathbf{I}_{\mathbf{b}[k]\psi} &\stackrel{\text{def}}{=} \text{Re} \{ j \Phi^{-k} \mathbf{G}^* \mathbf{A}^H \mathbf{A} \mathbf{G} \Phi^k \mathbf{B}[k] \} \\ \mathbf{I}_k &\stackrel{\text{def}}{=} \left[ \begin{array}{c|ccc} \mathbf{I}_{\mathbf{b}[k]\theta} & & & \\ & \mathbf{I}_{\mathbf{b}[k]f} & & \\ & & \mathbf{I}_{\mathbf{b}[k]\rho} & \\ & & & \mathbf{I}_{\mathbf{b}[k]\psi} \end{array} \right] \end{aligned}$$

where the  $\mathbf{I}_k$ 's are  $d \times 4d$  matrices. The FIM is then:

$$\mathcal{I}_\gamma = \frac{2}{\sigma^2} \left[ \begin{array}{ccc|ccc} \mathbf{H}_1 & & \mathbf{0} & & & \mathbf{I}_1 \\ & \ddots & & & & \vdots \\ \mathbf{0} & & \mathbf{H}_N & & & \mathbf{I}_N \\ \hline \mathbf{I}'_1 & \dots & \mathbf{I}'_N & & & \mathcal{I}_\alpha \end{array} \right]$$

The proof is not provided since it is a direct calculation.

The various CRBs are the diagonal elements of the inverse of the FIM, which results in this case in a  $(N + 4d)$  square matrix. This might be a too large matrix to invert due to computational cost, however we can use the Schur complement theorem (see Appendix B.1) on  $\mathcal{I}_\gamma$  to get the next proposition:



**Proposition 5.2.5** *Define:*

$$\begin{aligned}\mathbf{B}' &= \mathcal{I}_\alpha - \sum_{k=1}^N \mathbf{A}_k^T \mathbf{H}_k^{-1} \mathbf{A}_k \\ \mathbf{O}_{ij} &= \mathbf{H}_i^{-1} \mathbf{A}_i \mathbf{B}'^{-1} \mathbf{A}_j^T \mathbf{H}_j^{-1}\end{aligned}$$

assuming that  $\mathcal{I}_\alpha$ , the  $\mathbf{H}_k$ 's, and then  $\mathcal{I}_\gamma$  are invertible. The inverse of  $\mathcal{I}_\gamma$  is:

$$\mathcal{I}_\gamma^{-1} = \left[ \begin{array}{ccc|c} \mathbf{H}_1^{-1} + \mathbf{O}_{11} & & \mathbf{O}_{1N} & -\mathbf{H}_1^{-1} \mathbf{A}_1 \mathbf{B}'^{-1} \\ & \ddots & & \vdots \\ \mathbf{O}_{N1} & & \mathbf{H}_N^{-1} + \mathbf{O}_{NN} & -\mathbf{H}_N^{-1} \mathbf{A}_N \mathbf{B}'^{-1} \\ \hline -\mathbf{B}'^{-1} \mathbf{A}_1^T \mathbf{H}_1^{-1} & \dots & -\mathbf{B}'^{-1} \mathbf{A}_N^T \mathbf{H}_N^{-1} & \mathbf{B}'^{-1} \end{array} \right] \quad (5.11)$$

Since we are interested only in the diagonal elements of the inverse, this formulation allows us to save some computations.

## 5.3 Simulations

In order to check the quality of the bounds, we compare the various Cramer-Rao Bounds. The deterministic bounds are different for each new realization of  $\mathbf{B}$ . The stochastic bound incorporates the knowledge of the statistic of  $\mathbf{B}$ , so no realization are needed. The goal of this section is to determine if we can use one bound for the other (we don't know the matrix  $\mathbf{B}$  beforehand, so it is more practical to use the stochastic bound).

The simulations are based on 200 independent runs, where the parameters are fixed but the binary matrix  $\mathbf{B}$  and the noise matrix  $\mathbf{N}$  are varied randomly. We compare the Cramer-Rao bounds corresponding to the cases  $\beta$ , and  $\alpha$ . The scenario consists of  $d = 2$  sources impinging on an array of  $M = 4$  elements with directions  $\{80, 100\}$  degrees, and with residual carriers  $\pm 0.02T$  (i.e.  $\pm 10$  kHz). The SNR was 30 dB per source, and the number of samples was  $N = 100$ . We present two different simulations; in the first one, the number of samples varies from 64 to 32768 by a power of 2, and in the second one, the SNR varies from 0 dB to 60 dB.

For case  $\alpha$ , we show the average of 200 independent runs.

Figure 5.1 and 5.2 show the CRBs for  $\theta$  and  $f$  as function of  $N$ , with a SNR of 30 dB. From Figures 5.1 and 5.2, we note the closeness of both methods, which indicates that the stochastic and the deterministic CRBs can be exchanged. The only case where the CRBs differ, is at small numbers of samples, which is not surprising since the CRBs are by definition valid for large SNRs and number of samples.

Figure 5.3 and 5.4 show the CRBs for  $\theta$  and  $f$  as function of SNR, with  $N = 100$ : also the two bounds give the same result.

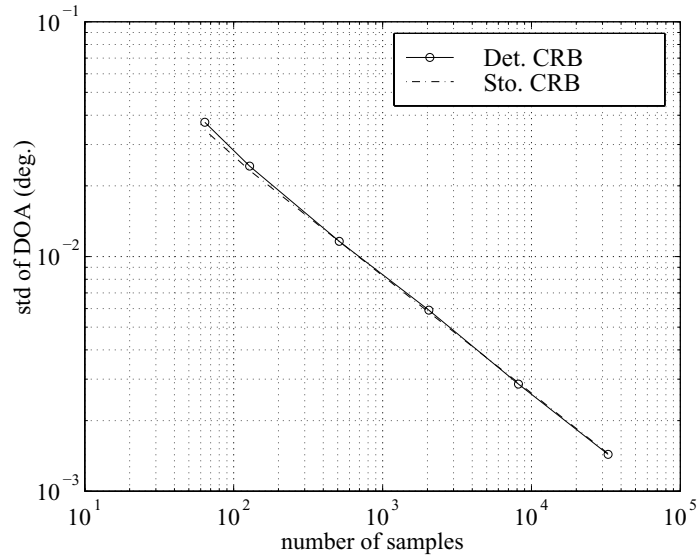


Figure 5.1: Standard deviation of the DOA as function of the number of samples for the CRB bound  $\alpha$  and  $\beta$ .

## 5.4 Conclusion

In this chapter, we have presented Cramer-Rao Bounds for three cases: deterministic known  $\mathbf{B}$ , deterministic unknown  $\mathbf{B}$ , stochastic  $\mathbf{B}$ . The simulations have shown good agreement between the CRBs for deterministic known  $\mathbf{B}$  and stochastic  $\mathbf{B}$ . Thus in the latter simulations, we will compare the algorithms with the stochastic CRB only, as it is simpler to compute.

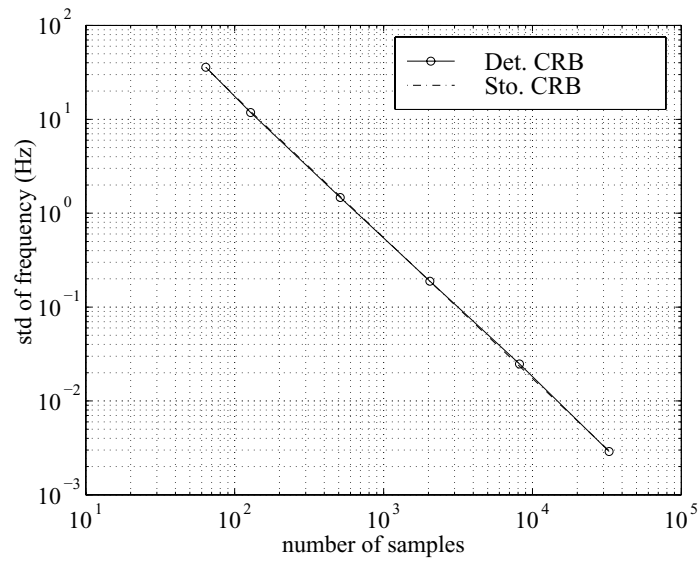


Figure 5.2: Standard deviation of the residual frequency as function of the number of samples for the stochastic CRB bound  $\alpha$  and  $\beta$ .

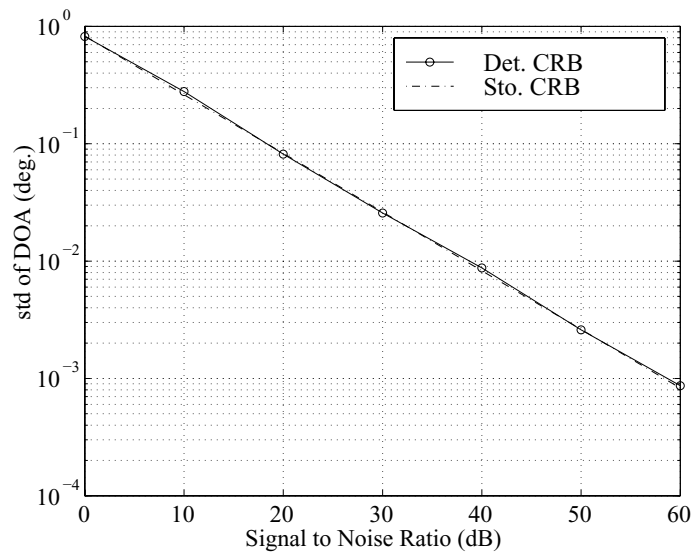


Figure 5.3: Standard deviation of the DOA as function of the SNR for the stochastic CRB bound  $\alpha$  and  $\beta$ .

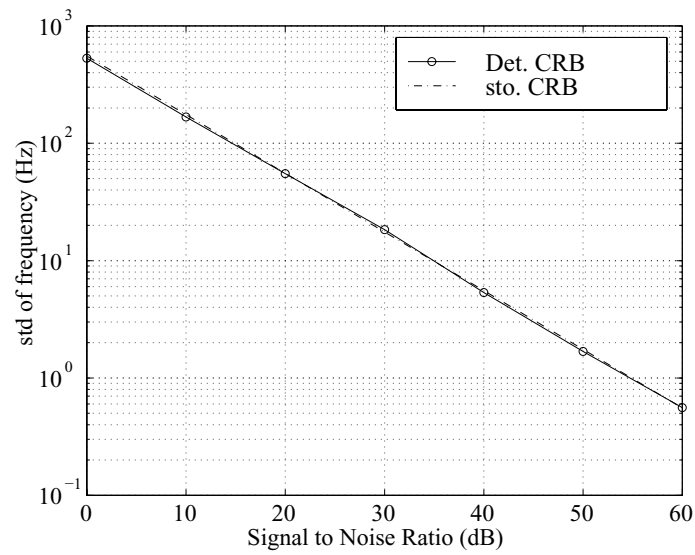


Figure 5.4: Standard deviation of the residual frequency as function of the SNR for the stochastic CRB bound  $\alpha$  and  $\beta$ .

## Chapter 6

# Algorithms

The goal of this thesis is to study how SSR replies can be separated using algebraic techniques. In the previous chapters, we defined the problem and its relevance, we studied identifiability —is it possible to solve the problem?—, and we considered the Cramer-Rao Bounds —what would be the quality of the best estimators? The next step is to give practical solutions.

In this Chapter, we propose and define algorithms to separate the replies and estimate their parameters. One conclusion of Chapter 3 is that the SSR sources are rich in structure, therefore many different properties may be used. Each section in this Chapter will focus on a specific property of the SSR sources and thus will lead to a different algorithm. In section 6.2, we exploit Properties 3.1.2: the sources have a Zero-Constant Modulus. These properties lead to the already existing algorithm AZCMA by Van der Veen [21], and the improved multi-shift ZCMA. In Section 6.3, we use Correlation Property 3.2.1 to extend the SOBI algorithm to a new algorithm called ESPRIT-SOBI. Lastly, section 6.4 presents an algorithm that uses the data Manchester Encoding of the different modes, based on Properties 3.1.1. But first we recall the model, propose a simplified version, and recall some algebraic results.

### 6.1 The problem statement and useful results

#### 6.1.1 The problem statement

For the convenience of the reader, we recall the signal model from Chapter 3.

We have a scenario where an array of  $M$  elements receives  $d$  SSR sources. We denote by  $T$  the sampling period, and  $x_i[n]$  the sampled version of the signal received on the  $i$ -th element of the array at the time  $t = nT$ . We denote the  $n$ -th received signal  $\mathbf{x}[n] = [x_1[n], \dots, x_M[n]]^T$ . We collect these vectors for the samples  $[1, \dots, N]$  into a received signal matrix  $\mathbf{X} = [\mathbf{x}[1], \dots, \mathbf{x}[N]]$ . Then  $\mathbf{X}$  has the model:

$$\mathbf{X} = \mathbf{A}\mathbf{G}\mathbf{S} + \mathbf{N} \tag{6.1}$$

Here,  $\mathbf{N}$  is the  $M \times N$  noise matrix constructed in the same fashion as  $\mathbf{X}$ .  $\mathbf{A}$  is the  $M \times d$  steering matrix that contains the steering vectors  $\mathbf{a}(\theta_i)$ ,  $1 \leq i \leq d$ , where the  $\theta_i$ 's are the directions of arrivals.  $\mathbf{G}$  is the  $d \times d$  diagonal gain matrix.  $\mathbf{S}$  is the  $d \times N$  transmitted sources matrix, and has the structure:

$$\mathbf{S} = [\mathbf{F} \odot \mathbf{B}]$$

where  $\odot$  is the Schur-Hadamard (element-wise) matrix multiplication between two matrices.  $\mathbf{F}$  is the frequency matrix that contains the residual frequencies over the time: the  $i$ -th row of  $\mathbf{F}$  is  $\mathbf{f}_i = [\phi_i, \dots, \phi_i^N]$ , where  $\phi_i = \exp(2\pi j f_i T)$ ,  $\forall i \in [1, \dots, d]$ .  $\mathbf{B} = [\mathbf{b}_1^T, \dots, \mathbf{b}_d^T]^T$  is the binary matrix that contains the bit information with  $\mathbf{b}_i = [b_i[1], \dots, b_i[N]]$  and  $\forall i \in [1, \dots, d]$ ,  $\forall n \in [1, \dots, N]$ ,  $b_i[n]$  is taken on the alphabet  $\{0, 1\}$ , with equal probability.

In this Chapter, we do not use the properties of the antenna array, so for simplicity we consider that the sources are mixed at the receiver by an unstructured matrix  $\mathbf{M}$ :

$$\mathbf{X} = \mathbf{M}\mathbf{S} + \mathbf{N}$$

where in fact  $\mathbf{M} = \mathbf{A}\mathbf{G}$ . Note that with this model,  $\mathbf{M}$  may also reflect the imperfections of the array such as calibration errors, coupling errors, or inaccuracies in the position of the elements. We only assume the matrix  $\mathbf{M}$  to be left-invertible.

To restore the sources, we look for a series of beamformers  $\{\mathbf{w}_i\}$ , such that  $\forall i \in \{1, \dots, d\}$ :

$$\hat{s}_i[n] = \mathbf{w}_i^H \mathbf{x}[n]$$

or in matrix form:

$$\hat{\mathbf{S}} = \mathbf{W}^H \mathbf{X} = \mathbf{W}^H \mathbf{M}\mathbf{S} + \mathbf{W}^H \mathbf{N}$$

where we try to make  $\hat{\mathbf{S}}$  to have properties similar to  $\mathbf{S}$ . The main advantage of this approach is its insensitivity to model mis-matches of the array.

### 6.1.2 Prior processing

Throughout this chapter, we assume that the number of sources has been accurately estimated. For instance, this estimation can be performed by a White Noise Test (WNT, see [9]), which assumes that the noise is spatially white with a known noise power. Since most of the noise consists of the thermal noise of the receiver, this is a plausible assumption. Denote by  $\lambda_i$ ,  $i \in \{1, \dots, M\}$ , the ordered eigenvalues of the sample covariance matrix of  $\mathbf{X}$ . The WNT compares the sum  $S_d = (M - d)^{-1} \sum_{n=d+1}^M \lambda_n$  to a threshold  $\gamma$  to detect the number of sources  $d$ , where  $\gamma$  is determined by the desired probability of false alarm.

Prior to any algorithm, we first reduce the dimension  $M$  of the received data vector  $\mathbf{x}(n)$  to the number of sources,  $d$ , and we whiten the data covariance matrix. The dimension reduction is necessary to avoid the existence of nullspace beamformers:  $\mathbf{w}_0$ , such that  $\mathbf{w}_0^H \mathbf{M} = 0$ . Indeed, such beamformers could be added to a valid separating beamformer  $\mathbf{w}_i$  without changing the output signal, and only change

the output noise. Hence they would destroy the uniqueness of the solution, and complicate the estimation algorithms.

The data covariance whitening is not as essential, but has been applied in similar algorithms because it causes the beamformers to converge asymptotically in  $N$  to the Wiener beamformer [49]. Indeed, let  $\mathbf{R}_x = \mathbb{E}\{\mathbf{x}\mathbf{x}^H\}$  be the data covariance matrix. Then the whitened data matrix is

$$\tilde{\mathbf{X}} = \mathbf{R}_x^{-1/2}\mathbf{X} = \tilde{\mathbf{M}}\mathbf{S} + \tilde{\mathbf{N}}.$$

where  $\tilde{\mathbf{M}} = \mathbf{R}_x^{-1/2}\mathbf{M}$ . Let  $\hat{\tilde{\mathbf{M}}}$  be an asymptotically unbiased estimate of  $\tilde{\mathbf{M}}$  in the whitened domain, then for large  $N$  we have  $\hat{\tilde{\mathbf{M}}} \approx \tilde{\mathbf{M}}$ . A matched beamformer in the whitened domain is  $\tilde{\mathbf{W}} = \tilde{\mathbf{M}}$ . In the original domain the corresponding beamformer acting on  $\mathbf{X}$  is

$$\mathbf{W} = \mathbf{R}_x^{-1/2}\hat{\tilde{\mathbf{M}}} \approx \mathbf{R}_x^{-1/2}\tilde{\mathbf{M}} = \mathbf{R}_x^{-1}\mathbf{M}.$$

This is recognized as the Wiener beamformer. Wiener beamformers are attractive because they optimize the output Signal to Interference and Noise Ratio (SINR). Note that after the prewhitening step, the noise is not spatially white anymore.

The usual method to compute the prewhitened data matrix is to use a Singular Value Decomposition (SVD) on  $\mathbf{X}$ , which factorizes  $\mathbf{X}$  matrix into a product of three matrices,

$$\mathbf{X} = \mathbf{U}\mathbf{\Sigma}\mathbf{V}$$

where  $\mathbf{U}$  is a  $M \times M$  unitary matrix,  $\mathbf{\Sigma}$  is an  $M \times M$  diagonal matrix, whose diagonal entries are real positive and ordered, and  $\mathbf{V}$  is an  $M \times N$  matrix, whose rows are orthonormal.

Note that the diagonal entries of  $\mathbf{\Sigma}$  are the square roots of the eigenvalues of the sample covariance matrix  $\hat{\mathbf{R}}_x = (1/N)\mathbf{X}\mathbf{X}^H$ , thus the detection of number of sources can be computed from  $\mathbf{\Sigma}$  at this point.

We split the matrix  $\mathbf{V}$  into two sub-matrices:

$$\mathbf{V} = \begin{bmatrix} \mathbf{V}_r \\ \mathbf{V}_n \end{bmatrix}$$

where  $\mathbf{V}_r$  is  $d \times N$ . We define as well  $\mathbf{U}_r$  the  $d$  first columns of  $\mathbf{U}$ , and  $\mathbf{\Sigma}_r$ , the upper left  $d \times d$  corner of  $\mathbf{\Sigma}$ . The prewhitened and dimension-reduced data matrix is now defined as

$$\tilde{\mathbf{X}} = \mathbf{V}_r$$

Indeed,  $\mathbf{V}_r$  contains the  $d$  dominant components in the row span of  $\mathbf{X}$ , and  $\mathbf{X}'\mathbf{X}'^H = \mathbf{V}_r\mathbf{V}_r^H = \mathbf{I}$  so the data is whitened.

The dimension reduction/prewhitening can also be written as a prefiltering on  $\mathbf{X}$ , since if we premultiply the data by<sup>1</sup>  $\mathbf{\Sigma}_r^{-1}\mathbf{U}_r^H$ , then we obtain

$$\mathbf{\Sigma}_r^{-1}\mathbf{U}_r^H\mathbf{X} = \mathbf{V}_r = \tilde{\mathbf{X}}.$$

<sup>1</sup>Note that  $\mathbf{U}_r\mathbf{\Sigma}_r^{-1}$  is a valid square root of  $\mathbf{R}_x$ , although it is not the usual symmetric square root.

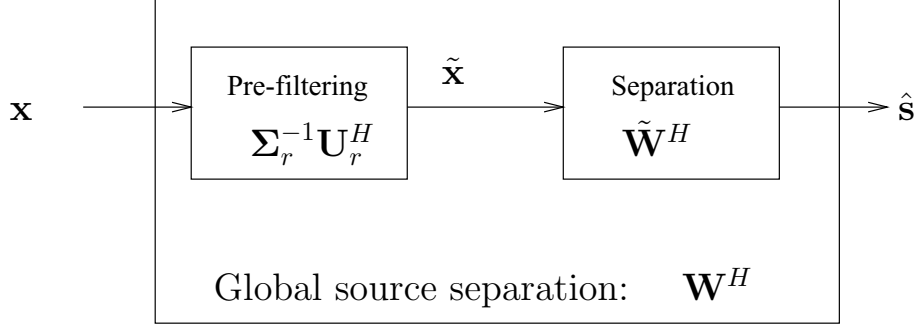


Figure 6.1: Sketch of preprocessing and beamforming.

This shows that the data model in the whitened domain is

$$\tilde{\mathbf{X}} = \tilde{\mathbf{M}}\mathbf{S} + \tilde{\mathbf{N}} \quad (6.2)$$

with

$$\tilde{\mathbf{M}} = \Sigma_r^{-1} \mathbf{U}_r^H \mathbf{M} \quad (6.3)$$

a  $d \times d$  square invertible mixing matrix, and  $\tilde{\mathbf{N}}$  a noise matrix with covariance  $\tilde{\mathbf{R}}_n = \sigma^2 \Sigma_r^{-2}$ .

Finally, once a beamforming matrix on  $\tilde{\mathbf{X}}$  is found, say  $\tilde{\mathbf{W}}$  such that  $\tilde{\mathbf{W}}^H \tilde{\mathbf{X}} = \hat{\mathbf{S}}$ , then the corresponding beamformer on the original data matrix is

$$\mathbf{W} = \mathbf{U}_r \Sigma_r^{-1} \tilde{\mathbf{W}}.$$

In the remaining of this Chapter we will work with the whitened data model (6.2) but to simplify the notation we will drop the tilde notation.

## 6.2 Zero/Constant modulus algorithms

In Subsection 6.2.1, we recall the ZCM properties, and we transform them into a more useful formulation. In Subsection 6.2.2, we then present the two algorithms proposed in [21], and their shortcomings. To overcome them, we present an adaptation of the preceding algorithms in Subsection 6.2.4, as well as some algorithmic details.

### 6.2.1 ZCM properties

#### Initial properties

From chapter 3, we recall the ZCM Properties 3.1.2 for a SSR source  $s[k]$ . The first property is instantaneous in time:  $s[k] = 0$  or  $|s[k]| = 1$ ,  $\forall k \in \{1, \dots, N\}$ , which is equivalent to:

$$s[k]s^*[k]s[k] = s[k] \quad (6.4)$$



For the second property, we consider the residual carrier of the sources. Denote by  $\phi$  the phase shift associated with the residual carrier  $f$  of a source  $s[k]$ :  $\phi = \exp(2\pi j f T)$ , where  $T$  is the sampling period. The shift-ZCM Property states that for any integer  $\tau$ , two non-zero samples with a distance of  $\tau$  in time have a phase difference of  $\phi^\tau$ . So either the product is zero:  $s[k]s^*[k-\tau] = 0$ , or it is  $s[k]s^*[k-\tau] = \phi^\tau$ ,  $\forall k \in \{1, \dots, N\}$ . Combining the two conditions, we obtain the relation:

$$s[k]s^*[k-\tau][s[k]s^*[k-\tau] - \phi^\tau] = 0 \quad (6.5)$$

Note that Equation (6.5) encompasses Equation (6.4) when  $\tau = 0$ .

### Refined static ZCM property

We look for beamformers  $\mathbf{w}$  such that  $s[k] = \mathbf{w}^H \mathbf{x}[k]$  in the noiseless case. Inserting this in Equation (6.4) leads to:

$$\mathbf{w}^H \mathbf{x}[k] \mathbf{w}^T \mathbf{x}^*[k] \mathbf{w}^H \mathbf{x}[k] = \mathbf{w}^H \mathbf{x}[k]$$

Let  $\alpha = \mathbf{w}^H \mathbf{w}$  be the square of the norm of  $\mathbf{w}$ . Multiplying the right hand side by  $1 = \frac{1}{\alpha} \mathbf{w}^H \mathbf{w}$ , and using the properties of the Kronecker product, the equation becomes:

$$[\mathbf{x}[k] \otimes \mathbf{x}^*[k] \otimes \mathbf{x}[k]]^T (\mathbf{w}^* \otimes \mathbf{w} \otimes \mathbf{w}^*) = \frac{1}{\alpha} \text{vec}(\mathbf{I}_d \otimes \mathbf{x}[k])^T (\mathbf{w}^* \otimes \mathbf{w} \otimes \mathbf{w}^*)$$

For any complex vector  $\mathbf{a}$ , we define  $\mathbf{a}^{\otimes 3}$  to be a  $d^2(d+1)/2$  vector that contains only the non-redundant elements of the Kronecker product ( $\mathbf{a}^* \otimes \mathbf{a} \otimes \mathbf{a}^*$ ). We define also  $\mathbf{J}$  to be the  $d^3 \times (d^2(d+1)/2)$  matrix that allows to reconstruct ( $\mathbf{a}^* \otimes \mathbf{a} \otimes \mathbf{a}^*$ ) from  $\mathbf{a}^{\otimes 3}$ , *i.e.*,  $\mathbf{a}^* \otimes \mathbf{a} \otimes \mathbf{a}^* = \mathbf{J} \mathbf{a}^{\otimes 3}$ . We denote by  $\mathbf{p}_A^{(1)}[k]$  the product  $(\mathbf{x}[k] \otimes \mathbf{x}^*[k] \otimes \mathbf{x}[k])^T \mathbf{J}$ , and by  $\mathbf{p}_A^{(2)}[k]$  the product  $\text{vec}(\mathbf{I}_d \otimes \mathbf{x}[k])^T \mathbf{J}$ . Then the preceding equation is equal to:

$$\alpha \mathbf{p}_A^{(1)}[k] \mathbf{w}^{\otimes 3} = \mathbf{p}_A^{(2)}[k] \mathbf{w}^{\otimes 3} \quad (6.6)$$

We create the matrices  $\mathbf{P}_A^{(1)}$  and  $\mathbf{P}_A^{(2)}$  by stacking the rows  $\mathbf{p}_A^{(1)}[k]$  and  $\mathbf{p}_A^{(2)}[k]$ ,  $\forall k \in \{1, \dots, N\}$ . We thus obtain a matrix formulation for the first ZCM property:

$$\alpha \mathbf{P}_A^{(1)} \mathbf{w}^{\otimes 3} = \mathbf{P}_A^{(2)} \mathbf{w}^{\otimes 3} \quad (6.7)$$

where the matrices  $\mathbf{P}_A^{(1)}$  and  $\mathbf{P}_A^{(2)}$  are  $N \times d^2(d+1)/2$ .

### Refined shift ZCM property

Similarly, we transform Equation (6.5) to:

$$\mathbf{w}^H \mathbf{x}[k] \mathbf{w}^T \mathbf{x}^*[k-\tau] \mathbf{w}^H \mathbf{x}[k] \mathbf{w}^T \mathbf{x}^*[k-\tau] = \phi^\tau \mathbf{w}^H \mathbf{x}[k] \mathbf{w}^T \mathbf{x}^*[k-\tau]$$

Using the Kronecker product properties, the equation becomes:

$$\begin{aligned} [\mathbf{x}[k] \otimes \mathbf{x}^*[k-\tau] \otimes \mathbf{x}[k] \otimes \mathbf{x}^*[k-\tau]]^T & \cdot (\mathbf{w}^* \otimes \mathbf{w} \otimes \mathbf{w}^* \otimes \mathbf{w}) \\ & = \phi^\tau [\mathbf{x}[k] \otimes \mathbf{x}^*[k-\tau]]^T (\mathbf{w}^* \otimes \mathbf{w}) \end{aligned}$$

We define  $\mathbf{a}^{\otimes 4}$  a  $(d(d+1)/2)^2$  vector that contains only the non-redundant elements of the Kronecker product  $(\mathbf{a}^* \otimes \mathbf{a} \otimes \mathbf{a}^* \otimes \mathbf{a})$ . We define also  $\mathbf{J}'$  the  $d^4 \times (d(d+1)/2)^2$  matrix such that  $(\mathbf{a}^* \otimes \mathbf{a} \otimes \mathbf{a}^* \otimes \mathbf{a}) = \mathbf{J}' \mathbf{a}^{\otimes 4}$ . For the sake of simplicity, we also define

$$\begin{aligned} \mathbf{a}^{\otimes 2} & = \mathbf{a}^* \otimes \mathbf{a} \\ \mathbf{p}_\tau^{(1)}[k] & = (\mathbf{x}[k] \otimes \mathbf{x}^*[k-\tau] \otimes \mathbf{x}[k] \otimes \mathbf{x}^*[k-\tau])^T \mathbf{J}' \\ \mathbf{p}_\tau^{(2)}[k] & = (\mathbf{x}[k] \otimes \mathbf{x}^*[k-\tau])^T \end{aligned}$$

Then the preceding equation is equal to:

$$\mathbf{p}_\tau^{(1)}[k] \mathbf{w}^{\otimes 4} = \phi^\tau \mathbf{p}_\tau^{(2)}[k] \mathbf{w}^{\otimes 2} \quad (6.8)$$

We create the matrices  $\mathbf{P}_\tau^{(1)}$  and  $\mathbf{P}_\tau^{(2)}$  by stacking the rows  $\mathbf{p}_\tau^{(1)}[k]$  and  $\mathbf{p}_\tau^{(2)}[k]$ ,  $\forall k \in \{\tau, \dots, N\}$ . We thus obtain a matrix formulation for the second ZCM property:

$$\mathbf{P}_\tau^{(1)} \mathbf{w}^{\otimes 4} = \phi^\tau \mathbf{P}_\tau^{(2)} \mathbf{w}^{\otimes 2} \quad (6.9)$$

where the matrix  $\mathbf{P}_\tau^{(1)}$  has size  $(N-\tau) \times (d(d+1)/2)^2$ , and  $\mathbf{P}_\tau^{(2)}$  is  $(N-\tau) \times d^2$ .

## 6.2.2 The existing algorithms

Using the preceding properties, two algorithms were proposed in [21], which we summarize in this section.

### First algorithm

The Analytical Zero/Constant modulus Algorithm (AZCMA) aims at solving Equation (6.7),

$$\alpha \mathbf{P}_A^{(1)} \mathbf{w}^{\otimes 3} = \mathbf{P}_A^{(2)} \mathbf{w}^{\otimes 3} \quad (6.10)$$

which is a matrix pencil problem (generalized eigenvalue problem for rectangular matrices), where the set of solutions  $\{\alpha\}$  are the eigenvalues, and the corresponding  $\{\mathbf{w}^{\otimes 3}\}$  the eigenvectors. The algorithm assumes that  $\mathbf{P}_A^{(1)}$  is full rank, and remarks that  $\mathbf{P}_A^{(2)}$  has only  $d$  non-zero columns. Hence, there are at most  $d$  non-zero eigenvalues, which then are equal to the  $\alpha$ 's. If there are no repeated eigenvalues, the corresponding beamformers  $\{\mathbf{w}\}$  are directly obtained from the eigenvectors  $\{\mathbf{w}^{\otimes 3}\}$  after scaling by  $\alpha^{\frac{1}{2}} = \|\mathbf{w}\|$ .

In their implementation, Equation (6.7) was solved via premultiplication by the pseudo-inverse of the first matrix in order to obtain:

$$\left[ \mathbf{P}_A^{(1)\dagger} \mathbf{P}_A^{(2)} \right] \mathbf{w}^{\otimes 3} = \alpha \mathbf{w}^{\otimes 3} \quad (6.11)$$

where the matrix in brackets is square. This is a standard eigenvalue problem and can be solved. From the eigenvectors  $\mathbf{w}^{\otimes 3}$  and the relation  $\mathbf{w}^* \otimes \mathbf{w} \otimes \mathbf{w}^* = \mathbf{J}\mathbf{w}^{\otimes 3}$ , the beamformers  $\mathbf{w}$  can be computed. In particular, if we let  $\mathbf{W}$  be a reshaping of the vector  $\mathbf{J}\mathbf{w}^{\otimes 3}$  into a  $d \times d^2$  matrix such that  $\text{vec}(\mathbf{W}) = \mathbf{J}\mathbf{w}^{\otimes 3}$ , then  $\mathbf{W} = \mathbf{w}^*(\mathbf{w}^* \otimes \mathbf{w})^H$ , and the conjugate of the dominant left singular vector of  $\mathbf{W}$  is the desired beamformer  $\mathbf{w}$ , up to a scaling which can be determined from  $\alpha$ .

Note that the set of solutions of Equation (6.11) contains the solutions of Equation (6.7), and potentially others. However, since  $\mathbf{P}_A^{(2)}$  is of rank  $d$ , there are only  $d$  non-zero eigenvalues to the matrix in Equation (6.11), and these must correspond to the solutions of (6.7).

### Second algorithm

The Analytical Frequency/ZCM Algorithm (AFZA) in [21] considers property (6.9) for the delays  $\tau = 0$  and  $\tau = 1$ :

$$\begin{cases} \mathbf{P}_0^{(1)} \mathbf{w}^{\otimes 4} = \mathbf{P}_0^{(2)} \mathbf{w}^{\otimes 2} \\ \mathbf{P}_1^{(1)} \mathbf{w}^{\otimes 4} = \phi \mathbf{P}_1^{(2)} \mathbf{w}^{\otimes 2} \end{cases}$$

By defining the vector  $\mathbf{y} = [(\mathbf{w}^{\otimes 4})^T \ (\mathbf{w}^{\otimes 2})^T]^T$ , and the matrices  $\mathbf{A}$  and  $\mathbf{B}$  as:

$$\mathbf{A} = \begin{bmatrix} \mathbf{P}_0^{(1)} & -\mathbf{P}_0^{(2)} \\ \mathbf{P}_1^{(1)} & \mathbf{0} \end{bmatrix}, \quad \mathbf{B} = \begin{bmatrix} \mathbf{0} & \mathbf{0} \\ \mathbf{0} & \mathbf{P}_1^{(2)} \end{bmatrix}$$

we can write the set of equations as

$$\mathbf{A}\mathbf{y} = \phi\mathbf{B}\mathbf{y} \tag{6.12}$$

which is again a matrix pencil problem. The article [21] assumed that  $\mathbf{A}$  and  $\mathbf{P}_1^{(2)}$  are of full rank, and used the same pseudo-inverse method to arrive at

$$[\mathbf{A}^\dagger \mathbf{B}]\mathbf{y} = \phi^{-1}\mathbf{y}$$

As in the preceding algorithm, the new eigenvalue problem contains the solutions of the original matrix pencil problem, but now, because  $\mathbf{P}_1^{(2)}$  is full rank, the implicit projection that is part of the pseudo-inversion might have introduced other non-trivial solutions as well. To cite [21], there are  $d^2$  solutions from which “we must choose the  $d$  eigenvalues that are on the unit circle”.

### Discussion

Let us consider two non-overlapping sources in time,  $s_1$  and  $s_2$ , and no noise, see Figure 6.2. We denote by  $\mathbf{w}_1$  and  $\mathbf{w}_2$  two beamformers that restore exactly  $s_1$  and  $s_2$  from  $\mathbf{x}$ . From Figure 6.2, we note that for any pair of complex  $(a, b)$  on the unit circle, namely with  $|a| = 1$  and  $|b| = 1$ , the vector  $\mathbf{w} = a\mathbf{w}_1 + b\mathbf{w}_2$  is also an acceptable beamformer for the criterion (6.4). This demonstrates that AZCMA



Figure 6.2: Two non-overlapping sources

cannot separate the two sources in this case. In terms of the matrix pencil problem, note that in the case of two non-overlapping sources, the rank of  $\mathbf{P}_A^{(1)}$  is too small, and thus there will appear additional eigenvectors that will cause the other eigenvectors to be non-unique.

The AFZA should work for non-overlapping sources, since it uses the frequency information which is different for two sources with different frequencies. Unfortunately, simulations have shown that also for AFZA it might happen that  $\mathbf{A}$  is not full rank. In that case, premultiplication by  $\mathbf{A}^\dagger$  to obtain the standard square eigenvalue problem does not work well, because there is always an ambiguity in the result. To improve our understanding, in the next subsection we study the matrix pencil problem  $\mathbf{A}\mathbf{y} = \phi\mathbf{B}\mathbf{y}$  in more detail.

### 6.2.3 The matrix pencil problem

In this subsection, we first transform the matrix pencil problem to an equivalent problem of smaller dimensions without introducing new solutions. We study a generic case in more detail, and state under which conditions the reduced problem is solvable with unique solutions and no additional solutions. The last Subsection contains a few remarks on non-generic cases.

#### Reformulation

Since we already noted that the ZCM property used by AZCMA does not allow to separate two non-overlapping sources uniquely, we will study the pencil problem for AFZA only. We consider the noiseless case for the equation:

$$\mathbf{A}\mathbf{y} = \phi\mathbf{B}\mathbf{y} \quad (6.13)$$

Recall that  $\mathbf{A}$  and  $\mathbf{B}$  are tall matrices of size  $N \times L$ , where  $L \stackrel{\text{def}}{=} [d(d+1)/2]^2$  and  $N \geq L$ . In order for there to be any solution to (6.13), it is necessary that the column spans of  $\mathbf{A}$  and  $\mathbf{B}$  have a non-empty intersection. Thus let  $\mathbf{U}$  be a matrix whose columns form an orthonormal basis of  $\mathcal{U}$ , the intersection of the column spaces of  $\mathbf{A}$  and  $\mathbf{B}$ , and let  $q$  be the number of columns of  $\mathbf{U}$ . Note that any solution  $\mathbf{y}$  to Equation (6.13) must be such that

$$\mathbf{A}\mathbf{y} \in \mathcal{U} \quad \text{and} \quad \mathbf{B}\mathbf{y} \in \mathcal{U} \quad (6.14)$$

To construct  $\mathbf{U}$ , we perform a QR factorization of  $\mathbf{A}$  and  $\mathbf{B}$ :

$$\begin{aligned}\mathbf{A} &= \mathbf{Q}_A \mathbf{R}_A \\ \mathbf{B} &= \mathbf{Q}_B \mathbf{R}_B\end{aligned}$$

where  $\mathbf{Q}_A$  and  $\mathbf{Q}_B$  are tall rectangular matrices with orthonormal columns spanning  $\text{col}(\mathbf{A})$  and  $\text{col}(\mathbf{B})$  respectively, and where we construct  $\mathbf{R}_A$  and  $\mathbf{R}_B$  to have full row rank, possibly being rectangular if  $\mathbf{A}$  or  $\mathbf{B}$  are rank deficient. Now, we define  $\mathbf{T}_A$  to be a unitary matrix that transforms  $\mathbf{Q}_A$  such that it places  $\mathbf{U}$  on the first columns:  $\mathbf{Q}_A \mathbf{T}_A = [\mathbf{U} \mid \mathbf{U}_A]$ , where  $\mathbf{U}_A$  is a matrix whose columns are an orthonormal basis of the complementary space of  $\mathcal{U}$  on the space spanned by  $\mathbf{A}$ . Also let be  $\tilde{\mathbf{R}}_A = \mathbf{T}_A^{-1} \mathbf{R}_A$ . We perform a similar transformation on  $\mathbf{B}$ , which results in:

$$\begin{aligned}\mathbf{A} &= [\mathbf{U} \mid \mathbf{U}_A] \tilde{\mathbf{R}}_A \\ \mathbf{B} &= [\mathbf{U} \mid \mathbf{U}_B] \tilde{\mathbf{R}}_B\end{aligned}$$

We now partition the matrix  $\tilde{\mathbf{R}}_A^H$  into two sub-matrices which correspond to the columns of  $\mathbf{U}$  and  $\mathbf{U}_A$ :  $\tilde{\mathbf{R}}_A^H = [\mathbf{A}_c \mid \mathbf{A}_{nc}]$ , where  $\mathbf{A}_c$  and  $\mathbf{A}_{nc}$  are full column rank. (The subscript  $(\ )_c$  stands for ‘‘common’’, and  $(\ )_{nc}$  for ‘‘not common’’.) Doing the same to  $\tilde{\mathbf{R}}_B^H$  leads to transform the preceding set of equations into:

$$\mathbf{A} = [\mathbf{U} \mid \mathbf{U}_A] \begin{bmatrix} \mathbf{A}_c^H \\ \mathbf{A}_{nc}^H \end{bmatrix} \quad (6.15)$$

$$\mathbf{B} = [\mathbf{U} \mid \mathbf{U}_B] \begin{bmatrix} \mathbf{B}_c^H \\ \mathbf{B}_{nc}^H \end{bmatrix} \quad (6.16)$$

where all sub-matrices  $\mathbf{A}_i$  and  $\mathbf{B}_i$ , for  $i \in \{c, nc\}$  are full column rank, and  $\mathbf{A}_c$  and  $\mathbf{B}_c$  have the same number of columns  $q$  as  $\mathbf{U}$ . The point of all these transformations is that we will be able to work with  $\mathbf{A}_c$  and  $\mathbf{B}_c$ , which have only order  $d^4/4$  rows rather than  $N$ .

Indeed, this factorization leads us to consider the decomposition of the space of  $\mathbf{y}$ ,  $\mathbb{C}^L$  into three orthogonal subspaces  $\mathcal{Z}_0$ ,  $\mathcal{Z}_c$ , and  $\mathcal{Z}_n$ :

$$\mathbb{C}^L = \mathcal{Z}_0 \oplus \mathcal{Z}_c \oplus \mathcal{Z}_n$$

Since these subspaces are orthogonal and span the complete space, we can write any vector  $\mathbf{y} \in \mathbb{C}^L$  in a unique way as  $\mathbf{y} = \mathbf{y}_0 + \mathbf{y}_c + \mathbf{y}_n$ , where  $\mathbf{y}_i$  belongs to  $\mathcal{Z}_i$  with  $i \in \{0, n, c\}$ . The subspaces  $\mathcal{Z}_i$  are defined as follows:

- $\mathcal{Z}_n$  is the intersection of the kernel of the matrices  $\mathbf{A}$  and  $\mathbf{B}$ .

For any  $\mathbf{y}_n \in \mathcal{Z}_n$ :  $\mathbf{A}\mathbf{y}_n = \mathbf{B}\mathbf{y}_n = 0$ , which implies:

$$\mathbf{A}_c^H \mathbf{y} = \mathbf{A}_{nc}^H \mathbf{y} = \mathbf{B}_c^H \mathbf{y} = \mathbf{B}_{nc}^H \mathbf{y} = 0 \quad (6.17)$$

- $\mathcal{Z}_c$  is the union of the subspaces spanned by the matrices  $\mathbf{A}_{nc}$  and  $\mathbf{B}_{nc}$ , or the column span of  $[\mathbf{A}_{nc} \ \mathbf{B}_{nc}]$ . For any  $\mathbf{y}_c \neq \mathbf{0} \in \mathcal{Z}_c$ :  $\mathbf{A}_{nc}^H \mathbf{y}_c$  and/or  $\mathbf{B}_{nc}^H \mathbf{y}_c$  is non null.

Note that for any vector  $\mathbf{y}_n \in \mathcal{Z}_n$ , Equation (6.17) shows that  $\mathbf{y}_n^H [\mathbf{A}_{nc} \ \mathbf{B}_{nc}] = 0$ , so that  $\mathcal{Z}_c$  is indeed orthogonal to  $\mathcal{Z}_n$ .

- $\mathcal{Z}_0$  is the complementary space orthogonal to the union of  $\mathcal{Z}_c$  and  $\mathcal{Z}_n$ :  $\mathcal{Z}_0 = (\mathcal{Z}_n \oplus \mathcal{Z}_c)^\perp$ . The most interesting property is: for any  $\mathbf{y}_0 \in \mathcal{Z}_0$ :

$$\mathbf{y}_0 \perp \mathcal{Z}_c \quad \Rightarrow \quad \mathbf{A}_{nc}^H \mathbf{y}_0 = \mathbf{B}_{nc}^H \mathbf{y}_0 = 0 \quad (6.18)$$

Note that by definition the subspaces are orthogonal and their direct sum is equal to  $\mathbb{C}^L$ .

When we insert this partitioning of  $\mathbf{y}$  in Equation (6.12), we obtain

$$\left[ \mathbf{U} \mid \mathbf{U}_A \right] \begin{bmatrix} \mathbf{A}_c^H \\ \mathbf{A}_{nc}^H \end{bmatrix} (\mathbf{y}_0 + \mathbf{y}_c + \mathbf{y}_n) = \phi \left[ \mathbf{U} \mid \mathbf{U}_B \right] \begin{bmatrix} \mathbf{B}_c^H \\ \mathbf{B}_{nc}^H \end{bmatrix} (\mathbf{y}_0 + \mathbf{y}_c + \mathbf{y}_n)$$

which results in:

$$\left[ \mathbf{U} \mid \mathbf{U}_A \mid \mathbf{U}_B \right] \begin{bmatrix} \mathbf{A}_c^H (\mathbf{y}_0 + \mathbf{y}_c) - \phi \mathbf{B}_c^H (\mathbf{y}_0 + \mathbf{y}_c) \\ \mathbf{A}_{nc}^H \mathbf{y}_c \\ \mathbf{B}_{nc}^H \mathbf{y}_c \end{bmatrix} = \mathbf{0}$$

The first matrix compound is a tall orthonormal matrix. We can therefore pre-multiply the equation by its Hermitian conjugate, which gives:

$$\mathbf{A}_c^H (\mathbf{y}_0 + \mathbf{y}_c) = \phi \mathbf{B}_c^H (\mathbf{y}_0 + \mathbf{y}_c) \quad (6.19)$$

$$\begin{bmatrix} \mathbf{A}_{nc} & \mathbf{B}_{nc} \end{bmatrix}^H \mathbf{y}_c = \mathbf{0} \quad (6.20)$$

Recall that  $\mathbf{y}_c \in \mathcal{Z}_c$ , so by definition of the subspace of subspace  $\mathcal{Z}_c$ , if  $\mathbf{y}_c \neq \mathbf{0}$  at least  $\mathbf{A}_{nc}^H \mathbf{y}_c$  or  $\mathbf{B}_{nc}^H \mathbf{y}_c$  is non-zero. So Equation (6.20) implies  $\mathbf{y}_c = \mathbf{0}$ , and hence any solution  $\mathbf{y}$  of (6.13) must be of the form  $\mathbf{y} = \mathbf{y}_0 \in \mathcal{Z}_0$ , with

$$\mathbf{A}_c^H \mathbf{y}_0 = \phi \mathbf{B}_c^H \mathbf{y}_0 \quad (6.21)$$

To express the condition  $\mathbf{y} = \mathbf{y}_0 \in \mathcal{Z}_0$ , let  $\mathbf{Z}_0$  be a  $q \times L$  matrix whose columns are a basis of the subspace  $\mathcal{Z}_0$ , where  $q > L$ . Then any  $\mathbf{y}_0 \in \mathcal{Z}_0$  can be written as

$$\mathbf{y}_0 = \mathbf{Z}_0 \mathbf{y}_r$$

where  $\mathbf{y}_r$  is an  $L$ -dimensional ‘‘reduced’’ vector. Also let  $\mathbf{A}_r = \mathbf{A}_c \mathbf{Z}_0$  and  $\mathbf{B}_r = \mathbf{B}_c \mathbf{Z}_0$ , then Equation (6.21) becomes:

$$\mathbf{A}_r \mathbf{y}_r = \phi \mathbf{B}_r \mathbf{y}_r \quad (6.22)$$

where the matrices are now square of size  $q \times q$ . This equation represents a generalized eigenvalue problem, and we denote its solutions as  $\mathbf{y}_r^{(i)}$ ,  $q = 1, \dots, q$ .

By this sequence of steps, we can state that all solutions  $\mathbf{y}^{(i)}$  of Equation (6.13) are of the form

$$\mathbf{y}^{(i)} = \mathbf{Z}_0 \mathbf{y}_r^{(i)} + \mathbf{y}_n^{(i)} \quad (6.23)$$

where  $\mathbf{y}_r^{(i)}$  is a solution of Equation (6.22), and  $\mathbf{y}_n^{(i)} \in \mathcal{Z}_n$ . Ideally,  $\mathcal{Z}_n = \emptyset$ , so that the latter terms are absent.

### The “generic” case

We first study the “generic” case, *i.e.*, the ideal case where there are only  $d$  unique solutions which correspond exactly to the desired beamformers, and the eigenvalues are exactly on the unit circle. The interest of studying first the “generic” case is two-fold, 1) the generic case allows a straightforward solution of the pencil problem, and 2) understanding the generic case facilitates the understanding of the non-generic case.

The generic case is defined by:

$$\dim(\mathcal{Z}_c) = L - d \quad (6.24)$$

Note that it is equivalent to state:

$$\begin{aligned} \dim(\mathcal{Z}_n) &= 0 \\ \dim(\mathcal{Z}_0) &= d \end{aligned}$$

because  $d \geq \dim(\mathcal{Z}_0 \oplus \mathcal{Z}_n) \geq \dim(\mathcal{Z}_0) \geq d$ . In order to get  $\mathcal{Z}_0$  zero-dimensional, it is sufficient that  $\mathbf{A}$  is full column rank. But it is not clear under which conditions  $\dim(\mathcal{Z}_0) = d$ , or equivalently the rank of  $\mathbf{U}$  is exactly equal to  $d$ .

In the generic case there are only  $d$  solutions to Equation (6.22), and we know that there are  $d$  solutions to Equation (6.13), so there is a one-to-one mapping which allows us to state the next Proposition:

**Proposition 6.2.1** *Assume the “generic case” in which  $\mathbf{A}$  is full column rank,  $\dim(\mathcal{U}) \stackrel{\text{def}}{=} q = d$ , and the residual frequencies  $\phi$  are different. Then there are exactly  $d$  solutions to the matrix pencil problem (6.12), they can be obtained by solving the standard eigenvalue problem (6.22); the eigenvalues are the desired frequency residuals, and the eigenvectors correspond to the desired beamformers.*

**Proof:** The original AFZA problem admits at least  $d$  beamformers, hence the matrix pencil problem (6.12) has at least  $d$  solutions. We have to show that there are precisely  $d$  solutions, and that they are unique. Since all steps in the derivation of (6.22) were reversible, it suffices to solve the latter problem instead of (6.12). Since  $q = d$  by assumption, it is a  $d \times d$  generalized eigenvalue problem, and we have to show that the  $d$  eigenvectors are unique. This is the case if  $\mathbf{A}_r$  is full rank  $d$ , and the eigenvalues are different.

Note that because  $\mathbf{A}$  is full rank,  $\mathbf{A}_c^H \mathbf{y}_0 \neq \mathbf{0}$  for all  $\mathbf{y}_0 \in \mathcal{Z}_0$ , hence the matrix  $\mathbf{A}_r$  is a full rank  $d \times d$  square matrix, and can be inverted in Equation (6.22), so that there are precisely  $d$  eigenvectors to this eigenvalue problem.

Since by assumption the residual frequencies differ, the eigenvalues  $\phi$  in (6.22) differ, hence the eigenvectors  $\mathbf{y}_r^{(i)}$  are unique. The fact that  $\mathbf{A}$  is full rank also implies that  $\dim(\mathcal{Z}_n) = 0$ , so that there is no vector  $\mathbf{y}_n$  in equation (6.23), and the solutions of (6.12) are  $\mathbf{y}^{(i)} = \mathbf{Z}_0 \mathbf{y}_r^{(i)}$ , for  $i \in \{1, \dots, d\}$ , and unique. Thus they must correspond to the desired beamformers.  $\square$

### Non-Generic case

Assuming that there is no source for which all the bits are equal to zero (which with our a priori assumptions would be an improbable event), we know that Equation (6.22) has at least  $d$  solutions. This implies

$$\begin{aligned} d &\leq \dim(\mathcal{Z}_0) \\ d &\leq \dim(\text{range}(\mathbf{A}_c)) \end{aligned}$$

where the first inequality comes from the fact there are at least  $d$  solutions to the eigenvalue problem, and the second one from the fact that for each source Equation (6.5) holds for every  $k \in \{1, \dots, N\}$ .

We can also find a relation between the dimension of  $\mathcal{Z}_0$  and  $\dim(\text{range}(\mathbf{A}_c))$ . First note that  $\dim(\text{range}(\mathbf{A}_c)) = \dim(\text{range}(\mathbf{B}_c)) = q$  since they are full column rank and therefore equal to the size of  $\mathbf{U}$ . Now we consider any  $\mathbf{y}_0 \in \mathcal{Z}_0$ :

$$\begin{aligned} \mathbf{y}_0 \notin \mathcal{Z}_n &\Rightarrow \mathbf{A}\mathbf{y}_0 \neq \mathbf{0} \\ &\Rightarrow \mathbf{U}\mathbf{A}_c^H \mathbf{y}_0 \neq \mathbf{0} \\ &\Rightarrow \dim(\mathcal{Z}_0) \leq \dim(\text{range}(\mathbf{A}_c)) = \dim(\mathcal{U}) \end{aligned}$$

which allows us to claim that the number of solutions is smaller than the dimension of the common space  $\mathcal{U}$  between  $\mathbf{A}$  and  $\mathbf{B}$ .

Assume that the dimension of  $\mathcal{Z}_n$  is  $p > 0$ , and let  $[\mathbf{z}_1, \dots, \mathbf{z}_p]$  be a basis of  $\mathcal{Z}_n$ . We also assume that the number of solutions to Equation (6.22) is  $q \geq d$ . Then the solutions to the initial problem (6.13) are of the form

$$\mathbf{y}^{(j)} = \mathbf{y}_r^{(j)} + \sum_{i=1}^p \lambda_{i,j} \mathbf{z}_i, \quad j = 1, \dots, q \quad (6.25)$$

From this we see that there are two problems in the AFZA algorithm: 1) the number of solutions  $q$  doesn't have to be precisely equal to  $d$ , 2) if  $p = \dim(\mathcal{Z}_n) \neq 0$ , then arbitrary vectors from  $\mathcal{Z}$  can be added to the solutions. In both cases, it is very hard to recover the beamformers because from the set  $\mathbf{y}^{(j)}$  we would have to find out which vectors in that space have the required Kronecker structure. There are no techniques yet to deal with such situations.

We discovered a few cases that differ from the generic case, for which we expose now the physical origin and their connections with the previous proposition. In order to have a clear insight, we restrict ourself to the reception of two non-mixed sources ( $\mathbf{M} = \mathbf{I}_2$ ), and to the noiseless case.

- The most common case is non-overlapping signals, meaning that the second signal begins only after the first one end. Then all cross-products between the two sources are equal to zero, and the corresponding columns of the matrices  $\mathbf{P}_0^{(2)}$ ,  $\mathbf{P}_0^{(1)}$  and  $\mathbf{P}_1^{(1)}$  are equal to the zero vector. Consequently the matrix  $\mathbf{A}$  is not full column rank.



- In case of slightly overlapping signals, the aforementioned problem may appear. But also, because some columns that contain the cross-products have only one non-zero element in  $\mathbf{P}_1^{(1)}$  and in  $\mathbf{P}_1^{(2)}$  at the same place, the common space  $\mathcal{U}$  increases.
- A more unusual case that we observed is as follows: if the sampling rate is chosen equal to half the data rate of the mode A/C, then because of Property (3.2.1), the terms of equation (6.12) are always equal to zero, and by construction AFZA cannot restore mode A/C sources.

The last case can be avoided by choosing the sampling rate carefully. To overcome the drawbacks of the two first cases, one remedy to restore the rank properties of  $\mathbf{A}$  and  $\mathcal{U}$  is to consider more than one time-lag. This is investigated in the next subsection.

## 6.2.4 The multi-shift ZCMA

### Principle

From the preceding subsection, we understand that when the subspace  $\mathcal{Z}_c$  is of dimension  $L-d$  we have the “generic case” which admits a unique solution. We now discuss a technique to “fill” the subspace  $\mathcal{Z}_c$  to its maximal size. As a consequence,  $\dim(\mathcal{Z}_n) = 0$ ,  $\dim(\mathcal{Z}_0) = d$ , and  $\dim(\mathcal{U}) = d$ . The idea is to consider several different time-lags. For each time-lag we stack in a matrix  $\mathbf{Z}_C$  a basis of the estimated subspace  $\mathcal{Z}_c$  for that time-lag. When this matrix reaches the appropriate size:  $L-d$ , the subspace that contains the beamformer is the orthogonal complementary subspace of the subspace spanned by  $\mathcal{Z}_c$ .

### Method

Consider Equation (6.9) for all  $\tau \in \mathbb{N}$ :

$$\mathbf{P}_\tau^{(1)} \mathbf{w}^{\otimes 4} = \phi^\tau \mathbf{P}_\tau^{(2)} \mathbf{w}^{\otimes 2}$$

where  $\mathbf{P}_\tau^{(1)}$  is  $N \times L$ , and  $\mathbf{P}_\tau^{(2)}$  is  $N \times d^2$ . Using the same notation as in the preceding subsection, let  $\mathcal{U}$  be the common subspace spanned by the columns of the matrices  $\mathbf{P}_\tau^{(1)}$  and  $\mathbf{P}_\tau^{(2)}$  for all  $\tau$ . Then we can write

$$\begin{aligned} \mathbf{P}_\tau^{(1)} &= \left[ \mathbf{U} \mid \mathbf{U}_\tau^{(1)} \right] \begin{bmatrix} (\mathbf{P}_{\tau,c}^{(1)})^H \\ (\mathbf{P}_{\tau,nc}^{(1)})^H \end{bmatrix} \\ \mathbf{P}_\tau^{(2)} &= \left[ \mathbf{U} \mid \mathbf{U}_\tau^{(2)} \right] \begin{bmatrix} (\mathbf{P}_{\tau,c}^{(2)})^H \\ (\mathbf{P}_{\tau,nc}^{(2)})^H \end{bmatrix} \end{aligned}$$

where  $\mathbf{U}_\tau^{(1)}$  and  $\mathbf{U}_\tau^{(2)}$  are the orthogonal complements of  $\mathbf{U}$  over  $\mathbf{P}_\tau^{(1)}$  and  $\mathbf{P}_\tau^{(2)}$ , and  $(\mathbf{P}_{\tau,nc}^{(i)})^H$ ,  $i \in \{1, 2\}$  are of full row rank.

Similarly as before, we consider solutions  $\mathbf{y}$  of equation (6.12), the  $\mathbf{y}_i = [(\mathbf{w}_i^{\otimes 4})^T \ (\mathbf{w}_i^{\otimes 2})^T]^T, \forall i \in \{1, \dots, d\}$ :

$$\left[ \mathbf{U} \mid \mathbf{U}_\tau^{(1)} \mid \mathbf{U}_\tau^{(2)} \right] \begin{bmatrix} (\mathbf{P}_{\tau,c}^{(1)})^H \mathbf{w}_i^{\otimes 4} - \phi^\tau (\mathbf{P}_{\tau,c}^{(2)})^H \mathbf{w}_i^{\otimes 2} \\ (\mathbf{P}_{\tau,nc}^{(1)})^H \mathbf{w}_i^{\otimes 4} \\ -\phi^\tau (\mathbf{P}_{\tau,nc}^{(2)})^H \mathbf{w}_i^{\otimes 2} \end{bmatrix} = \mathbf{0}$$

where the first matrix compound is full column rank by definition. Then the second compound is equal to zero, and particularly, we have the following properties:

$$(\mathbf{P}_{\tau,c}^{(1)})^H \mathbf{w}_i^{\otimes 4} - \phi^\tau (\mathbf{P}_{\tau,c}^{(2)})^H \mathbf{w}_i^{\otimes 2} = \mathbf{0}$$

$$(\mathbf{P}_{\tau,nc}^{(1)})^H \mathbf{w}_i^{\otimes 4} = \mathbf{0}$$

and:

$$(\mathbf{P}_{\tau,nc}^{(2)})^H \mathbf{w}_i^{\otimes 2} = \mathbf{0} \tag{6.26}$$

We use Equation (6.26) in order to estimate the subspace orthogonal to the subspace spanned by the  $\mathbf{w}_i^{\otimes 2}$ 's.

We stack the matrix  $(\mathbf{P}_{\tau,nc}^{(2)})^H$  in the matrix  $\mathbf{Z}_C$  for  $L$  different  $\tau \in \mathbb{N}$ :

$$\mathbf{Z}_C^H = \begin{bmatrix} (\mathbf{P}_{0,nc}^{(2)})^H \\ (\mathbf{P}_{1,nc}^{(2)})^H \\ (\mathbf{P}_{2,nc}^{(2)})^H \\ \vdots \\ (\mathbf{P}_{L,nc}^{(2)})^H \end{bmatrix}$$

Note that the matrix has only  $d^2$  columns, and  $\forall i \in \{1, \dots, d\}$ :

$$\mathbf{Z}_C^H \mathbf{w}_i^{\otimes 2} = \mathbf{0} \tag{6.27}$$

We now assume that we have taken a sufficient number of time-lags such that the matrix  $\mathbf{Z}_C$  is of rank  $d^2 - d$ . The rank cannot be larger, because we know that there are  $d$  independent vectors, which are orthogonal to the columns of the matrix  $\mathbf{Z}_C$ . So we assume “de facto” that the matrix achieves its highest rank.

Let  $\mathcal{W}_1$  be the subspace spanned by the columns of  $\mathbf{Z}_C$ , and  $\mathcal{W}_0$  its orthogonal complementary subspace over  $\mathbb{C}^{d^2}$ , whose dimension is  $\dim(\mathcal{W}_0) = d$ . We denote by  $\mathbf{Y}$  a basis of  $\mathcal{W}_0$ , and we stack the collection of vectors  $\mathbf{w}_i^{\otimes 2}$  into the matrix  $\mathbf{W}^{\otimes 2} = [\mathbf{w}_1^{\otimes 2}, \dots, \mathbf{w}_d^{\otimes 2}]$ . Since  $\mathbf{Y}$  and  $\mathbf{W}^{\otimes 2}$  span the same subspace, there is an invertible matrix  $\mathbf{Q} = [q_{ij}]$  such that:

$$\mathbf{Y} = \mathbf{W}^{\otimes 2} \mathbf{Q}$$

We use now the Unvec operator defined in Section 1.7, which transforms a vector of dimension  $d^2$  into a matrix of size  $d \times d$ . For each column of  $\mathbf{Y}$  we obtain a  $d \times d$

matrix:  $\mathbf{Y}_i$   $i \in \{1, \dots, d\}$ , for which we have the relation:

$$\begin{aligned}\mathbf{Y}_i &= \sum_{j=1}^d \mathbf{w}_j \mathbf{w}_j^H q_{i,j} \\ &= \mathbf{W} \text{diag}(q_{i,1}, \dots, q_{i,d}) \mathbf{W}^H\end{aligned}$$

From the above equation, we see that the collection of the  $\mathbf{Y}_i$ 's accept a common basis  $\mathbf{W}$  in which they are all diagonal. We say that they are “jointly diagonalizable” by the basis  $\mathbf{W}$ , and in fact by any of its column permutations and/or unit column scalings.

The next step of the algorithm is to perform this joint diagonalization (JD). We can use existing algorithms, see [12] or [45]. The basis of the diagonalization  $\mathbf{W}$  contains the desired beamformers which will separate the sources:

$$\hat{\mathbf{s}}[k] = \mathbf{W}^H \mathbf{x}[k] \quad \forall k \in \{1, \dots, N\}$$

Moreover, the frequency residuals can be calculated using Equation (6.5).

The last step is to use Equation (6.3) to get an estimate of the matrix  $\mathbf{M}$ . With the estimated matrix  $\widehat{\mathbf{M}}$ , we can recover the Direction Of Arrival (DOA) for each source, for example by applying the ESPRIT algorithm to each column of  $\widehat{\mathbf{M}}$ .

We summarize the algorithm in Table 6.1.

1	For $\tau \in \{\tau_1, \dots, \tau_L\}$ , do.
a	Derive $\mathbf{P}_\tau^{(1)}$ and $\mathbf{P}_\tau^{(2)}$ from the data.
b	Calculate the common subspace $\mathcal{U}$ .
c	Derive the matrix $\mathbf{P}_{\tau,nc}^{(2)}$
d	Stack it to $\mathbf{Z}_C^H$ .
2	Perform an SVD of $\mathbf{Z}_C$ .
3	Keep the left singular vectors corresponding to the $d$ smallest eigenvalues to form the matrix $\mathbf{Y}$ .
4	Unvec $\mathbf{Y}$ to obtain the $\mathbf{Y}_i$ 's.
5	Perform joint diagonalization on the $\mathbf{Y}_i$ 's to obtain $\mathbf{W}$ .
6	$\hat{\mathbf{S}} = \mathbf{W}^H \mathbf{X}$ .
7	Estimate $\widehat{\mathbf{M}}$ , and the DOA's.
8	Estimate the residual frequencies.

Table 6.1: Multi-shift ZCM Algorithm.

### Remarks

In our implementation, the joint diagonalization algorithm used in step 5 is the Jacobi angle method from [12].

The set of time delays  $\{\tau_1, \dots, \tau_L\}$  can be chosen arbitrarily, as long as the matrix  $\mathbf{Z}_C$  is expected to achieve its maximal full rank. In our implementation, the

following set has given satisfactory results:

$$\left\{ 0, 1, -1, 2, -2, \frac{N}{10}, \frac{-N}{10}, \frac{N}{4}, \frac{-N}{4}, \frac{N}{2}, \frac{-N}{2} \right\}$$

In order to save some computational cost, the algorithm implementation worked in an iterative fashion: the  $\tau$  were taken one by one in the order: 0, 1, -1,  $N/2$ ,  $-N/2$ , 2, -2,  $N/10$ ,  $-N/10$ ,  $N/4$ ,  $-N/4$ , until the estimate of the subspace spanned by  $\mathbf{Y}$ ,  $\mathcal{W}_0$ , was declared stable, *i.e.* the subspace at the iteration  $k + 1$ , and  $k$  were similar. The distance was measured by the dimension of the common subspace between  $(\mathcal{W}_0)_k$  and  $(\mathcal{W}_0)_{k+1}$ .

The computational cost is dominated by the search of the subspace  $\mathcal{U}$  for each  $\tau$ . The most expensive in this search is the QR factorization of  $\mathbf{P}_\tau^{(1)}$ , which is of the order  $N \times L^2/2$ . Thus the computational cost is of order  $LNd^8/8$ . Note that the most expensive step in AFZA is the QR of  $\mathbf{A}$ , of order  $Nd^8/4$ .

### 6.2.5 Discussion

It has been seen from the simulations that the multi-shift ZCM algorithm resolved all simulated cases, even those with non-overlapping sources. The algorithm is deterministic, and thus requires only a few number of samples, as opposed to stochastic algorithms which need many samples to reach good performance.

Unfortunately, there are a few drawbacks. The computational cost is rather high, a joint diagonalization is required (unlike the AFZA), the frequency estimates are obtained in the last step and do not have good performance.

For future research, the iterative method should be investigated as it has the potential to reduce the computational cost, but one has to find a strategy for choosing the  $\tau$ 's such that 1) the numbers of iterations is minimal, 2) the stability of the subspace  $\mathcal{W}_0$  is detectable.

## 6.3 ESPRIT-Second-Order Blind Identification algorithm

One of the two conclusions of Section 3.2 was the statement of Property 3.2.1, which expresses the residual carrier presence on the recovered source symbols correlation. To simplify this property, we consider only a mixture of SSR mode S replies, and we assume that we have an interval of length  $T_L$  on which these sources are present throughout the interval, so that we can assume the statistical properties to be stationary. Define the auto-correlation of a source  $s[k]$  by  $\underline{\gamma}[\tau] \stackrel{\text{def}}{=} \text{E}\{s[k]s^*[k - \tau]\}$ . Then for any integer  $\tau$ , such that  $16 < \tau \ll T_L$ , the next property holds:

$$\underline{\gamma}[\tau] = \frac{1}{4}\phi^\tau \tag{6.28}$$

where  $\phi = \exp(2\pi jfT)$ , with  $T$  the sampling period and  $f$  the residual carrier of the source  $s[k]$ .

The Second-Order Blind Identification (SOBI) algorithm [17] is a technique to blindly separate sources based on differences in second-order spectral content. Our aim in this Section is to extend the SOBI to also take the SSR property (6.28) into account. We first recall the original SOBI in Subsection 6.3.1. Next, in Subsection 6.3.2, we describe our extension using the additional knowledge of (6.28). Finally, we discuss the merits of this algorithm.

### 6.3.1 The original SOBI: principle

Consider the data model  $\mathbf{x}[k] = \mathbf{M}\mathbf{s}[k] + \mathbf{n}[k]$ , where the vector signal  $\mathbf{s}[k]$  consists of  $d$  independent wide-sense stationary sources  $s_i[k]$  with different non-white spectral content. For each  $i \in \{1, \dots, m\}$ , the  $i$ -th component of the noise  $b_{n_i}[k]$  is additive zero-mean Gaussian noise, temporally independently identically distributed. Let  $\underline{\gamma}_i[\tau] = \mathbb{E}\{s_i[k]s_i^*[k-\tau]\}$ , and define the non-central auto-covariance of the vector  $\mathbf{x}$  at time-lag  $\tau$  as

$$\mathbf{R}_\tau \stackrel{\text{def}}{=} \mathbb{E}\{\mathbf{x}[k]\mathbf{x}^H[k-\tau]\} \quad (6.29)$$

We denote by  $\mathbf{m}_i$  the  $i$ -th column of  $\mathbf{M}$ . Inserting this in Equation (6.29), we obtain for any integer  $\tau \in \mathbb{N}$ :

$$\begin{aligned} \mathbb{E}\{\mathbf{x}[k]\mathbf{x}^H[k-\tau]\} &= \sum_{i=1, j=1}^d \mathbf{m}_i \mathbf{m}_j^H \mathbb{E}\{s_i[k]s_j^*[k-\tau]\} + \sum_{i=1}^d \mathbf{m}_i \mathbb{E}\{s_i[k]\mathbf{n}^H[k-\tau]\} \\ &+ \sum_{j=1}^d \mathbb{E}\{s_j^*[k-\tau]\mathbf{n}[k]\}\mathbf{m}_j^H + \mathbb{E}\{\mathbf{n}[k]\mathbf{n}^H[k-\tau]\} \end{aligned}$$

which consists of the sum of four terms. When  $\tau \neq 0$ , the last three terms are null due to the statistical properties of the noise:

$$\begin{aligned} \mathbb{E}\{\mathbf{n}\} &= 0 \\ \mathbb{E}\{\mathbf{n}[k]\mathbf{n}^H[k-\tau]\} &= 0 \quad \text{if } \tau \neq 0 \end{aligned}$$

The first term simplifies because there is no correlation for two different sources:  $\mathbb{E}\{s_j[k]s_i^*[k-\tau]\} = 0$ , if  $i \neq j$ ,  $\forall \tau \in \mathbb{N}$ . Thus, the auto-covariance matrices become

$$\mathbf{R}_\tau = \sum_{i=1}^d \underline{\gamma}_i[\tau] \mathbf{m}_i \mathbf{m}_i^H$$

with  $\tau \neq 0$ , or equivalently:

$$\mathbf{R}_\tau = \mathbf{M} \begin{bmatrix} \underline{\gamma}_1[\tau] & \dots & 0 \\ \vdots & \ddots & \vdots \\ 0 & \dots & \underline{\gamma}_d[\tau] \end{bmatrix} \mathbf{M}^H = \mathbf{M}\mathbf{\Gamma}_\tau\mathbf{M}^H \quad (6.30)$$

We collect  $L$  matrices  $\mathbf{R}_\tau$  with different  $\tau$ ,  $\tau \in \{\tau_1, \dots, \tau_L\}$ . Note that all the  $\mathbf{R}_\tau$  have a diagonal form in the same basis,  $\mathbf{M}$ . One can prove that if the  $\mathbf{\Gamma}_\tau$  are

sufficiently different and  $\mathbf{M}$  is full rank, the only matrix that jointly diagonalizes this collection is  $\mathbf{M}$ , up to a column permutations and/or a unit-norm column scaling.

There are various algorithms for computing  $\mathbf{M}$ . Consider for example two matrices  $\mathbf{R}_1, \mathbf{R}_2$ , then  $\mathbf{R}_1\mathbf{R}_2^{-1} = \mathbf{M}(\mathbf{\Gamma}_1\mathbf{\Gamma}_2^{-1})\mathbf{M}^{-1}$ , hence  $\mathbf{M}$  can be estimated from an eigenvalue decomposition of  $\mathbf{R}_1\mathbf{R}_2^{-1}$ . Better joint diagonalization algorithms take all available matrices into account and also work if the  $\mathbf{\Gamma}_i$  are not invertible. The proposed algorithm in [17] uses the joint diagonalization of Cardoso [45].

### Discussion

In an implementation of the algorithm, the true  $\mathbf{R}_\tau$  are unknown and have to be estimated by  $\hat{\mathbf{R}}_\tau = (N - \tau)^{-1} \sum_{k=\tau+1}^N \mathbf{x}[k]\mathbf{x}[k - \tau]$ . When the number of samples is small, the cross-terms in the correlation (6.29) do not become precisely zero, and the matrices  $\hat{\mathbf{R}}_\tau$  will not be exactly diagonalizable. This is true even in the noise-less case, since the method heavily relies on the cross-correlation of the sources to be zero for all lags. Hence, SOBI is not consistent as the Signal to Noise Ratio (SNR) tends to infinity.

Nonetheless, for a small number of samples, SOBI is often an improvement over fourth-order methods because the second order sample moments will converge to their asymptotic values much faster than the fourth order sample moments, and their functions such as e.g. the kurtosis tensor.

SOBI also has a lower computational cost, determined mostly by the computation of the matrices  $\hat{\mathbf{R}}_\tau$ , which is of order  $LNd^2$  multiplications.

### 6.3.2 An evolution: ESPRIT-SOBI

In this Subsection, we extend on SOBI by also using the property that  $\gamma_i[\tau] = \frac{1}{4}\phi_i^\tau$ , where the  $\phi_i$  are complex on the unit circle:  $\phi_i = \exp(2\pi j f_i T)$ .

Recall that  $\mathbf{m}_i$  is the  $i$ -th column of  $\mathbf{M}$ , and define the vector  $\tilde{\mathbf{m}}_i$  as  $\tilde{\mathbf{m}}_i \stackrel{\text{def}}{=} \text{Vec}(\mathbf{m}_i\mathbf{m}_i^H) = \mathbf{m}_i^* \otimes \mathbf{m}_i$ . We also define

$$\tilde{\mathbf{M}} = [\tilde{\mathbf{m}}_1, \dots, \tilde{\mathbf{m}}_d] = [\mathbf{m}_1^* \otimes \mathbf{m}_1, \dots, \mathbf{m}_d^* \otimes \mathbf{m}_d] \stackrel{\text{def}}{=} \mathbf{M}^* \circ \mathbf{M}$$

where  $\circ$  denotes a column-wise Kronecker product (also known as the Khatri-Rao product). Using Equation (1.5) in Equation (6.30) leads to

$$\mathbf{r}_\tau \stackrel{\text{def}}{=} \text{Vec}(\mathbf{R}_\tau) = \frac{1}{4}\tilde{\mathbf{M}} \begin{bmatrix} \phi_1^\tau \\ \vdots \\ \phi_d^\tau \end{bmatrix} \quad \forall \tau \in \{\tau_1, \dots, \tau_L\} \quad (6.31)$$

We collect the  $\mathbf{r}_\tau$ ,  $\forall \tau \in \{\tau_1, \dots, \tau_L\}$ , in a matrix  $\mathbf{R}^\circ$ :

$$\mathbf{R}^\circ \stackrel{\text{def}}{=} [\mathbf{r}_{\tau_1} \dots \mathbf{r}_{\tau_L}] \quad (6.32)$$

Thus we obtain from Equation (6.31) that

$$\mathbf{R}^\circ = \frac{1}{4} \tilde{\mathbf{M}} \begin{bmatrix} \phi_1^{\tau_1} & \dots & \phi_1^{\tau_L} \\ \vdots & & \vdots \\ \phi_d^{\tau_1} & \dots & \phi_d^{\tau_L} \end{bmatrix}$$

We now choose the  $\tau_i$ 's as successive integers:  $\tau_i = \tau_1 + i - 1$ , for  $i = 1, \dots, L$ . Then  $\mathbf{R}^\circ$  becomes:

$$\mathbf{R}^\circ = \frac{1}{4} \tilde{\mathbf{M}} \text{diag}([\phi_1^{\tau_1}, \dots, \phi_d^{\tau_1}]) \begin{bmatrix} 1 & \phi_1 & \dots & \phi_1^{L-1} \\ \vdots & & & \vdots \\ 1 & \phi_d & \dots & \phi_d^{L-1} \end{bmatrix} \quad (6.33)$$

$$= \frac{1}{4} \tilde{\mathbf{M}} \mathbf{D} \mathbf{F} \quad (6.34)$$

At this point, note that  $\mathbf{F}$  has a Vandermonde structure. The shift invariance property of that matrix suggests the use of the ESPRIT algorithm to estimate the  $\phi_i$ , see Subsection 3.3.2. In particular, if  $\mathbf{F}_x$  contains columns  $0, \dots, L-2$  of  $\mathbf{F}$ , and  $\mathbf{F}_y$  contains columns  $1, \dots, L-1$ , then the shift-invariance property is

$$\mathbf{F}_y = \Phi \mathbf{F}_x, \quad \Phi \stackrel{\text{def}}{=} \text{diag}(\phi_1, \dots, \phi_d) \quad (6.35)$$

where we note that  $\mathbf{D} = \Phi^{\tau_1}$ .

In summary, our algorithm first computes an estimate of the matrix  $\mathbf{R}^\circ$ :  $\hat{\mathbf{R}}^\circ$ , which contains  $L$  successive time-lags with  $L \geq d+1$ . Since  $\mathbf{R}^\circ$  has rank  $d$ , we then perform a Singular Value Decomposition (SVD) on  $\hat{\mathbf{R}}^\circ$  in order to get a low rank factorization:  $\hat{\mathbf{R}}^\circ = \mathbf{U} \Sigma \mathbf{V}$ , where  $\mathbf{V}$  is  $d \times L$ . From the model in (6.34), note that there exist an invertible matrix  $\mathbf{T}$  such that  $\mathbf{V} = \mathbf{T} \mathbf{F}$ . We apply ESPRIT: let  $\mathbf{V}_x$  contain the columns of  $\mathbf{V}$  except for the last, and  $\mathbf{V}_y$  the columns of  $\mathbf{V}$  except for the first, then from (6.35),  $\mathbf{V}_y = \mathbf{T} \Phi \mathbf{T}^{-1} \mathbf{V}_x$ , hence<sup>2</sup>

$$\mathbf{V}_y \mathbf{V}_x^\dagger = \mathbf{T} \Phi \mathbf{T}^{-1},$$

and an eigenvalue decomposition of  $\mathbf{V}_y \mathbf{V}_x^\dagger$  reveals both  $\mathbf{T}$  and  $\Phi$ , hence the  $\phi_i$ 's. We can reconstruct  $\tilde{\mathbf{F}} = \mathbf{T}^{-1} \mathbf{V}$  and  $\tilde{\mathbf{D}} = \text{diag}([\phi_1^{\tau_1}, \dots, \phi_d^{\tau_1}])$ , and estimate  $\tilde{\mathbf{M}}$  as:

$$\tilde{\mathbf{M}} = 4 \hat{\mathbf{R}}^\circ \tilde{\mathbf{F}}^\dagger \tilde{\mathbf{D}}^{-1} \quad (6.36)$$

The estimation of  $\mathbf{M}$  from  $\tilde{\mathbf{M}}$  is in fact a series of  $d$  smaller problems: the estimation of the  $\mathbf{m}_i$ 's from the columns  $\tilde{\mathbf{m}}_i$  of  $\tilde{\mathbf{M}}$ , for  $i = 1, \dots, d$ . Using the definition

$$\tilde{\mathbf{m}}_i \stackrel{\text{def}}{=} \text{Vec}(\mathbf{m}_i \mathbf{m}_i^H) \Leftrightarrow \text{Unvec}(\tilde{\mathbf{m}}_i) = \mathbf{m}_i \mathbf{m}_i^H$$

we can estimate each  $\mathbf{m}_i$  by taking the dominant left singular vector of the matrix  $\text{Unvec}(\tilde{\mathbf{m}}_i)$ . Next,  $\hat{\mathbf{S}}$  is obtained as:

$$\hat{\mathbf{S}} = \hat{\mathbf{M}}^{-1} \mathbf{X}$$

We summarize the algorithm in Table 6.2.

---

<sup>2</sup>()<sup>†</sup> stands for pseudo-inverse.

1	Calculate $\hat{\mathbf{R}}_k$ for $k = 1$ to $L$ .
2	Stack the $\text{vec}(\hat{\mathbf{R}}_k)$ into $\hat{\mathbf{R}}^\circ$ .
3	Perform a SVD of $\hat{\mathbf{R}}^\circ$ , to extract $\mathbf{V}$ .
4	Apply ESPRIT on $\mathbf{V}$ to obtain $\phi_i, i \in \{1, \dots, d\}$ .
5	Use the $\phi_i$ to reconstruct $\tilde{\mathbf{F}}$ and $\mathbf{D}$ .
6	Estimate $\tilde{\mathbf{M}}$ from $\tilde{\mathbf{\Phi}}$ .
7	Estimate $\hat{\mathbf{M}}$ , and then $\hat{\mathbf{S}}$ .

Table 6.2: ESPRIT-SOBI algorithm.

### 6.3.3 Discussion

As for SOBI, the computational cost is dominated by the construction of  $\mathbf{R}^\circ$ , which costs order  $Ld^2N$  flops.

The number of lags  $L$  in the algorithm is a design parameter. The minimal number is  $L = d + 1$ , the maximal number is determined by  $T_L$ , the length of the time interval on which the data is taken. The optimal choice for  $L$  is not known. One consideration is that for robustness reasons, it is desirable to have more shifts than the minimal number. In general, the accuracy of the ESPRIT step increases with  $L$ . However, the accuracy of the covariance estimates  $\mathbf{R}_\tau$  decreases for larger lags, since with finite data we can average over fewer samples, and incorporating these lags in the ESPRIT step will decrease the performance. Hence there is a trade-off. Also note that the computational cost is linear with the number of shifts.

The ESPRIT-SOBI has several advantages: the computational cost is lower than for the multi-shift-ZCMA, unlike SOBI there is no need for a joint diagonalization, more sources than sensors can be detected, as demonstrated by simulations in Chapter 7. Furthermore, the detection of the number of sources  $d$  might be done more accurately on  $\mathbf{R}^\circ$  than the usual White Noise Test (WNT) directly on the data (we have not verified this statement). All statistics are of second-order, so in number of samples the method converges faster than High-Order Statistics (HOS) methods.

On the other hand, like for SOBI, the algorithm is not consistent as SNR goes to infinity and the number of samples is finite, because the algorithm relies on the decorrelation of the sources. This will limit the performance of the algorithm for high SNRs as compared to other algorithms that are asymptotically consistent, such as the multi-shift-ZCMA. Simulations indicate that the poor finite-sample performance is indeed a significant limitation of this type of algorithms.

#### Mode A/C replies

Mode A/C replies have the same property (6.28) as Mode S replies, but with different characteristic times, as discussed in Section 3.2. Thus, a mixture of only mode A/C replies can be separated using the same principle, but a mixture of both types of signals needs additional attention.

For future research, we suggest to use initially time-lags  $\tau$ 's larger than the time life of the mode A/C replies. This will suppress the mode A/C signals in the



correlations  $\mathbf{R}_r$ . Applying the ESPRIT-SOBI algorithm to these matrices allows us to estimate the columns of  $\mathbf{M}$  that concerns mode S replies only. It is then possible to project out the subspace spanned by these columns, and to concentrate on the mode A/C replies with their more specific properties.

## 6.4 Manchester Decoding Algorithm

In chapter 3, we have shown that the SSR replies have a special encoding. Indeed, the Mode S source are encoded in a ‘‘Manchester encoding’’ scheme, which means that a bit 0 is coded as [01], and a bit 1 as [10]. If the receiver is synchronized to the time of arrival, a mode S reply has a data stream  $b[k]$  that obeys:

$$b[k]b[k + 1] = 0 \quad (6.37)$$

with a sampling rate as  $T = 0.5 \mu s$ . Otherwise, when un-synchronized, the data stream obeys:

$$b[k - 1]b[k]b[k + 1] = 0 \quad (6.38)$$

Since mode A/C and mode S replies have different data-rates, and different properties, it is complicated to consider an algorithm that can process both of them. In this section, we will consider only a mixture of mode S replies. We will derive the ‘‘Manchester Decoding Algorithm’’ (MDA) that will separate the sources based on property (6.38).

In Subsection 6.4.1, we introduce the principle of separation based on Property (6.37), and we present the Manchester Decoding Algorithm, the MDA2, where 2 stands for second-order. In Subsection 6.4.2, using the Property (6.38), we propose an alternative algorithm using the third-order Kronecker product of the beamformer, which is called MDA3. Subsection 6.4.3 is dedicated to a specific step of the MDA3: the final third-order joint diagonalization. After a discussion of the merits and problems of the MDA’s in Subsection 6.4.4, we give in the last Subsection a few hints how to deal with a mixture of replies with different modes.

### 6.4.1 Principle of the MDA2

Property (6.37) states that, if we are synchronized, then from two consecutive samples of a mode S source one sample must be zero. The problem we face is that we do not know the time synchronization. Indeed, we cannot assume that the receivers are synchronized with the replies, since the problem is blind. Moreover, two replies from different planes cannot be synchronized, therefore we are dealing with a mixture of fully un-synchronized mode S replies.

As a consequence, Property (6.37) is true only every two samples. The idea is then to consider the next two products:

$$p_1[k] = s[2k]s[2k + 1] \quad (6.39)$$

$$p_2[k] = s[2k + 1]s[2k + 2] \quad (6.40)$$

where  $s[k]$  is a mode S source. Depending on the synchronization, one product of the two is always equal to 0, and the other is random.

We now consider a beamformer  $\mathbf{w}$  such that its application to  $\mathbf{x}[k]$  gives an estimate of one of the replies:  $\hat{s}_i[k] = \mathbf{w}^H \mathbf{x}[k]$ , which satisfies the Property (6.37). Inserting this in (6.39) and (6.40), we obtain

$$\mathbf{P}_1(\mathbf{w} \otimes \mathbf{w}) = \mathbf{0} \quad \text{or} \quad \mathbf{P}_2(\mathbf{w} \otimes \mathbf{w}) = \mathbf{0}$$

where  $\mathbf{P}_i$  is the collection into a tall matrix of the  $N/2$  rows:  $[\mathbf{x}[2k+i] \otimes \mathbf{x}[2k+1+i]]^H$ , for  $i \in \{1, 2\}$ , and  $\forall k \in \{0, \dots, N/2-1\}$ .

For each beamformer  $\mathbf{w}_i$ , the vector  $\mathbf{w}_i \otimes \mathbf{w}_i$  belongs then either to the kernel of  $\mathbf{P}_1$  or to the kernel of  $\mathbf{P}_2$ . Under conditions of Proposition 6.4.1, we state that for sufficiently large  $N$  there are no other vectors in the union of the kernels, so that we have a one-to-one mapping of an arbitrary basis of each kernel to the corresponding basis of beamformers  $\mathbf{w}_i \otimes \mathbf{w}_i$  of the sources that have the corresponding synchronization. In that case, we can detect the number of sources with a particular synchronization from the dimension of the corresponding kernel, and we can estimate the beamformers from a joint diagonalization procedure applied to each basis.

In the next proposition, we state that as the number of samples increases and the sources are completely overlapping, then the union of the kernels of  $\mathbf{P}_1$ , and  $\mathbf{P}_2$  will be precisely of dimension  $d$ . This implies that there are no other solutions than  $\mathbf{w}_i \otimes \mathbf{w}_i$ ,  $i = 1, \dots, d$ , so that the problem is identifiable.

**Proposition 6.4.1** *Assume that  $\mathbf{M}$  is invertible, the sources are totally overlapping, and that there is no noise. Then for large number of samples  $N$ , the union of the kernel of the matrices  $\mathbf{P}_1$  and  $\mathbf{P}_2$  will almost surely be of dimension  $d$ .*

**Proof:** We define  $\mathbf{S}_2^{(i)}$  as the stacking into a tall matrix of the  $N/2$  rows:  $[\mathbf{s}[2k+i] \otimes \mathbf{s}[2k+1+i]]^H$ , for  $i \in \{1, 2\}$ , and  $\forall k \in \{0, \dots, N/2-1\}$ . Some derivations shows then:

$$\begin{aligned} \mathbf{P}_1 &= \mathbf{S}_2^{(1)}(\mathbf{M} \otimes \mathbf{M})^H \\ \mathbf{P}_2 &= \mathbf{S}_2^{(2)}(\mathbf{M} \otimes \mathbf{M})^H \end{aligned}$$

Since  $\mathbf{M}$  is invertible, Lemma 1.7.1 insures that  $(\mathbf{M} \otimes \mathbf{M})$  is invertible as well, so there is equality between the rank of the  $\{\mathbf{P}_i\}$  and the  $\{\mathbf{S}_2^{(i)}\}$ , for  $i \in \{1, 2\}$ : We define the covariance matrix of  $\mathbf{S}_1$  as  $\hat{\mathbf{R}}_1 = \frac{1}{N} \mathbf{S}_1^H \mathbf{S}_1$ , and the covariance matrix of  $\mathbf{S}_2$  as  $\hat{\mathbf{R}}_2 = \frac{1}{N} \mathbf{S}_2^H \mathbf{S}_2$ . For  $i \in \{1, 2\}$ ,  $\hat{\mathbf{R}}_i$  has the same rank as  $\mathbf{S}_i$  as soon as  $N \geq d^2$ . We investigate the rank of  $\hat{\mathbf{R}}_i$  as  $N$  tends to infinity, which is equal to the rank of  $\mathbf{R}_i$  almost surely.

Denote the  $m$ -th source at time  $k$  as  $s_m[k] = b_m[k] \phi_m^k$ , where  $b_m[k]$  is the transmitted symbol (0 or 1 with equal probability) and  $\phi_m$  is the residual phase rotation,

random on the unit circle. The  $i, j$ -th entry of  $\hat{\mathbf{R}}_\alpha$ ,  $\alpha \in \{1, 2\}$  is

$$\left(\hat{\mathbf{R}}_\alpha\right)_{i,j} = \frac{1}{N} \sum_{k=0}^{N/2-1} b_m[2k+\alpha]b_n[2k+\alpha-1]b_o[2k+\alpha]b_p[2k+\alpha-1] \\ \phi_m^{-2k-\alpha}\phi_n^{-2k-\alpha+1}\phi_o^{2k+\alpha}\phi_p^{2k+\alpha-1}$$

where  $i = md + n$ , and  $j = od + p$ , for  $m, n, o, p = 1, \dots, d$ . As  $N \rightarrow \infty$ ,  $\hat{\mathbf{R}}_\alpha$  converges to  $\mathbf{R}_\alpha$ .

For doublets that are not equal up to a permutation,  $\{m, n\} \neq \{o, p\}$ , the residual carrier induces the terms  $(\hat{\mathbf{R}}_\alpha)_{i,j}$  to tend towards zero. By re-ordering the rows and columns of  $\mathbf{R}_\alpha$ , we transform it into a block-diagonal matrix, with two kinds of sub-matrices.

1. The first kind of sub-matrices are of size  $1 \times 1$  for triplets of the form  $\{n, n\}$ , for  $n = 1, \dots, d$ , with value

$$\left(\hat{\mathbf{R}}_\alpha\right)_{i,i} = \frac{1}{N} \sum_{k=2}^{N-1} b_n[2k-1]b_n[2k]$$

with  $i = n(d+1)$ , it corresponds to the source  $n$ . Because of Property (6.37), one of the two elements  $(\hat{\mathbf{R}}_\alpha)_{i,i}$ ,  $\alpha \in \{1, 2\}$ , is always equal to 0, and the other tends to  $\frac{1}{4}$  as  $N \rightarrow \infty$ . The matrix, which element is zero, corresponds to the sub-sampled series  $s_n[2k+\alpha]$  synchronized to the source  $n$ , the other matrix is un-synchronized. So the sub-matrix is zero only in one of the two matrices  $\mathbf{R}_\alpha$ . There are precisely  $d$  sub-matrices of this kind on both matrices. Moreover, there are not placed at the same position in the matrix. They thus contribute  $d$  dimensions to the union of the kernel of  $\mathbf{R}_1$  and  $\mathbf{R}_2$ .

2. The second kind of sub-matrices are of size  $2 \times 2$  for doublets of forms  $\{n, m\}$  and  $n \neq m$ . Denote the corresponding sub-matrices by  $\mathbf{R}'$ . Let  $\psi = \phi_m\phi_n^*$  and  $\mathbf{C}_2 = \text{diag}\{1, \psi\}$ , then  $\mathbf{R}' = 1/16 \mathbf{C}_2^* (3\mathbf{I}_2 + \mathbf{1}^H \mathbf{1}) \mathbf{C}_2$ , which is full rank.

Hence, the union of the kernels of  $\{\mathbf{R}_1, \mathbf{R}_2\}$  is asymptotically of dimension  $d$ . By continuity, this will almost surely be the case for finite but sufficiently large  $N$ .  $\square$

Note that if two sources  $s_1$  and  $s_2$  have non-overlapping time-support domains, as in Figure 6.2, then all columns of the matrices  $\mathbf{S}_2^{(1)}$  and  $\mathbf{S}_2^{(2)}$  that contain a cross-product of these two sources will zero. As a result, the size of the union of the kernels will be larger than  $d$ , making the algorithm fail.

We denote by  $d_i$  the dimension of the kernel of  $\mathbf{P}_i$ ,  $i \in \{1, 2\}$ , with  $d = d_1 + d_2$ , and we define  $\mathbf{U}_i$  as a  $d^2 \times d_i$  matrix whose columns are a basis of the kernel of  $\mathbf{P}_i$ . We assume that the conditions of proposition 6.4.1 are fulfilled, so we have:

$$\mathbf{U}_i = (\mathbf{W}_i \circ \mathbf{W}_i) \mathbf{T}_i, \quad i = 1, 2$$

where  $\mathbf{W}_i$  contains the  $d_i$  beamformers  $\mathbf{w}$ 's related to the kernel of  $\mathbf{P}_i$ , and  $\mathbf{T}_i$  is a  $d_i \times d_i$  invertible matrix.

First, we consider the case  $i = 1$ . We denote  $\mathbf{u}_i$ , the  $i$ -th column of  $\mathbf{U}_1$ . By using the unvec operator we obtain:

$$\text{unvec}(\mathbf{u}_i) = \sum_{j=1}^{d_1} (\mathbf{T}_1)_{ij} \mathbf{w}_j \mathbf{w}_j^T$$

where we note that the  $\{\text{unvec}(\mathbf{u}_i)\}$  have a diagonal form in the basis  $\mathbf{W}_1$ . It is a joint diagonalization problem, on which we can use the algorithm in [12]. We do the same joint diagonalization with the columns of  $\mathbf{U}_2$  to obtain  $\mathbf{W}_2$ , then we obtain  $\mathbf{W}$  as  $\mathbf{W} = [\mathbf{W}_1 \mathbf{W}_2]$ .

Once the beamformers are determined, we separate the sources:  $\hat{\mathbf{s}}[k] = \mathbf{W}^H \mathbf{x}[k]$ ,  $\forall k \in \{1, \dots, N\}$ . As in the multi-shift-ZCM Algorithm, the residual frequencies and the matrix  $\mathbf{M}$  are estimated with Equation (6.5), and Equation (6.3), respectively. Finally, we can estimate the Directions of Arrival (DOAs) from each column of the estimated matrix  $\widehat{\mathbf{M}}$  separately, e.g. by applying a simplified version of the ESPRIT algorithm.

The outline of the algorithm is restated in Table 6.3.

- |   |   |
|---|---|
| 1 | Construct $\mathbf{P}_1, \mathbf{P}_2$ from $\mathbf{X}$ .  |
| 2 | Extract $\mathbf{U}_1$ , and $\mathbf{U}_2$ from the kernels of $\mathbf{P}_1$ , and $\mathbf{P}_2$ . |
| 3 | Jointly diagonalize the columns of the $\{\mathbf{U}_i\}$ to get $\mathbf{W}$ .                       |
| 4 | Separate the sources via $\hat{\mathbf{S}} = \mathbf{W}^H \mathbf{X}$ .                               |
| 5 | Estimate $\widehat{\mathbf{M}}$ , and the DOA's.  |
| 6 | Estimate the residual frequencies.  |

Table 6.3: MDA2 Algorithm.

The most expensive step is the QR factorization of the  $\mathbf{P}_i$ 's, required in the computation of the kernels in step 2, with an associated cost of order  $Nd^4$  flops.

### 6.4.2 Principle of the MDA3

To avoid the problem of estimating the kernels of two different matrices, we investigate in this Subsection if it is possible to use the combined Property (6.38), to arrive at only one, but bigger, matrix.

As in the preceding Subsection, we consider a beamformer  $\mathbf{w}$  such that  $\hat{s}_i[k] = \mathbf{w}^H \mathbf{x}[k]$ . From Equation (6.38), we can derive:

$$\hat{s}_i[k+1] \hat{s}_i[k] \hat{s}_i[k-1] = 0. \quad (6.41)$$

Using twice Equation (1.3), we get:

$$[\mathbf{x}[k+1] \otimes \mathbf{x}[k] \otimes \mathbf{x}[k-1]]^H (\mathbf{w} \otimes \mathbf{w} \otimes \mathbf{w}) = 0 \quad (6.42)$$

We define the matrix  $\mathbf{P}_3 : N \times d^3$  as the collection of the rows  $[\mathbf{x}[k+1] \otimes \mathbf{x}[k] \otimes \mathbf{x}[k-1]]^H$  for  $k \in \{2, \dots, N-1\}$ , and obtain:

$$\mathbf{P}_3 \mathbf{w}^\diamond = 0, \quad \mathbf{w}^\diamond \stackrel{\text{def}}{=} \mathbf{w} \otimes \mathbf{w} \otimes \mathbf{w} \quad (6.43)$$

When there are  $d$  sources, there are  $d$  linearly independent separating beamformers  $\mathbf{w}_i$ ,  $i = 1, \dots, d$ . Thus we have  $d$  linearly independent vectors  $\mathbf{w}_i^\diamond$  that belong to the kernel of  $\mathbf{P}_3$ . If the kernel is  $d$ -dimensional, then the subspace spanned by the  $\mathbf{w}_i^\diamond$  is exactly equal to the kernel, and a basis for the kernel must be a linear combination of the  $\mathbf{w}_i^\diamond$ . The algorithm will be to estimate an arbitrary basis for the kernel, then to find the linear combinations to map the basis to the structured vectors  $\mathbf{w}_i^\diamond$ , and subsequently to estimate the corresponding  $\mathbf{w}_i$  for each vector.

In the next proposition, we state that as the number of samples increases and the sources are completely overlapping, then the kernel of  $\mathbf{P}_3$  will be precisely of dimension  $d$ . This implies that there are no other solutions than  $\mathbf{w}_i^\diamond$ ,  $i = 1, \dots, d$ , so that the problem is identifiable.

**Proposition 6.4.2** *Assume that  $\mathbf{M}$  is invertible, the sources are totally overlapping, and that there is no noise. Then for large number of samples  $N$ , the matrix  $\mathbf{P}_3$  will almost surely have rank  $(d^3 - d)$ , equivalently its kernel will almost surely be of dimension  $d$ .*

**Proof:** A short derivation shows that

$$\mathbf{x}[k+1] \otimes \mathbf{x}[k] \otimes \mathbf{x}[k-1] = (\mathbf{M} \otimes \mathbf{M} \otimes \mathbf{M}) [\mathbf{s}[k+1] \otimes \mathbf{s}[k] \otimes \mathbf{s}[k-1]] \quad (6.44)$$

After defining  $\mathbf{S}_3$  as the collection of the rows  $[\mathbf{s}[k+1] \otimes \mathbf{s}[k] \otimes \mathbf{s}[k-1]]^H$ , for  $k \in \{2, \dots, N-1\}$ , we get:

$$\mathbf{P}_3 = \mathbf{S}_3 (\mathbf{M} \otimes \mathbf{M} \otimes \mathbf{M})^H \quad (6.45)$$

Since  $\mathbf{M}$  is invertible, Lemma 1.7.1 insures that  $(\mathbf{M} \otimes \mathbf{M} \otimes \mathbf{M})$  is invertible as well, so the rank of  $\mathbf{P}_3$  is equal to the rank of  $\mathbf{S}_3$ . Define the covariance matrix of  $\mathbf{S}_3$  as  $\hat{\mathbf{R}}_{ss}^{(3)} = \frac{1}{N} \mathbf{S}_3^H \mathbf{S}_3$ . It has the same rank as  $\mathbf{S}_3$  as soon as  $N \geq d^3$ . We will verify the rank of  $\hat{\mathbf{R}}_{ss}^{(3)}$  as  $N$  tends to infinity.

Denote the  $m$ -th source at time  $k$  as  $s_m[k] = b_m[k] \phi_m^k$ , where  $b_m[k]$  is the transmitted symbol (0 or 1 with equal probability) and  $\phi_m$  is the residual phase rotation, random on the unit circle. The  $i, j$ -th entry of  $\hat{\mathbf{R}}_{ss}^{(3)}$  is

$$\begin{aligned} \left( \hat{\mathbf{R}}_{ss}^{(3)} \right)_{i,j} &= \frac{1}{N} \sum_{k=2}^{N-1} b_m[k-1] b_n[k] b_l[k+1] b_o[k-1] b_p[k] b_q[k+1] \\ &\quad \phi_m^{-k+1} \phi_n^{-k} \phi_l^{-k-1} \phi_o^{k-1} \phi_p^k \phi_q^{k+1} \end{aligned}$$

where  $i = md^2 + nd + l$ , and  $j = od^2 + pd + q$ , for  $m, n, l, o, p, q = 1, \dots, d$ . As  $N \rightarrow \infty$ ,  $\hat{\mathbf{R}}_{ss}^{(3)}$  converges to  $\mathbf{R}_{ss}^{(3)}$ .

Before demonstrating that the rank of  $\mathbf{R}_{ss}^{(3)}$  is  $d^3 - d$ , we show it in the case  $d = 2$  for the reader's convenience. Define  $\psi = \phi_1 \phi_2^*$ , and re-order the columns and the rows in order to follow the triplets  $(m, n, l) = (1, 1, 1), (1, 1, 2), (1, 2, 1), (2, 1, 1)$ ,

$(1, 2, 2), (2, 1, 2), (2, 2, 1), (2, 2, 2)$ . Then the matrix converges to:

$$\mathbf{R}_{ss}^{(3)} = \frac{1}{32} \begin{bmatrix} 0 & 0 & 0 & 0 & 0 & 0 & 0 & 0 \\ 0 & 4 & \psi & \psi^2 & 0 & 0 & 0 & 0 \\ 0 & \psi^* & 4 & \psi & 0 & 0 & 0 & 0 \\ 0 & \psi^{*2} & \psi^* & 4 & 0 & 0 & 0 & 0 \\ 0 & 0 & 0 & 0 & 4 & \psi & \psi^2 & 0 \\ 0 & 0 & 0 & 0 & \psi^* & 4 & \psi & 0 \\ 0 & 0 & 0 & 0 & \psi^{*2} & \psi^* & 4 & 0 \\ 0 & 0 & 0 & 0 & 0 & 0 & 0 & 0 \end{bmatrix}$$

which is of rank  $6 = 2^3 - 2$ . There are precisely  $d = 2$  columns equal to zero, which give the kernel a dimension of 2. The rest of the matrix is block-diagonal with non-singular blocks of size  $3 \times 3$ .

Now, we consider the general case. For triplets that are not equal up to a permutation,  $\{m, n, l\} \neq \{o, p, q\}$ , the residual carrier induces the term  $(\hat{\mathbf{R}}_{ss}^{(3)})_{i,j}$  to tend toward zero. By re-ordering the row and the columns of  $\mathbf{R}_{ss}^{(3)}$ , we transform it into a block-diagonal matrix, with three kinds of sub-matrices.

1. The first kind of sub-matrices are of size  $1 \times 1$  for triplets of the form  $\{n, n, n\}$ , for  $n = 1, \dots, d$ , with value

$$\left(\hat{\mathbf{R}}_{ss}^{(3)}\right)_{i,i} = \frac{1}{N} \sum_{k=2}^{N-1} b_n[k-1]b_n[k]b_n[k+1]$$

with  $i = n(d^2 + d + 1)$ . As  $N \rightarrow \infty$ , these elements converge to zero because of property 6.38. There are precisely  $d$  sub-matrices of this kind. They thus contribute  $d$  dimensions to the kernel of  $\mathbf{R}_{ss}^{(3)}$ .

2. The second kind of sub-matrices are of size  $3 \times 3$  for triplets of forms  $\{n, n, m\}$  and  $n \neq m$ . Denote the corresponding submatrices by  $\mathbf{R}_2$ . Let  $\psi = \phi_m \phi_n^*$  and  $\mathbf{C}_2 = \text{diag}\{1, \psi, \psi^2\}$ , then  $\mathbf{R}_2 = 1/32 \mathbf{C}_2^* (3\mathbf{I}_3 + \mathbf{1}^H \mathbf{1}) \mathbf{C}_2$ , which is full rank.
3. The third kind of sub-matrices are of size  $6 \times 6$  for triplets of forms  $\{n, m, l\}$  and  $m \neq n \neq l$ . Denote by  $\mathbf{R}_3$  the corresponding sub-matrices. Let  $\psi_1 = \phi_m \phi_n^*$ ,  $\psi_2 = \phi_l \phi_n^*$ , and  $\mathbf{C}_3 = \text{diag}\{\psi_2, \psi_1, \psi_1^* \psi_2, \psi_1^*, \psi_1 \psi_2^*, \psi_2^*\}$ , and define:

$$\mathbf{D} = \begin{bmatrix} 8 & 2 & 2 & 1 & 1 & 2 \\ 2 & 8 & 1 & 2 & 2 & 1 \\ 2 & 1 & 8 & 2 & 2 & 1 \\ 1 & 2 & 2 & 8 & 1 & 2 \\ 1 & 2 & 2 & 1 & 8 & 2 \\ 1 & 1 & 1 & 2 & 2 & 8 \end{bmatrix}$$

which is full rank. Then  $\mathbf{R}_3 = 1/64 \mathbf{C}_3^* \mathbf{D} \mathbf{C}_3$ , which is full rank.

Hence, the rank of  $\mathbf{R}_{ss}^{(3)}$  is equal to  $d^3 - d$ . Thus, as the number of samples tends towards infinity,  $\mathbf{S}_3$  and  $\mathbf{P}_3$  will have rank  $(d^3 - d)$ . By continuity, this will almost surely be the case for finite but sufficiently large  $N$ .  $\square$

Note that the same limitation as for the previous algorithm (MDA2) will occur in case of two sources with non-overlapping time-support. In that case all columns of the matrix  $\mathbf{S}_3$  containing a cross-product of these two sources will be zero, which will increase the dimension of its kernel and make the algorithm fail.

Let  $\mathbf{U}_0$  be a matrix whose columns form a basis for the kernel of  $\mathbf{P}_3$ , and define  $\mathbf{W}^\diamond = [\mathbf{w}_1^\diamond, \dots, \mathbf{w}_d^\diamond]$ . If the kernel of  $\mathbf{P}_3$  is  $d$ -dimensional, then  $\mathbf{W}^\diamond$  is also a basis for the kernel. There is a one-to-one relation between the two bases, so that

$$\mathbf{U}_0 = \mathbf{W}^\diamond \mathbf{T} \quad (6.46)$$

where  $\mathbf{T}$  is a  $d \times d$  invertible matrix. Denote by  $\mathbf{u}_i$  the  $i$ -th column of  $\mathbf{U}_0$ . Equation (6.46) gives for all  $i$  in  $\{1, \dots, d\}$ :

$$\mathbf{u}_i = \sum_{j=1}^d (\mathbf{T})_{ij} \mathbf{w}_j^\diamond$$

Recall from Section 1.7 that the Unvec operator is the operator that transforms a  $d^2$  vector into a  $d \times d$  matrix. We now denote similarly by Unvec3 the “three-dimensional Unvec operator” which transforms a  $d^3$  vector into a  $d \times d \times d$  “cube”. We denote the resulting cube:  $\text{unvec3}(\mathbf{u}_i) = \mathbb{U}_i$ , for all  $i$  in  $[1, \dots, d]$ . Note that application of this operator on  $\mathbf{w}_j^\diamond$  gives an elementary rank-1 cube,  $(\mathbb{W}_j)_{mnp} = \mathbf{w}_j(n)\mathbf{w}_j(m)\mathbf{w}_j(p)$ . So each cube  $\mathbb{U}_i$  is a linear combination of  $d$  elementary cubes  $\mathbb{W}_j$ ,

$$\mathbb{U}_i = \sum_{j=1}^d (\mathbf{T})_{ij} \mathbb{W}_j$$

In the basis of the  $\mathbf{w}_i$ 's, the cube  $\mathbb{U}_i$  would then be only with non-zero components on the main tridiagonal. It is a joint diagonalization problem in three dimensions, and the generalized eigenvectors are the  $\mathbf{w}_i$ 's. Since it is a difficult question, we keep this problem for the next Subsection, and assume from now that we have estimated  $\mathbf{W}$ .

Once the beamformers are determined, the remaining of the algorithm is the same as for the MDA2.

The outline of the algorithm is restated in Table 6.4.

The cost of this algorithm is driven by the cost of estimating the kernel of  $\mathbf{P}_3$ :  $N \times d^3$ . The main cost of this is formed by a QR factorization of  $\mathbf{P}_3$ , which is of order  $Nd^6/2$ .

### 6.4.3 The third-order joint diagonalization

The most difficult point of the algorithm is the joint diagonalization of a collection of cubes (see [50]). A “simpler” problem is the joint diagonalization of a collection of matrices.

1	Construct $\mathbf{P}_3$ from the $\mathbf{x}$ 's.
2	Extract $\mathbf{U}_0$ from the kernel of $\mathbf{P}_3$ .
3	Jointly diagonalize the columns of $\mathbf{U}_0$ to get $\mathbf{W}$ .
4	Separate the sources via $\hat{\mathbf{S}} = \mathbf{W}^H \mathbf{X}$ .
5	Estimate $\widehat{\mathbf{M}}$ , and the DOA's.
6	Estimate the residual frequencies.

Table 6.4: MDA3 Algorithm.

Towards this simplification, we propose the next procedure. Let  $\mathbf{u}_i$  be the  $i$ -th column of  $\mathbf{U}_0$  with size  $d^3$ , and recall that  $\mathbf{u}_i = \sum_{j=1}^d (\mathbf{T})_{ij} \mathbf{w}_j^\circ$ . We reshape  $\mathbf{u}_i$  into a  $d^2 \times d$  matrix  $\mathbf{U}_i$ , such that  $\text{vec}(\mathbf{U}_i) = \mathbf{u}_i$ . Then

$$\mathbf{U}_i = \sum_{j=1}^d (\mathbf{T})_{ij} (\mathbf{w}_j \otimes \mathbf{w}_j) \mathbf{w}_j^T = (\mathbf{W} \circ \mathbf{W}) \text{diag}(\mathbf{t}_i) \mathbf{W}^T \stackrel{\text{def}}{=} (\mathbf{W} \circ \mathbf{W}) \mathbf{\Lambda}_i \mathbf{W}^T$$

We can define the  $d^2 \times d^2$  matrix  $\mathbf{U}'$  as

$$\mathbf{U}' \stackrel{\text{def}}{=} [\mathbf{U}_1, \dots, \mathbf{U}_d] = (\mathbf{W} \circ \mathbf{W}) [\mathbf{\Lambda}_1 \mathbf{W}^T, \dots, \mathbf{\Lambda}_d \mathbf{W}^T]$$

This shows that  $\mathbf{U}'$  should be of rank  $d$ . Thus let  $\mathbf{V}$  be an estimated  $d$ -dimensional basis for the column span of  $\mathbf{U}'$ , obtained via an SVD of  $\mathbf{U}'$ , and let  $\mathbf{Q} = \mathbf{V}^H (\mathbf{W} \circ \mathbf{W})$ , with size  $d \times d$ . Then  $\mathbf{V}^H \mathbf{U}'$  is a dimension-reduced ( $d \times d^2$ ) matrix with square  $d \times d$  blocks  $\mathbf{V}^H \mathbf{U}_i$ , each of the form

$$(\mathbf{V}^H \mathbf{U}_i) = \mathbf{Q} \mathbf{\Lambda}_i \mathbf{W}^T, \quad i = \{1, \dots, d\}$$

Thus, the problem is reduced to a standard (unsymmetric) joint diagonalization problem, and the algorithm in [12] can be applied to estimate  $\mathbf{W}$ .

#### 6.4.4 Discussion

The MDA2 and MDA3 methods have a lower cost than the Multi-Shift ZCMA, and they are not iterative. They are deterministic, so they have better performance than SOBI-ESPRIT for finite number of samples and good SNR. Unfortunately, a joint diagonalization is needed and as for AZCMA the method is highly sensitive to the presence of non-overlapping sources.

MDA2 has the advantage over MDA3 that the dimensions of the matrices are much smaller, and that the data is cross-multiplied only to order two rather than 3 or 4, which should lead to better numerical properties. A related advantage of this method is its lower computational cost. Indeed, the cost of MDA2 is about  $Nd^4$  flops, whereas MDA3 has  $Nd^6/2$  flops.



### 6.4.5 Mode A/C replies

Mode A/C is the main problem in this method. Indeed, even without time-synchronization  $s[t]s[t - T_C/2] = 0$  holds true for mode A/C replies, which results in a too large kernel of  $\mathbf{S}_3$ .

To solve this problem, a two-stage algorithm is proposed: 1) the mode A/C replies are detected in a similar fashion, and filtered out; 2) the MDA is applied to the remaining signal.

We define  $\tilde{\mathbf{x}}[k] = \mathbf{x}[t = k\frac{T_C}{2}]$ , we consider the matrix  $\mathbf{P}_2$  that contains the rows  $[\tilde{\mathbf{x}}[k] \otimes \tilde{\mathbf{x}}[k+1]]^H$ . We denote by  $\mathbf{w}_c$  a beamformer that receives a mode A/C reply, then from Equation 3.4, we derive:

$$\mathbf{P}_2(\mathbf{w}_c \otimes \mathbf{w}_c) = 0$$

By performing a joint diagonalization on the kernel of  $\mathbf{P}_2$ , we recover all the mode A/C replies. We collect the  $\mathbf{w}_c$ 's in a tall matrix  $\mathbf{W}_c$ , and we denote by  $\mathbf{Q}$  the orthogonal projector to the sub-space spanned by  $\mathbf{W}_c$ . Then  $\mathbf{Q}\mathbf{X}$  is a mixture of mode S replies only, on which we can apply the MDA algorithm.

## 6.5 Post-processing

Unfortunately, we observe that the frequency estimate given by Equation (6.5) for the MS-ZCMA and the MDA's algorithms is far from the CRB. The idea is to estimate the frequency shift on the separated data, one advantage is that there should be only one source remaining in a time serie, the obvious drawback occurs when the separation is not efficient. While slightly better than Equation (6.5), a phase rotation based method (as ESPRIT on the time serie) performed on the estimated source signal had poor performance as well. So, we propose to minimize the following cost function with respect to the frequency estimate  $f'$  on the estimated source  $\hat{\mathbf{s}}$ , without knowing the bits:

$$\min_{f'} (N - \|\hat{\mathbf{s}}\mathbf{f}^H\|^2)$$

where  $\hat{\mathbf{s}}$  is the estimated signal,  $N$  the number of samples, and  $\mathbf{f} = [1, \phi, \dots, \phi^{N-1}]$ , where  $\phi = \exp^{2\pi j f' T}$ . In the noiseless case, we show that this cost is minimum when the frequency estimate  $f'$  is equal to the frequency shift of  $\hat{\mathbf{s}}$ . Indeed consider that  $\hat{\mathbf{s}}(k) = s_0 b(k) \exp^{2\pi j k f T}$ , with an unknown  $s_0 \in \mathbb{C}$ , and  $|s_0| = 1$ , then:

$$\begin{aligned} \|\hat{\mathbf{s}}\mathbf{f}^H\|^2 &= \left| \sum_{k=0}^{N-1} s_0 b(k) \exp^{2\pi j k f T} \exp^{-2\pi j k f' T} \right|^2 \\ &\leq \sum_{k=0}^{N-1} |s_0 b(k) \exp^{2\pi j k (f-f') T}|^2 \\ &\leq N_b i \end{aligned}$$

where  $N_b$  is the number of bits equal to one. So we obtain that the cost function is always larger to  $N - N_b$ . Note that if  $f = f'$ , there is equality, so the cost is minimum at  $f = f'$ .

## 6.6 Conclusion

This chapter have presented several algorithms to separate the SSR sources. Depending the property on which each algorithm is based, we have described what is likely to be the performance of each algorithm for certain conditions. One algorithm is stochastic, while the others are deterministic.

## Chapter 7

# Simulations

In the previous chapter, we proposed algorithms to separate SSR sources. At this point, we desire to test and confirm the conclusions of the preceding chapter using computer simulations. With the simulations, we also desire to assess the quality of the proposed algorithms, and possibly to discover any unpredicted behavior. In addition, the simulations can be used to predict the behavior of the experimental antenna developed within TU Delft.

First we describe the simulation scenario, then we present a series of different simulations and their results, and finally we draw conclusions on the quality of the algorithms.

### 7.1 Simulation scenario

For the simulations, we have considered an array of four elements, with an inter-element distance of a half wavelength. This choice is compatible with the experimental setup which has only four elements. We have considered scenarios with only two sources, each with an unframed structure. Hence, the sources are modeled as continuous data streams without the specific framing of the various modes, nor the preamble, nor the redundancy code of mode S. This is done so that we can vary the number of symbol easily, and can compare to the CRBs. As we consider only mode S, the signal is raw Manchester encoded data shifted in frequency, without any pulse-shape.

Six parameters were varied: the input SNR, the number of samples, the angle difference between the two sources, their frequency difference, and the power ratio of the two sources. The sixth one is a different simulation, in this one we consider two packets, and we vary the ratio of their common time support. Since the multi-dimensional space of the parameters is quite large, we have performed the simulations by changing only one parameter per set. The common point for all sets of simulations has the following characteristics: two equal powered sources with a SNR of 30 dB, 100 samples (so 50 symbols), DOAs of  $[70, 110]$  degree, frequency shifts of  $[-5 \cdot 10^4, 5 \cdot 10^4]$

Hz. The source packets are totally overlapping.

For each set of parameters, we performed 1000 independent Monte-Carlo runs, except for the SNR simulations series, where only 100 independent runs were performed. We present performance curves of the following results: the failure rate (a failure occurs when the estimated output SNIR of one of the sources is below 4 dB), the output SINR, and the standard deviation of the estimated DOA and the frequency shift. The definition of output SINR is the ratio between the output power of the desired source and the sum of the output noise power plus the output power of the undesired sources (after the beamformer). Since the output SINR has a direct relation to the degradation of the symbol estimate, it is a more interesting performance measure than the output SNR and the output SIR.

All algorithms start by a detection of the number of sources with the White Noise Test described in Section 6.1. Most algorithms end with the estimation of the frequency shift with the method of section 6.5.

In the SINR plots, a black line indicates the best achievable output SINR for one source, it is a maximum bound. In the legend, it is called “Single” (as single user). We compute it by multiplying the SNR by the number of elements of the antenna array. In the same plots, we also present the performance of the Wiener beamformer, in dashed lines. This beamformer is defined as the minimum of the MSE criterion under the assumption that the transmitted data matrix  $\mathbf{S}$  is known (see Section 3):

$$\mathbf{W} = (\mathbf{X}\mathbf{X}^H)^{-1} \mathbf{X}\mathbf{S}^H$$

In the plots presenting the performance of the estimation of the DOA and of the frequency, the stochastic CRB is included to give a limit on the variance of the best achievable unbiased estimation.

The failure rate is defined as the ratio of the number of failed simulations over the total number of simulations for a given set of parameters. The failed simulations are discarded from the estimation of the SINR, and the standard deviations of the DOA or the frequency shift.

All the plots present also the multi-shifts ZCMA (denoted MS-ZCMA), the ESPRIT-SOBI (denoted from now E-SOBI), and the two versions of the MDA algorithm (denoted MDA 2 and MDA 3). When the parameters of two sources had totally symmetric values, their estimates were averaged together.

## 7.2 SNR

In the first set of simulations, the input SNR is varied from 10 to 50 dB. This range represents well the SNR of the received signals encountered in practice. The results are presented in the Figures 7.1 to 7.5.

Figure 7.1 shows the failure rate as a function of the input SNR. The MDA 3 and E-SOBI have a few failures at low SNR, while the MS-ZCMA and MDA 2 algorithms are robust with respect to the noise level.

Figure 7.2 shows the SINR as a function of the input SNR. The output SINR is linear with the input SNR for all algorithms. Due to the large range of input SNR,

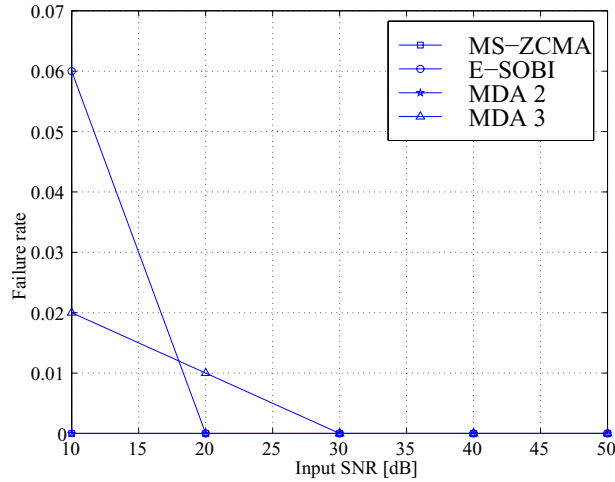


Figure 7.1: The failure rate as a function of input SNR.

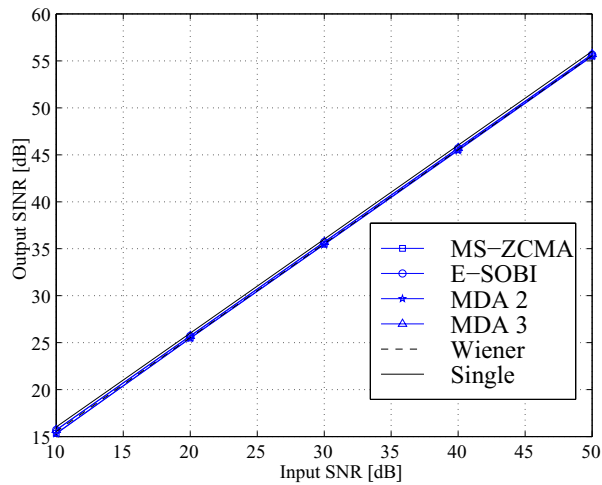


Figure 7.2: The SINR as a function of input SNR.

it is more interesting to consider the difference of the output SINR and the input SNR, see Figure 7.3. It shows that the MS-ZCMA and the MDA 2 tend towards the Wiener solution, while the MDA 3 and E-SOBI have better performance, but still remains under the ultimate limit of one signal alone (the “Single” curve).

Figures 7.4 and 7.5 present the estimation performance for the frequency and the DOA as a function of input SNR. We also show the stochastic Cramer-Rao bounds derived in Proposition 5.2.2. In both plots we note that the deterministic algorithms have a better behavior than E-SOBI, which reaches a floor above a certain input

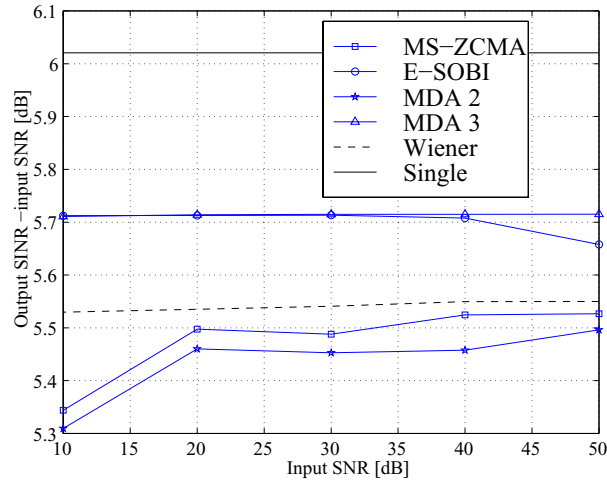


Figure 7.3: *Compensated SINR by input SNR as a function of input SNR.*

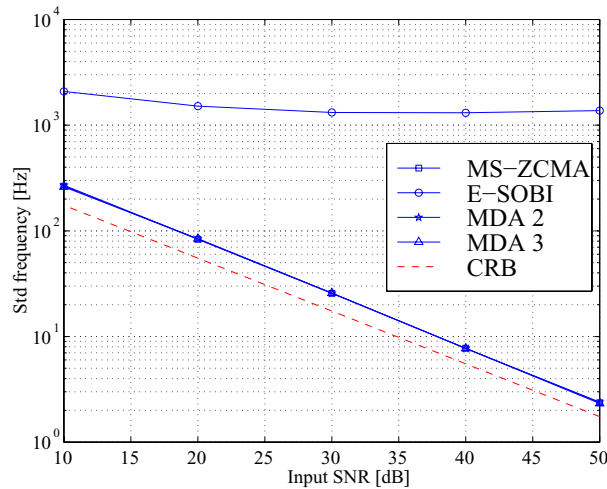


Figure 7.4: *Standard deviation of the frequency estimate as a function of input SNR.*

SNR. This floor is due to the finite sample effect, indeed the E-SOBI algorithm uses an estimate of various covariance matrices. These sample covariance matrices require a certain amount of samples to converge to their expected values. At low SNR, the finite sample effect will be masked by the noise power. Oppositely, at high input SNR, the finite sample noise limits the accuracy of the covariance matrices and the estimation of the frequency shifts is less reliable, which can be observed by the floor effect on Figure 7.4. In summary, the estimates of E-SOBI are not consistent.

This frequency mis-estimation should have dramatic consequences for the E-SOBI

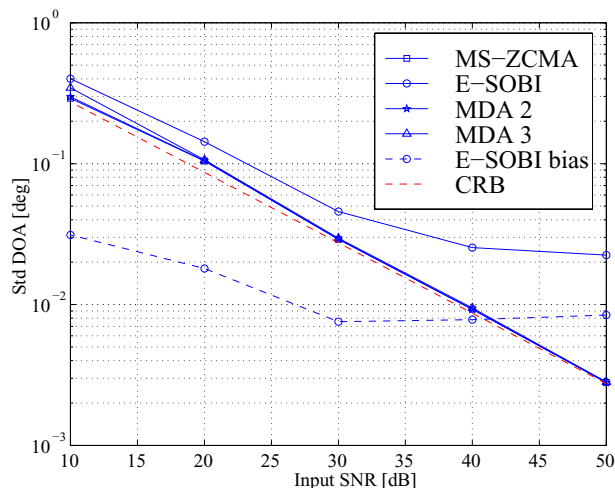


Figure 7.5: Standard deviation of the DOA estimate as a function of input SNR.

separation performance. Indeed, this algorithm uses the knowledge of the frequency to estimate the mixing matrix, see Equation (6.36). As the estimate of the mixing matrix is used to estimate the beamformers, the output SINR should have been degraded, unlike what we observe in Figure 7.3. The Unvec operation used for the estimation of the columns of the mixing matrix is probably compensating for the frequency mis-match.

We also note that the deterministic algorithms are near the Cramer-Rao bounds, which indicates they have a good performance. For an input SNR of 30 dB, the standard deviation of the estimated frequency is only 25 Hz, which would allow to recover the Doppler shift. If this accuracy can be repeated in practice, it would be possible to derive the vectorial speed of the aircrafts at the central management by comparing the different Doppler shifts from each receiving base station. The standard deviation of the DOA is 0.03 degree for a input SNR of 30 dB for the deterministic algorithms. Since the current SSR radars typically have only 0.2 degree of accuracy, it seems a good result, but we have to keep in mind that this is a theoretical result for a perfect antenna array.

As an additional problem, the E-SOBI algorithm has a non-negligible bias for the estimate of the Direction of Arrival, which is shown in the Figure 7.5 under the name “E-SOBI bias”. The other bias were well below their associated standard deviation.

### 7.3 Number of Samples

In this series of simulations, we only vary the number of samples, from 50 to 200 samples, keeping the other parameters fixed.

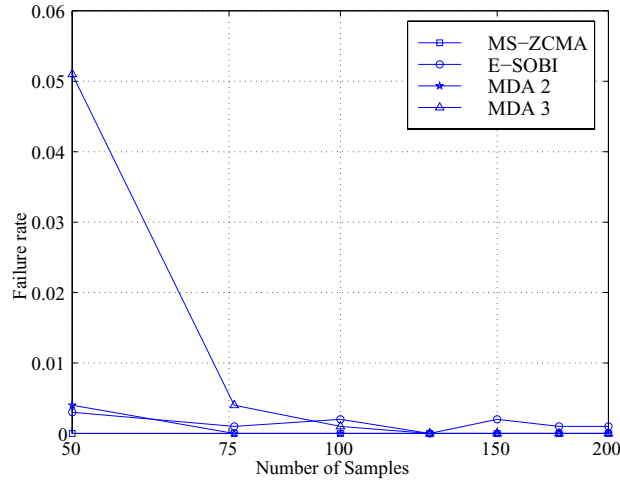


Figure 7.6: *The failure rate as a function of the number of samples.*

Figure 7.6 shows the failure rate as a function of the number of samples. It appears that the MDA 3 algorithm is the first to fail at low number of samples, while the other algorithms rarely fail. In order to have tall matrices, the MS-ZCMA algorithm needs to have  $N \geq d^4/2$ , and the MDA 3 needs  $N \geq d^3$ . Note that with  $d = 2$ , the limits are the same,  $N \geq 8$ . In the general case, we expect that MS-ZCMA is more sensitive than MDA 3. In fact MS-ZCMA uses an average of the subspace obtained by considering several shifts, thus it is more robust than MDA 3, which uses only one matrix.

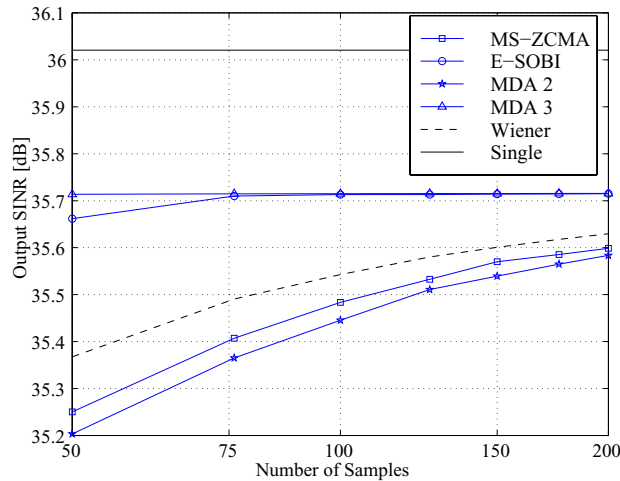


Figure 7.7: *The output SINR as a function of the number of samples.*



Figure 7.7 shows the SINR as a function of the number of samples. We note that the SINR of the Wiener solution is increasing with the number of samples, but remains below the single-user maximum SINR. The MS-ZCMA and the MDA 2 algorithms follow the trend of the Wiener solution. E-SOBI and MDA 3 have a nearly constant SINR, which degrades a little for the E-SOBI at a low number of samples. Their SINR is better than the Wiener solution, this is due to the fact that the beamformers for these algorithms were derived as parametric Wiener beamformer.

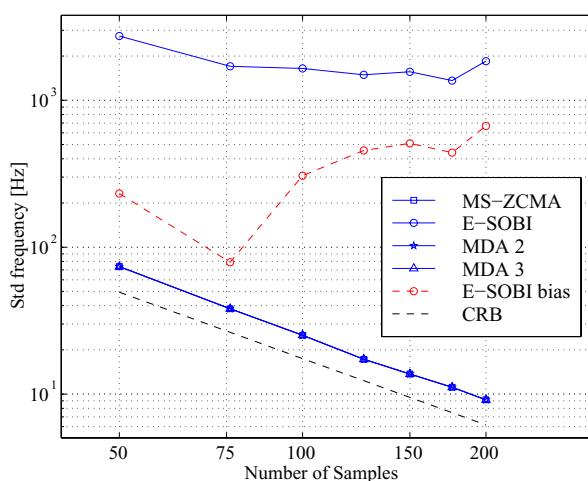


Figure 7.8: Standard deviation of the frequency estimate as a function of the number of samples.

Figure 7.8 shows the standard deviation of the frequency estimate as a function of the number of samples. We note that all deterministic algorithms follow the CRB for the frequency. E-SOBI reaches some floor as in the preceding series of simulations. In an unreasonable way, a bias even appears for a large number of samples. This effect remains without any explanation.

Figure 7.9 presents the standard deviation of the DOA as a function of the number of samples. We note that the deterministic algorithms follow quite well the CRB, while E-SOBI remains significantly above, and for a low number of samples exhibits a degradation in performance. This comes from the fact that E-SOBI needs that the covariance matrices reach their expected values. The deterministic algorithms are consistent, but unfortunately not asymptotically efficient.

## 7.4 Angle difference

In this series of simulations, we only vary the DOA of the impinging sources, keeping the other parameters fixed. The DOAs are changed according to the relation:  $[\theta_1, \theta_2] = [90 - \theta, 90 + \theta]$  where  $\theta$  is the index used in the plots.

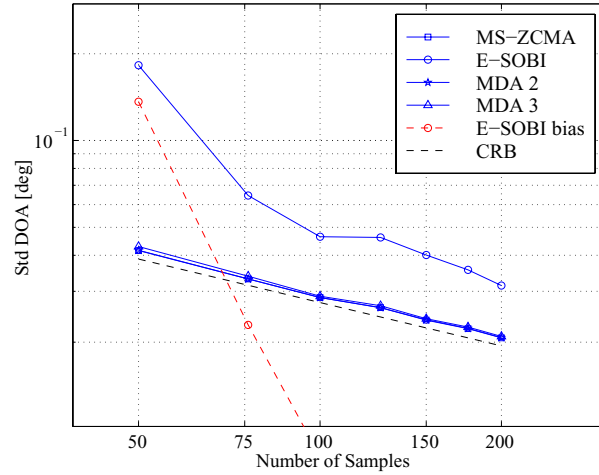


Figure 7.9: Standard deviation of the DOA estimate as a function of the number of samples.

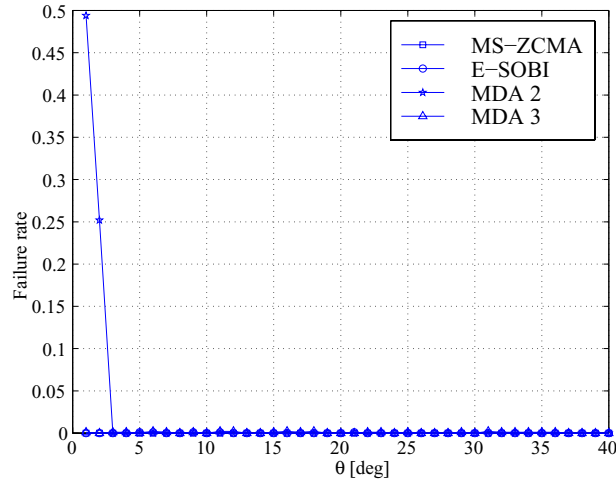


Figure 7.10: The failure rate as a function of half the angular difference.

Figure 7.10 presents the failure rate as a function of the parameter  $\theta$ . We observe that MDA 2 can not cope with low angular separation. As MDA 3 uses a similar concept, it is interesting to compare them. For MDA 2, the solution subspace is extracted from the kernels of two different matrices, while for MDA 3, it is extracted from the kernel of only one matrix. If one of the two matrices used by MDA 2 does not give the correct subspace, the final detection will be wrong. Thus, MDA 3 is more robust than MDA 2 at low angular separation.

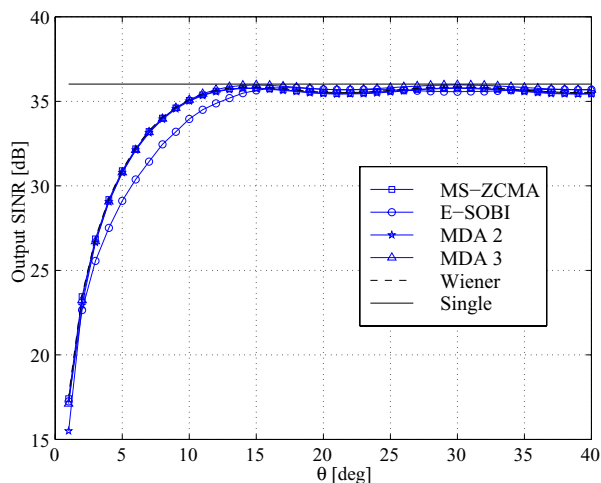


Figure 7.11: *The SINR as a function of half the angular difference.*

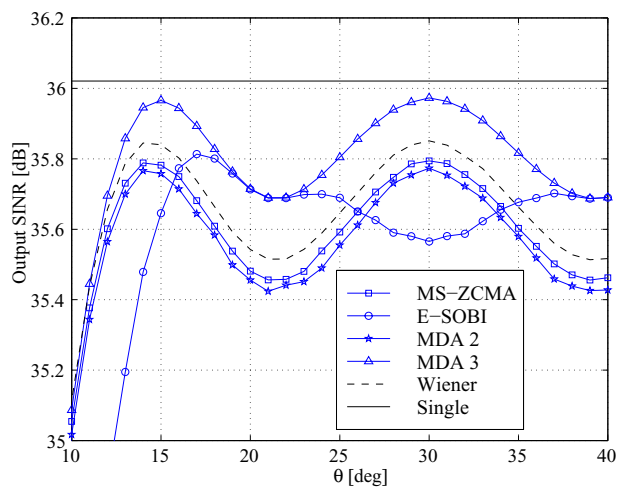


Figure 7.12: *A detail of the SINR as a function of half the angular difference.*

Figure 7.11 shows the output SINR as a function of the parameter  $\theta$ . All algorithms have decreased performances in SINR for a lower angular separation than 24 degrees. The E-SOBI also shows a loss over the other algorithms of a few dB over the range  $[3^\circ, \dots, 14^\circ]$  degrees. Figure 7.12 is a zoom of Figure 7.11 in the range  $[10^\circ, \dots, 40^\circ]$ . We observe that the MS-ZCMA and the MDA 2 algorithms are below the Wiener solution, and MDA 3 is above. These 4 curves have an oscillating behavior.

Figure 7.13 shows the standard deviation of the frequency estimate as a function

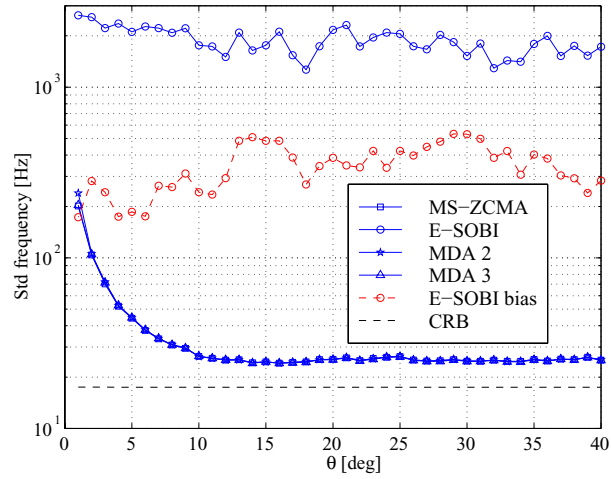


Figure 7.13: *Standard deviation of the frequency estimate as a function of half the angular difference.*

of the parameter  $\theta$ . The frequency estimate is almost constant above 20 degrees separation, with E-SOBI two orders of magnitude above the deterministic algorithms. There was no observable bias for the deterministic algorithm, while E-SOBI had a slight bias.

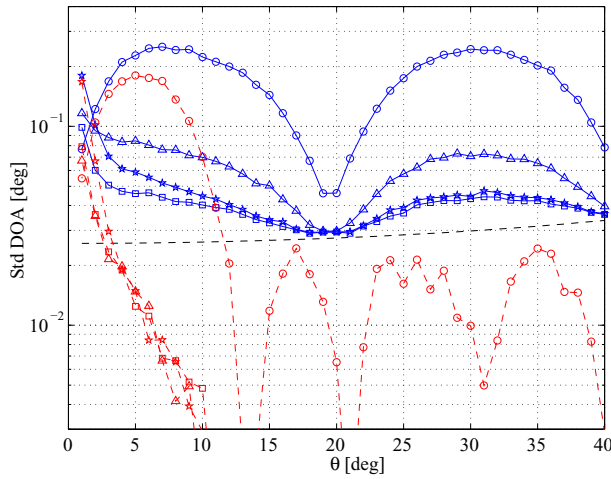


Figure 7.14: *Standard deviation of the DOA as a function of half the angular difference.*

Figure 7.14 shows the standard deviation of the DOA as a function of the

parameter  $\theta$ . For reasons of space, the legend is not displayed in this figure, the line types are the same as for the previous plots, with the addition of the dashed lines, which represent the bias of each method. We first note that all algorithms have a bias at low angular separation. Second, surprisingly, the standard deviations of all methods show the same pattern with different levels of amplitude. Last, the Cramer-Rao bound rises slightly with the angular separation, which is counter-intuitive.

## 7.5 Frequency difference

In this series of simulations, we only vary the frequency shifts, keeping the other parameters fixed. The new frequency shifts are defined accordingly to the relation:  $[f_1, f_2] = [-f, f]$ , where  $f$  in Hz is the index used in the plots.

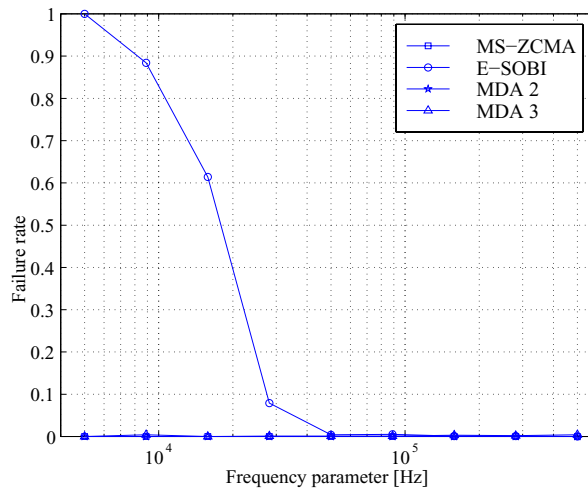


Figure 7.15: *The failure rate as a function of frequency.*

Figure 7.15 presents the failure rate as a function of the parameter  $f$ . The E-SOBI algorithm does not work with small frequency differences, and below 30 kHz begins to fail. Usually, the ESPRIT step can resolve small frequency differences in noise-free case, but here the sample covariance noise is probably too strong. The deterministic algorithms are robust for all simulated frequencies.

Figure 7.16 presents the output SINR as a function of the parameter  $f$ . The SINR of the deterministic algorithms are almost independent of the frequency shift, while the E-SOBI is performing well only between 30 and 300 kHz. As the frequency difference tends to zero, the ESPRIT step of the E-SOBI algorithm is more sensitive to the sample covariance noise, which explains the bad performance for the low frequency. For high frequency difference, E-SOBI has bad performance as well, the natural explanation would be the aliasing effect, but Figure 7.17 contradicts this hypothesis.

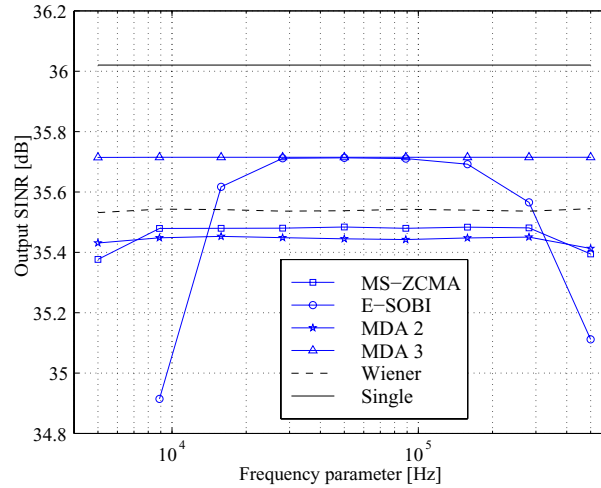


Figure 7.16: *The SINR as a function of frequency.*

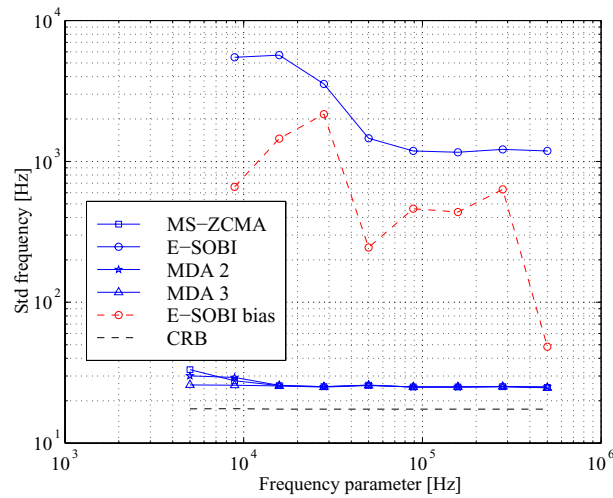


Figure 7.17: *The standard deviation of the frequency as a function of frequency.*

Figure 7.17 presents the standard deviation of the estimate of the frequency shift as a function of the parameter  $f$ . We note again that E-SOBI works only with a difference of frequency larger than 30 kHz, and we remark that the mean of the E-SOBI is not negligible. The deterministic algorithms have a performance near the Cramer-Rao bound, and only a slight degradation of quality at low frequency differences.

Figure 7.18 presents the standard deviation of the estimate of the DOA as a

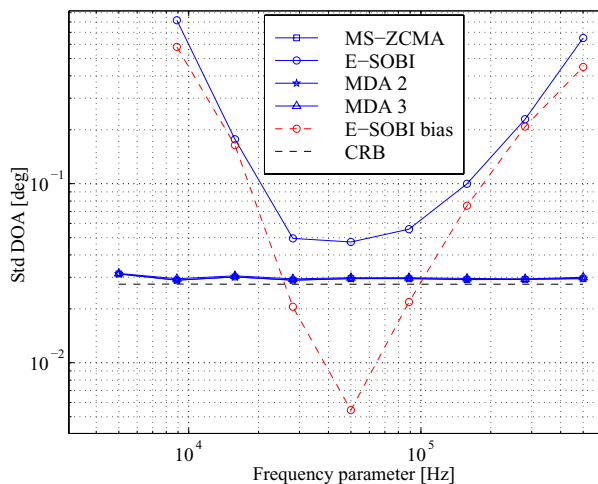


Figure 7.18: *The standard deviation of the DOA as a function of frequency.*

function of the frequency difference of the two sources. The deterministic algorithms have a similar behavior, and are near the Cramer-Rao bound. E-SOBI has acceptable performance only between 30 and 100 kHz, but outside this range the bias and the variance are significant.

From this set of simulations, we can conclude that the deterministic algorithms do not depend on the difference in residual carrier, which was expected since the MS-ZCMA and the MDAs do not depend on the frequency. It also appears that E-SOBI has a limited range where its performance is reliable.

## 7.6 Power Ratio

In this series of simulations, we only vary the ratio of the source power,  $P_1$ ,  $P_2$ , while keeping the other parameters fixed. It is done by keeping  $P_1$  constant, while  $P_2$  vary such that the relative power varies over  $[-20, \dots, 20]$  dB. The SNR of source 2 varies then in the range  $[10, \dots, 50]$  dB.

Figure 7.19 presents the failure rate as a function of the power ratio. We note that if the power ratio of the two source is too large, E-SOBI fails. This effect is due to the finite sample effect: the non diagonal entries of the source covariance matrix are larger or of the same order of magnitude as the smallest diagonal entry. At low power ratio, the MDA 2 unexpectedly fails, we can only assume that the problem is due to the choice of the null subspace from the pair of matrices  $\{\mathbf{R}_1, \mathbf{R}_2\}$ .

Figure 7.20 presents the output SINR of source 1 as a function of the power ratio. Figure 7.21 presents the output SINR of source 2 compensated by the relative power, as a function of the relative power. In both figures, MS-ZCMA and MDA 3 have a good behavior, while at low power ratios MDA 2 for source 2 has 2 dB loss.

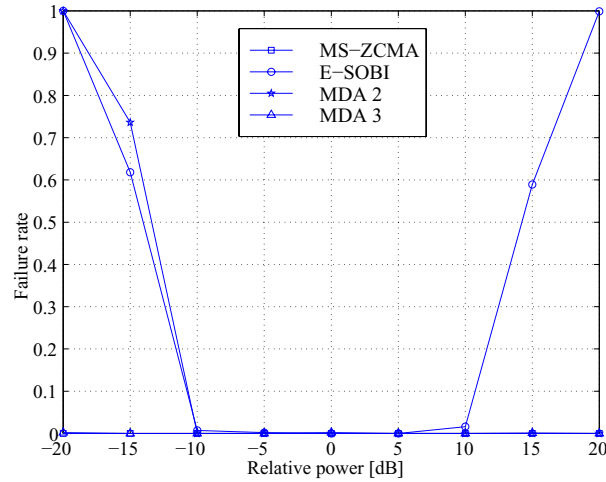


Figure 7.19: *The failure rate as a function of the power ratio.*

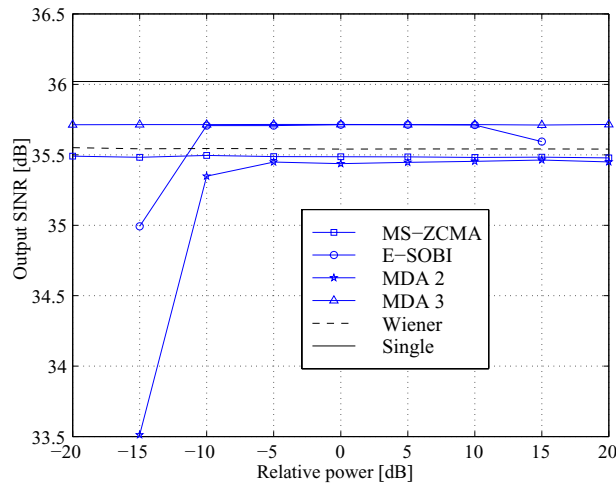


Figure 7.20: *The SINR of the source 1 as a function of the power ratio.*

The two figures are not each other's image, because at low power ratios the sources have the following SNR:  $[30, 10]$  dB, and at high SNR they have the SNR  $[30, 50]$ ; these two situations are not symmetric with respect to the noise.

Figure 7.22 presents the standard deviation of the estimate of the frequency shift as a function of the power ratio. Figure 7.23 presents the standard deviation of the estimate of the DOA as a function of the power ratio. As the SNR is different for each sources, the performance for each of the two sources is shown separately. In both figures, we note that the deterministic algorithms behave near the Cramer-Rao



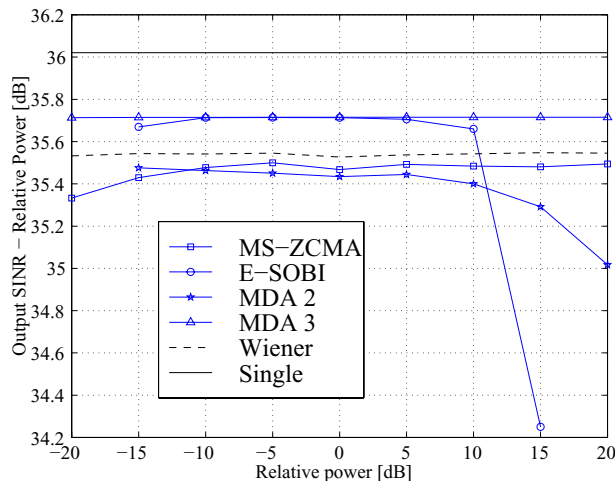


Figure 7.21: The SINR of the source 2 as a function of the power ratio.

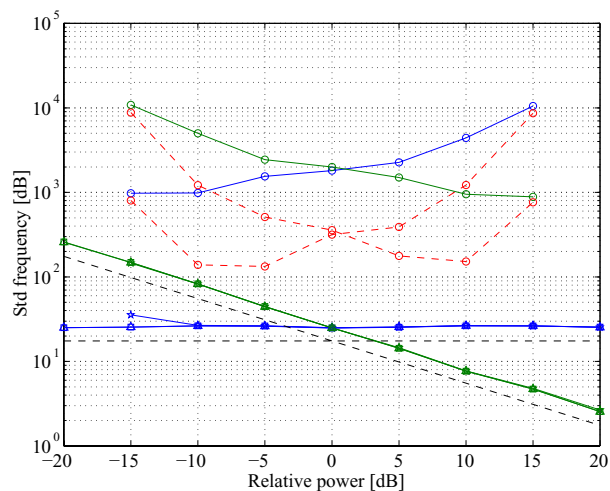


Figure 7.22: The standard deviation of the frequency as a function of the power ratio.

bound, while for E-SOBI always one of the two sources has degraded performance, unless their powers are equal. Furthermore, the bias for the E-SOBI can be as high as the standard deviation.

This set of simulations totally excludes the E-SOBI algorithm from real-life applications where the dynamic range of the sources can be high. It is worthwhile to note that MS-ZCMA and MDA 3 can cope with this high variability in power ratio.

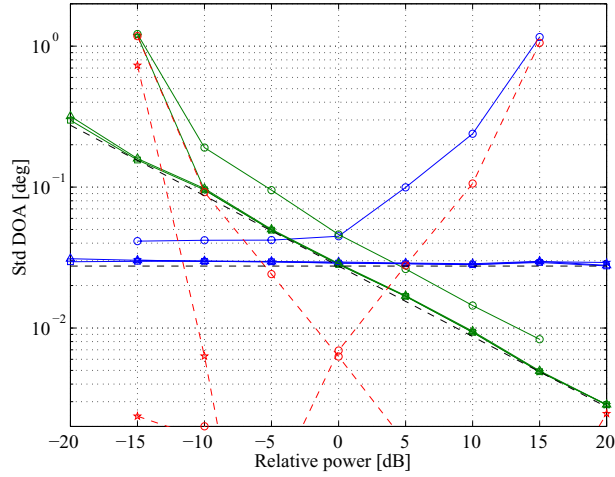


Figure 7.23: The standard deviation of the DOA as a function of the power ratio.

## 7.7 Packet overlapping

In this series of simulations, we investigate the influence of the time delay offset between the beginning of two signals with an equal length, while keeping the other parameters fixed. Both source signals have the same packet length (100 symbols). The length of the observation window is equal to the number of samples plus the time delay, so for each simulation the data block has a different number of samples. If the time delay offset is bigger than 100, then the two signals are non-overlapping.

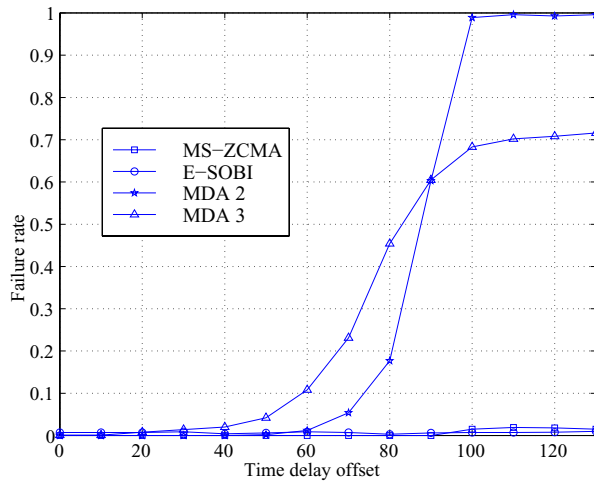


Figure 7.24: The failure rate as a function of the time delay offset.

Figure 7.24 presents the failure rate as a function of the time delay offset. This figure confirms our expectations that MDAs cannot cope with non-overlapping signals, but also shows us that already with a time delay offset equal to 50% these methods begin to fail. For time delay offsets below 90, MDA 2 performs better than MDA 3, but for non-overlapping sources it always fails, while MDA 3 still has a “success rate” of 30%. Figure 7.24 also shows that MS-ZCMA only has a few percent failures for non-overlapping sources. It is interesting because in real-life there should be a pre-processing unit that tries to isolate smaller set of data samples before using the algorithms. If this step fails and do not isolate two non-overlapping signals, then our algorithm has to be able to resolve also this kind of situation. For non-overlapping sources, the covariance matrices  $\mathbf{R}_r$  should not have cross-signal terms (even for finite samples), hence we expect E-SOBI to behave better in that case. But its failure rate is still a few percent for large time delay offsets.

Given that the failure rate for MDA 2 is almost 1 for a number of samples superior to 90, the other statistics are not making sense, and are not presented in the remaining figures for the range of samples  $[100, \dots, 130]$ .

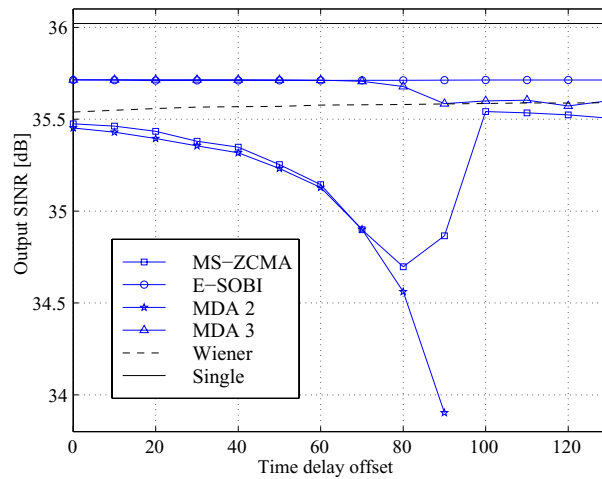


Figure 7.25: *The SINR as a function of time delay offset.*

Figure 7.25 presents the SINR as a function of the index of separation. We note that E-SOBI algorithm has a constant SINR. The SINRs of MDA 2 and MS-ZCMA have similar behavior until the time delay offset is equal to 70, then the MDA 2 has its SINR degrading even more, while the SINR of MS-ZCMA raises to almost the Wiener solution for time delay offsets above 100. Note that the variation of the SINR for MS-ZCMA is less than 1 dB on an average of 35 dB, so this behavior is acceptable.

Figure 7.26 presents the standard deviation of the estimate of the frequency shift as a function of the index of separation. E-SOBI algorithm has a constant standard deviation, and so is unaffected by the time delay offset, but the bias of this method is

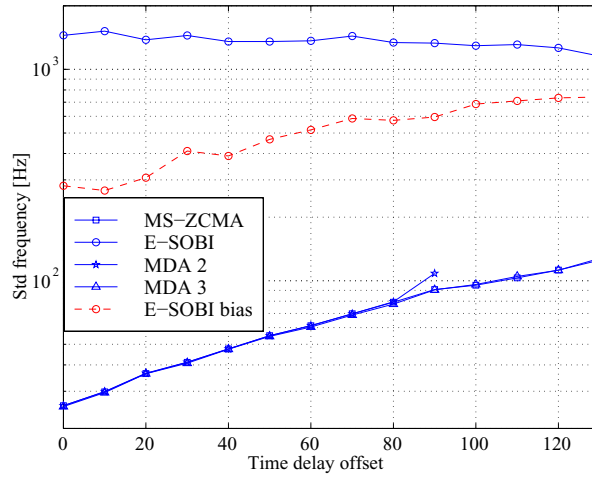


Figure 7.26: *The standard deviation of the frequency as a function of the time delay offset.*

rising with the time delay offset. The deterministic algorithms have similar curves, which are log-linear with the time delay offset.

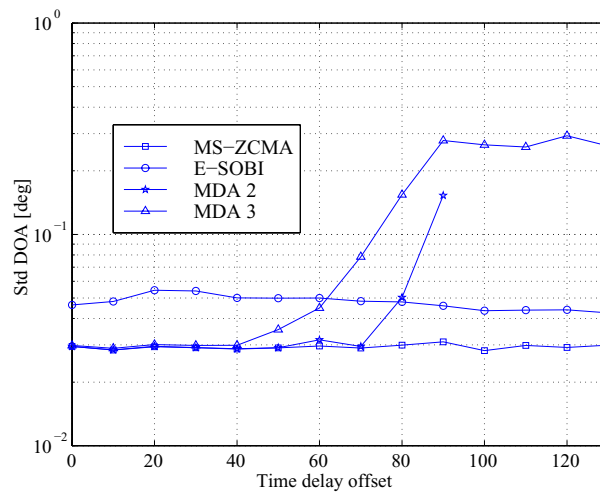


Figure 7.27: *The standard deviation of the DOA as a function of the time delay offset.*

Figure 7.27 presents the standard deviation of the estimate of the DOA as a function of the time delay offset. E-SOBI and MS-ZCMA algorithms have constant curves, while there is a slight improvement for E-SOBI at high time delay offsets.

MS-ZCMA remains the algorithm with the best standard deviation for DOA.

We can conclude that the only overlapping-resistant algorithms are E-SOBI and MS-ZCMA. This is consistent with Chapter 6, where we derived Propositions 6.4.1 and 6.4.2 only for totally overlapping sources, so the MDAs were not supposed to cope with non-overlapping sources.

## 7.8 Conclusions

In this section, we have studied by means of simulation the behavior of each algorithm for different situations. Our goal was to verify our predictions on the behavior from the preceding chapter, and to discover some unpredicted behavior. At this point, we can draw a first conclusion on the quality of each algorithm.

First, E-SOBI presents too many restrictions in frequency difference and power ratio. Furthermore, the standard deviation of its frequency and DOA estimate are always much above the other algorithms. Given these points, we can discard E-SOBI.

Next to E-SOBI, MDA 2 behaves slightly better. Indeed the method fails only at small angle differences, or at low power ratios, or with non-overlapping sources. When the method is not failing, the SINR is near the Wiener solution, and the estimates are near their CRBs.

Finally, if we do not consider the “overlapping” simulations, we conclude that MDA 3 and MS-ZCMA are of equal quality, they have low failure rate, and the standard deviations for their estimates are near their CRBs.

The only difference is for non-overlapping sources. As MDA 3 was not designed for it, it is not surprising that the algorithm is out-performed by MS-ZCMA. Note that MDA 3 uses simpler mathematics, and has a simpler numerical implementation.



## Chapter 8

# Experimental results

In the previous chapter, we used simulations to verify which of the algorithms can perform well with the data model. In this chapter we describe the work done in our groups within TU Delft to try the new algorithms with real measurement data.

During the preparation of the thesis, we built several experimental setups. Here, we present in the first section only the last one for the sake of space. In the second section, the measured data is presented and we present some experimental considerations on it. The last section derives some statistics out of synthesized overlapping packets extracted from the data set, and present an overlapping case completely based on measurement data.

### 8.1 Experimental setup

The experimental device consists of 4 parts: the antennas, the receiving chain, the digital oscilloscope, and a PC computer. The impinging signals are received by the antennas, which are feeding the receivers. The receiving chains down-convert the signal from the radio frequency, 1090 MHz (RF), to the Intermediary frequency, 10 MHz (IF). They also amplify the signal and filter out the other bands. The digital oscilloscope samples, digitizes and records the output data. Then, via a General Purpose Interface Board link (GPIB), the computer receives the measured data and saves it on the hard-disk and CD-ROM for off-line processing.

First, we present the analog part of the setup, then its digital counterpart.

#### 8.1.1 Design of the receivers

The receiver is intended to convert the signal from RF to IF, and its design is shown in Figure 8.1.

After the antenna, an RF band-pass filter (BP) is placed before the RF-amplifier. Its purpose is to protect the amplifier from increasing the power of other signals<sup>1</sup>.

---

<sup>1</sup>The nearest interference can be produced by DME, a system used for navigation.

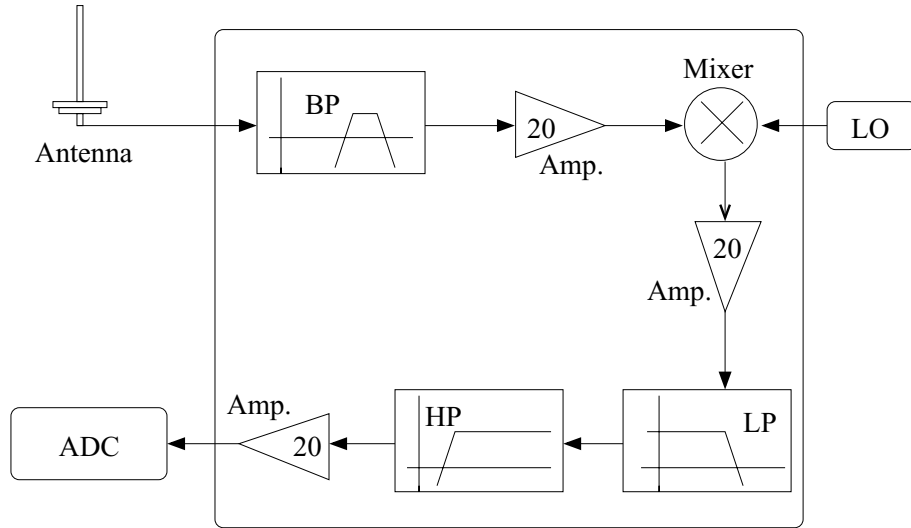


Figure 8.1: *Design of the receiving chain.*

This RF-filter has a bandpass of 10 MHz, and is centered at 1090 MHz. The amplifier has a gain of 20 dB. The next stage is a mixer, which multiplies by a Local Oscillator (LO). The LO has a frequency of 1080 MHz, so the IF will be 10 MHz. Since the mixer is not perfect, there are also some harmonics, and the most important are the second harmonic at 20 MHz, and the third one at 30 MHz. The other harmonics do not have an important influence as they are filtered out by the low-pass filter, in the last stage. The LO is produced by a Marconi waveform generator and is quite stable in frequency. The next stage consists of a bandpass filter implemented by a LP and a HP filter. The low-pass filter is centered on 10 MHz, and has a bandpass of 10 MHz. The measurements made by the technician have shown that the filter has a constant time-delay over this bandpass.

We built 6 antennas, and 4 receiving chains. The first and last antenna are loaded with the correct impedance and intended to reduce the coupling between antennas.

We simulated the transformations that a mode S signal undergoes if it is processed by this receiving chain. The spectrum of the digital output of the receiver is shown in Figure 8.2.

In Figure 8.2, there are 3 spectra: the desired output, the second harmonic, and the third harmonic. The vertical bar shows the band of the spectrum that is kept after digital transformation. From the plot, we note that there is around 40 dB between the desired signal and the second harmonic, so this design is acceptable.



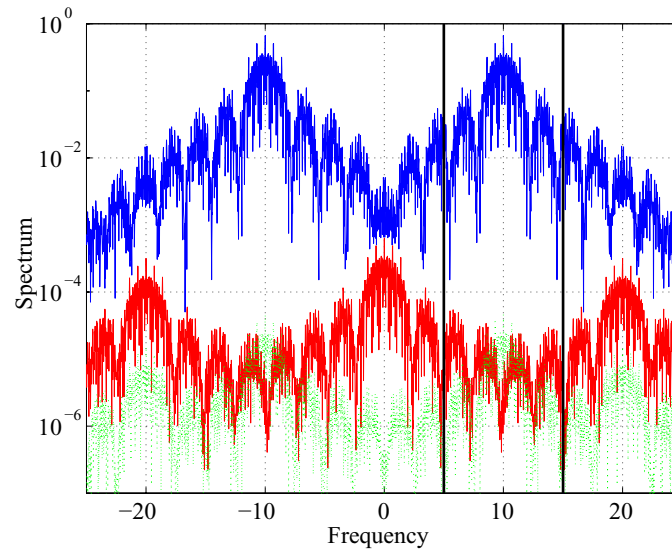


Figure 8.2: *Simulation of the spectra of the first three harmonics. The vertical bar represent the cut-off frequency of subsequent digital filters.*

### 8.1.2 The digital part

The digital part consists of a digital oscilloscope, which is linked to a computer by a GPIB link, and an off-line digital pre-processing phase done in matlab.



Figure 8.3: *The Tektronix TDS 784 A.*

The oscilloscope, a Tektronix **TDS 784A** (see Figure 8.3), has a vertical resolution of 8 bits.

The sampling rate for the measurement is 50 Megasamples per second. As the oscilloscope has a limited memory, it was mandatory to export the data in a fast and reliable way.

The data is loaded from the digital oscilloscope into the computer, which eventually stores it onto CDROM for offline processing. The offline processing consists of three stages. First a Hilbert transform is applied, then a digital filtering with a bandwidth of 10 MHz. The last stage is to down-sample the data to 2 M-samples per second, which is the frequency for which the algorithms are designed. No synchronization scheme is implemented.

## 8.2 Experimental considerations

Due to a tight schedule, we could only perform a limited amount of measurements during two hours on Aug. 23, 2001. During these two hours, we could record 28 different data sets. Most of them have a short time duration,  $300\mu\text{s}$ , which was chosen to get a mode S reply or some interesting features. Four of the experiments were recorded over a long time duration in order to estimate the frequency of appearance of the various modes. The recorded data contained 8 clean mode S replies and one case with two overlapping mode S replies.

### 8.2.1 Reply density

In the scope of this thesis, we assumed that soon only mode S replies would be emitted by the airplanes, and that these mode S replies would overlap at the reception. So we are interested in estimating the density of the replies at reception.

To estimate the reply density, we recorded the output of the antenna for a long time of observation without any special triggering, and we obtained 4 block-records this way. When considering the 4 block-records, we counted 120 mode A/C replies, and 2 mode S replies for a time length of 2.6 ms per record. This is disappointing, because the Eurocontrol commission was supposed to enforce the mode S standard by 1999. Furthermore, it could reduce the importance of the work produced in this thesis, but the motivation of the thesis remains valid, and it is just a matter of years before source separation algorithms will be mandatory.

### 8.2.2 Verification of the signal model

In this subsection, we study the agreement between the true and the modeled signal.

#### The frequency drift

First, we check the source behavior, so we consider one signal on one antenna, and we down-sample a received mode S to a frequency of 2 MHz. The absolute values are consistent up to the noise with the simplified model of Equation (3.9). But the phase of the received replies is not always consistent with the model. In Figures 8.4 to 8.6, we consider the phase of three mode S replies, numbered 7, 2 and 6. We present the

original phase with the frequency shift, and the phase after compensation by the estimated frequency shift for the 3 sources.

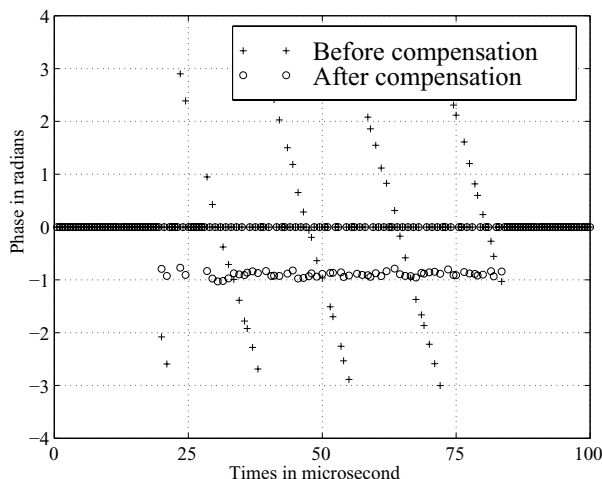


Figure 8.4: *Received phase of source 7, for which a remaining frequency drift of  $-60238$  Hz has been estimated, and compensated phase of the same source.*

Figure 8.4 shows that the match between the model and the true signal is quite good, indeed the compensated signal has almost a constant phase.

Figure 8.5 presents the phase of source 2. We note that the compensated phase is not constant as in the preceding case. Moreover, the shape of the compensated phase is too regular to indicate that only noise is present. We contemplate that the output of the transponder was not as modeled.

Figure 8.6 presents the phase of the source 6. We note that the phase does not follow any regular pattern, and the algorithm could not compensate any phase-shift. It is obvious that the emitted signal had a random phase.

To conclude, it appears that the transponders do not follow any rules for the stability of their phases. Some are quite stable, while others are not. Since the ICAO does not enforce this point, it was previsible that the transponder manufacturers would not spend any money on it.

### Calibration

High-resolution algorithms are sensitive to so-called “calibration” errors, which arise from non-identical behavior of the analog transducers that transform the impinging electromagnetic waves into electric signals. It was necessary to investigate array calibration algorithms, in particular, we considered AB algorithms [51], and the ESPRIT-like Algorithms [52].

Using these algorithms did not help to estimate the direction of arrival of the impinging sources. We assume that the errors in the received signal originate from

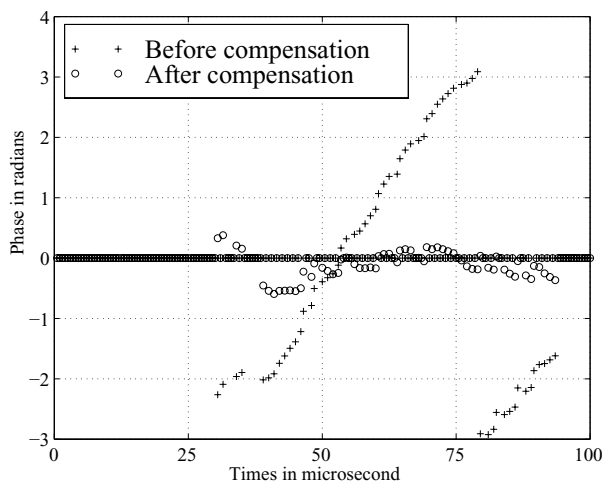


Figure 8.5: Received phase of source 2, for which a remaining frequency drift of 19258 Hz has been estimated, and compensated phase of the same source.

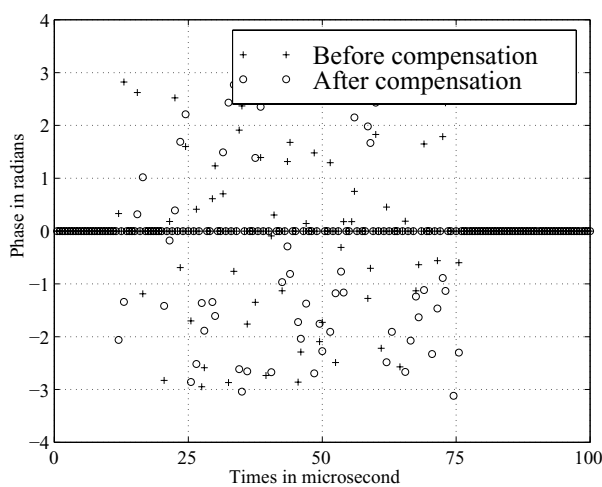


Figure 8.6: Received phase of source 5, for which no remaining frequency drift could be estimated, and compensated phase of the same source.

different reasons. Two causes can immediately be identified: first, there can be a “coupling” problem, which is caused by the reflections from one element to another element. Second, the roof on which the measurement equipment was installed contains (too?) many metallic objects, which can be the source of secondary paths.

Given that the array response does not follow the model in Equation (3.8), it is

not possible to evaluate the DOAs. So we limit ourselves to source separation in the remaining of this chapter.

### Test of the methods

To verify whether the algorithms can cope with real signals, we check Properties 3.1.1 and 3.1.2.

Property 3.1.1 states that the delayed cross-products should be equal to zero. We checked this property on data segment 2.

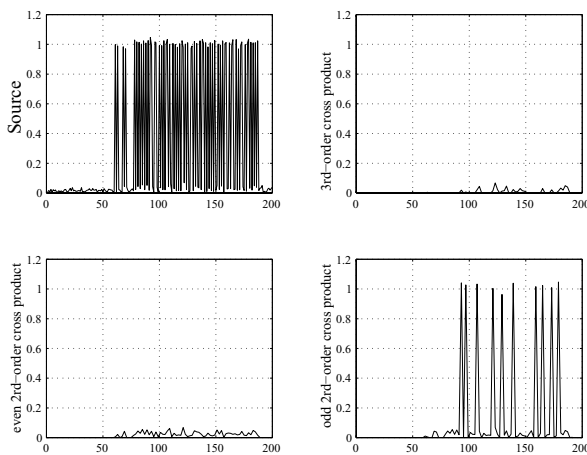


Figure 8.7: Absolute value of the data segment 2, and the test on the third-order cross-product, and the two second-order cross-product.

In Figure 8.7, we observe the signal, the third-order cross-product, and the two second-order cross-products. As stated in the property 3.1.1, the third-order, and one of the second-order cross-products are equal to zero (up to the noise). This validate the basic assumptions for the MDA algorithms.

Next, we check the Property 3.1.2. As our algorithm, the MS-ZCMA, compares iteratively 2 vectors, it is reasonable to estimate if these two vectors are parallel. The way to compare if they are parallel is to take an unit-norm version of them, and to perform a SVD on them, we should get two tall vectors multiplied by a  $2 \times 2$  diagonal matrix and a small square transform matrix. The first vector is supposed to be the mean, and the second vector the difference. We will plot each vector multiplied by its corresponding singular value, and compare them graphically. The original AZCMA also compares 2 vectors, so we can perform this test. We consider the vector containing the  $(s^*s^2)(k)$  for all  $k \in [1, \dots, N]$ , and the vector containing the  $s(k)$ 's for the original AZCMA. For MS-ZCMA, we consider the vector containing the  $[s^*(k-1)s(k)]^2$  for all  $k \in [1, \dots, N]$ , and the vector containing the  $s^*(k-1)s(k)$  for all  $k \in [1, \dots, N]$ . The output of the procedure are displayed for comparison in Figure 8.8.

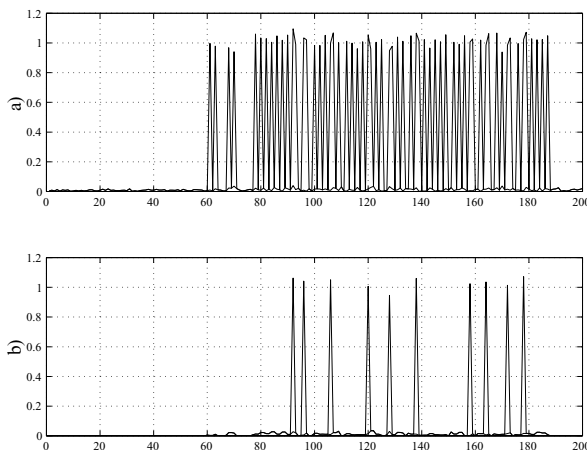


Figure 8.8: (a) presents the results of the procedure for the first and third-order product of the source (the original AZCMA). (b) displays the results of the procedure of the second and the fourth-order cross-product of the signal (MS-ZCMA).

We note that in both plots of Figure 8.8, the second vector of the testing procedure is at the level of the noise. Thus the algorithm will be able to extract the correct subspace for each case.

### 8.3 Experimental results

In this section, we first study the statistical properties of the algorithms, then the only true overlapping packets we could measure is investigated.

#### 8.3.1 Semi-synthesized results

As we could measure only a very few number of true mode S replies, with only one overlapping case, we had to add them manually to create a mixture of two sources. An advantage is that the delay offset and the SNR can be varied.

We choose the best received mode S signal (8 in total). The signals have a SNR in the range  $[10, \dots, 30]$  dB, they are 128 samples long. The signals are already down-sampled. We add them pairwise with some Gaussian white noise, so we have 56 possible combinations to study the performance of the algorithms.

There are two series of experiments: in the first series, we vary the power of the added noise. In the second series, we include a time delay between the two sources.

In the first series, for every couple of sources, we add them pairwise without time delay offset. We take the sources with an equal power, and we calculate the noise level. If this noise level is below the SNR we investigate, we adjust the noise level by adding some complex Gaussian noise, otherwise we discard this couple.

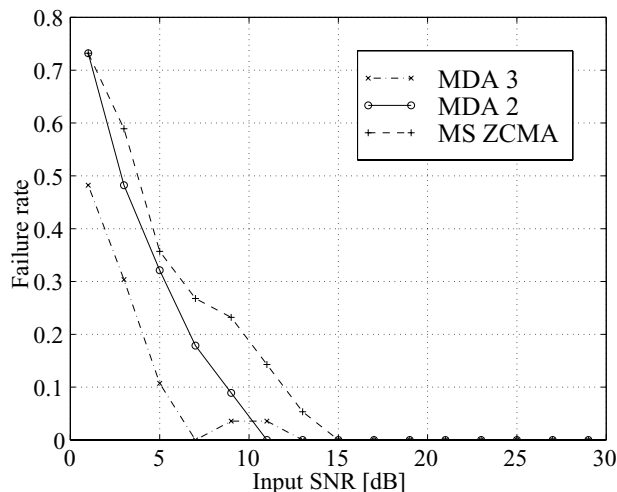


Figure 8.9: The failure rate as a function of the input SNR.

Figure 8.9 shows the failure rate as a function of the SNR. Unlike in the simulation, MS-ZCMA fails earlier: at 13 dB. These experiments also learn us that MDA 2 soon joins MS-ZCMA, while MDA 3 stay 25% below them. MDA 3 appears to be more robust than the two other at low SNR.

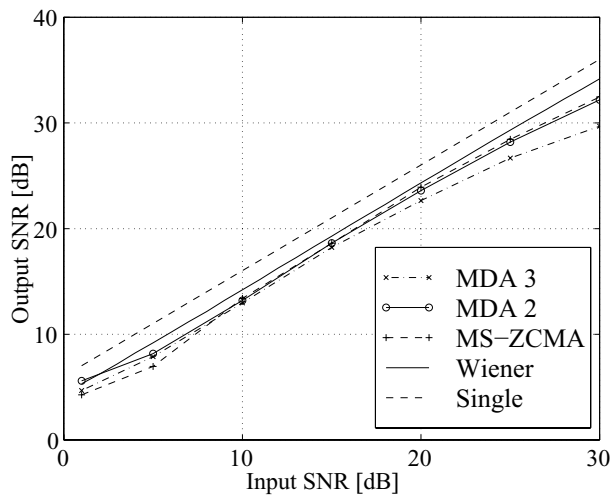


Figure 8.10: The output SINR as a function of the input SNR.

Figure 8.10 shows the output SINR as a function of the SNR. The three algorithms tend to follow the Wiener solution, as in the simulations. Only at an SNR of

30 dB, the performance is degrading a little for MDA2 and MS-ZCMA, and more seriously for MDA3 (2 dB more). Unfortunately, we do not have recording of reply signals with less noise to explore if this is a systematic trend or not.

In the next series of experiment, we use equi-powered sources with a SNR equal to 20 dB, we only vary the time delay offset.

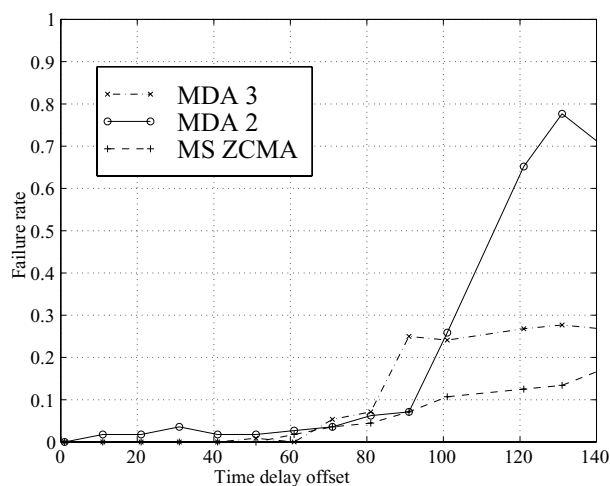


Figure 8.11: *The failure rate as a function of the delay of the second source.*

Figure 8.11 presents the failure rate as a function of the delay of the second source. We recognize the same trend as in Figure 7.24. The MDAs have some problems in the non-overlapping zone, but MDA 3 now has a failure rate of 30%, while it was 70% in the simulated data. Also, MS-ZCMA has an improved failure rate in that zone, although it remains below the others.

Figure 8.12 presents the output SINR as a function of the delay of the second source. As in the simulations, the performance of MS-ZCMA is insensitive to the time delay offset, but is not as close to the Wiener solution as in the simulations (it is 2 dB lower now). MDA 2 has the same bad performance as in the simulations. A new fact is the loss of 8 dB for MDA 3 for cases with a large time delay offset.

We can summarize this semi-synthetic study by mentioning that we obtained more or less the same behavior of the algorithms as in the simulations, and we did not get too many surprises. MS-ZCMA stays the most interesting algorithm for a real blind approach, and MDA 3 in case we know that the sources have a large support in common.

### 8.3.2 Real case data: influence of the down-sampling

In this subsection, we consider the only real overlapping measured data we obtained. First, we present the situation of this measurement, and the signals. Then we present the results of the down-sampling study, and why some cases did not work out.



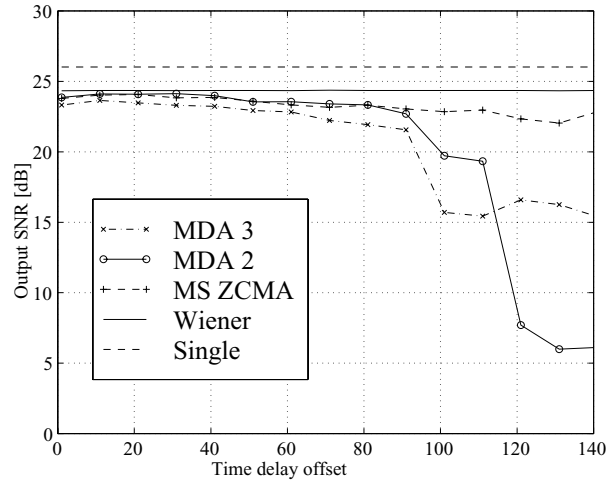


Figure 8.12: *The output SINR as a function of the delay of the second source.*

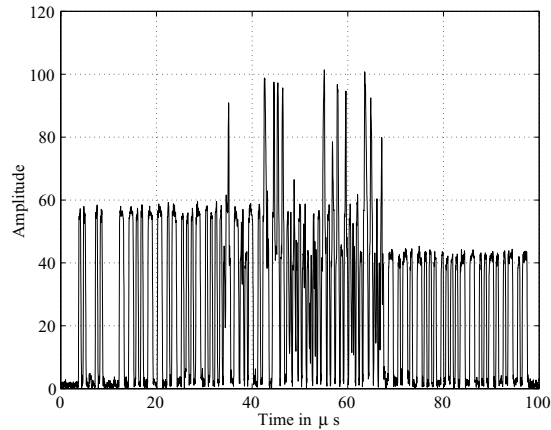


Figure 8.13: *Two overlapping mode S replies at a sampling rate of 50 MHz.*

Figure 8.13 presents the absolute value of the first antenna. We observe two mode S replies overlapping with a similar power. This plot is still sampled at the initial digitalization frequency of 50 MHz. We separated the two sources by another means to estimate the mixing matrix, which we can invert to separate the sources.

Figure 8.14 shows the absolute value of the first source obtained this way, and the Figure 8.15 shows its angular phase. The same is shown for the second source in Figures 8.16 and 8.17.

The first source has its magnitude quite constant or equal to zero, but its angular phase is totally random. This is an example of a received signal not matching with

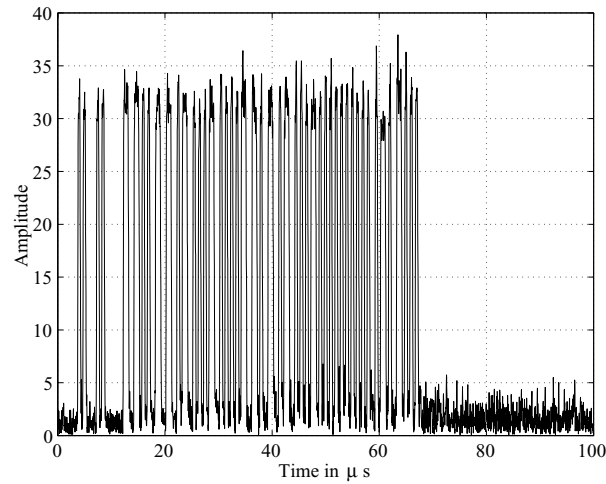


Figure 8.14: *Absolute value of the first recovered source.*

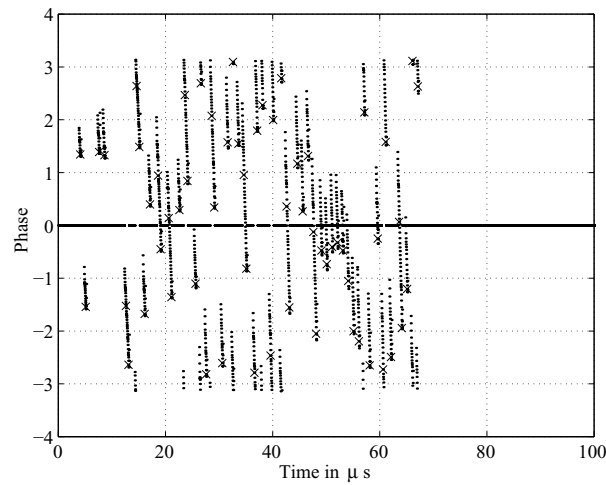
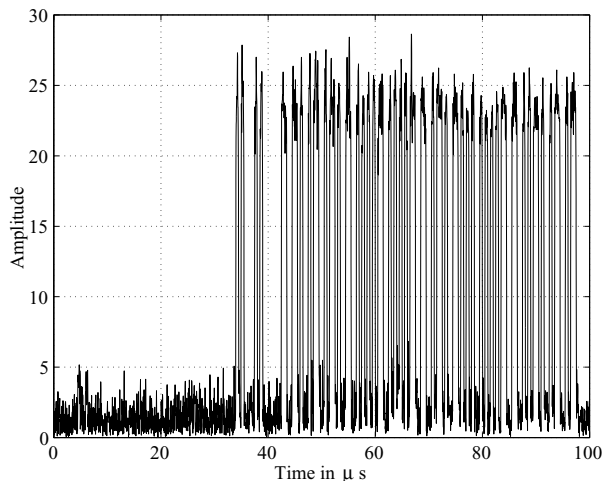
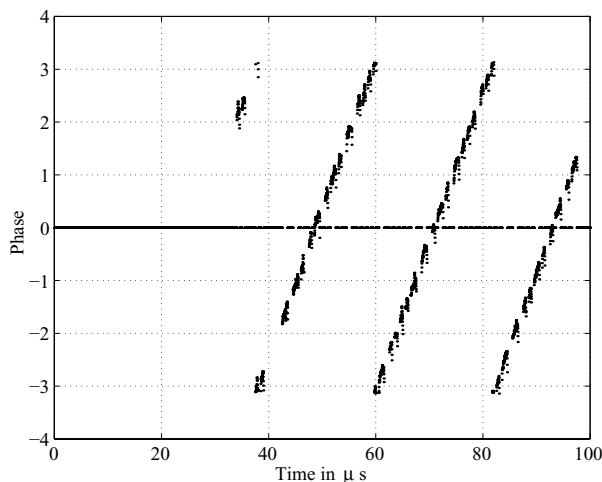


Figure 8.15: *Angular phase of the first recovered source. Every 25 samples, a sample is represented by a cross.*

our model.

The second source is totally matching the model, in amplitude and in phase.

Before using the algorithms, we have to reduce the number of samples from 50 per microsecond to 2 per microsecond. If we chose a good initial offset point for the down-sampling, all algorithms perform well. Oppositely, with a bad initial offset point, none of the algorithms is able to separate the sources. Since in practice the downsampler should be totally blind on the choice of the initial point, we need to

Figure 8.16: *Absolute value of the second recovered source.*Figure 8.17: *Angular phase of the second recovered source.*

know the influence of the initial point on the results of the algorithms. So for each initial point we tried to separate the source, and if one of the two sources has an output SINR smaller than 3 dB, the trial was considered as a failure. Table 8.1 presents the resulting rates.

It appears clearly that the Manchester based algorithms are more robust than MS-ZCMA. For this case, the phase of the first source does not follow our model, this may explain that the MDAs are more robust. The latter only use the absolute values of the samples.

Method	MD2	MD3	MS-ZCM
Failure rate	0.24	0.24	0.36

Table 8.1: Failure rate over all the possible starts of the down-sampling.

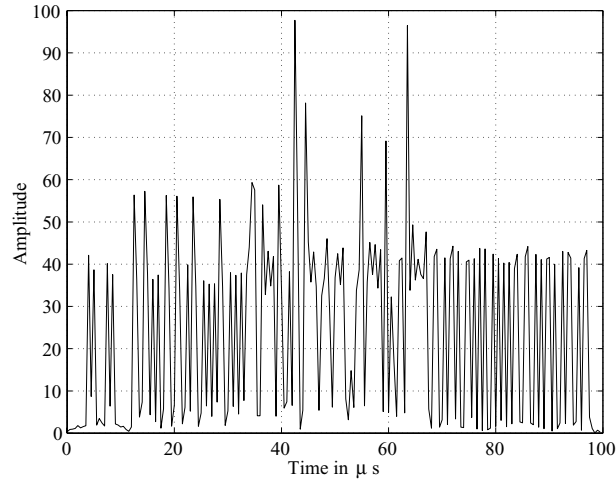


Figure 8.18: Case of down-sampling which results in a failure.

Figure 8.18 presents a case where the initial sampling point was chosen badly. One can observe that in this case the amplitude is constant almost everywhere, and thus we do not have the 0/1 property for the sources.

## 8.4 Conclusion

The measured data have shown that the model chosen at the beginning of the thesis does not always match the reality. The experiments show that even with these mismatches the algorithms continue to perform well.

The last experiment demonstrates that now the most important aspect to be investigated is the downsampling. To be insensitive to the sample moment, we have to oversample the received data, and the algorithms have to be modified for this.

## Chapter 9

# Conclusion

During the work of this thesis, I was offered a rare opportunity: to deeply investigate a subject from the beginning to the end. I had to demonstrate the feasibility of a new extension to the SSR radar: the multi-static configuration. The critical point was to create a passive receiving antenna array, this is the focus of my thesis. Antenna array is not a new tool, but never used in the scope of SSR. So the limits of this approach had to be found, algorithms dedicated for this case to be imagined, and a real antenna to be built.

Before any data processing, it is important to know if a solution exists and is unique. Many results on antenna array identifiability exist, but most of them concern infinite number of samples. For a finite number of samples, only probability bounds exist and are constellation-dependent; none of them is related to the SSR case. I found a novel bound for identifiability of the SSR problem using the source properties.

It is common practice to evaluate the best performance achievable by signal processing for a given scenario. This performance is the Cramer-Rao Bound, unfortunately in many cases some parameters influence the bound while they are not desired: we commonly call them the *unwanted parameters*. Often the symbols are unwanted parameters, I derived a proof for a stochastic Cramer-Rao Bound, which averages them.

As many algorithms dedicated to antenna arrays already exist, it is more interesting to elaborate new algorithms or refinements based on the specific properties of the SSR sources. I mainly investigated three different directions. Using the special Manchester Encoding of the SSR replies, I created two algorithms, called MDA2 and MDA3. I have adapted the SOBI algorithm to the SSR case, in order to make it more reliable. While it is not interesting in our context, it can be used in the landing phase of the aircrafts at the airport, where there is no variability in dynamic range. Lastly, I have used the principle of the AZFA algorithm to recreate a many subspace intersections algorithm, the MS-ZCMA.

Finally, I added a new value by designing and programming the whole physical receiving chain to validate those algorithms. With the antenna array built during the

thesis, we could perform a limited number of measurements. It was a semi-success, in the sense that while the results were good, not enough measurements could be done, due to lack of time.

As a general conclusion, the MDA 3 and the MS-ZCMA are recommended to be implemented in the future in the airports, as they have shown good robustness to difficult situations, and low failure rates.

In the future, as far as theoretical aspect are concerned, one should perform a first order error study of the algorithms. As the experimental device is up and running, it is a pity to not use it for further measurements, I suggest to use the device to enforce or to change the conclusion of Chapter 8. Practical utilization will be possible only after investigating the down-sampling issue: how it influences the results, and how to adapt the algorithms?

High-resolution algorithms are sensitive to so-called “calibration” errors, which arise from non-identical behavior of the analog transducers that transform the impinging electromagnetic waves into electric signals. As the thesis has a strong experimental final component, it was necessary to investigate array calibration algorithms. To do so, I gathered an extensive bibliography on the subject and I directed a student to study the AB algorithms [51] and the ESPRIT-like Algorithms [52] with synthesized data. Due to lack of time, I could not continue my investigations beyond these first steps. My desire is to continue to work in this direction and to imagine elegant new algorithms.

# Appendix A

## Proof of Lemma 4.3.5

### A.1 Reminder

We consider here  $d$  ZCM sources,  $s_i[n]$ , for which the absolute values belong to the set  $\{0, 1\}$  with equal probability, and for which the phases are uniformly distributed over  $[0, 2\pi)$ . It can be summarized as:

$$P(s_i[n] = 0) = P(|s_i[n]| = 1) = \frac{1}{2}$$

In Chapter 4, we have considered a  $N \times d^2(d+1)/2$  matrix  $\Psi$  constructed as:

$$\Psi = [\Psi_a | \Psi_b] \tag{A.1}$$

with:

$$\Psi_a = \left[ \begin{array}{ccc|ccc} s_1[1] & \dots & s_d[1] & (s_1^* s_1 s_2)[1] & \dots & (s_d^* s_d s_{d-1})[1] \\ \vdots & \vdots & \vdots & \vdots & \vdots & \vdots \\ s_1[N] & \dots & s_d[N] & (s_1^* s_1 s_2)[N] & \dots & (s_d^* s_d s_{d-1})[N] \end{array} \right]$$

$$\Psi_b = \left[ \begin{array}{ccc} (s_1^* s_2^2)[1] & \dots & (s_d^* s_{d-1}^2)[1] \\ \vdots & \vdots & \vdots \\ (s_1^* s_2^2)[N] & \dots & (s_d^* s_{d-1}^2)[N] \end{array} \right]$$

whose rows contain all the non redundant elements  $s_i^* s_j s_l[n]$ ,  $\forall \{i, j, l\} \in [1, \dots, d]^3$ ,  $\forall n \in [1, \dots, N]$ . The rows are sorted with the time index, the columns are sorted such that the elements for which  $i = j = l$  are placed first, then the elements with  $j \neq l$ , and lastly the elements such that  $j = l$ , and  $i \neq j$ .

We also have stated that this matrix has its columns independent, with at least the probability stated in Lemma 4.3.5. The next section presents the proof of this Lemma.

## A.2 Proof of Lemma 4.3.5

Given  $N$  samples of  $\mathbf{s}[n]$ ,  $\Psi$  is full column rank if and only if:

$$\Psi\boldsymbol{\alpha} = \mathbf{0} \implies \boldsymbol{\alpha} = \mathbf{0} \quad (\text{A.2})$$

For the sake of convenience, the vector  $\boldsymbol{\alpha}$  is indexed as  $\alpha_{ijl}$ , where  $\{i, j, l\}$  is conformal to the list of arguments in  $\Psi$ .

The proof is constructive: we derive a probability bound such that all elements of  $\boldsymbol{\alpha}$  are zero, hence  $\Psi$  full rank. Consider Figure A.1 where the coefficients  $\alpha_{ijl}$  are stacked in a volume, as in a half cube. We note that the elements  $\alpha_{ijl}$ , which are connected with the first source, represent a layer of the volume, and that the smaller volume is a scale-reduced version of the total volume.

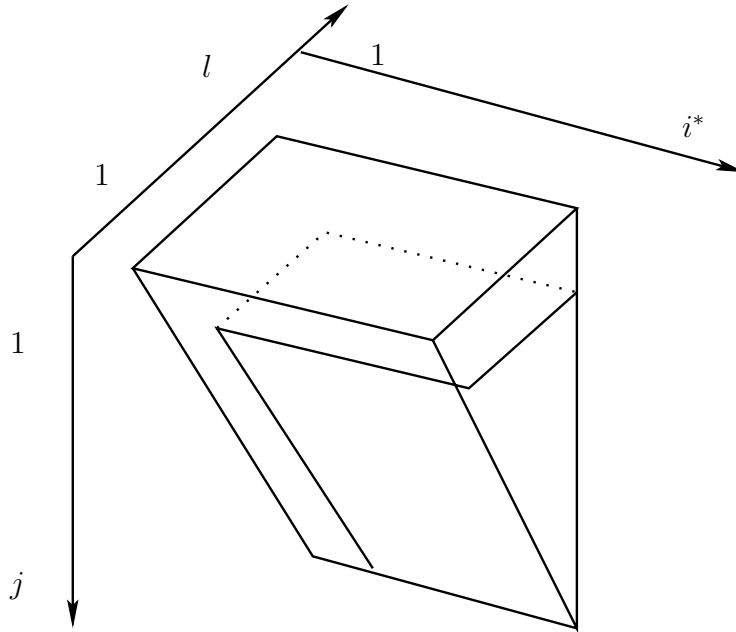


Figure A.1: The coefficient  $\alpha_{ijl}$  are re-organized in a volume which is a half-cube. In the upper-left are placed the coefficients containing a 1 in their indices.

The objective of this proof is to consider one layer after the other, and by using the independence of the sources to demonstrate that the  $\alpha_{ijl}$  are all equal to 0.



**Source 1:** We consider the first source  $s_1[n]$ . Reformulating Equation (A.2), we obtain for every  $n$  the following equation:

$$\begin{aligned}
(\Psi\alpha)[n] = 0 &\Leftrightarrow \tag{A.3} \\
\alpha_{111}s_1[n] &+ \sum_{2 \leq i \leq j}^d \alpha_{1ij}s_1^*[n]s_i[n]s_j[n] + \sum_{2 \leq i}^d \alpha_{11i}s_1^*[n]s_1[n]s_i[n] \\
+ \sum_{2 \leq \{i,j\}}^d \alpha_{i1j}s_i^*[n]s_1[n]s_j[n] &+ \sum_{2 \leq i}^d \alpha_{i11}s_i^*[n]s_1^2[n] + \sum_{2 \leq j < l}^d \alpha_{ijl}s_i^*[n]s_j[n]s_l[n] \tag{A.4}
\end{aligned}$$

For the samples  $n$  such that  $s_1[n] \neq 0$ , define the sample set  $\mathbb{N}_1$  of size  $N_1$ . This set exists with the probability:

$$P_c(N_1/N) = \frac{1}{2^N} \frac{N!}{(N - N_1)!N_1!}$$

For each sample  $n \in \mathbb{N}_1$ , we multiply the equations in (A.4) by  $s_1[n]$ , and using  $s_1s_1^* = 1$ , we obtain:

$$\begin{aligned}
&\left[ \sum_{2 \leq i \leq j}^d \alpha_{1ij}s_i[n]s_j[n] \right] + \left[ \sum_{2 \leq i}^d \alpha_{11i}s_i[n] \sum_{2 \leq j < l}^d \alpha_{ijl}s_i^*[n]s_j[n]s_l[n] \right] s_1[n] \\
&+ \left[ \alpha_{111} + \sum_{2 \leq \{i,j\}}^d \alpha_{i1j}s_i^*[n]s_j[n] \right] s_1^2[n] + \left[ \sum_{2 \leq i}^d \alpha_{i11}s_i^*[n] \right] s_1^3[n] = 0
\end{aligned}$$

It is a set of polynomial equations in  $s_1$ :

$$a[n] + b[n]s_1[n] + c[n]s_1^2[n] + d[n]s_1^3[n] = 0$$

for which G. Cardan (see [53] and [54, page 12]) gave us an exact solution:

$$s_1[n] = G[a[n], b[n], c[n], d[n]]$$

Since  $a[n]$ ,  $b[n]$ ,  $c[n]$ , and  $d[n]$  depend on  $\{s_2[n], \dots, s_d[n]\}$ , it implies  $s_1[n] = F(s_2[n], \dots, s_d[n]) = F[n]$ , which contradicts the independence assumption. Indeed, as  $|s_1[n]| = 1$ , and its probability distribution is uniform in phase, the probability such that  $s_1[n] = F[n]$  is zero, because it is a set of measure zero (one point on a circle). Therefore, either  $a[n]$  or  $d[n]$  is zero. Repeating this reasoning on the remaining quadratic equation, and on the linear equation, implies:

$$a[n] = b[n] = c[n] = d[n] = 0, \quad \forall n \in \mathbb{N}_1$$

or equivalently:

$$\begin{cases} a[n] = \sum_{2 \leq i \leq j}^d \alpha_{1ij} s_i[n] s_j[n] & = 0 \\ b[n] = \sum_{2 \leq i}^d \alpha_{11i} s_i[n] + \sum_{\substack{2 \leq j \leq l \\ 2 \leq j \leq l}}^d \alpha_{ijl} s_i^*[n] s_j[n] s_l[n] & = 0 \\ c[n] = \alpha_{111} + \sum_{2 \leq \{i,j\}}^d \alpha_{i1j} s_i^*[n] s_j[n] & = 0 \\ d[n] = \sum_{2 \leq i}^d \alpha_{i11} s_i^*[n] & = 0 \end{cases}$$

Note that we have discarded one sample.

1. We first study  $a[n] = 0$ . The probability to get a sample  $n \in \mathbb{N}_1$ , such that  $s_2[n] \neq 0$  is  $p_0(N_1) = 1 - 1/2^{N_1}$ . For this  $n$ , factoring  $s_2[n]$  out of the sum gives:

$$\alpha_{122} s_2^2[n] + \left( \sum_{j=3}^d \alpha_{12j} s_j[n] \right) s_2[n] + \left( \sum_{3 \leq i \leq j}^d \alpha_{1ij} s_i[n] s_j[n] \right) = 0$$

This  $s_2[n]$  is the solution of a quadratic equation:  $a'[n]s_2^2[n] + b'[n]s_2[n] + c[n] = 0$ , with the same reasoning like in the preceding alinea, it follows that the probability to get  $s_2[n] = \left[ \frac{-b'[n] \pm \sqrt{4a'c - b'^2}}{2a'} \right] [n]$  is zero, thus implying:

$$\begin{cases} \alpha_{122} = 0 \\ \sum_{j=3}^d \alpha_{12j} s_j[n] = 0 \\ \sum_{3 \leq i \leq j}^d \alpha_{1ij} s_i[n] s_j[n] = 0 \end{cases}$$

Next, we consider the  $N_1 - 1$  equations  $\sum_{j=3}^d \alpha_{12j} s_j[n] = 0$ . Similarly, the probability that we obtain at least one non-zero  $s_3[n]$  is  $p_0(N_1 - 1) = 1 - 1/2^{N_1 - 1}$ . We then have the equation  $\alpha_{123} s_3[n] = -\sum_{j=4}^d \alpha_{12j} s_j[n]$ , because of the independence of the sources,  $\alpha_{123} = 0$ . Inductively, we deduce the probability to have all  $\alpha_{12i} = 0$ ,  $i \geq 2$  is:

$$\prod_{i=2}^d p_0(N_1 - i + 2)$$

Next, we consider the  $N_1 - 2$  equations  $\sum_{3 \leq i \leq j}^d \alpha_{1ij} s_i[n] s_j[n] = 0$ , applying inductively the same reasoning than at the beginning of this alinea, we can state that  $\forall \{i, j\}$  such that  $2 \leq i \leq j \leq d$ ,  $\alpha_{1ij} = 0$  with the probability:

$$P_1(N_1) = \prod_{i=1}^{d(d-1)/2} p_0(N_1 - i + 1)$$

**Note** that we have identified  $\frac{d(d-1)}{2}$  parameters, the  $\alpha_{1ij}$  with  $2 \leq i \leq j$ , but we also discarded  $\frac{d(d-1)}{2}$  samples.

2. We now study  $c[n] = \left[ \alpha_{111} + \sum_{2 \leq \{i,j\}}^d \alpha_{i1j} s_i^*[n] s_j[n] \right] = 0$ . We denote  $N_2 = N_1 - \frac{d(d-1)}{2}$ , and we assume there exists a time  $n$  in the remaining set of  $\mathbb{N}_1$  such that  $|s_2[n]| = 1$ , then we can multiply  $c[n]$  by  $s_2[n]$ :

$$\left( \left[ \alpha_{111} + \sum_{3 \leq i,j}^d \alpha_{i1j} s_i^* s_j \right] + \alpha_{212} |s_2|^2 \right) s_2[n] + \left[ \sum_{2 \leq j}^d \alpha_{21j} s_j \right] + \left[ \sum_{2 \leq j}^d \alpha_{i11} s_i^* \right] s_2^2[n] = 0 \quad (\text{A.5})$$

$s_2[n]$  has to be the solution of the above quadratic equation. Since the probability to obtain randomly the ideal  $s_2[n]$  is zero, for the same reason as in the preceding aineas, it implies:

$$\Rightarrow \begin{cases} \sum_{2 \leq j}^d \alpha_{21j} s_j & = 0 \\ \sum_{2 \leq i}^d \alpha_{i12} s_i^* & = 0 \\ \alpha_{111} + \alpha_{212} |s_2|^2 + \sum_{3 \leq i,j}^d \alpha_{i1j} s_i^* s_j & = 0 \end{cases}$$

Using the same techniques as in item 1, we show that with probability  $\prod_{i=3}^d p_0(N_2 - i + 2)$ :

$$\alpha_{21j} = 0, \forall j \geq 3$$

and with probability  $\prod_{j=3}^d p_0(N_2 - d + 2 - j + 2)$ :

$$\alpha_{i21} = 0, \forall i \geq 3$$

By iterating the process, with the probability:

$$P_2(N_2) = \prod_{i=1}^{(d-2)(d-1)+1} p_0(N_2 - i + 1)$$

we obtain:

$$\alpha_{i1j} = 0, 2 \leq i \neq j \leq d$$

Note that we identified  $(d-1)(d-2)$  coefficients and discarded  $d(d-2)$  samples. The  $(d-2)$  unused samples remain and form the following equations:

$$\begin{bmatrix} 1 & 1 & * & \cdots & * \\ \vdots & * & \ddots & \ddots & \vdots \\ \vdots & \vdots & \ddots & \ddots & \vdots \\ 1 & * \cdots & * & 1 & * \end{bmatrix} \begin{bmatrix} \alpha_{111} \\ \vdots \\ \vdots \\ \alpha_{d1d} \end{bmatrix} = \mathbf{0} \quad (\text{A.6})$$

where  $* \in \{0, 1\}$ , so the matrix is binary

Considering again the beginning this ainea, we obtain that if  $|s_1| = 1$ :

$$c[n] = \alpha_{111} + \sum_{2 \leq j}^d \alpha_{i1i} |s_i|^2 = 0 \quad (\text{A.7})$$

3.  $d[n] = \sum_{2 \leq i}^d \alpha_{i11} s_i^* [n] = 0$ . We denote  $N_3 = N_2 - (d-1)(d-2)$ . By isolating the contribution of each source as in the first ainea, we then have the probability  $P_3(N_3) = \prod_{i=1}^{d-1} p_0(N_3 - i + 1)$  to obtain  $\alpha_{i11} = 0 \quad \forall i \leq 2$

Note that  $(d-1)$  coefficients and samples are discarded.

4. We denote  $N_4 = N_3 - (d-1)$ . We first consider Equation (A.4) with the terms, that have not yet been canceled:

$$\alpha_{111} s_1 + \sum_{2 \leq i}^d \alpha_{i1i} |s_i|^2 s_1 + \sum_{2 \leq i}^d \alpha_{11i} |s_1|^2 s_i + \sum_{\substack{2 \leq j \leq l \\ 2 \leq i \leq l}}^d \alpha_{ijl} s_i^{*2} s_j s_l = 0 \quad (\text{A.8})$$

If Equation (A.7) is true when  $|s_1| = 1$ , then Equation (A.7) multiplied by  $s_1$  is true for all  $s_1$ :

$$\left[ \alpha_{111} + \sum_{2 \leq i}^d \alpha_{i1i} |s_i|^2 \right] s_1 = 0$$

Thus Equation (A.8) reduces to:

$$\begin{aligned} & \left[ \sum_{2 \leq i}^d \alpha_{11i} s_i \right] |s_1|^2 + \left[ \sum_{\substack{2 \leq j \leq l \\ 2 \leq i \leq l}}^d \alpha_{ijl} s_i^* s_j s_l \right] = 0 \\ \Leftrightarrow & a'[n] b_1[n] + c'[n] = 0 \end{aligned} \quad (\text{A.9})$$

where  $b_1[n]$  is the associated bit to  $s_1[n]$ . Assume that  $a[n] \neq 0$  so that  $b_1[n] = \frac{c'[n]}{a'[n]} = f[n]$ .

Necessarily, both sides must have the same probability distribution:

$$\begin{cases} P(1) & = & \frac{1}{2} \\ P(0) & = & \frac{1}{2} \end{cases}$$

but are independent since  $f[n] = F(s_2[n], \dots, s_d[n])$ . The probability to get an equation as “0 = 1” is:  $P_4 = 1 - \frac{1}{2^{N_4}}$ , which shows that by necessity  $a'[n] = 0$ , and thus  $c'[n]$  as well.

Denote  $N_5 = N_4 - 1$ . We consider now  $a'[n] = \sum_{2 \leq i}^d \alpha_{11i} s_i [n] = 0$  as in the previous case, with probability  $P_5 = \prod_{i=1}^{d-1} p_0(N_5 - i + 1)$ ,  $\alpha_{11i} = 0$  for  $i \geq 2$ .

Finally, we managed to reduce Equation (A.8), and Equation (A.4), to:

$$\sum_{\substack{2 \leq i \leq l \\ 2 \leq j \leq l}}^d \alpha_{ijl} s_i^* s_j s_l = 0$$

with the probability:

$$P_T^{(1)}(N) = \sum_{N_1=l_d}^N P_C \left( \frac{N_1}{N} \right) \left[ \prod_{i=1}^{l_d} p_0(N_1 - i_1) \right]$$

where  $l_d = d \left\lceil \frac{3d-1}{2} \right\rceil - 1$ .

Note that now the Equation does not contain any  $\alpha_{ijl}$  whose indices would contain a 1. We are placed back at the beginning of the demonstration, but with  $d-1$  sources only.

**Source 2:** We consider the second source  $s_2[n]$ . With the same method as in the previous paragraph, we determine the probability to isolate the “half-cube” containing the  $\alpha_{ijl}$  with all indices superior to 2 to be:

$$P_T^{(2)} = \sum_{N_2=l_{d-1}}^{N-l_d} P_C \left( \frac{N_2}{N-l_d} \right) \left[ \prod_{i=1}^{l_{d-1}} p_0(N_2 - i + 1) \right]$$

with  $l_{d-1} = (d-1) \left\lceil \frac{3(d-1)-1}{2} \right\rceil - 1$ , and to obtain:

$$\begin{cases} \alpha_{2ij} = 0 & \forall i, j \in \{3, \dots, d\} \\ \alpha_{i2j} = 0 & 3 \leq i \neq j \leq d \\ \alpha_{22i} = 0 & 3 \leq i \\ \alpha_{i22} = 0 & i \geq 3 \end{cases}$$

Note that we left on the side several coefficient as in the preceding paragraph: the  $\alpha_{i2i}$ , for all the  $i \geq 2$ .

**Source 3 to  $d-2$ :** • The same method is iterated from the third source to the  $(d-2)^{th}$  source, and for each source the probability is:

$$P_T^{(i)} = \sum_{N_i=l_{d-i+1}}^{N-L_{d+1-i}} P_C \left( \frac{N_i}{N-L_{d+1-i}} \right) \left[ \prod_{j=1}^{l_{d+1-i}} p_0(N_i - j + 1) \right]$$

with  $L_{d+1-i} = \sum_{j=1}^{i-1} l_{d+1-j}$ .

**Source  $d - 1$ :** We finally consider the  $(d - 1)^{th}$  source, Equation (A.4) is now reduced to:

$$\sum_{\substack{d-1 \leq i \leq d \\ d-1 \leq j \leq d}} \alpha_{ijl} s_i^* s_j s_l = 0$$

or equivalently:

$$\begin{aligned} & \alpha_{ddd} s_d + \alpha_{d-1,d-1,d-1} s_{d-1} + \alpha_{d-1,d-1,d-1} |s_{d-1}|^2 s_d \\ & + \alpha_{d-1,d,d} s_d^2 s_{d-1} + \alpha_{d,d-1,d-1} s_d^* s_{d-1}^2 + \alpha_{d,d-1,d} |s_d|^2 s_{d-1} = 0 \end{aligned} \quad (\text{A.10})$$

- a) The probability there is a time  $n$  such that  $s_d = 0$  and  $s_{d-1} \neq 0$  is  $\frac{1}{4}$ . We denote  $N' = N - L_{d-2}$  the number of unused samples, then the probability to get this combination is  $P_a = 1 - \left(\frac{3}{4}\right)^{N'}$ . Equation (A.10) is simplified to:

$$\alpha_{d-1,d-1,d-1} s_{d-1} = 0 \Rightarrow \alpha_{d-1,d-1,d-1} = 0$$

- b) Identically, with probability  $P_b = 1 - \left(\frac{3}{4}\right)^{N'-1}$ , there is a  $t$  such that  $s_{d-1} = 0$  and  $s_d \neq 1$ , which simplifies Equation (A.10) to:

$$\alpha_{d,d,d} s_d = 0 \Rightarrow \alpha_{d,d,d} = 0$$

- c) Consider now that both  $s_d$  and  $s_{d-1}$  are non-zero, and multiply Equation (A.10) by  $s_d$ :

$$[\alpha_{d,d-1,d-1}] + [\alpha_{d,d-1,d} s_{d-1}] s_d + [\alpha_{d-1,d-1,d} |s_{d-1}|^2] s_d^2 + [\alpha_{d-1,d,d} s_{d-1}^*] s_d^3 = 0$$

with  $|s_{d-1}| = 1$ . For the same reason than in the previous steps of the demonstration, the probability such that  $s_d = F(s_{d-1})$  is zero. Thus the coefficients of the polynomial should be zero, and remind that  $s_{d-1} \neq 0$ :

$$\begin{cases} \alpha_{d,d-1,d-1} & = 0 \\ \alpha_{d,d-1,d} s_{d-1} & = 0 \Rightarrow \alpha_{d,d-1,d} = 0 \\ \alpha_{d-1,d-1,d} |s_{d-1}|^2 & = 0 \Rightarrow \alpha_{d-1,d-1,d} = 0 \\ \alpha_{d-1,d,d} s_{d-1}^* & = 0 \Rightarrow \alpha_{d-1,d,d} = 0 \end{cases}$$

with  $P_c = 1 - \left(\frac{3}{4}\right)^{N'-2}$ .

**Last terms:** The last part of the demonstration is to cancel the terms  $\alpha_{iji}$  with  $i \geq j$ . We have the following relations, for all  $t \in [1, \dots, N]$ :

$$\begin{cases} \left[ \alpha_{111} + \sum_{2 \leq i}^d \alpha_{i1i} b_i[n] \right] s_1[n] & = 0 \\ \left[ \alpha_{222} + \sum_{3 \leq i}^d \alpha_{i2i} b_i[n] \right] s_2[n] & = 0 \\ & \vdots \\ \left[ \alpha_{d-2,d-2,d-2} + \sum_{d-1 \leq i}^d \alpha_{i,d-2,i} b_i[n] \right] s_{d-i}[n] & = 0 \end{cases} \quad (\text{A.11})$$

We assume that we can find  $d$  samples,  $\{n_1, \dots, n_d\}$ , such that the columns of the signal form an upper-triangular  $d \times d$  source matrix, with non-zero elements on the diagonal, such as:

$$S_F = \begin{bmatrix} s_1[n_1] & s_1[n_2] & \cdots & s_1[n_d] \\ 0 & s_2[n_2] & \ddots & \vdots \\ \vdots & \ddots & \ddots & * \\ 0 & \cdots & 0 & s_d[n_d] \end{bmatrix}$$

where  $S_F$  is full rank. Given  $N_F$  remaining samples, the probability to get such an arrangement is:  $P_\alpha(N_F) = \prod_{i=1}^d \left[ 1 - \left( 1 - \frac{d+1-i}{2^{d+1-i}} \right)^{N-i+1} \right]$ .

For each  $i \in \{1, \dots, d-2\}$ , we transform  $S_F$  into a matrix  $S_F^{(i)}$  by multiplying the square of the element of the absolute value of  $S_F$  by a diagonal matrix which contains on the diagonal the  $i$ -th row of  $S_F$ . We denote the square of the element of absolute value of  $|S_F|$  by  $\underline{S}_F$ , the  $S_F^{(i)}$  are:

$$\begin{aligned} S_F^{(i)} &= \underline{S}_F \times \text{diag}[(s_i[n_1]), \dots, (s_i[n_d])] \\ S_F^{(i)} &= \begin{bmatrix} (|s_1|^2 s_i)[n_1] & (|s_1|^2 s_i)[n_2] & \cdots & (|s_1|^2 s_i)[n_d] \\ 0 & (|s_2|^2 s_i)[n_2] & & \vdots \\ \vdots & \ddots & \ddots & \vdots \\ 0 & \cdots & 0 & (|s_d|^2 s_i)[n_d] \end{bmatrix} \end{aligned} \quad (\text{A.12})$$

where the lower right  $(d-i) \times (d-i)$  corner of the matrices  $S_F^{(i)}$  are full rank matrices.

We define the notation  $(\overline{\mathbf{M}})_i$ , which reduce a matrix  $\mathbf{M}$  to its lower right  $(d-i) \times (d-i)$  corner. Equation (A.11) can be re-written as:

$$\left\{ \begin{array}{l} [\alpha_{111}, \alpha_{212}, \dots, \alpha_{d1d}] \left( \overline{S_F^{(1)}} \right)_i = 0 \\ [\alpha_{222}, \dots, \alpha_{d2d}] \left( \overline{S_F^{(2)}} \right)_i = 0 \\ \vdots \\ [\alpha_{d-2,d-2,d-2}, \alpha_{d-1,d-2,d-1}, \alpha_{d,d-2,d}] \left( \overline{S_F^{(d-2)}} \right)_i = 0 \end{array} \right. \quad (\text{A.13})$$

which demonstrates that  $\forall d \geq i \geq j \geq 1: \alpha_{iji} = 0$ .

Because this last step need a lot of samples in order to have  $P_\alpha(N_F)$  near 1, it is more interesting to select good samples at the beginning and to keep it on the side for the end, so that the probability is  $P_\alpha(N)$ .

**Conclusion** We demonstrated that with the probability:

$$P_F = P_\alpha(N) \left[ P_T^{(1)} P_T^{(2)} \cdots P_T^{(d-2)} \right] (N-d) P_a P_b P_c$$

for all  $i, j, l \in \{1, \dots, d\}$ , we have obtained that:

$$\alpha_{ijl} = 0$$

So with the same probability, the matrix  $\Psi$  has independent columns. If  $N \geq L_2 + d + 3$ ,  $\Psi$  is full rank.  $\square$



## Appendix B

# CRB proofs

### B.1 Inversion of $\mathcal{I}_\gamma$ by the Schur complement theorem

Consider a matrix  $M$ , which has the following partition:

$$\mathbf{M} = \begin{bmatrix} \mathbf{A} & \mathbf{B} \\ \mathbf{B}^H & \mathbf{C} \end{bmatrix}$$

then assuming  $\mathbf{A}$  and  $\mathbf{C}$  to be square and that  $\mathbf{A}$ ,  $\mathbf{C}$ , and  $\mathbf{M}$  are invertible, the Schur complement theorem yields ([55, p. 472]):

$$\begin{bmatrix} \mathbf{A} & \mathbf{B} \\ \mathbf{B}^H & \mathbf{C} \end{bmatrix}^{-1} = \begin{bmatrix} (\mathbf{A} - \mathbf{B}\mathbf{C}^{-1}\mathbf{B}^H)^{-1} & \mathbf{A}^{-1}\mathbf{B}(\mathbf{B}^H\mathbf{A}^{-1}\mathbf{B} - \mathbf{C})^{-1} \\ (\mathbf{B}^H\mathbf{A}^{-1}\mathbf{B} - \mathbf{C})^{-1}\mathbf{B}^H\mathbf{A}^{-1} & (\mathbf{C} - \mathbf{B}^H\mathbf{A}^{-1}\mathbf{B})^{-1} \end{bmatrix} \quad (\text{B.1})$$

Then using the matrix inversion lemma:

$$(\mathbf{A} + \mathbf{B}\mathbf{C}\mathbf{D})^{-1} = \mathbf{A}^{-1} - \mathbf{A}^{-1}\mathbf{B}(\mathbf{C}^{-1} + \mathbf{D}\mathbf{A}^{-1}\mathbf{B})^{-1}\mathbf{D}\mathbf{A}^{-1}$$

and denoting the matrix:  $(\mathbf{C} - \mathbf{B}^H\mathbf{A}^{-1}\mathbf{B})^{-1} = \mathbf{C}'$ , the above matrix simplifies to:

$$\begin{bmatrix} \mathbf{A} & \mathbf{B} \\ \mathbf{B}^H & \mathbf{C} \end{bmatrix}^{-1} = \begin{bmatrix} \mathbf{A}^{-1} + \mathbf{A}^{-1}\mathbf{B}\mathbf{C}'\mathbf{B}^H\mathbf{A}^{-1} & -\mathbf{A}^{-1}\mathbf{B}\mathbf{C}' \\ -\mathbf{C}'\mathbf{B}^H\mathbf{A}^{-1} & \mathbf{C}' \end{bmatrix} \quad (\text{B.2})$$

Replacing the matrices  $\{\mathbf{A}, \mathbf{B}, \mathbf{C}\}$  by their actual value gives Prop. 5.2.5.

### B.2 Proof for lemma (5.2.3)

#### B.2.1 Reminders

**FACT I** For a real Gaussian noise with variance  $\sigma_{\mathbb{R}}^2$ , the probability density function is:

$$p(n) = \frac{1}{2\pi\sigma_{\mathbb{R}}^2} e^{-\frac{\|n\|^2}{2\sigma_{\mathbb{R}}^2}}$$

define  $m_i = \mathbb{E}\{n^i\}$ , then we get:

$$\begin{cases} m_0 &= 1 \\ m_1 &= 0 \\ m_2 &= \sigma_{\mathbb{R}}^2 \end{cases} \quad (\text{B.3})$$

**FACT II** For a complex Gaussian noise with variance  $\sigma_{\mathbb{C}}^2$ , the p.d.f. is:

$$p(x) = \frac{1}{\pi\sigma_{\mathbb{C}}^2} e^{-\frac{\|x\|^2}{\sigma_{\mathbb{C}}^2}}$$

with  $\sigma_{\mathbb{C}}^2 = 2 \cdot \sigma_{\mathbb{R}}^2$ . Define  $m_{ij} = \mathbb{E}\{x^i x^{*j}\}$ , since complex Gaussian noise are circular, if  $i \neq j$ ,  $m_{ij} = 0$ . Also:

$$\begin{cases} m_{00} &= 1 \\ m_{11} &= \sigma_{\mathbb{C}}^2 \end{cases} \quad (\text{B.4})$$

## B.2.2 Preliminary lemmas

**Lemma B.2.1** *Define*

$$F_{ab} = \int \frac{e^{-|x-a|^2} \times e^{-|x-b|^2}}{e^{-|x-a|^2} + e^{-|x-b|^2}} dx$$

if  $\|a - b\|^2 \gg 1$  ( $a$  and  $b$  are enough separated), then  $|F_{ab}| \ll |F_{aa}|$ , meaning  $F_{ab}$  can be neglected with respect to  $F_{aa}$ .

**Proof** Let us cut the domain of integration into two regions: A and B, respectively centered around  $a$  and  $b$ . Since we assume  $a$  and  $b$  to be “far enough”, for each region one exponential is highly dominant.  $F_{ab}$  and  $F_{aa}$  simplify as:

$$F_{aa} \simeq \int_B \frac{e^{-2|x-a|^2}}{e^{-|x-b|^2}} dx + \int_A e^{-|x-a|^2} dx$$

and

$$F_{ab} \simeq \int_B e^{-|x-a|^2} dx + \int_A e^{-|x-b|^2} dx$$

Comparing both expression, it appears that  $F_{aa}$  got most (all) of the energy of  $\int \exp^{-|x-a|^2}$ , while  $F_{ab}$  not, which is then neglectable with respect to  $F_{aa}$ .  $\square$

**Lemma B.2.2** *Define:*

$$\begin{aligned} \mathbf{F}_{11} &= \int \cdots \int_{\mathbb{C}^M} \frac{e^{-\frac{2}{\sigma^2} \|\mathbf{y}\|^2}}{\sum_{\mathbf{b}_l \in \mathcal{B}} e^{-\frac{1}{\sigma^2} \|\mathbf{y} + \mathbf{M}_k(\mathbf{b}_k - \mathbf{b}_l)\|^2}} \mathbf{y} \mathbf{y}^H d\mathbf{y} \\ \mathbf{F}_{12} &= \int \cdots \int_{\mathbb{C}^M} \frac{e^{-\frac{2}{\sigma^2} \|\mathbf{y}\|^2}}{\sum_{\mathbf{b}_l \in \mathcal{B}} e^{-\frac{1}{\sigma^2} \|\mathbf{y} + \mathbf{M}_k(\mathbf{b}_k - \mathbf{b}_l)\|^2}} \mathbf{y} \mathbf{y}^T d\mathbf{y} \end{aligned}$$

where  $\mathcal{B}_d$  denotes the set of all the binary vector of length  $d$ . Given that  $\frac{1}{\sigma^2} \|\mathbf{M}_k(\mathbf{b}_k - \mathbf{b}_l)\|^2$  is large enough for  $\mathbf{b}_k \neq \mathbf{b}_l$ , we can accept the following approximation:

$$\begin{aligned}\mathbf{F}_{11} &\simeq \sigma^2(\pi\sigma^2)^M \mathbf{I}_M \\ \mathbf{F}_{12} &\simeq \mathbf{0}\end{aligned}$$

**Proof** Let us begin with  $\mathbf{F}_{11}$ :

$$\mathbf{F}_{11} = \int \cdots \int_{\mathbb{C}^M} \frac{\mathbf{y}\mathbf{y}^H e^{-\frac{2}{\sigma^2} \|\mathbf{y}\|^2}}{\sum_{\mathbf{b}_l \in \mathcal{B}} e^{-\frac{1}{\sigma^2} \|\mathbf{y} + \mathbf{M}_k(\mathbf{b}_k - \mathbf{b}_l)\|^2}} d\mathbf{y}$$

Considering that  $\frac{1}{\sigma^2} \|\mathbf{M}_k(\mathbf{b}_k - \mathbf{b}_l)\|^2$  is large enough for  $\mathbf{b}_k \neq \mathbf{b}_l$ , we can admit a similar reasoning as in the previous lemma and limits ourselves on the area around 0:

$$\begin{aligned}\mathbf{F}_{11} &\simeq \int \cdots \int_{(\text{Around } 0)^M} \mathbf{y}\mathbf{y}^H e^{-\frac{1}{\sigma^2} \|\mathbf{y}\|^2} d\mathbf{y} \\ &\simeq \int \cdots \int_{(\text{Around } 0)^M} \begin{bmatrix} y_1 y_1^* & \cdots & y_1 y_M^* \\ \vdots & & \vdots \\ y_M y_1^* & \cdots & y_M y_M^* \end{bmatrix} e^{-\frac{1}{\sigma^2} \|\mathbf{y}\|^2} d\mathbf{y}\end{aligned}$$

then the elements are:

$$\begin{aligned}(\mathbf{F}_{11})_{ij} &\simeq \int \cdots \int_{(\text{Around } 0)^M} y_i y_j^* e^{-\frac{1}{\sigma^2} \sum_{l=1}^M \|y_l\|^2} dy_1 \dots dy_M \\ (\mathbf{F}_{12})_{ij} &\simeq \int \cdots \int_{(\text{Around } 0)^M} y_i y_j e^{-\frac{1}{\sigma^2} \sum_{l=1}^M \|y_l\|^2} dy_1 \dots dy_M\end{aligned}$$

with Eqn. (B.4) relates to:

$$(\mathbf{F}_{11})_{ij} \simeq \sigma^2(\pi\sigma^2)^M \cdot \delta(i - j)$$

while for  $\mathbf{F}_{12}$ , by circularity:

$$(\mathbf{F}_{12})_{ij} \simeq 0$$

then the result holds.  $\square$

For the next Lemma, recall that  $\mathbf{b}$  is a equiprobable i.i.d. binary vector.

**Lemma B.2.3** Denote  $\mathcal{B}_d$  the set of all the binary vector of length  $d$ , and define  $\mathbf{C}_B^{(d)} = \frac{1}{4}(\mathbf{1}^T \cdot \mathbf{1} + \mathbf{I}_d)$ , then:

$$\sum_{\mathbf{b}_k \in \mathcal{B}_d} \mathbf{b}_k \mathbf{b}_k^T = 2^d \mathbf{C}_B^{(d)}$$

**Proof** the proof is by induction. Beforehand, let us remind that:

$$\sum_{\mathbf{b}_k \in \mathcal{B}_d} \mathbf{b}_k = 2^d \mathbb{E}\{\mathbf{b}\} = 2^{d-1} \mathbf{1}_d$$

Now let us consider the case  $d = 2$ :

$$\mathbf{0} + \begin{bmatrix} 1 & 0 \\ 0 & 0 \end{bmatrix} + \begin{bmatrix} 0 & 0 \\ 0 & 1 \end{bmatrix} + \begin{bmatrix} 1 & 1 \\ 1 & 1 \end{bmatrix} = \begin{bmatrix} 2 & 1 \\ 1 & 2 \end{bmatrix} = 2^2 \begin{bmatrix} \frac{1}{2} & \frac{1}{4} \\ \frac{1}{4} & \frac{1}{2} \end{bmatrix}$$

Consider now the property true for any order  $d$ , and let us determine it for  $d + 1$ :

$$\begin{aligned} \sum_{\mathbf{b}'_k \in \mathcal{B}_{d+1}} \mathbf{b}'_k \mathbf{b}'_k{}^T &= \sum_{\mathbf{b}_k \in \mathcal{B}_d} \begin{bmatrix} \mathbf{b}_k \\ 0 \end{bmatrix} \cdot [\mathbf{b}_k^T \ 0] + \sum_{\mathbf{b}_k \in \mathcal{B}_d} \begin{bmatrix} \mathbf{b}_k \\ 1 \end{bmatrix} \cdot [\mathbf{b}_k^T \ 1] \\ &= \begin{bmatrix} 2^d C_b^{(d)} & \mathbf{0} \\ \mathbf{0}^T & 0 \end{bmatrix} + \begin{bmatrix} 2^d C_b^{(d)} & \sum_{\mathbf{b}_k \in \mathcal{B}_d} \mathbf{b}_k \\ (\sum_{\mathbf{b}_k \in \mathcal{B}_d} \mathbf{b}_k)^T & 2^d \end{bmatrix} \\ &= \begin{bmatrix} 2^{d+1} C_b^{(d)} & 2^{d-1} \mathbf{1}_d \\ 2^{d-1} \mathbf{1}_d^T & 2^d \end{bmatrix} = \mathbf{C}_B^{d+1} \end{aligned}$$

which demonstrates that we have the property for the order  $d + 1$ .  $\square$

### B.2.3 Main body

We assume:  $\mathbf{x}_k = \mathbf{M}_k \cdot \mathbf{b}_k + \mathbf{n}_k$  with the conditional probability:

$$p(\mathbf{x}_k / \mathbf{M}_k, \mathbf{b}_k) = \frac{1}{(\pi\sigma^2)^M} \exp^{-\frac{1}{\sigma^2} \|\mathbf{x}_k - \mathbf{M}_k \cdot \mathbf{b}_k\|^2}$$

We sum over all the  $\mathbf{b}_k$  in  $\mathcal{B}_d$  to get the conditional probability:

$$p(\mathbf{x}_k / \mathbf{M}_k) = \sum_{\mathbf{b}_k \in \mathcal{B}_d} p(\mathbf{x}_k / \mathbf{M}_k, \mathbf{b}_k) \times p(\mathbf{b}_k)$$

where  $\mathcal{B}_d$  is the set of all the possible  $\mathbf{b}_k$  of length  $d$ . Since  $p(\mathbf{b}_k) = \frac{1}{2^d}$ , it is equal to:

$$p(\mathbf{x}_k / \mathbf{M}_k) = \frac{1}{2^d} \frac{1}{(\pi\sigma^2)^M} \sum_{\mathbf{b}_k \in \mathcal{B}_d} \exp^{-\frac{1}{\sigma^2} \|\mathbf{x}_k - \mathbf{M}_k \cdot \mathbf{b}_k\|^2}$$

where with some abuse of notation, we drop now the  $d$  on  $\mathcal{B}_d$  to use it as  $\mathcal{B}$ . The Fisher Information Matrix for the sample  $k$  is defined as:

$$\mathcal{I}_{i,j}^{(k)} = \mathbb{E} \left\{ \frac{\partial \ln p}{\partial \lambda_i} \cdot \frac{\partial \ln p^*}{\partial \lambda_j} \right\} = \int \dots \int_{\mathbb{C}^M} \frac{\partial \ln p(\mathbf{x}_k / \mathbf{M}_k)}{\partial \lambda_i} \cdot \frac{\partial \ln p(\mathbf{x}_k / \mathbf{M}_k)}{\partial \lambda_j} p(\mathbf{x}_k / \mathbf{M}_k) d\mathbf{x}_k$$

and the derivation of the log-likelihood gives:

$$\begin{aligned} \frac{\partial \ln p(\mathbf{x}_k / \mathbf{M}_k)}{\partial \lambda_i} &= \frac{1}{\sum_{\mathbf{b}_k \in \mathcal{B}} \exp^{-\frac{1}{\sigma^2} \|\mathbf{x}_k - \mathbf{M}_k \cdot \mathbf{b}_k\|^2}} \\ &\times \sum_{\mathbf{b}_l \in \mathcal{B}} \frac{1}{\sigma^2} \left[ \mathbf{b}_k^H \frac{\partial \mathbf{M}_k^H}{\partial \lambda_i} \mathbf{n}_k + \mathbf{n}_k^H \frac{\partial \mathbf{M}_k}{\partial \lambda_i} \mathbf{b}_k \right] \exp^{-\frac{1}{\sigma^2} \|\mathbf{x}_k - \mathbf{M}_k \cdot \mathbf{b}_l\|^2} \end{aligned}$$

After several manipulations, we get:

$$\begin{aligned} \mathcal{I}_{i,j}^{(k)} &= \frac{1}{2^d} \frac{1}{(\pi\sigma^2)^M} \frac{1}{\sigma^4} \\ &\sum_{\mathbf{b}_l, \mathbf{b}_k \in \mathcal{B}} \left[ \mathbf{b}_k^H \frac{\partial \mathbf{M}_k^H}{\partial \lambda_i} F_{(11)}(\mathbf{b}_k, \mathbf{b}_l) \frac{\partial \mathbf{M}_k}{\partial \lambda_j} \mathbf{b}_l + \mathbf{b}_k^H \frac{\partial \mathbf{M}_k^H}{\partial \lambda_i} F_{(12)}(\mathbf{b}_k, \mathbf{b}_l) \frac{\partial \mathbf{M}_k^*}{\partial \lambda_j} \mathbf{b}_l^* \right. \\ &\quad \left. + \mathbf{b}_k^T \frac{\partial \mathbf{M}_k^T}{\partial \lambda_i} F_{(21)}(\mathbf{b}_k, \mathbf{b}_l) \frac{\partial \mathbf{M}_k}{\partial \lambda_j} \mathbf{b}_l + \mathbf{b}_k^T \frac{\partial \mathbf{M}_k^T}{\partial \lambda_i} F_{(22)}(\mathbf{b}_k, \mathbf{b}_l) \frac{\partial \mathbf{M}_k^*}{\partial \lambda_j} \mathbf{b}_l^* \right] \end{aligned}$$

with the matrices  $\mathbf{F}_{(ij)}(\mathbf{b}_k, \mathbf{b}_l)$  defined as:

$$\begin{aligned} \mathbf{F}_{(11)}(\mathbf{b}_k, \mathbf{b}_l) &= \int \cdots \int_{\mathbb{C}^M} [\mathbf{x}_k - \mathbf{M}_k \mathbf{b}_k] [\mathbf{x}_k - \mathbf{M}_k \mathbf{b}_l]^H \\ &\quad \cdot \frac{\exp^{-\frac{1}{\sigma^2} \|\mathbf{x}_k - \mathbf{M}_k \cdot \mathbf{b}_k\|^2} \cdot \exp^{-\frac{1}{\sigma^2} \|\mathbf{x}_k - \mathbf{M}_k \cdot \mathbf{b}_l\|^2}}{\sum_{\mathbf{b}_i \in \mathcal{B}} \exp^{-\frac{1}{\sigma^2} \|\mathbf{x}_k - \mathbf{M}_k \cdot \mathbf{b}_i\|^2}} d\mathbf{x}_k \\ \mathbf{F}_{(22)}(\mathbf{b}_k, \mathbf{b}_l) &= \mathbf{F}_{(11)}^*(\mathbf{b}_k, \mathbf{b}_l) \\ \mathbf{F}_{(12)}(\mathbf{b}_k, \mathbf{b}_l) &= \int \cdots \int_{\mathbb{C}^M} [\mathbf{x}_k - \mathbf{M}_k \mathbf{b}_k] [\mathbf{x}_k - \mathbf{M}_k \mathbf{b}_l]^T \\ &\quad \cdot \frac{\exp^{-\frac{1}{\sigma^2} \|\mathbf{x}_k - \mathbf{M}_k \cdot \mathbf{b}_k\|^2} \cdot \exp^{-\frac{1}{\sigma^2} \|\mathbf{x}_k - \mathbf{M}_k \cdot \mathbf{b}_l\|^2}}{\sum_{\mathbf{b}_i \in \mathcal{B}} \exp^{-\frac{1}{\sigma^2} \|\mathbf{x}_k - \mathbf{M}_k \cdot \mathbf{b}_i\|^2}} d\mathbf{x}_k \\ \mathbf{F}_{(21)}(\mathbf{b}_k, \mathbf{b}_l) &= \mathbf{F}_{(12)}^*(\mathbf{b}_k, \mathbf{b}_l) \end{aligned}$$

Given that  $\frac{1}{\sigma^2} \|\mathbf{M}_k(\mathbf{b}_k - \mathbf{b}_l)\|^2$  is large enough for  $\mathbf{b}_k \neq \mathbf{b}_l$ , we can use the Lemma B.2.1 and neglect  $\mathbf{F}_{(ij)}(\mathbf{b}_k, \mathbf{b}_l)$ . The FIM becomes:

$$\mathcal{I}_{i,j}^{(k)} = \frac{1}{2^d} \frac{1}{(\pi\sigma^2)^M} \sum_{\mathbf{b}_k \in \mathcal{B}} \frac{1}{\sigma^4} \mathbf{b}_k^T \mathbf{M}_{i,j} \mathbf{b}_k \quad (\text{B.5})$$

with

$$\mathbf{M}_{i,j} = 2\text{Re} \left\{ \frac{\partial \mathbf{M}_k^H}{\partial \lambda_i} \mathbf{F}_{(11)}(\mathbf{b}_k, \mathbf{b}_k) \frac{\partial \mathbf{M}_k}{\partial \lambda_j} + \frac{\partial \mathbf{M}_k^H}{\partial \lambda_i} \mathbf{F}_{(12)}(\mathbf{b}_k, \mathbf{b}_k) \frac{\partial \mathbf{M}_k^*}{\partial \lambda_j} \right\}$$

Let us change the origin:  $\mathbf{y} = \mathbf{x} - \mathbf{M}_k \cdot \mathbf{b}_k$ , the matrices then become:

$$\begin{aligned} \mathbf{F}_{(11)}(\mathbf{b}_k, \mathbf{b}_k) &= \int \cdots \int_{\mathbb{C}^M} \frac{\mathbf{y} \mathbf{y}^H \exp^{-\frac{2}{\sigma^2} \|\mathbf{y}\|^2}}{\sum_{\mathbf{b}_l \in \mathcal{B}} \exp^{-\frac{1}{\sigma^2} \|\mathbf{y} + \mathbf{M}_k(\mathbf{b}_k - \mathbf{b}_l)\|^2}} d\mathbf{y} \\ \mathbf{F}_{(12)}(\mathbf{b}_k, \mathbf{b}_k) &= \int \cdots \int_{\mathbb{C}^M} \frac{\mathbf{y} \mathbf{y}^T \exp^{-\frac{2}{\sigma^2} \|\mathbf{y}\|^2}}{\sum_{\mathbf{b}_l \in \mathcal{B}} \exp^{-\frac{1}{\sigma^2} \|\mathbf{y} + \mathbf{M}_k(\mathbf{b}_k - \mathbf{b}_l)\|^2}} d\mathbf{y} \end{aligned}$$

The Lemma B.2.2 allows us to approximate these quantities to:

$$\begin{aligned} \mathbf{F}_{(11)}(\mathbf{b}_k, \mathbf{b}_k) = \mathbf{F}_{(22)}(\mathbf{b}_k, \mathbf{b}_k) &= \sigma^2 (\pi\sigma^2)^M \cdot \mathbf{I}_M \\ \mathbf{F}_{(12)}(\mathbf{b}_k, \mathbf{b}_k) = \mathbf{F}_{(21)}(\mathbf{b}_k, \mathbf{b}_k) &\ll \mathbf{F}_{11}(\mathbf{b}_k, \mathbf{b}_k) \\ &\approx \mathbf{0} \end{aligned}$$

From Eqn. (B.5), we can transform the next quantity:

$$\sum_{\mathbf{b}_k \in \mathcal{B}} \mathbf{b}_k^T \mathbf{M}_{i,j} \mathbf{b}_k = \text{Tr} \left\{ \mathbf{M}_{i,j} \cdot \left( \sum_{\mathbf{b}_k \in \mathcal{B}} \mathbf{b}_k \mathbf{b}_k^T \right) \right\}$$

Using Lemma B.2.3 and the preceding value of  $\mathbf{F}_{11}$ , we find:

$$\mathcal{I}_{i,j}^{(k)} = \frac{2}{\sigma^2} \text{Tr} \left\{ \text{Re} \left\{ \frac{\partial \mathbf{M}_k^H}{\partial \lambda_i} \cdot \frac{\partial \mathbf{M}_k}{\partial \lambda_j} \right\} \cdot \mathbf{C}_B^{(d)} \right\}$$

When integrating over  $k \in [1, \dots, N]$ , it leads to the general formula:

$$\boxed{\mathcal{I}_{i,j} = \frac{2}{\sigma^2} \sum_{k=1}^N \text{Tr} \left\{ \text{Re} \left\{ \frac{\partial \mathbf{M}_k^H}{\partial \lambda_i} \cdot \frac{\partial \mathbf{M}_k}{\partial \lambda_j} \right\} \cdot \mathbf{C}_B^{(d)} \right\}} \quad (\text{B.6})$$

But in our case it appears that the matrix  $\mathbf{M}_k$  has only one column that depends on a given parameter  $\lambda_i$  at a time  $k$ ,  $\mathbf{m}_k^i$ , the derivative simplifies to:

$$\frac{\partial \mathbf{M}_k}{\partial \lambda_i} = \left[ \mathbf{0} \mid \frac{\partial \mathbf{m}_k^i}{\partial \lambda_i} \mid \mathbf{0} \right]$$

replacing the derivative of  $\mathbf{M}_k$  in Equation (B.6) gives the result in lemma (5.2.3).  
□

# Bibliography

- [1] M. Stevens, *Secondary Surveillance Radar*. Artech house, Norwood, MA, 1988.
- [2] S. Kingsley and S. Quegan, *Understanding Radar Systems*. Mc Graw-Hill, London, UK, 1992.
- [3] J. Shaw, *Radar data processing with new generation monopulse SSR radar*.
- [4] J. J. Renes and M. R. Best, "Theoretical background to the reconstruction facility MURATREC," Rep. NLR TR 84008 L, National Aerospace Laboratory, Amsterdam, 1984.
- [5] N. Petrochilos and A. Trindade, "Application of JAFE to multi-static radar for air speed measurement," in *Proc. International Symposium on Antennas for Radar Earth Observation*, (Delft, The Netherlands), 8-9 June 2000.
- [6] J. Tol, "Improvement of the SSR mode S data link using a distributed groundsystem," Graduate project Report S-xxx-99, IRCTR, Sept. 1995.
- [7] P. Bezousek, "A passive radar surveillance system VERA for ATC," in *IRS'98*, (Munich, Germany), 1998.
- [8] H. Krim and M. Viberg, "Two decades of array signal processing research," *IEEE Sig. Proc. Magazine*, pp. 67-94, July 1996.
- [9] S. Haykins, *Radar Array Processing*. Springer-Verlag, 1993.
- [10] W. A. Gardner, *Cyclostationarity in Communications and Signal Processing*. IEEE press, 1994.
- [11] P. Comon, "Independent component analysis, a new concept?," *Signal Processing, Special issue on Higher-Order Statistics*, vol. 36, pp. 287-314, April 1994.
- [12] A. van der Veen and A. Paulraj, "An analytical constant modulus algorithm," *IEEE Trans. Signal Processing*, vol. 44, pp. 1136-1155, May 1996.
- [13] S. Talwar, M. Viberg, and A. Paulraj, "Blind separation of synchronous co-channel digital signals using an antenna array. Part I. algorithms," *IEEE Trans. on Signal Processing*, vol. 44, pp. 1184-1197, May 1996.

- 
- [14] A. van der Veen, "Analytical method for blind binary signal separation," *IEEE Trans. Signal Processing*, vol. 45, pp. 1078–1082, Apr. 1997.
- [15] O. Grellier and P. Comon, "Blind separation of discrete sources," *IEEE Signal Processing Letters*, vol. 5, pp. 212–214, Aug. 1998.
- [16] O. Grellier and P. Comon, "Analytical blind discrete source separation," in *Eusipco*, (Tampere, Finland), 5-8 sept. 2000.
- [17] A. Belouchrani, K. A. Meraim, J.-F. Cardoso, and E. Moulines, "A blind source separation technique based on second order statistics," *IEEE Trans. Signal Processing*, vol. 45, pp. 434–444, feb 1997.
- [18] L. Tong, "Joint blind signal detection and carrier recovery over fading channels," in *Proc. IEEE ICASSP*, (Detroit, MI), pp. 1205–1208, 1995.
- [19] A. van der Veen, "Blind separation of BPSK sources with residual carriers," *Signal Processing*, vol. 73, pp. 67–79, Jan. 1999.
- [20] E. Chaumette, P. Comon, and D. Muller, "An ICA-based technique for radiating sources estimation; application to airport surveillance," *IEE Proceedings - Part F*, vol. 140, pp. 395–401, Dec. 1993. Special issue on Applications of High-Order Statistics.
- [21] A. van der Veen and J. Tol, "Separation of zero/constant modulus signals," in *Proc. IEEE ICASSP*, (Munich (FRG)), pp. 3445–3448, April 1997.
- [22] N. Petrochilos, A. Trindade, D. Matic, and R. Prasad, "Blind Channel Synchronisation and Equalisation Algorithm for OFDM wireless communications," in *Proc. of WPMC 2001*, vol. 3, (Aalborg, Denmark), pp. 1357–1361, 9-12 September 2001.
- [23] D. Matić, N. Petrochilos, A. Trindade, F. Schoute, P. Comon, and R. Prasad, "OFDM synchronisation based on the phase rotation of sub-carriers," in *Proc. of 51st IEEE Vehicular Technology conference VTC*, vol. 2, (Tokyo, Japan), pp. 1260–1264, 15-18 May 2000. VTC 2000.
- [24] D. Matic, N. Petrochilos, A. Coenen, F. Schoute, and R. Prasad, "Acquisition of synchronisation parameters for OFDM using a single training symbol," in *Second International Workshop on Multi-Carrier Spread-Spectrum and related Topics*, (Oberpfafenhofen, Germany), 15-17 September 1999. published as a book by Kluwer.
- [25] N. Petrochilos and A. van der Veen, "Blind time delay estimation in asynchronous CDMA via subspace intersection and ESPRIT," in *Proc. of IEEE ICASSP 2001*, vol. 4, (Salt Lake City (UT)), pp. 2217–2220, May 2001.
- [26] N. Petrochilos and P. Comon, "Blind identification of linear-quadratic channels with usual communication inputs," in *Proc. of SSAP 2000*, (Pennsylvania, USA), pp. 181–185, 14-16 Aug 2000.



- 
- [27] N. Petrochilos and P. Comon, "Nonlinear channel identification and performance analysis," in *Proc. of 2000 IEEE ICASSP*, vol. 1, (Istanbul, Turkey), pp. 209–202, 5-9 Jun 2000.
- [28] N. Petrochilos, A. Leshem, and A. van der Veen, "Finite sample identifiability of multiple constant modulus sources," in *Proc. of GRETSI 2001*, (Toulouse, France), 10-13 September 2001.
- [29] International Civil Aviation Organisation, *International standards and recommended practices, aeronautical telecommunications: Annex 10*, 1985.
- [30] N. Petrochilos, "Reflectors detection by clustering," Master Report et 10-84, IRCTR, Feb. 1998.
- [31] M. S. Bartlett, "Smoothing Periodograms from Time Series with Continuous Spectra," *Nature*, no. 161, pp. 686–687, 1948.
- [32] M. Zoltowski, "On the performance analysis of the MVDR beamformer in the presence of correlated interference," *IEEE Transactions on Acoustics, Speech and Signal Processing*, vol. 36, pp. 945–947, jun 1988.
- [33] J. Capon, "High-Resolution Frequency-Wavenumber Spectrum Analysis," *proc. IEEE*, vol. 57, pp. 2408–2418, Aug 1969.
- [34] P. Stoica and A. Nehorai, "MUSIC, Maximum Likelihood and Cramer-Rao Bound," *IEEE Trans. on ASSP*, vol. 37, pp. 720–741, may 1989.
- [35] R. O. Schmidt, "A Signal Subspace Approach to Multiple Emitter Location and Spectral Estimation," phd thesis, Stanford Univ., Stanford, CA, Nov 1981.
- [36] P. Stoica and K. Sharman, "Novel eigenanalysis method for direction estimation," *IEE Proceedings F - Radar and Signal Processing*, vol. 137, feb 1990.
- [37] R. Roy and T. Kailath, "ESPRIT estimation of signal parameters via rotational invariance techniques," *IEEE Trans. on acoustics, speech, and Signal Processing*, vol. 37, pp. 984–995, July 1989.
- [38] A. van der Veen, M. Vanderveen, and A. Paulraj, "Joint angle and delay estimation using shift-invariance techniques," *IEEE Tr. Signal Processing*, vol. 46, pp. 405–418, Feb. 1998.
- [39] A. N. Lemma, A.-J. van der Veen, and E. Deprettere, "Analysis of Joint Angle-Frequency Estimation Using ESPRIT," *IEEE trans. on Acoustics, speech, and signal processing*, 1999. to appear.
- [40] M. Zoltowski, "Novel techniques for estimation of array signal parameters based on matrix pencils, subspace rotations, and total least squares ," in *Proceeding of ICASSP*, vol. 5, (Ney York, USA), pp. 2861–2864, April 1988.

- 
- [41] M. Haardt and J. Nossék, "Unitary ESPRIT: how to obtain increased estimation accuracy with a reduced computational burden," *IEEE Transactions on Signal Processing*, vol. 43, pp. 1232–1242, may 1995.
- [42] N. Yuen and B. Friedlander, "Asymptotic performance analysis of esprit, higher order esprit, and virtual esprit algorithms," *IEEE Trans. on Signal Processing*, vol. 44, October 1996.
- [43] A. L. Swindlehurst, S. Daas, and J. Yang, "Analysis of a decision directed beamformer," *IEEE Trans. on Signal Processing*, vol. 43, pp. 2920–2927, Dec. 1995.
- [44] G. Golub and V. Pereyra, "The differentiation of pseudo-inverses and non-linear least square problems whose variables separate," *SIAM J. Num. Anal.*, vol. 10, pp. 413–432, 1973.
- [45] J.-F. Cardoso and A. Souloumiac, "Jacobi angles for simultaneous diagonalization," *SIAM J. Mat. Anal. Appl.*, vol. 17, pp. 161–164, Jan. 1996.
- [46] N. Petrochilos and P. Comon, "ML estimation of SSR signals, identifiability, and Cramer-Rao bounds," in *Proc. of EUSIPCO 2000*, (Tampere, Finland), 5-8 Sept 2000.
- [47] N. Petrochilos, A. Leshem, and A. van der Veen, "Finite sample identifiability of multiple constant modulus sources," *IEEE letter on Sig. Proc.*, 2002. to be submitted.
- [48] S. M. Kay, *Fundamentals of statistical signal processing: estimation theory*. Prentice Hall, 1993.
- [49] A.-J. van der Veen, "Asymptotic properties of the algebraic constant modulus algorithm," *IEEE trans. on Acoustics, speech, and signal processing*, Aug. 2001.
- [50] L. D. Lathauwer, "Signal Processing based on Multilinear Algebra," phd thesis, K.U.Leuven, Leuven, Belgium, Sep 1997.
- [51] A. Weiss and B. Friedlander, "Almost blind steering vector estimation using second-order moments," *IEEE Transactions on Signal Processing*, vol. 44, pp. 1024–1027, April 1996.
- [52] D. Astely, A. Swindlehurst, and B. Ottersten, "Spatial signature estimation for uniform linear arrays with unknown receiver gains and phases," *IEEE Transactions on Signal Processing*, vol. 47, pp. 2128–2138, Aug 1999.
- [53] G. Cardan, *Ars Magna*. Milan University Press, 1545.
- [54] J. Stillwell, *Elements of algebra*. Springer, 1994. ISBN 0-387-94290-4.
- [55] R. A. Horn and C. R. Johnson, *Matrix Analysis*. Cambridge University Press, 1985.

## Summary

Air Traffic Control (ATC) centers aim at ensuring safety of aircrafts cruising in their area. The information required to face this mission includes the data provided by primary and Secondary Surveillance Radar (SSR). The first one indicates the presence of an aircraft, whereas the second gives information on its identity and altitude. All aircrafts contain a transponder, which send replies to the secondary radar in a semi-automatic mode, indeed it is an exchange. The increase of the air traffic implies that in a near future the actual SSR radar will not be able to perform correctly, and that requires to improve the quality of the SSR radar. This thesis proposes a possible improvement of the SSR.

We propose to replace at reception the rotating antenna by an antenna array to gain spatial diversity, in order to perform beamforming. Given the density of the traffic, high-resolution techniques are mandatory to separate the sources. This is a blind source separation problem, but unlike standard cases, the sources are sending packets (not continuously), the packets do not completely overlap (non-stationary situation), the alphabet is binary but not antipodal ( $\{0, 1\}$  instead of  $\{+1, -1\}$ ). And the carrier frequencies are not identical. Among the problems to solve, two main issues are the non-synchronisation of the sources, and the non-calibration of the antenna.

This thesis presents new contributions to this field, including the identifiability of parameters and related Cramer-Rao bounds, and the design of receiver algorithms taking into account the specific encoding of the data (such as the MDA and the ZCMA algorithms presented herein). The performance of these algorithms is tested by extensive computer simulations as well as actual measurements; the setup of the experimental platform is also part of the thesis framework.



## samenvatting

### Algoritmes voor het scheiden van "Secondary Surveillance Radar" (SSR) transpondersignalen

De luchtverkeersleidingcentra zijn verantwoordelijk voor de veiligheid van vliegtuigen in hun gebied. De informatie die hiervoor nodig is komt van twee radarsystemen: het hoofdradar en het "Secondary Surveillance Radar" (SSR). De eerste geeft een indicatie van de aanwezigheid van vliegtuigen aan de hand van hun reflecties, terwijl de tweede informatie geeft over de identiteit en de hoogte van een vliegtuig. Alle vliegtuigen hebben een transponder aan boord, die half-automatisch databerichten terugstuurt naar het SSR radarstation. De toegenomen dichtheid in het luchtruim betekent dat in de nabije toekomst het SSR systeem niet meer correct zal kunnen fungeren, tenzij de kwaliteit van het systeem verbeterd wordt. Deze thesis stelt een mogelijke verbetering voor.

We stellen voor om de roterende ontvangstantenne van het SSR systeem te vervangen door een antenne array om spatiële vrijheidsgraden te creëren, en selectieve bundelvorming mogelijk te maken. Gegeven de dichtheid van het vliegverkeer is het noodzakelijk om hoge-resolutie algoritmes toe te passen om de bronsignalen te scheiden. Dit is een zogenaamd "blind" probleem (de boodschap en het kanaal zijn beide onbekend), maar met verschillen ten opzichte van het standaard geval: de bronnen zenden korte databerichten (niet continue), de berichten kunnen half overlappen (geen stationariteit), het alfabet is binair maar niet symmetrisch ( $\{0, 1\}$  in plaats van  $\{-1, 1\}$ ), en de draaggolf-frequenties zijn niet precies aan elkaar gelijk. Bijkomende problemen is het feit dat de bronnen niet gesynchroniseerd zijn en de antennes niet gecalibreerd.

Dit proefschrift presenteert nieuwe bijdragen in dit vakgebied, waaronder de identificeerbaarheid van de parameters en de gerelateerde Cramer-Rao ondergrens op de parametervariantie, alsmede het ontwerp van ontvangsalgoritmes die van de specifieke codering van de data gebruik maken (de MDA en ZCMA algoritmes in deze thesis). De kwaliteit van de algoritmes wordt getest door middel van uitgebreide computersimulaties maar ook door echte metingen; het ontwerp en uitvoering van een experimenteel platform hiervoor valt ook binnen het kader van het proefschrift.



## Acknowledgments

Thanks to P. Dewilde, P. Comon and P. van Genderen for supervising me. Thanks to A.-J. van der Veen for being my everyday supervisor. Thanks to J.T. Fokkema (Rector magnificus), G. Galati, M. Moonen, and Ph. A. Regalia to be part of the dutch jury. Thanks specially to G. Galati for asking a broad range of meaningful questions before the defence.

Thanks to the members of the French jury, I. Fijalkow, J. Le Roux, E. Moreau, D. Slock, for their review, presence, questions and for making me a doctor.

Thanks to P. Aubry for the GPIB help. Thanks to J. Heijnoort for the PCB help. Thanks to A.-J. Boonstra for the ADC help. Thanks E. Platzbecker and A. Frehe for being very competent system managers.

Thanks to MF. Bacchialoni for freeing me from some of my secondary school duties. Thanks to H. Rivano for offering me a computer to write this thesis. Thanks to A. Trindade for receiving me and feeding me in Delft. Thanks to my IUFM supervisors, MB. Pages, MC. Abrahamian, Y. Weiss, for making this year sweeter. Thanks to S. Mermier, P. Sixdenier, P. Lapraz for showing me the full range of pedagogy. Thanks to D. Courte and F. Euleuche (SNALC) for defending me from the Ministry of Education.

Thanks to Abdelbrahim, Adil, Ahmet, Alex, Anna, António, Arnold, Aziz, Bruno, Christina, Daniele, Dany, Dušan, Fiona, Francisco, Georgios, Jean-Pierre, Klaus, Luuk, Marco, Marteen, Maya, Michiel, Miguel, Miki, Nuno, Paul, Pedro, Pirhos, Plamy, Relja, Reto, Roger, Rute, Silke, Simon, Sotiris, Thanos, Victoria, Vlad, Yannis, Jan-Willem, and Mhr. Crouwer (my last landlord) for their best effort to make Holland a decent place where to live.

Thanks to the friends that made their best effort to make Nice a decent place where to live: Aurore, Blaise, Carine, Caroline (G. and B.), David, Herve (again R. and G.), Jerome, Isabelle, and Marie.

Thanks to my IUFM-mates Bachera, Caroline, Eva, Frederic, Laurent, Nicolas (P. and G.), Olivier, Pierre, Stephan, Tanguy, to make me pass the IUFM reality-check.

Thanks to my friends from Toulon for their support: Guillaume, Mylene, Zook, Mickey, Anne, David, Celine, Guitou... and also to all my friends I lost in this wonderful and dangerous world. I apologize to whoever I forgot. Let us meet again, and have a night of "Jenever".

Thanks to my family, Lea's family, and close relatives for their constant support.

Special thanks to Lea.

*We were delighted, we all realized we were leaving confusion and non-sense behind and performing our one and noble function of the time, move."*

– Jack Kerouac, "On the road" –



## Curriculum vitae

N. Petrochilos was born in Paris, France on the 10th of July 1970. He obtained his “Baccalauréat” C in 1988, at the “Lycée Bonaparte”, Toulon, France. He got his “Maîtrise” of physics in 1994 at “École Normale Supérieure de Lyon”. Subsequently, he was employed as a research officer during one year in a navy computer center. In 1996, he graduated the D.E.A of signal and image processing of E.N.S.E.A in Cergy-Pontoise, co-promoted by the E.N.S. Lyon, with the distinctions of the jury and as the major of promotion. In 1997, he passed the “Agrégation de physique”, ranked 56 over 1200 candidates. Since October 1997, he was working towards the Ph.D. title at TU Delft, first within IRCTR, then within CAS. This thesis was done under a cooperative supervision with the University of Nice Sophia Antipolis, laboratory I3S.

Since September 2001, he is working as a physics teacher in the secondary education for the Ministry of Education of France in Carros, then in Hyères, France. The 10th of July 2002, he obtained the title of Doctor with highest distinctions from the University of Nice Sophia Antipolis.